Swansea University

2025

Development of a combination therapy to destabilize ovarian cancer and its tumor microenvironment through inducible Nitric Oxide Synthase (iNOS) inhibition.

Submitted to Swansea University in fulfillment of the requirements for the degree of Doctor of Philosophy

Gianmarco Melone

MSc

Declarations

This work has not previously been accepted in substance for any degree and is not being concurrently submitted in candidature for any degree.

Signed .[redacted] ....

Date ...01/06/2026..

STATEMENT 1

This thesis is the result of my own investigations, except where otherwise stated. Where correction services have been used, the extent and nature of the correction is clearly marked in a footnote(s).

Other sources are acknowledged by footnotes giving explicit references. A bibliography is appended.

Signed [redacted]..

Date ...01/06/2026...

STATEMENT 2

I hereby give consent for my thesis, if accepted, to be available online in the University's Open Access Repository and for inter-library loan, and for the title and summary to be made available to outside organisations.

Signed [redacted] ....

Date ...01/06/2026..

Location of the PhD/research

The following PhD research project was conducted at both Swansea University (SU) and the Houston Methodist Research Institute (HMRI). The initial literature review to understand the topic and the challenges associated with ovarian cancer, as well as training in in vitro cell culture techniques and the application of non-coding RNA treatments, were carried out at Swansea University. The studies involving the administration of L-NMMA, cisplatin, the combination of both drugs, and the development of the two in vivo models were conducted at the Houston Methodist Research Institute. As part of an ongoing collaboration between the Houston Methodist Research Institute, the Department of Histopathology at Galway University Hospital (Ireland), and the Discipline of Pathology at the University of Galway (Ireland), the pathological evaluation of mouse tissues from the syngeneic in vivo model was performed at those institutions.

Abstract

Ovarian cancer represents a significant challenge in oncology, largely because reliable strategies for early detection are still lacking. In its initial stages, the disease is frequently asymptomatic or associated with vague and nonspecific symptoms that often resemble different gynecological or abdominal disorders. Consequently, most patients receive a diagnosis only when the disease has already progressed to an advanced stage, typically after extensive peritoneal dissemination has occurred. This late diagnosis severely limits therapeutic options and is associated with poor clinical outcomes. The management of ovarian cancer is further complicated by the high rate of relapse and by the immunosuppressive characteristics of the tumour microenvironment. Among these factors, nitric oxide (NO) plays a particularly relevant role. In many cancers, including ovarian cancer, NO is predominantly produced by inducible nitric oxide synthase (iNOS), and elevated NO levels have been associated with enhanced tumour progression as well as suppression of antitumour immune responses. Given the challenges posed by late-stage diagnosis, the presence of an immunologically "cold" tumour microenvironment, and the aggressive dissemination of ovarian cancer cells, this study explores an alternative therapeutic strategy to complement conventional chemotherapy. Specifically, the work investigates the potential of the iNOS inhibitor L-NMMA as a means of modulating nitric oxide

production, both as a single agent and in combination with Cisplatin. The experimental approach integrates in vitro and in vivo models to evaluate whether targeting NO signalling can simultaneously impair tumour cell behaviour and disrupt protumoural interactions within the tumour microenvironment. The main objective of this research is therefore to develop a therapeutic strategy capable not only of directly affecting ovarian cancer cells but also of altering the tumour microenvironment by limiting excessive nitric oxide production. This goal was addressed through the identification of Vimentin, a marker of epithelial–mesenchymal transition (EMT), as a molecular target affected by L-NMMA treatment. In OVCAR8 ovarian cancer cells, L-NMMA administration resulted in a reduction of Vimentin expression exceeding 50%. To further investigate the role of nitric oxide in tumour biology, OVCAR8 NOS2 knockout cell lines were specifically developed and used for both in vitro and in vivo studies. In addition, the combined treatment with Cisplatin and L-NMMA was associated in a syngeneic in vivo model with enhanced immune activation, characterized by increased markers of $CD4^{+}$ T-cell activation and a reduction in $CD4^{+}$ naïve T-cell markers, together with an overall increase in T cells and natural killer (NK) cells. This combination therapy demonstrated the capacity to modulate the immune response while simultaneously reducing total tumour cell number, percentages of tumour cell numbers and tumour area. Complementary evidence was obtained using a xenograft model based on NSG mice implanted with OVCAR8 NOS2 knockout cells. In this system, reduced peritoneal dissemination was observed, suggesting diminished migratory capacity associated with decreased Vimentin expression and impaired nitric oxide production. Furthermore, mice treated with Cisplatin displayed prolonged survival and improved control of tumour progression when compared with models using NOS2 parental OVCAR8 cell lines. Overall, the results presented in this work highlight the potential of targeting nitric oxide signalling as a strategy to enhance the efficacy of standard chemotherapy in ovarian cancer. By integrating experimental approaches across two research institutions, this project expands current understanding of the role of nitric oxide in ovarian cancer biology and provides evidence supporting the development of therapeutic interventions aimed at modulating the tumour microenvironment. In conclusion, the findings presented in this study, may contribute to the design of more effective treatment strategies capable of improving clinical outcomes for patients affected by ovarian cancer.

Acknowledgments

I would like to express my sincere gratitude to Dr. Recep Bayraktar, Dr. Jenny C. Chang, and Professor Lewis Francis for their continuous guidance, support, and mentorship throughout the course of this PhD project. I am deeply grateful to Professor Lewis Francis for his understanding, encouragement, and for sharing the same vision and ambition for this research. His constant support and guidance were fundamental in the development of my expertise in non-coding RNA research during my time at Swansea University as well as opening a new frontier of research in the RBGO group. I would also like to thank Dr. Jenny Chang for welcoming me into her laboratory and for fostering a supportive and stimulating research environment at the Houston Methodist Research Institute. My sincere thanks also go to Dr. Hong Zhao and Agne Baseviciene for their essential assistance in the RNA-seq data analysis. I am grateful to the RBGO research group for their training in fundamental in vitro techniques, which were essential for the screening of innovative therapeutic strategies in ovarian cancer within this project. Special thanks to Dr. Marcos Quintela-Vazquez. for his guidance and training in Western blot, qPCR, and RT-qPCR techniques. I would also like to thank Dr. David Howard and Dr. Kadie Edwards for their training in cell culture techniques and for our conversation about nanoparticle formulation, now extremely useful for future scenarios of this research. I extend my appreciation to the members of Dr. Jenny C. Chang's laboratory for their valuable support in the design and execution of innovative experiments that contributed significantly to this thesis. I am grateful to Nermin Kahraman for providing OVCAR8 cell lines and Dr. Polina Matre for her intermediary role between us. I am particularly thankful to Dr. Liliana Guzman for providing key experimental materials and for assisting with the generation of knockout models. I would also like to thank Dr. Thomas Christophoros for sharing his expertise on the biological principles underlying knockout model generation and on the use of L-NMMA. My thanks also go to Jenying Deng for her training in flow cytometry and data analysis, and to Maria Florencia Chervo for her assistance in preparing samples for RNA-seq analysis. I am grateful to Mailin Li for her helpful suggestions regarding the cytokine mixture used to stimulate iNOS expression. I would like to acknowledge Ivonne Uzair and Karina Ortega Martinez for their support during experimental work and for their constructive feedback. I am also thankful to Kristina D. Zambo and Fotis Nikolos for providing the flow cytometry panel used in this research, and to Fotis Nikolos for his assistance with the operation of the flow cytometer. I am grateful to Jianying Zhou and Wei Qian for their training and support in the animal facility, particularly during experiments requiring the processing of large numbers of mice, and to Aireana Phillips for her assistance during extensive animal analyses. Finally, I would like to thank Sean Hynes, Adam Freegrove, and Fidelma Kaar for their support with the histological analysis of the mouse peritoneum.

List of contents

Chapter 4 – iNOS knockout cell line reveals a higher sensitivity to Cisplatin in vitro and in vivo

List of figures

Chapter 1 – Ovarian cancer and its microenvironment

Chapter 2 – Ovarian cancer cell lines show basal expression of iNOS and increased sensitivity to Cisplatin in combination with L-NMMA

Chapter 3 – L-NMMA increases the efficacy of Cisplatin in vivo and stimulates the immune response

List of tables

Key words and abbreviations

ACTB – β-Actin (gene or mRNA)

β-Actin - β-Actin protein

α-SMA - α-smooth muscle actin

CAFs - Cancer-associated fibroblasts

CCLE - Cancer Cell Line Encyclopedia

DC1 - Type 1 dendritic cells

DC2 - Type 2 dendritic cells

DC(s) - Dendritic cells

EMT - Epithelial to Mesenchymal Transition

EndOC - Endometrioid ovarian cancer

eNOS - Endothelial Nitric oxide synthase (protein)

EVs - extracellular vesicles

GO - Gene Ontology

HGSOC - High-grade serous ovarian cancer

IFN- Y - Interferon-Y

IL-6 - Interleukin-6

IL-β1 - Interleukin-beta 1

iNOS - Inducible Nitric oxide synthase (protein)

IP - Intraperitoneal

KO - Knockout

L-NIL - N6-(1-iminoethyl)-L-lysine

L-NMMA - N^G-Monomethyl-L-arginine

LPS – Lipopolysaccharide

MDSCs - Myeloid-derived suppressor cells

MEOC - Murine epithelial ovarian cancer cell line

MMPs - Matrix metalloproteinases

MSCs - Mesenchymal stem cells

NE – Neutrophils

NK - Natural killer

NO - Nitric oxide

nNOS - Neuronal Nitric oxide synthase protein

NOS - Nitric Oxide Synthases

NOS1 - Neuronal Nitric oxide synthase (gene or mRNA)

NOS2 - Inducible Nitric oxide synthase (gene or mRNA)

NOS3 - Endothelial Nitric oxide synthase (gene or mRNA)

nTPM - Number of transcripts per million

NSG - NOD Scid Gamma

OC-TME - Ovarian cancer tumor microenvironment

OSE - Ovarian surface epithelium

OvCa – Ovarian cancer

PCA – Principal component analysis

PARP - Poly adenosine diphosphate-ribose polymerase

PDXs - Patient-Derived Xenografts

RNAi - RNA interference

RNAseq - RNA sequencing

ROIs - Regions of interest

ROS - Reactive oxygen species

RT-qPCR - Quantitative Real-Time PCR

siRNAs - short interfering RNA

TAMC - Tumor-associated Mast cells

TAMs - Tumor-associated macrophages

TME - Tumor microenvironment

TIME - Tumor Immune microenvironment

TNBC - Triple-negative breast cancer

TNF-α - Tumor necrosis factor alpha

Tregs - Regulatory T cells

VEGF - Vascular endothelial growth factor

The results and material obtained from the thesis have been published in the research journal Molecular Therapy Nucleic Acids in April 2026

Melone G, Bayraktar R, Zhao H, Hynes SO, Kaar F, Freegrove A, Deng J, Baseviciene A, Uzair I, Martinez KO, Guzman-Rojas L, Chervo MF, Li M, Qian W, Zhou J, Phillips A, Zambo KDA, Nikolos F, Chan KS, Thomas C, Francis L, Chang JC, Nitric Oxide Dependent Stabilization of Vimentin Confers Chemoresistance in Ovarian Cancer, Molecular Therapy - Nucleic Acids (2026), doi: https://doi.org/10.1016/j.omtn.2026.102924.

As well as this paper the skills and training were also utilized in other papers connected to HGSOC, namely:

1. RNAseq skills - Vaiasicca, S., **Melone, G.**, James, D.W. et al. Transcriptomic analysis of stem cells from chorionic villi uncovers the impact of chromosomes 2, 6 and 22 in the clinical manifestations of Down syndrome. Stem Cell Res Ther 14, 265 (2023). https://doi.org/10.1186/s13287-023-03503-4
2. RNAseq skills and EV characterization – Salvatore Vaiasicca, **Gianmarco Melone**, David W James, Marcos Quintela, Jing Xiao, Seydou Yao, Richard H Finnell, Robert S Conlan, Lewis W Francis, Bruna Corradetti, Transcriptomic analysis reveals the anti-cancer effect of gestational mesenchymal stem cell secretome, Stem Cells Translational Medicine, Volume 13, Issue 7, July 2024, Pages 693–710
3. RNAseq skills and co-colture analysis - Vaiasicca, S., James, D.W., **Melone, G.** et al. Amniotic fluid-derived mesenchymal stem cells as a therapeutic tool against cytokine storm: a comparison with umbilical cord counterparts. Stem Cell Res Ther 16, 151 (2025). https://doi.org/10.1186/s13287-025-04262-0

Chapter 1 – Ovarian cancer and its microenvironment

1.1 Ovarian cancer, a global gynecological challenge

Ovarian cancer (OvCa) is a multifaceted malignancy where 310,000 new cases and up to 200,000 deaths are estimated every year [1]. Due to the lack of early detection methods and the ambiguity of its symptoms, it is often diagnosed at an advanced stage and the 5-year survival rate is less than 50% with poor prognosis [2, 3]. Approximately 90% of primary malignant ovarian tumors are epithelial and are originated from the ovarian surface epithelium (OSE) [4]. The four major classifications of these epithelial ovarian tumors are High Grade Serous, Endometroid, Clear cell, Mucinous and Low Grade Serous [5]. Among these subtypes, High-grade serous ovarian cancer (HGSOC) represents the 70% of all the OvCa subtypes and it is often diagnosed at stage III (51%) and IV (29%) when the metastasis progression has already started [6]. Recent discoveries suggested as, the metastasis process doesn't only happen from the primary tumor site with a predilection from the omentum [7, 8], but there are recent discoveries suggesting metastatic spread from tumor cells found in the blood, as it has been identified from different investigations [9, 10]. This other metastasis formation scenario could potentially change the idea about how metastasis is formed, but what remains clear is the deleterious role that has in all the patients due to their wide dissemination. Different advanced therapy are currently adopted in addition to surgery and chemotherapy, such as antiangiogenic agents, poly adenosine diphosphate-ribose polymerase (PARP) inhibitors, hormone receptor modulators, and immune checkpoint inhibitors [11]. The first approach however is still based on tumor debulk and carboplatin/paclitaxel chemotherapeutic treatment [12]. Even if most patients initially respond positively to the standard therapeutic approaches, recurrence typically occurs in a median time of 15 months from the first diagnosis [13] and this is due to genetic and epigenetic mutations that may lead to the extrusion or inactivation of cytotoxic drugs [14], impaired apoptosis and enhanced induction of repair mechanisms.

Another key factor for OvCa complexity and recurrence, is the presence of a 'cold immune microenvironment' where immune cells are either inactive or have a pro-cancer effect, implementing the deleterious effect of the tumor niche [15]. In addition to the immune component, often described as "cold" due to its limited activity, the tumour microenvironment is highly heterogeneous. This heterogeneity arises from the presence of multiple cell populations, including cancer-associated fibroblasts at different activation stages, endothelial cells, stromal cells, and adipocytes. These components coexist with the malignant cells themselves. [16-18]. All together, these factors contribute to making OvCa an open challenge in the scientific and clinical communities. In **Figure 1.1 it is possible** to observe the main populations of the tumor microenvironment (TME).

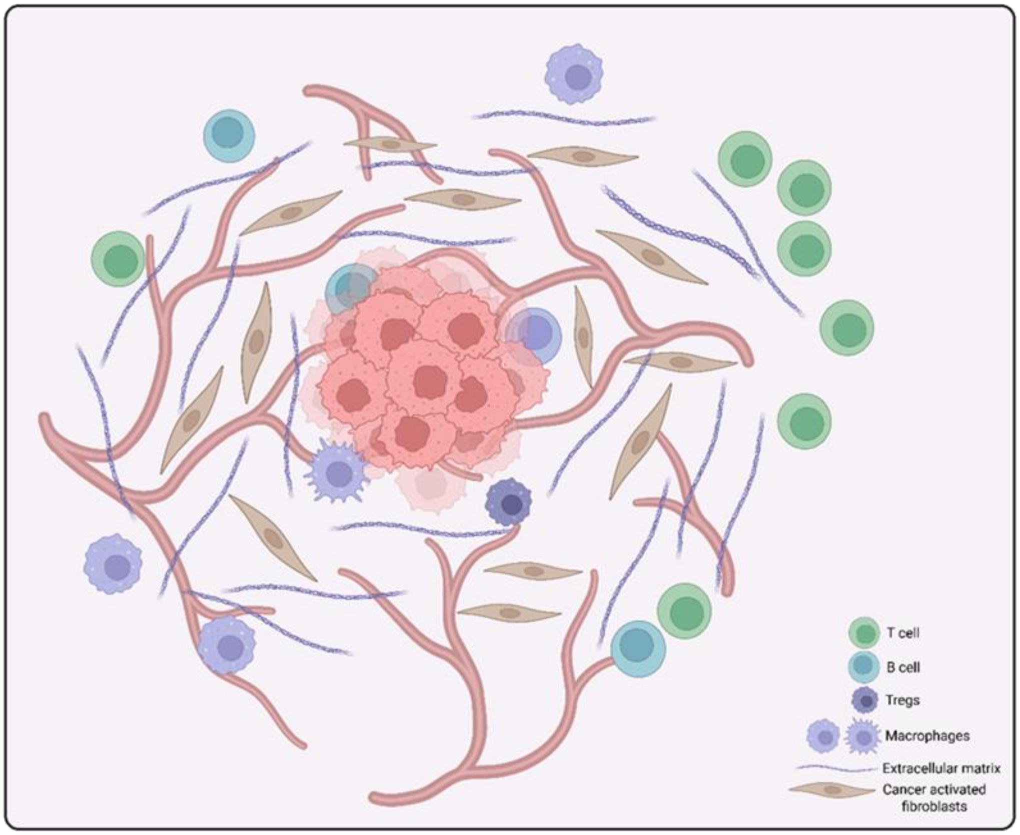

Figure 1.1. The heterogeneity of the tumor microenvironment. Cancer cell growth is supported by cancer activated fibroblasts and the extracellular matrix secreted by them with the role of supporting angiogenesis and representing a physical barrier for immune cells infiltration. Another key factor in ovarian cancer is the presence of immunosuppressive immune cell populations that, together with CAFs and stromal cells, contribute to generate a "cold" tumour microenvironment. Created in https://BioRender.com.

The main events happening into the tumor microenvironment related to each single population of the TME are shown in **Figure 1.2.**

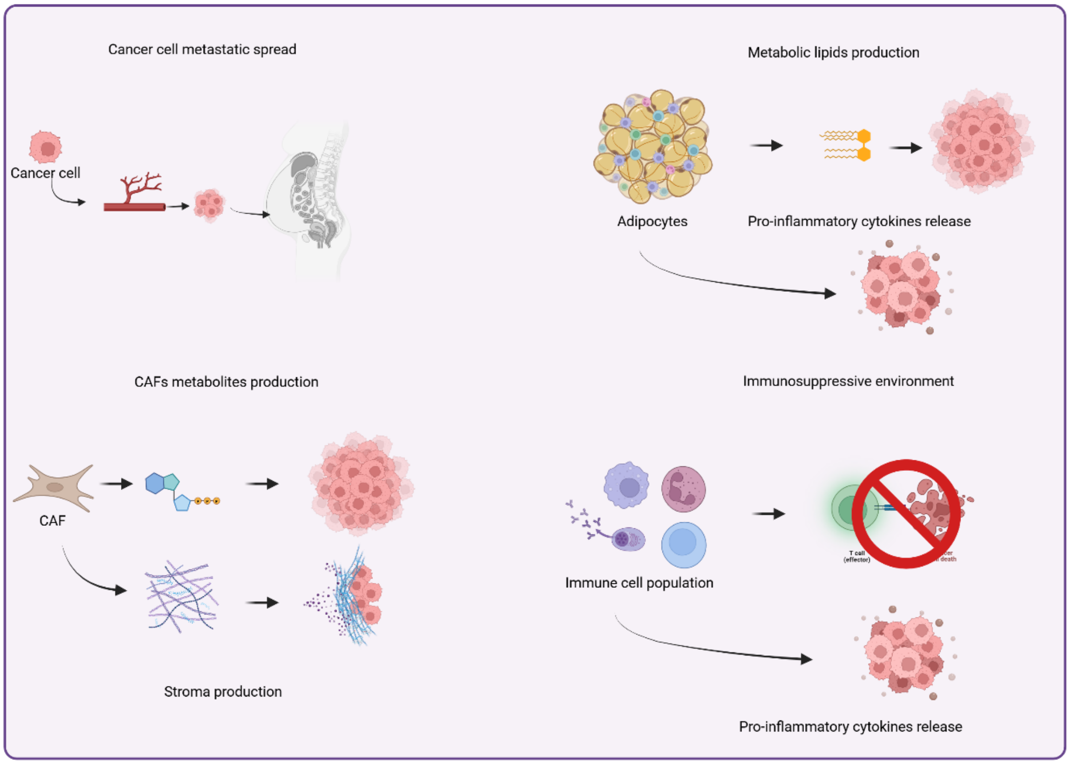

Figure 1.2. NO related activities in the TME. It is possible to see as each cell line into the tumour niche drives cancer cell metastasis. CAFs activity supports cancer growth, adipose tissue provides metabolic support to cancer cells and releases inflammatory cytokine and the immunosuppressive cell population prevents immune response and supports cancer growth. . Created in https://BioRender.com.

1.2 The ecology of the ovarian cancer tumor microenvironment (OC-TME) and the metastatic process

Ovarian cancer (OvCa) is often diagnosed at advanced stages, making it difficult to treat due to already established metastatic progression. In many patients, the disease has already spread to the omentum and the peritoneum. **Figure 1.3** illustrates the anatomical regions of the ovary, omentum, and peritoneum. Considering these factors and the dissemination of cancer cells, tumor debulking through surgery is an important and essential step to arrest the metastatic spread. Chemotherapy is also necessary to arrest the duplication and spread of ovarian cancer cells. The TME plays a key role in in supporting tumor growth, stimulating the Epithelial to Mesenchymal Transition (EMT), protecting cancer cells growth and stimulating the EMT. Cancer-associated fibroblasts (CAFs), derived from resident fibroblasts, mesenchymal stem cells (MSCs), adipocytes, and mesothelial cells, secrete pro-inflammatory cytokines and remodeling enzymes that promote EMT, invasion, and therapy resistance [19]. Mesenchymal stem cells contribute to CAFs populations and support tumor growth by differentiating into myofibroblasts under TME cues such as hypoxia and inflammation [20]. Adipocytes, particularly in the omentum, undergo dedifferentiation into fibroblast-like cells, releasing fatty acids that fuel cancer cell metabolism and enhance metastatic potential [21]. Lymphocytes, including regulatory T cells and tumor-infiltrating cytotoxic T cells, are modulated by stromal signals to promote immune evasion, further influencing EMT and tumor aggressiveness. Indeed, this integrated stromal network not only facilitates peritoneal dissemination but also contributes to chemoresistance and immune suppression, making it a critical target for therapeutic intervention in HGSOC [22].

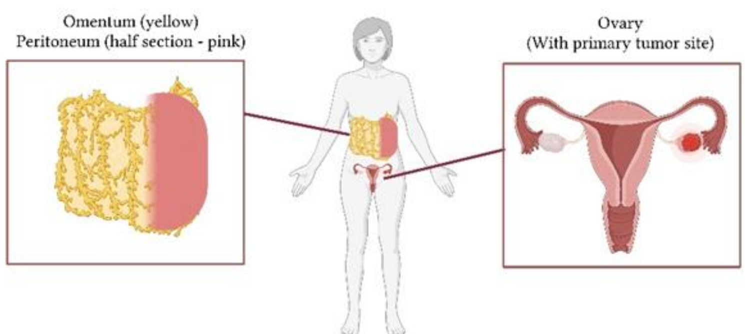

Figure 1.3 Anatomical regions of the ovary with a primary cancer spot, omentum and peritoneum. Created in https://BioRender.com.

1.2.1 Cancer-associated fibroblasts (CAFs)

Cancer-associated fibroblasts (CAFs) are key components of the tumor microenvironment, characterized by high heterogeneity, diverse phenotypes, and varied functional activities. They are typically located within or adjacent to the tumor mass, where they provide direct support to cancer cells [23]. Another peculiarity of fibroblasts is their diverse origins, which contribute to their heterogeneity. In particular, they can be derived from resident fibroblasts, bone marrow mesenchymal stem cells (MSCs), epithelial cells, endothelial cells, or adipocytes [24-29]. CAFs can exist in two distinct states: quiescent and activated. The activated state is often associated with the expression of various markers, including α-smooth muscle actin (α-SMA), fibroblast activation protein, low levels of caveolin-1, CD10, integrin β1, platelet-derived growth factor receptors α and β, and G protein-coupled receptor 77 [30-36]. Once activated, fibroblasts exhibit increased proliferation rates and a heightened metabolic state. The primary function of cancer-activated fibroblasts (CAFs) is to support tumor growth, invasion, and the proliferation of cancer cells. One way they achieve this is by releasing cytokines that modulate various signaling pathways. Among these cytokines, TGF-β is one of the most well-known, playing a crucial role in promoting tumor initiation and facilitating immune escape [37]. Many TGF-β-related genes expressed by CAFs play key roles in their interaction with ovarian cancer. These include Periostin, Collagen type XI alpha 1, Collagen triple helix repeat containing 1, and Versican [38-44]. Another important function of CAFs is to supply nutrients to cancer cells. In the early stages of cancer, when nutrient availability is limited, CAFs support cancer cell growth by providing energy through the tricarboxylic acid cycle. This process helps maintain the biological activities necessary for tumor progression and is often referred to as the “reverse Warburg effect.” [45] The support that CAFs provide to cancer cells also contributes to promoting cancer cell stemness [46, 47]. In addition, CAFs can reduce or limit the effectiveness of Cisplatin. Since many drugs are delivered through blood vessels into the tumor vasculature, CAFs can hinder drug delivery not only by creating a physical barrier but also by producing glutathione and cysteine. These molecules inhibit the accumulation of Cisplatin in the nuclei of cancer cells, thereby reducing its cytotoxic effects [48]. In addition to providing support and replenishing energy for cancer cells, CAFs can also stimulate a critical process frequently observed in ovarian cancer: the epithelial-to-mesenchymal transition (EMT). Specifically, it has been demonstrated that CAF-conditioned medium can induce EMT by regulating and modulating the expression of key markers such as E-cadherin and vimentin. Moreover, it influences other genes involved in metastasis, including MMP2 and VEGF, both in vitro and in vivo [49]. CAFs also participate in communication with cancer cells through the release of exosomes. Notably, exosomes released by CAFs contain higher levels of TGF-β1 compared to those from normal fibroblasts [50]. These exosomes can induce EMT by activating the SMAD signaling pathway, along with increasing the release of IL-6, which is linked to STAT3 activation. Together, these factors contribute to the induction of EMT [51]. Another important factor that induces EMT and protects cancer cells from drug penetration is the stiffness of the extracellular matrix, which results from the accumulation of matrix components secreted by CAFs. This increased stiffness can promote the formation of lamellipodia and invadosomes [52]. A further important function of CAFs is the stimulation of chemoresistance in cancer cells. Beyond matrix stiffness, CAFs can contribute to acquired chemoresistance by upregulating the expression of immune checkpoint molecules PD-1 and CTLA-4 on regulatory T cells (Tregs), thereby promoting an immunosuppressive environment [53]. In addition to this role, fibroblasts also support and stimulate angiogenesis by providing a scaffold that facilitates blood vessel formation, ensuring nutrient supply to cancer cells. In particular, CAFs are a significant source of VEGFA [54, 55]. In summary, CAFs have a relevant role in different functions of ovarian cancer and for that reason they are one of the key elements into the ovarian cancer TME.

1.2.2 Mesenchymal stem cells

Mesenchymal stem cells (MSCs) are controversial elements in cancer research, with some studies reporting their ability to suppress cancer activity. For example, it has been shown that MSCs can inhibit the proliferation of MCF-7 breast cancer cells by suppressing the Wnt signaling pathway [56]. Conversely, other studies have reported that MSCs can promote tumorigenesis. For example, MSCs have been shown to enhance the proliferation of melanoma cells [57]. Another study on breast cancer demonstrated that through cross-talk with breast cancer cells, MSCs were stimulated to produce CCL5, which in turn promotes breast cancer cell motility and invasion [58]. A study by McLean et al. reported the presence of MSCs in ovarian cancer and demonstrated that, upon interaction with cancer cells, MSCs promote tumor growth in vivo [20]. Considering all these different studies and what still to be elucidated about this population, MSCs have all the potential to be considered important players in the tumor microenvironment.

1.2.3 Adipocytes

Adipocytes are important components of the tumor microenvironment, especially given recent findings supporting their potential role in chemoresistance. Considering the abundance of adipocytes in the omentum, the primary site of metastatic spread in ovarian cancer, their interaction with cancer cells is particularly significant. Notably, conditioned media derived from adipocytes has been reported to increase cancer cell viability following Cisplatin treatment [59]. Other studies have shown that co-cultures of adipocytes and ovarian cancer cells result in the direct transfer of lipids from adipocytes to cancer cells, promoting tumor development both in vitro and in vivo. Additionally, omental adipocytes are known to secrete cytokines such as IL-8, which enhance the invasiveness of cancer cells. Adipocytes, also, undergo synchronized development alongside ovarian cancer cells, supported by the release of Interleukin-8 (as mentioned earlier), Interleukin-6 (IL-6), Monocyte chemoattractant protein-1, Tissue inhibitor of metalloproteinase-1, and Adiponectin, all of which contribute to ovarian cancer progression. Interestingly, similar to what is observed in peritoneal metastasis, omental adipocytes can transfer fatty acids directly to cancer cells through cell-to-cell contact, thereby influencing the metabolic activity of these carcinogenic cells [21].

1.2.4 The immune microenvironment

In the OC-TME one of the main features is the heterogeneity of the cell population into the niche. In particular, the heterogeneity of the immune cells population makes it difficult to develop a unique targeted therapy for the immune system control and reactivation. The difficulty lies in the fact that there are multiple cells to target, and one single therapy is not wide and at the same time specific enough to target multiple cell lines at the same time. Another factor which makes things more complicated is that as the tumor develops and the tumor microenvironment adapts to support the growth, at the same time immune cells can switch their function making it difficult to find the exact timing to start a potential immunotherapy. In **Figure 1.4** a summary of the immune cells population that is possible to find in the ovarian cancer tumor microenvironment (OC-TME) is shown.

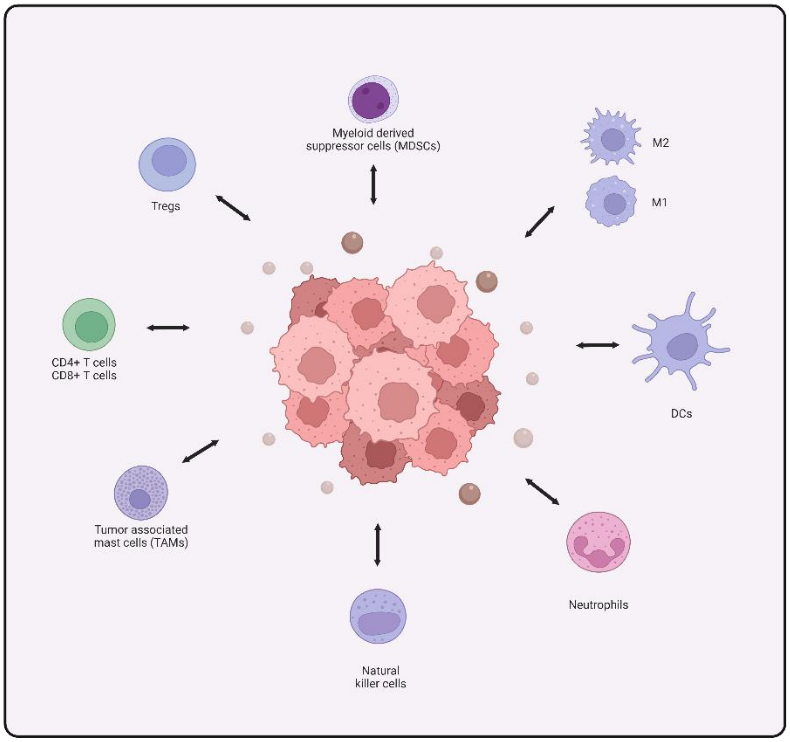

Figure 1.4. The immune population into the OC-TME. Immune cells in the tumor microenvironment undergo functional inactivation through reciprocal interactions with cancer cells and other immune cells, contributing to immune suppression and tumor progression.

Understanding the heterogeneity and complexity of the immune population will be beneficial not only to expand the actual knowledge about the ovarian cancer immune microenvironment, but also to develop a specific and more targeted immunotherapy. For that reason, it is an important element to comprehend the crosstalk between these different cells, to inhibit the immunosuppressive role operated by some specific subtypes. The heterogeneity of the immune population is given by the presence of different immune components such as components of the innate immune response like Macrophages (M1, M2), Dendritic cells (DCs), Neutrophils (NE), Natural killer (NK) cells, Tumor-associated Mast cells (TAMC). There are also components of the adaptive immune response where we can mention T-cells and all of their different categories like cytotoxic CD8+ T-cells, Helper CD4+ T-cells (and the subdivision in Th1 cells and Th2 cells) and also T-regulatory cells (Tregs). To complete the components of the adaptive immune components, it is also important to mention B-cells. These populations can also be divided into immunosuppressive (pro-tumor) populations where M2 Macrophages, Tregs, Myeloid-derived suppressor cells (MDSCs), Th2 cells and Tumor-associated Mast cells belong. The second group is composed of M1 Macrophages, Cytotoxic CD8+ T-cells, Th1 Cells (CD4+), NK cells and Dendritic cells (even if their polarization might change their function). Together with these two groups there are also immune cells which have been found to have a dual function and for that they are a mixed population. These populations are B cells, even if much can vary according to their subtype and neutrophils.

1.2.5 Macrophages

Macrophages have an important role in the innate immune response and its homeostasis. They have different functions that can vary according to the site of activity, the niche where they can be found and their polarization. In general, their function is related to antigen presentation, phagocytosis and homeostasis of the TME which has on his hand the potential of influencing macrophages polarization [60]. Macrophages can reach the tumor niche through chemotaxis according to signals present into the niche [61]. The polarization of macrophages has two different scenarios which can transform non polarized macrophages into Tumour-associated macrophages (TAMs). In the first scenario the polarization drives macrophages in anti-tumourigenic M1 macrophages, in the second scenario they become pro-tumourigenic M2 macrophages [62].

M2 Tumor-associated macrophages are known as pro-tumourigenic and immunosuppressive macrophages because of the secretion of IL-4, IL-5 and IL-6 which have a role in the enhancement of angiogenesis and in the suppression of the immune response [63]. They are also involved in angiogenesis enhancing endothelial cell migration via IL-8 upregulation [64]. Their deleterious effects are not only reported in the stimulation of angiogenesis, but also suppressing T-cells response by secreting molecules such as CCL-22, B7-H4 and CD206. B7-H4+ macrophages, for example, are able to suppress T cell immunity driven by antigen driven [65].

M2 and M1 macrophages express both MHCII, but the difference between them is that M2 macrophages don't express MHCII at levels sufficient for all the functions of antigen presentation [66].

For that reason, M1 macrophages can be considered the efficient counterpart in anti-tumorigenic activity compared to M2 macrophages.

1.2.6 Dendritic cells – DCs

Dendritic cells are known to be Antigen Presenting Cells with relevant functions both in the innate and adaptive system. Due to their ability to present tumor antigens to naïve T cells, DCs are essential in the immune response against cancer [67], and many efforts are currently ongoing to develop efficient cancer vaccines based on DCs. For that reason, the immune escape operated by ovarian cancer cells could be related to the alteration of the DCs response in the tumor niche [68].

1.2.7 Neutrophils

Neutrophils play an important role in cancer-related inflammation which can be either pro-tumorigenic or anti-tumorigenic according to the TME crosstalk and factors release. It has been observed by Charles et al. that, in patients, neutrophils are recruited by different factors such as tumor necrosis factor alpha (TNF-α) in an Interleukin-17-dependant way and it is correlated with a pro-tumourigenic effect [69]. Also, TGF-beta plays an important role in the recruitment of neutrophils. In particular, it has been observed how TGF-beta is able to recruit Tumor associated neutrophils with an immunosuppressive and pro-tumourigenic role and contrarily, the blockade of TGF-beta has shown a higher recruitment of neutrophils with a more relevant antitumour phenotype [70].

1.2.8 Natural killer cells

Natural killer (NK) cells are part of the innate immune system. One key feature of these cells is their capability of killing cancer cells without prior sensitization [71]. Their activity is related to the CD16 receptor, the NKG2D receptor and the NKp30 cytotoxicity receptor. The dysfunction of NK cells can be related to an impaired cytotoxicity/cytokine secretion, alterations in the receptor or alteration in the ligand, reduced infiltration of NK cells into the tumor site due to the biological barriers of the tumor niche. [72] – Another examples of NK inactivation has been observed into patients ascites through the inhibition of NKG2D [73] and NKp30 [74, 75] According to Krockenberger et al., cancer cells express factors responsible for the transcriptional downregulation of NKG2D [73] . The release of the soluble factor B7-H6 which is known to bind to NKp30 is also responsible for reducing the cytotoxic activity of NK cells into ascites [74]. In addition to these inactivation elements observed in ovarian cancer and in particular in ascites, it has also been reported by Radke et al. and Trotta et al. how TGF-β and IL-8 are also able to suppress the activity of NK cells [76, 77].

1.2.9 Tumor associated mast cells (TAMCs)

Mast cells derive from a bone marrow progenitor cell, they migrate in the tissue where they grow and differentiate according to the conditions of the microenvironment. For that reason, there are different subdivision and possible developmental scenarios of mast cells according to the microenvironment, the release of cytokines and the potential crosstalk with different cell types influencing also their secretion profile in the tumor niche itself [78]. This cell population is so versatile in terms of differentiation and localization that in tumor they have been reported to have ambivalent roles. For example, TAMs secrete IL-8 which is a factor that influences angiogenesis and it is also known to be a tumor mitogen factor [79]. On the other hand, they are also capable of expressing, for example, IL-4 which by binding to the IL-4 receptor expressed by human breast carcinoma cells, it could induce apoptosis in breast cancer cells [80].

1.2.10 CD8+T cells

Multiple immunotherapies have the main goal of reactivating and stimulating CD8+ T cells as they are powerful effectors in the anti-cancer immune response [81]. Many studies highlighted how high infiltration of CD8+T cells is associated with a good clinical outcome [82-85], but even if the intraepithelial presence of CD8+T showed a favorable overall, Hamanishi et al. showed that the infiltration of CD8+T cells into the stroma didn't show the same positive overall positive progression in patients [86]. CD8+T cells exhaustion is associated with the expression of PD-1 and the blockade of PD-1 enhances T-cells immunity specifically in ovarian cancer [87]. Together, CD8+ and CD4+ TILs secrete cytokines such IFN-gamma and IL-2 [88] that can enhance the antitumor activity and promote longer survival [89].

1.2.11 CD4+T helper

CD4+ T cells are a broad range of immune cells that undergo specific functionalization and differentiation after the interaction with MHCII of Antigen Presenting Cells (APCs). In general, there are six subpopulations of CD4+ T cells which are Th1, Th2. Th9, Th17, Treg, follicular T helper [90]. As per the majority of the immune components in ovarian cancer, their role can be ambivalent according to their differentiation pathway, for example, Th1 are considered as positive elements against cancer [91] and regulatory T cells (Tregs) are considered, even if also in this case the literature shows contrasting evidences, pro-tumourigenic factors. In general, studies reported how CD4+T cells stimulate the immune response against the tumor by secreting cytokines like IL-2 and IFN-Y that are able to regulate and stimulate the response of APCs in order to keep cytolytic CD8+T cells active against tumor [92, 93]. They also stimulate APCs maturation via interaction of CD40 on APC cells and the ligand CD154 on T cells. This interaction stimulates the secretion of IL-12 and stimulates the maturation of naïve T cells against antigens [94-96]. Their activity is not only related to the support of the immune response or keeping CD8+ T cells active, but CD4+T cells can also have a role in directly targeting cancer cells and how reported by different authors, cytotoxic CD4+T cells (CD4-CTLs or Th-CTLs) are able to act similarly to CD8+T cells cytotoxic by secreting granzyme and perforin [97-99]. In particular, the cytotoxic functions related to these subtypes of CD4+T cells are related to transcription factors already present in natural killer (NK) and CD8+ T cells that are Eomes, T-bet and Blimp1 [100-102]. Another recent subtype that should be mentioned, in addition to the ones previously mentioned, is the counterpart related to the innate immune response. These subtypes are called Innate lymphoid cells [103-105] which don’t express antigen receptors. The progenitors of these cells are found in the bone marrow where mature ILCs are considered tissue- resident [106].

1.2.12 T-regulatory (Treg) cells

Treg cell infiltration is correlated with a metastatic phenotype and advanced cancer stage with a typical genomic signature with several immune related pathways involved [107]. Qiao et al. reported also how Tregs infiltration and the expression of its marker FOXP3 correlated with angiogenic factors like VEGFA and VASH1, all factors, together with FOXP3 related to a poor prognosis in patients [108]. FOXP3 in Tregs has also been associated with other pro-tumourigenic effects; in particular, as reported by Qiao et al. TAMs are able to secrete IL-12 which increase the frequency of Tregs by activating FOXP3 during the T-cell differentiation. Considering these factors and the negative correlation between poor prognosis and infiltration of Tregs, they can be used as potential targets for immunotherapeutic approaches.

1.2.13 Myeloid derived suppressor cells (MDSCs)

Another cell type which can inhibit the immune response is the Myeloid derived suppressor cells (MDSCs). They usually accumulate at the late stage of tumourigenesis when there is a level of cytokines release which is able to support MDSCs growth and recruitment [109] . These cell types can modulate immune response activity both in physiological and pathological conditions [110]. Another relevant factor is that MDSCs enhance cancer stem cell gene expression and sphere formation by inducing microRNA101 and suppressing the corepressor CtBP2 [111]. Recruitment of MDSCs in the TME is mainly mediated by chemokine receptors CXCR2, CCR2, CCR5 which mainly interact with CXC chemokines like CXCL1, CXCL2 and CXCL5 [112, 113]. As mentioned before for the immunosuppressive role of Tregs and their recruitment, also MDSCs can recruit Tregs through CD40-CD40 signaling [114]. The following figure (**Figure 1.5**) summarizes the immune cell populations and highlights the imbalance between the tumor microenvironment and the surrounding tissue. It also depicts the main molecules involved in immune suppression.

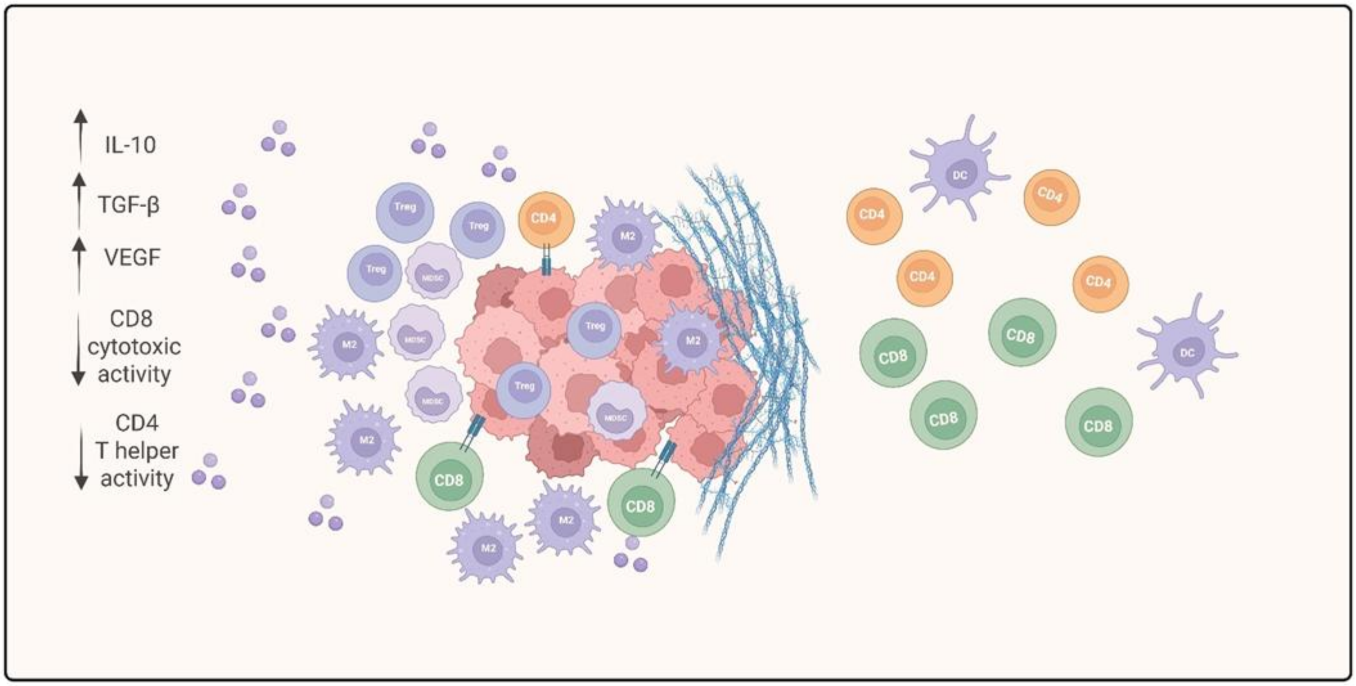

Figure 1.5. Representation of the immune-cold tumor microenvironment. Immune cell inactivation is primarily mediated by regulatory T cells (Tregs), M2-polarized macrophages, and myeloid-derived suppressor cells (MDSCs). Tregs and MDSCs contribute, among other mechanisms, to the release of immunosuppressive factors such as IL-10, TGF-β, and VEGF, which promote an immune-cold environment and inhibit the activity of CD8+ and CD4+ T cells. Created in https://BioRender.com

1.3 HGSOC Advanced therapies

One of the main challenging aspects of ovarian cancer is the detection at the late stage of the disease. Rarely patients are diagnosed with ovarian cancer at the early stages. For that reason, an essential aspect of the treatment is, when patients are diagnosed at the late stage, a surgical operation for tumor debulking [115], followed by chemotherapy which is a key strategy to reduce and prevent tumor growth [116-118], but considered the frequent relapses that characterize this tumor, the scientific community is seeking for new strategies to improve chemotherapy and/or offering valuable. As examples, immunotherapies have the main role of reactivation or engineering immune cells to target cancer cells [119]. Pan-drug microenvironment has the role of destabilizing the entire crosstalk between cells and their microenvironment [120]. These new approaches, together, will be extensively treated in the sections below.

1.3.1 Antibody based immunotherapy

Considering the high heterogeneity of the immune population resident in the tumor microenvironment, which is inactive or in a quiescent state, reactivating all the immune machinery is one of the main approaches that are taking place in the current scenario. In particular, the complexity of the tumor immune microenvironment (TIME) is given not only by the interaction among cancer cells, immune cells and CAFs, but also by the immunosuppressive role of some specific immune cells population which are recruited by cancer and components, with the role of inhibiting the immune response. This aspect is one of the main causes which allow cancer cells to proliferate. For this reason, reactivating the immune response may counteract immune escape and tumour progression. It may also enhance the effectiveness of treatments such as chemotherapy.

The antibody based therapy that is widely used in different types of cancer; they are well established for hematologic cancers, but there are increasingly antibody therapies that are started to use in ovarian cancer [121]. Examples of this therapy are Bevacizumab (Avastin®, Roche) which is a humanized monoclonal antibody (mAb) that binds to vascular endothelial growth factor (VEGF) receptor ligand. The reason for using this specific antibody is that in ovarian cancer, after biopsies VEGF gene expression is often correlated with a poor prognosis [122]. Another interesting antibody tested is Catumaxomab (Removab®, Fresenius Biotech GmbH) which has the dual function of binding to the epithelial cell adhesion molecule EpCAM and the T cell antigen CD3. EpCAM has already been reported by Bellone et al. to be expressed by primary and metastatic ovarian cancer [123] and the binding of this antibody could represent an important mechanism to arrest the proliferation and migration of ovarian cancer. The second function of this antibody is to bind to CD3 binding domains in order to recruit and activate immune effectors which are not active in the tumor site [124]. This antibody has also been adopted in chemotherapy – refractory ovarian cancer with malignant ascites and it is showing promising results [125].

1.3.2 TAM – targeting antibodies

Tumor-associated macrophages (TAMs) are a relevant component of the stroma in solid tumor. They are very active in the crosstalk between cells and in tumor progression. TAMs are classified into two subset with different cytokine profile, surface phenotypes, effects and influence on tumor progression [126]. In particular, the higher presence of M2 macrophages subset is often characterize by poorer prognosis compared to a higher presence of M1 macrophages. The immunosuppression exerted by M2 macrophages is often related to secretion of the chemokine CCL22 which enhances the activity of T regulatory cells (Tregs) and according to what reported by Curiel et al., treatment with anti-CCL22 decreased Tregs migration in tumors [127]. Considering the importance of cytokines both released by macrophages and their function in determining the polarization of these components, the use of anti-CCL22 mAb is one of the adopted strategies to reduce the migration of Tregs in order to block the deleterious effect of M2 macrophages in ovarian cancer. There is another function currently used to limit the activity of M2 macrophages which works on their depletion of the tumor microenvironment by blocking Macrophage Colony Stimulating Factor receptor by using an antibody (anti-CSF-1R mAb). How shown by Ries et al. the administration of this antibody significantly reduced the presence of TAMs together with an increased ratio of cytotoxic CD8+T cells and CD4+ T cells while decreasing the number of FoxP3+ T regs [128] .

1.3.3 Immune checkpoints inhibitors

Other strategies which are currently used to reactivate T cells functions are the immune checkpoints inhibitors. During an immune response, immune checkpoint signaling prevents self-tissue damage or collateral damage by regulating and controlling the immune response, but this mechanism could be used by the same cancer cells and other deleterious stromal components to secrete immunosuppressive molecules in the TME to evade the immune response and stimulating tumor progression [121] . Examples of these new therapies are reactivating CD4+ and CD8+ effector T cells through blocking the cytotoxic T-lymphocite-associated protein 4 (CTLA). In various preclinical models, the administration of an anatagonistic anti-CTLA-4 antibody induced tumor rejection [129].

1.3.4 Anti-PD-L1

Another potential target which is acquiring relevant importance in the field is the development of strategies to target PD-1 to stop PD-L1 effects. Maine et al. reported how PD-L1 expression on monocytes in the ascites of patients is correlated with a poorer outcome [130] and for that reason, adding this targets together with common strategies might represent an additional weapon to fight ovarian cancer and to reactivate the immune system in the TME.

1.3.5 Cancer vaccines

Vaccine strategies open to the possibility for patients to have their immune system “trained” in an individual and specific way to target cancer cells and malignant elements in tumor microenvironment. One of the most used and theorized approaches based on vaccines are dendritic cell vaccines [121]. Dendritic cells have the capability to drive and to direct the immune response and this feature could represent a key role especially in extreme cold immune microenvironment like ovarian cancer. Another interesting feature of DC vaccines is that they can be conducted both in vivo and ex vivo. By “training” DCs cells with long amminoacids, as reported by Bijker et al. it has been possible to stimulate and reactivate CD8+ effector and CD4+ T cells, also inducing immune memory [131]. Together with that, another interesting option is the development of DNA and RNA vaccines. Both have shown good immunogenicity and good safety for patients [132, 133]. Both types of nucleic acids can be extracted with excellent purity and can be easily amplified through Polimerase Chain Reaction. Also, for that reason, they don’t even require much patients’ material. DNA vaccines are developed from bacterial plasmids modified to express specific genes. DNA vaccines can either be administered intramuscularly, intradermally or subcutaneously with good results inducing CD8+ T cells [134], humoral response [135] and memory response [136, 137]. Same administration methods for RNA vaccines which could also be electroporated into DCs [138]. Another type of vaccines are the viral vectors which have the advantage of being immunogenic and have the propension for the infection of mammalian cells. Their risk is the possibility of integrating into the host genome in coding genes altering their function, but on the other hand they can also be loaded with relatively big amount of DNA for some double DNA stranded viruses like the ones from poxviridae family with the ability of infecting a broad range of hosts [139].

1.4 Targeting stromal components

Stromal components (extracellular matrix, fibroblasts, vascular structure etc.) that develop around the tumor have a key role in creating a safe environment for cancer to stimulate their growth, proliferation and migration. The formation of a tumor niche due to the stromal components is also responsible for a slower drug penetration in the tumoural niche and for a reduced infiltration of immune cells in addition to all the anti-immune stimuli that accumulates in the niche. The evidence of the stromal component relevance is given first by the consideration of the metastatic spread into the peritoneum and as second factor, they play a key role in supporting tumor growth. Ascites, in this point of view, have also a relevant role considering their support to the metastatic spread and their pro-tumourigenic activity in ovarian cancer [140]. Among the stromal components, some which have a key role are fibroblasts. Fibroblasts in cancer are known to support different processes like angiogenesis, remodeling of the extracellular matrix and modulation of the immune response [31, 141, 142]. The roles of activated CAFs are multiple starting from the extracellular matrix formation which represents a natural barrier from immune cell penetration and drug penetration too. Another function is the production of a protein scaffold which supports cancer cell proliferation and vascularization associated with cancer. One of the molecules mentioned above is TGF-beta. TGF-beta has also a role in the immune escape mechanism played by cancer cells to evade immune response [37]. TGF-beta is often secreted by stromal components, CAFs and myofibroblasts. The role of this molecule is also to regulate innate and adaptive immunity. NK cells are afflicted by this mechanism, CD4+ and CD8+ T cells, macrophages and various cells that are part of the immune system [143]. CAFs can also recruit immune cells with anti-immune activity by their release of cytokines and regulation of signaling pathways [144]. In terms of immune inactivation and exclusion, as reported by Debois et al. there are three methods to exclude T cells from tumors. The first is through the loss of MHC-I presentation tumor cells, the second is through TGF-beta with its role in the ECM formation and fibroblasts activation and the third is the activation of various stromal components which actively act in the exclusion of T-cells from the tumor niche [145]. Considering this aspect, fibroblasts play a key role in forming a selective and protective tumour niche through extensive signalling with other stromal components. Their activation from a quiescent to an activated state alters their metabolism and reshapes the tumour microenvironment, affecting both extracellular vesicle (EV) cargo and cytokine secretion. Notably, recent studies have also suggested a potential beneficial role of cancer-associated fibroblasts (CAFs) in pancreatic ductal adenocarcinoma (PDAC). Odzemar et al. reported how fewer myofibroblasts are correlated with a reduced survival in PDAC patients [146]. Apart from sporadic examples, most of the time, even if CAFs are always correlated to negative roles in cancer. Another recent role discovered about CAFs is the enhancement of tumor progression providing energy through the tricarboxylic acid cycle (TCA) as reported by Curtis et al. [45] . Taking together all these aspects related to CAFs, the hypothesis emerges on how they can be considered potential target for innovative strategies. For example, there is a current strategy which is related to targeting TGF-beta 1 and TGF-beta 2 now under investigation in clinical trials [147]. Other possible approaches could also be the depletion of CAFs via specific surface markers, conversion of activated fibroblasts into quiescent state by inhibitors or targeting downstream effectors related to CAFs pathways [144]. CAFs can be considered a potential target for therapies as well as elements that should be explored more to have a better understanding of their multiple effects in cancer. Another example is MSCs which, according to what stated above, are a controversial element which has still to be elucidated. An interesting perspective is using some specific miRNA like miR-18a-rp extracted from EVs isolated from this cell type which shows to have inhibitory effects on ovarian cancer proliferation, migration and invasion [148]. It has been also reported how MSCs epigenetic reprogramming happening into the tumor microenvironment is responsible for acquired pro-tumourigenic functions and interaction with cancer cells to drive metastasis through specific key pathways like WT1 and EZH2 [149]. Impairing these specific pathways into MSCs could represent also a possible approach to destabilize stromal component and their role in supporting cancer. Adipocytes, as also stated above, might have a role in tumor progression and metabolism [21, 59] and for that reason, they also represent potential targets for therapies. Treatment with hypomethylating agents such guadecitabine showed a reduced migration and invasion of ovarian cancer cells toward adipocytes themselves [150].

1.4.1 The role of NO across the stroma and in the TME

Nitric oxide (NO) is a versatile signaling molecule that plays diverse physiological roles in the human body. It functions as a neurotransmitter, a regulator of vascular tone, and a mediator of intracellular signaling in conjunction with reactive oxygen species (ROS) [151]. Additionally, NO is produced by cells of the immune system as a key effector in inflammatory responses [151]. NO synthesis is catalyzed by a family of enzymes known as Nitric Oxide Synthases (NOS), which exist as three distinct isoforms: neuronal NOS (nNOS when referred to the enzyme or NOS1 when referred to the gene or mRNA), inducible NOS (iNOS when referred to the enzyme or NOS2 when referred to the gene or mRNA), and endothelial NOS (eNOS when referred to the enzyme or NOS3 when referred to the gene or mRNA). While all isoforms generate NO, their expression is context-dependent, varying by cell type and physiological or pathological conditions. Neuronal NOS predominantly produces NO within the nervous system, consistent with its established role in neurotransmission. Endothelial NOS is constitutively expressed in endothelial cells, where it synthesizes NO to mediate vasodilation and maintain vascular homeostasis. In contrast, inducible NOS is expressed primarily in immune cells, such as macrophages, upon stimulation by pro-inflammatory cytokines or bacterial endotoxins, resulting in sustained and high-output NO production. Inflammatory stimuli critically regulate iNOS expression and consequent NO production [152]. Under chronic inflammatory conditions, such as those associated with tumorigenesis, NO can be overexpressed and facilitate tumor growth [153]. The role of inducible nitric oxide synthase (iNOS) and its related NO accumulation in the OC-TME, remains incompletely characterized. Given the immunosuppressive nature of the TME and the disease's high metastatic potential, nitric oxide (NO) signaling may significantly contribute to these pathological processes. Mechanistically, NO modulates diverse cellular pathways, notably through post-translational modifications such as S-nitrosylation [154]. This covalent modification, involving the attachment of a NO moiety to cysteine thiol groups, can alter protein function by affecting conformation, enzymatic activity, stability (e.g., via ubiquitination), and transcriptional regulation. Consequently, S-nitrosylation represents a critical regulatory mechanism through which NO influences cellular signaling networks. In the context of the TME, dysregulated S-nitrosylation may facilitate tumor progression by promoting proliferation, survival, and metastatic dissemination [155]. For these reasons, iNOS likely plays a key role in cancer progression, and the inhibition of NO synthesis has been explored clinically in various cancer types. Several NOS inhibitors exist, among which N^G-

Monomethyl-L-arginine (L-NMMA) acts as a competitive enzymatic inhibitor that blocks NO production [156]. Although L-NMMA functions as a pan-NOS inhibitor, reducing NO levels in environments with NOS overexpression, particularly when combined with chemotherapy, immunotherapy, or both, has demonstrated therapeutic benefit. The Houston Methodist Research Institute conducted a Phase I/II clinical trials combining L-NMMA with a taxane in patients with triple-negative breast cancer (TNBC), a malignancy characterized by iNOS overexpression, enrolling a total of 35 patients. Previous in vivo models had demonstrated encouraging results in terms of tumor burden reduction; therefore, a similar therapeutic approach was applied to patients with chemorefractory, locally advanced breast cancer (LABC) or metastatic TNBC. Specifically, 35 patients with metastatic TNBC were enrolled: 15 in the Phase I trial and 24 in the Phase II trial (including 4 patients treated at the recommended Phase II dose from Phase I). The study reported positive outcomes for the combination of chemotherapy and L-NMMA. In particular, the overall response rate was 45.8% (11 of 24 patients): 81.8% (9 of 11) among patients with LABC and 15.4% (2 of 13) among those with metastatic TNBC. Additionally, among patients with LABC, three (27.3%) achieved a pathological complete response at surgery. Although grade ≥3 toxicity was observed in 21% of patients, no adverse events were attributed to L-NMMA, suggesting that this agent can be safely combined with other drugs without compromising efficacy or patient health status. More specifically, this study also investigated immune cell correlates of chemotherapy response, focusing not only on the direct effects of chemotherapy but also on the associated immune response. From an immunological perspective, CyTOF analysis revealed that chemotherapy nonresponders exhibited higher expression of markers associated with M2 macrophage polarization, along with increased circulating levels of IL-6 and IL-10. In contrast, responders showed an increase in $CD15^+$ neutrophils in peripheral blood and a decrease in arginase expression (a marker of protumor N2 neutrophils) in tumor biopsies collected at the end of treatment. Overall, the promising results of this combination suggest that similar therapeutic strategies could potentially be extended to other cancer types. [157]. Composed of a range of cells, from cancer cells, fibroblasts, immune cells, and cancer stem cells, the TME plays a key role in tumor progression and development. Cells are continuously engaged in crosstalk, forming pro-stimulatory niche environments, where immune system activity is reduced [158-160]. Also, tumor microenvironment factors known to stimulate the release of NO by NOS2 include hypoxia and proinflammatory cytokines such as Interferon-gamma

(IFN-γ), Tumor Necrosis Factor-alpha (TNF-α), and Interleukin-beta 1 (IL-β1) [161]. As mentioned before, within tumors, once released, NO can promote tumorigenesis due to its ability to nitrosylate multiple factors, thereby altering pathways related to cancer progression, development and Epithelial-to-Mesenchymal transition (EMT), such as the RAS pathway and NF-κB [162]. For this reason, therapies targeting NOS2 could have a significant impact on the entire tumor microenvironment ecosystem, given its important role in the tumor niche. The potential deleterious role of NO overexpression in ovarian cancer is represented in the following figure (Figure 1.6)

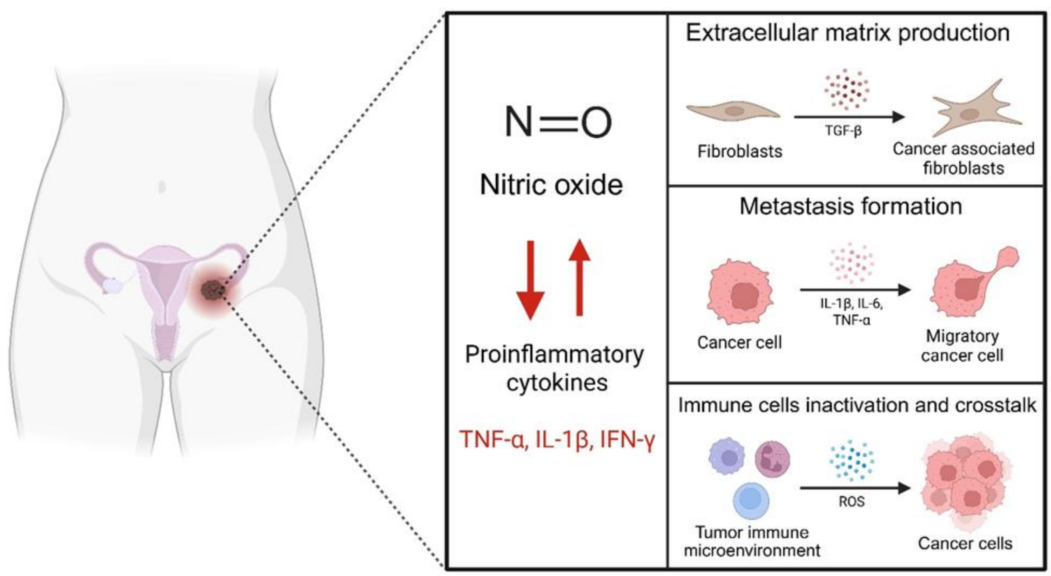

Figure 1.6. Potential role of nitric oxide (NO) overexpression in ovarian cancer. The release of pro-inflammatory cytokines promotes the production of NO, which in turn can further amplify cytokine release. Elevated NO levels, together with a pro-inflammatory microenvironment, may contribute to fibroblast activation into cancer-associated fibroblasts (CAFs), metastasis formation, and suppression of immune cell activity within the tumor niche. Created in https://BioRender.com.

1.4.2 Crosstalk Between iNOS and TIME Components in HGSOC

A key role of NO, as stated above, is to mediate not only proliferation and metastasis but also to act as a mediator between different cell populations in the tumor microenvironment (TME) [163]. It is important to mention that NO, being produced by different cellular types [164, 165], may exhibit distinct roles depending on the cell of origin and the specific location within the stroma where it is present. Generally, NO is a ubiquitous molecule capable of diffusing easily across the stroma. For this reason, its role as a mediator is considered highly significant. Cancer-associated fibroblasts (CAFs) can produce NO, a function linked to the stimulation of tumor growth and angiogenesis. Notably, CAFs are also known to secrete TGF-β, a molecule that not only promotes a pro-inflammatory environment but also induces nitric oxide production. Considering these aspects, the release of NO by CAFs likely plays an important role, especially given that CAFs contribute to the development and stimulation of chemoresistance [144]. CAFs stimulate chemoresistance and cancer progression not only through NO production but also by recruiting immunosuppressive cells that act as blockers of the immune response [166, 167]. Mesenchymal stem cells, as mentioned above, have a controversial role. They may either stimulate or inhibit cancer proliferation, thus exhibiting a dual function [56, 57]. It has also been demonstrated that these cells, under pro-inflammatory stimuli, can express iNOS [168]. The presence of pro-inflammatory stimuli is a well-established characteristic of various cancer types [169, 170], including ovarian cancer [171], and the induction of iNOS expression can exacerbate the detrimental effects associated with NO overexpression in cancer, such as enhanced angiogenesis, tumor growth promotion, and metastasis [172]. Interestingly, adipocytes are also associated with the release of pro-inflammatory stimuli. Several studies support their involvement in secreting cytokines that stimulate iNOS expression [173-175]. The role attributed to adipocytes extends beyond the release of pro-inflammatory cytokines, as they also provide lipids to cancer cells through direct mechanical contact [18]. Given their contribution to pro-inflammatory cytokine release [176], adipose tissue constitutes a major component that may negatively influence disease progression. Interactions between NO and other stromal components include processes involving TGF-β release and matrix metalloproteinases (MMPs). Some studies suggest that NO can induce the activity of metalloproteinases, particularly MMP2 and MMP10, which degrade collagen and protein components of the stroma, facilitating the release of TGF-β. This cytokine subsequently interacts with target cells [177], promoting CAF proliferation and enhancing the pro-inflammatory milieu, thereby increasing iNOS expression. As noted above, iNOS is also a mediator of immune responses; it is produced by macrophages, especially M2 macrophages with immunosuppressive activity [178], but also by myeloid-derived suppressor cells (MDSCs) [179], which possess immunosuppressive functions in the tumor niche. Furthermore, it has been observed that when expressed by regulatory dendritic cells, NO contributes to T cell inhibition.

1.4.3 Pan-tumor microenvironment agents

An interesting strategy for targeting the tumour microenvironment is to focus on the inflammatory stimuli and signalling pathways that regulate tumourigenesis and tumour progression An example could be targeting cytokines which are related to inflammatory status and often related to tumor progression. In particular, Infliximab, a monoclonal antibody against TNF-α has been tested in different studies [69, 180, 181]. Another option is Bevacizumab, a monoclonal antibody that targets VEGF-A [182, 183], a well know factor related to angiogenesis providing a vascularization system that provides supply to cancer cells. Another interesting approach, which has been extensively studied in the next chapters, is the role of NO in tumor development. iNOS is often related to the regulation of the immune response [184], and, in ovarian cancer an immunosuppressive response and at the same time to tumor progression [185, 186]. An interesting trial, proposed by Chung et al. for breast cancer is taking into clinics the use of a iNOS inhibiting drug, L-NMMA in triple negative breast cancer [157], very well-known cancer cell lines for the expression of iNOS [187]. This approach represents a promising and innovative strategy for targeting ovarian cancer, particularly given that iNOS is produced not only by epithelial cancer cells but also by immune cells and stromal components. As a key mediator within the tumor microenvironment, iNOS plays a critical role in intercellular communication that promotes tumor progression. Consequently, targeting iNOS offers the potential to simultaneously disrupt the immunosuppressive microenvironment, modulate stromal interactions, and directly affect cancer cells. This multi-faceted intervention could enhance the efficacy of chemotherapy by addressing several tumor-promoting factors concurrently, opening new avenues for combination therapies in ovarian cancer treatment. Under chronic inflammatory conditions, such as those associated with tumorigenesis, NO can exhibit dual and context-dependent roles [188]. In the tumor microenvironment

(TME), chronic inflammation often leads to recruitment of immunosuppressive cell populations rather than effector immune cells, thereby facilitating immune evasion. This phenomenon is exemplified in ovarian cancer, characterized by an immunologically “cold” microenvironment, where infiltration of immunosuppressive cells expressing iNOS contributes to immune suppression and tumor progression. The presence of immunosuppressive cells expressing iNOS may promote immune tolerance by dampening anti-tumor immune responses [189]. Furthermore, the TME is typically characterized by factors that inhibit effective immune cell infiltration and activate oncogenic signaling pathways that support tumor cell survival and proliferation. Within this milieu, NO may shift from a cytotoxic or regulatory molecule to one that supports tumor growth and metastasis [188]. Notably, several cancer cell lines, including those derived from breast carcinoma, have been shown to express iNOS, further amplifying NO production in the TME. This autocrine and paracrine production of NO may establish a positive feedback loop that promotes tumor survival, suppresses immune responses, and contributes to an aberrantly high NO concentration within the TME.

1.5 Targeting iNOS

The importance of targeting the tumor microenvironment has been discussed in the sections above. The presence of a molecule within the tumor microenvironment whose production is in most cases, significantly upregulated [169, 187], warrants particular attention, especially due to its broad ability to communicate among various cell populations within the tumor niche. This has prompted investigation into several preclinical models. A study was conducted using Melanoma Xenograft models, where N6-(1-iminoethyl)-L-lysine (L-NIL), a selective inhibitor of iNOS, demonstrated a clear inhibitory effect on tumor growth and reduced microvessel density. Moreover, when combined with chemotherapy, L-NIL enhanced the efficacy of the chemotherapeutic agent [190]. A third study, focused on Triple Negative Breast Cancer (TNBC) models, employed NG-Monomethyl-L-arginine (L-NMMA) and showed decreased cell proliferation, reduced migration, and suppression of EMT [157]. The relevance of these findings lies in the potential for combination therapies, not only using chemotherapy, but also incorporating agents that disrupt ovarian cancer crosstalk and pro-tumourigenic signaling pathways. Notably, nitric oxide (NO), through S-nitrosylation [155], can promote [EMT] via interactions with proteins such as HIF-1α [191-193] and MMPs [194]. Therefore, targeting these pathways, especially those linked to EMT, may not only limit tumor progression but also enhance the efficacy of chemotherapeutic agents. Such a strategy aims to impair cancer cell survival while concurrently modifying the tumor microenvironment to be less permissive for tumor growth and to block the activation of signaling pathways that sustain malignancy.

1.6 L-NMMA as a broad NOS inhibitor and potential implication of HGSOC

L-NMMA is structurally similar to L-arginine, the natural substrate for NOS. It binds to the active site of NOS enzymes, competing with L-arginine. By blocking L-arginine binding, L-NMMA prevents the enzymatic conversion of L-arginine to nitric oxide and L-citrulline. Considering the overexpression of iNOS in cancer and inflammation [195], L-NMMA may play a beneficial role by reducing NO release, thereby limiting EMT, acquired chemoresistance, and angiogenesis [196]. Although L-NMMA is a pan-inhibitor of NOS and not selective for iNOS, this characteristic may still yield therapeutic advantages. Among the three known isoforms of NOS, nNOS, eNOS, and iNOS, L-NMMA may exert cross-inhibitory effects. It is important to note that nNOS is predominantly expressed in the nervous system, where it performs specialized neuronal functions. However, regarding eNOS, L-NMMA may induce additional effects. This is particularly relevant given the role of angiogenesis and vascular remodeling in supporting tumor progression [197]. Thus, although inhibition of eNOS may be viewed as a potential side effect, it could also contribute positively by impairing the vascular support system of tumors. Importantly, iNOS is the principal isoform expressed within the tumor niche, being produced by cancer cells [169, 171], immune cells [198], and stromal cells [199]. This leads to a sustained presence and overexpression of iNOS, which is associated with the deleterious effects described above. Therefore, L-NMMA-based therapeutic strategies not only directly target iNOS but may also secondarily inhibit the transient expression of NO mediated by eNOS within the tumor microenvironment. A significant study evaluating the use of L-NMMA in combination with chemotherapy demonstrated positive outcomes, particularly in reducing EMT markers and inhibiting tumor growth [157]. This study was conducted in triple negative breast cancer, a subtype of cancer characterized by high iNOS expression. Based on these findings, other tumor types exhibiting elevated iNOS expression may also benefit from similar therapeutic approaches. In the context of the immunosuppressive, or "cold," tumor microenvironment characteristic of ovarian cancer, where immunosuppressive cells such as M2 macrophages and MDSCs, both associated with NO production, are present, additional contributors like CAFs, also linked to NO expression [167], may present new therapeutic opportunities. However, limited information is available regarding iNOS expression specifically in ovarian cancer. Further studies confirming iNOS expression in ovarian cancer cells could provide the rationale for initiating clinical investigations of L-NMMA in this malignancy.

1.7 Perspectives on future targeted therapies

Ovarian cancer is a highly heterogeneous tumor not only for the differences of its specific subtypes, but also for the differences between cell types into the tumor niche. These different cells collaborate and cross-interact to build a solid and safe niche to allow cancer proliferation. This crosstalk is the main characteristic that makes the ovarian cancer TME an extreme cold environment, makes a safe environment where drugs and immune cells struggle to penetrate and exploit their function. Considering this aspect, in the future single patient's approaches could be able to characterize each type of tumor with its specific niche and ratio between cells components, which may vary from patient to patient. With that perspective, genomics, single cell RNA sequencing and all the omics fields in science can guarantee a more tailored single patient treatment which can help to make treatment more efficient according to the patients' needs. Another relevant approach is the characterization of different cell types within the tumour microenvironment. This includes analysing their transcriptomic and genomic profiles to obtain a snapshot of their activity, as well as their RNA and protein expression patterns. Such analyses can provide a broader understanding of cancer biology. Rather than focusing on a single target, effective strategies may require destabilizing the tumour microenvironment and disrupting the cross-talk between its cellular components For that reason, the development of drugs more efficient in targeting cancer cells are essential, but also the combination of these drugs together with tumor microenvironment destabilizing agents will make a big change into the fight against cancer.

1.8 Thesis context

The crosstalk between cancer cells, stromal components and immunosuppressive immune cells lead to a high heterogeneous and complex tumor microenvironment where it is difficult to penetrate because of the extracellular matrix produced by stromal components and also, cytokines, EVs and molecules released in the tumor microenvironment create a niche favorable for cancer cells proliferation and growth. For those reasons, immune escape is favored in these conditions, allowing cancer cells to spread and proliferate regardless of the recruitment of the immune system. Taking together all these aspects, the importance of reactivating the immune population into the niche either targeting the immunosuppressive components and destabilizing the microenvironment components, is an approach which must be taken into consideration for future medicine. Combination therapies can represent a valid approach to allow multitargeting into the tumor niche. New approaches and strategies are in continuous expansion and further studies are required to develop a therapy which can effectively target multiple elements by contrasting cancer cell proliferation, metastatization, cross-talk between cells in the stroma and immune suppression trying to face the difficult change represented by ovarian cancer and its consequences on patients' life. This thesis focuses on exploring new possibilities for combining chemotherapy with L-NMMA, a drug that has the potential to interfere with and disrupt the cross-communication between cancer cells.

1.9 Thesis Hypothesis

The hypothesis for the project states that "The disruption of the crosstalk between cancer cells within their environment can suppress cancer cell proliferation, metastatic progression and reactivate the immune tumor microenvironment (TIME), to drive anti-cancer responses in ovarian cancer".

The major aim of this project is to define the role of iNOS in ovarian cancer, its implications in cancer progression, and its involvement in cancer proliferation within the tumor microenvironment (TME). To fulfil these aims, a series of objectives were identified:

1. Conduct a bioinformatic investigation to establish the expression of iNOS and downstream nitorsylated genes in HGSOC

2. Develop *in vitro* investigation of iNOS, considering the potential of different cell lines to express iNOS and its promotion of metastatic events

3. Optimize the *in vitro* use of iNOS inhibitor L-NMMA to target the Epithelial-to-Mesenchymal Transition and increase the efficacy of Cisplatin.

4. Develop a syngeneic *in vivo* model using ID8 murine epithelial ovarian cancer cells into C57BL/6 mice, to characterize the efficacy in reduction of tumor proliferation and immune system reactivation using a combination of Cisplatin and L-NMMA.

5. Develop an iNOS knockout ovarian cancer cell line to better investigate the role of iNOS in ovarian cancer.

6. Develop a xenograft *in vivo* model using NOD Scid Gamma (NSG) mice to compare metastasis formation and survival rates between knockout clones and parental cell lines

7. Treat the xenograft *in vivo* model with Cisplatin comparing the survival between knockout clones and parental cell lines.

These objectives map clearly to the thesis structure shown in **Figure 1.7**.

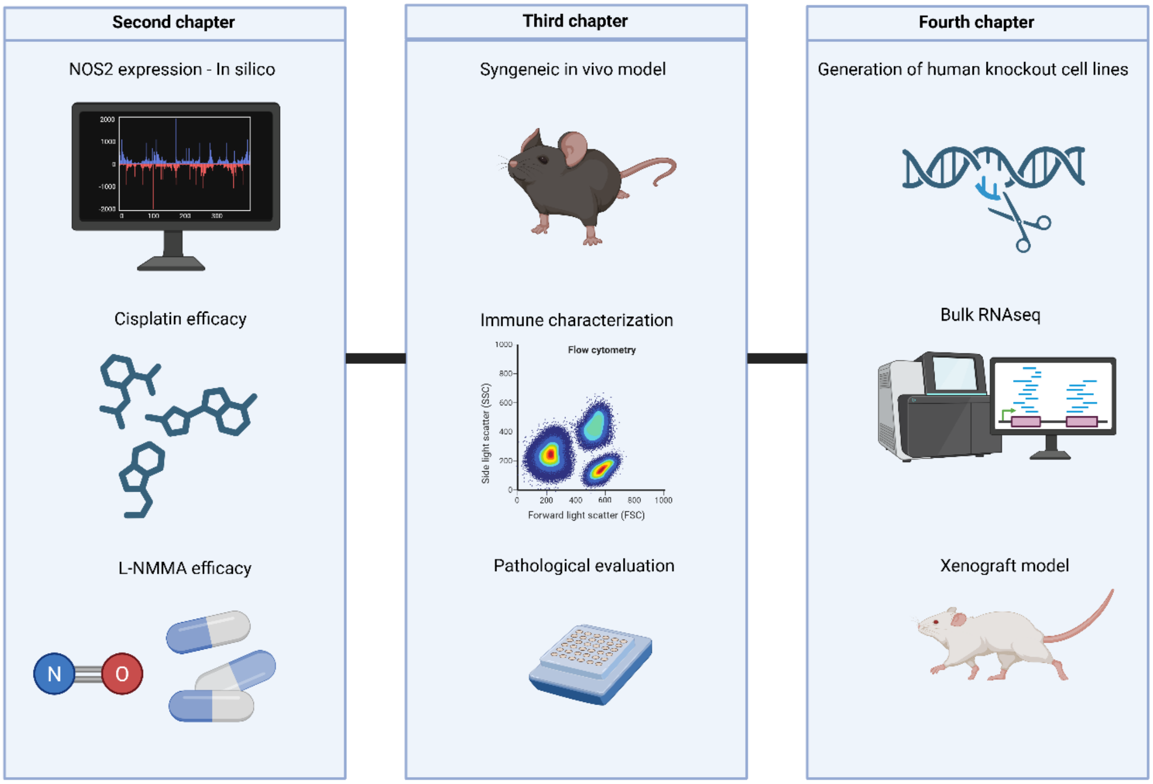

Figure 1.7. First chapter results are schematized per chapter. The second chapter has been based on iNOS detection in ovarian cancer cells (left). The third chapter continued with the development of a syngeneic in vivo model, ascites immune profiling and peritoneal metastasis analysis (center). The fourth chapter is based on the development of a human knockout cell line analyzed through RNAseq to identify the main dysregulated pathways related to NO and the development of a second in vivo model. Created in https://BioRender.com.

Chapter 2 – Ovarian cancer cell lines show basal expression of iNOS and increased sensitivity to Cisplatin in combination with L-NMMA

2.1 Introduction

The role of inducible nitric oxide synthase (iNOS) has still to be elucidated. As already mentioned, NO modulates diverse cellular pathways, notably through post-translational modifications such as S-nitrosylation [154]. This modification can afflict stability, can alter protein degradation cycles, but also their transcriptional regulation. S-nitrosylation represents a critical regulatory mechanism through which NO influences cellular signaling networks. Dysregulated S-nitrosylation promotes, as stated above, proliferation, survival, and metastatic dissemination [155]. For these reasons, iNOS represent a potential candidate as drug with the capability of targeting the communication across cells in the TME. **Figure 2.1** illustrates the consequences of an excessive accumulation of NO in the TME.

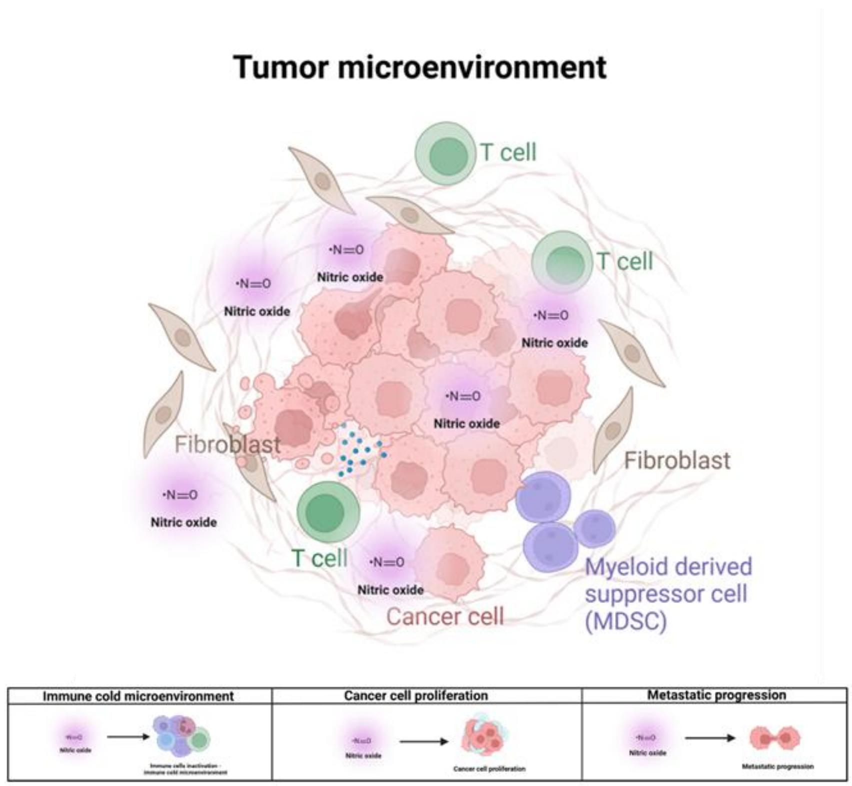

Figure 2.1. Role of NO in the tumour microenvironment. NO can influence the creation of a proinflammatory status and its overexpression leads to the S-nitrosylation of proteins which in turn lead to the dysregulation of many pathways in cancer [155]. Created in https://BioRender.com.

Given the clinical challenges associated with ovarian cancer, the combination of NOS inhibition with existing therapeutic approaches represents a promising strategy to overcome these limitations. In this context, the present study aimed to assess iNOS expression in OvCA, an area that remains relatively underexplored, and to investigate the potential therapeutic application of L-NMMA in targeting iNOS-associated deleterious functions in this malignancy. The development of suitable in vitro models is essential due to the marked heterogeneity of ovarian cancer. In particular, epithelial ovarian cancer comprises five major subtypes: HGSOC, endometrioid ovarian cancer (EndOC), mucinous ovarian cancer, clear cell ovarian cancer, and low-grade serous ovarian cancer. The frequency of each subtype is as follows: HGSOC 60%, EndOC 10%, mucinous ovarian cancer 3%, clear cell ovarian cancer 10%, and low-grade serous ovarian cancer < 5% according to World Cancer Report - IARC. Although these subtypes share certain features, they are primarily distinguished by specific genetic alterations, particularly mutations in p53 [200].

In addition, resistance to standard chemotherapeutics is a common and significant challenge in ovarian cancer [201], further contributing to the genetic and phenotypic diversity observed in tumor cells [202]. Therefore, it is critical to consider the diversity of ovarian cancer subtypes when designing experimental studies, as each subtype may respond differently to therapeutic agents. Although starting with specific cell lines may appear to streamline research efforts, this approach may overlook important biological variability, such as differences in tumor origin and histology [202]. This is particularly relevant when studying iNOS and, consequently, nitric oxide (NO), as their expression varies significantly across different cancer types and even among subtypes within those cancers. The emergence of omics technologies has provided valuable tools for characterizing the molecular features of different cancer subtypes and, also, ovarian cancer subtypes. These technologies enable patient-specific screening approaches that were unimaginable two decades ago. Bioinformatic analysis is now regarded as a critical initial step in identifying relevant genetic, transcriptomic, or proteomic profiles in cancer cell lines. In this study, three independent ovarian cancer cell line databases were consulted to guide the selection of cell models. This strategy was employed to reduce the risk of false positives and to assess the differential expression profiles of NOS2 across diverse cell lines.

The application of these omics-based tools constituted the foundational step of this investigation.

The selection of representative ovarian cancer cell lines for this study was based on the analysis of multiple publicly available databases, enabling the identification of the most suitable candidates for investigating NOS2 expression. Although NOS2 expression was found to be heterogeneous across ovarian cancer subtypes, and notably absent in clear cell ovarian cancer cell lines, the primary criteria guiding cell line selection were, first, the presence of specific cell lines in all three databases consulted and, second, their relative NOS2 expression levels. Among the ovarian cancer subtypes, HGSOC cell lines exhibited the highest NOS2 expression. Special attention was given to the OVCAR8 cell line, a widely studied model classified as HGSOC. OVCAR8 demonstrated the highest NOS2 expression across databases, and its chemoresistant variant exhibited an even greater expression level.

Based on these observations, additional representative cell lines of high-grade serous ovarian cancer (HGSOC) and endometrioid ovarian cancer (EndOC), which also showed NOS2 expression, were included to validate NOS2 levels using an in-house ovarian cancer cell line panel developed in this study. This in-house panel was developed to confirm both mRNA and protein-level expression of NOS2, specifically focusing on its protein product, inducible nitric oxide synthase (iNOS). Notably, only the cell lines that expressed iNOS also expressed Vimentin, a well-established epithelial-to-mesenchymal transition (EMT) marker. Vimentin expression has been associated with aggressive features, including enhanced migratory capacity and metastatic potential [203]. Furthermore, Vimentin is linked to the development of acquired chemoresistance [204], which is a major clinical concern given the high prevalence of chemoresistance in ovarian cancer [205]

Following this screening, OVCAR8 was selected for further investigation, as it demonstrated basal expression of both iNOS and Vimentin, features not observed in the other HGSOC cell lines included in the panel. Also, OVCAR8 is a well-characterized model frequently used in studies investigating chemoresistance and its underlying molecular mechanisms [206]. Therefore, this cell line was deemed the most suitable model for conducting functional studies on NOS2 and its role in ovarian cancer progression and therapy resistance. After establishing an appropriate in vitro model, the next step was to determine the optimal treatment conditions and dosing parameters for targeting NOS2-expressing ovarian cancer cells. Several studies have evaluated the administration of Cisplatin to OVCAR8, including both dosage and treatment duration [207, 208]. Based on prior research, this study tested a concentration range of 4 μM to 24 μM over a 72-hour period. Following Cisplatin treatment, the half-maximal inhibitory concentration (IC50) was calculated to establish the effective dose for potential combination treatments. Determining the IC50 is essential not only for identifying optimal drug concentrations in combination therapies but also for downstream experiments requiring accurate viability assessment, such as the RealTime-Glo™ viability assay. While the Cisplatin dosing aligned with values reported in the literature, the optimal concentration of L-NMMA had to be determined empirically, as it is not commonly used in ovarian cancer treatment protocols. A wide concentration range, from 2 mM to 30 mM, was tested to evaluate the cytotoxic effects of L-NMMA. Although L-NMMA has been studied in other cancer types, such as metaplastic breast cancer [209], its efficacy and impact in ovarian cancer remain largely unexplored. As previously mentioned, iNOS expression was a critical inclusion criterion for this study; however, the expression of Vimentin was also considered essential. One of the objectives was to investigate the potential relationship between iNOS and Vimentin in ovarian cancer, a topic that remains poorly characterized in the current literature. Vimentin expression was assessed both directly through immunoblotting and indirectly via a scratch wound assay, which will be discussed in the following section. Given the lack of existing studies on the combined use of L-NMMA and Cisplatin in ovarian cancer, an extensive range of drug combinations was tested to evaluate potential synergistic effects. The rationale for this approach was to assess whether L-NMMA, a less conventional therapeutic agent in the context of ovarian cancer, could enhance chemosensitivity when used in combination with Cisplatin and simultaneously impair epithelial-to-mesenchymal transition (EMT), a process associated with treatment resistance and metastasis. To this end, the impact of L-NMMA on Vimentin expression was specifically evaluated. In this study, Vimentin has been identified as an EMT marker associated with iNOS expression.

2.1.1 Hypothesis and Aims of the chapter

Building on prior evidence from other cancers, particularly breast cancer studies conducted at Houston Methodist Research Institute, we aimed to investigate the potential role of NOS inhibitors, specifically L-NMMA, in OvCA cell lines expressing iNOS. The therapeutic rationale for reducing NO levels in the TME, where iNOS is often overexpressed, includes attenuation of tumour progression, decreased cancer cell viability, and reprogramming of the immune microenvironment from an immunosuppressive ("cold") to an immunoreactive ("hot") state. The objectives of this study were two: to establish evidence of iNOS expression in ovarian cancer through analysis of publicly available databases as well as by constructing an in-house iNOS expression panel and to determine the effects of L-NMMA in ovarian cancer iNOS expressing cell lines. Following the establishment of this panel, we evaluated the effects of iNOS downregulation, and consequent NO reduction, on cell viability and EMT in selected ovarian cancer cell lines.

2.2 Materials and methods

Tissue culture. HGSOC OVCAR8 was a gift from Nermin Kahraman. Other High Grade Serous Ovarian Cancer cell lines SKOV3, OVCAR3 were a gift from Dr. Francesca Taraballi. High Grade Serous Ovarian Cancer cell line CAOV3 was purchased from ATCC (Cat# HTB75). Endometrioid Ovarian Cancer (EOC) A2780 (Cat# 93112519) and Endometrioid Ovarian Cancer Cisplatin resistant A2780cis (Cat# 93112517) were purchased from ECACC. OVCAR8-RFP-Luc were generated after transfection using a lentiviral vector. Murine epithelial ovarian cancer cell line (MEOC) ID8 was purchased from Sigma-Aldrich (Cat# 9Q04TP) and ID8-Luc were purchased from Creative Biolabs (Cat#IOC-ZP310). OVCAR8 and OVCAR8-RFP-Luc were cultured in RPMI1640 with 10% FBS and 1% Penicillin/Streptomycin at 37C supplied with 5% CO2. SKOV3 was cultured in McCoy's 5a medium with 10% FBS and 1% penicillin/streptomycin at 37% and 5% CO2. OVCAR3 were cultured in RPMI1640 with 20% FBS, 1% penicillin/streptomycin and 1 mg/mL of bovine insulin at 37C with 5% CO2. A2780 was cultured using RPMI1640 supplied with 10%FBS, 1% penicillin/streptomycin and 2 mM glutamine at 37C and 5% CO2. A2780cis were cultured at the same condition as A2780 with the addition of 1 μM of Cisplatin.

Cytokine mix and LPS administration. Cells were cultured under regular cell culture conditions. In order to stimulate iNOS expression, LPS (100ng/mL, Millipore Sigma # L2018- 5MG) or a cytokine mix composed by IFN-γ (25 ng/mL, Peprotech # 300-02-100UG), TNF-α (10ng/mL, Peprotech # 300-01A-50UG), IL1-β (10 ng/mL, Peprotech # 200-01B-10UG) were administered. Cytokines were administered only once and cells were maintained in culture after the cytokine or LPS administration for 72 hours. Experiments were conducted in triplicates and considered statistically significant when $p < 0.05$.

Bioinformatic analysis. Bioinformatic analyses were performed to evaluate NOS2 expression levels across various cell lines and tumour tissues using three different platforms. Specifically, RNA expression levels in different ovarian cancer cell lines were assessed via the Human Protein Atlas database, Cancer Cell Line Encyclopedia (CCLE) and NCI-60. Analyses of the CCLE and NCI-60 datasets were conducted with the assistance of Dr. Hong Zhao, who contributed to the filtering and classification of the multiple cell lines and groups represented in these databases. Additionally, expression levels in normal tissues, primary tumours, and metastases were analysed using the TNMplot database.

.

Immunoblotting. Whole-cell lysate was extracted using Cell Signaling lysis buffer (20 mM Tris-HCl (pH 7.5), 150 mM NaCl, 1 mM Na2EDTA, 1 mM EGTA, 1% Triton, 2.5 mM sodium pyrophosphate, 1 mM beta-glycerophosphate, 1 mM Na3VO4, 1 µg/ml leupeptin, Cat #9803). Proteins were separated by SDS-PAGE gel and transferred to a PVDF membrane (Millipore Sigma, Cat #NX0095). The membranes were blocked with 5% non-fat milk and incubated with primary antibody overnight at 4◦C with gentle agitation using the following antibody: rabbit anti-iNOS (1:1000, Cell Signaling, Cat #95423), rabbit anti-Vimentin (1:1000, Cell Signaling, Cat #5741), rabbit anti-β-Actin HRP conjugate (1:7000, Cell Signaling, Cat#5125). Signals from iNOS and Vimentin were detected and amplified by using a secondary anti-rabbit HRP-conjugated antibody (1:3000, Cell Signaling, Cat #7074). Signals were detected using Clarity ECL Western Blotting Substrates from Bio-Rad (Cat #1705060S)**.** Experiments were performed in triplicate (or in duplicate, where specified in the Results section) and considered statistically significant when $p < 0.05$.

RealTime-Glo™ MT Cell Viability Assay. 1.500 cells were seeded in white opaque 96-well plate (Greiner Bio-One, Cat# 655074). After 24 hours, gradients of Cisplatin (MCE®, Cat #HY-17394) concentration (from 4µM to 24 µM) and L-NMMA (from 2 mM to 30 mM) were added to the desired well together with MT Cell Viability Substrate and NanoLuc® luciferase (Promega, Catalog #G9711). Cells were maintained under regular culture conditions and luminescence was measured 72 hours after Cisplatin administration using a luminometer (GloMax navigator, Promega, Cat# E5302). Experiments were performed in triplicate (or in duplicate, where specified in the Results section) and considered statistically significant when $p < 0.05$.

siRNA transfection. siRNA transfection was performed using Dharmacon validated siRNA and transfection reagent, both purchased from Dharmacon®. The siRNA was prepared at a final concentration of 50 nM by diluting in 195 μL of serum-free medium. Separately, 5 μL of transfection reagent was also diluted in 195 μL of serum-free medium. Both solutions were incubated at room temperature for 5 minutes. Following this initial incubation, the siRNA and transfection reagent solutions were combined and gently mixed. The resulting complex was incubated for an additional 20 minutes at room temperature to allow for complex formation. The transfection mixture was then added dropwise to each well, followed by the addition of 1.6 mL of serum-free medium. After six hours, the transfection solution was removed and replaced with standard complete growth medium. Protein samples were collected after 48 hours of downstream analysis. The related immunoblot NOS2 siRNA knockdown was conducted once as proof of concept using validated Dharmacon anti-NOS2 siRNA.

Reverse Transcription, Quantitative Real-Time PCR (RT-qPCR). Total RNA was extracted using RNeasy mini kit from Qiagen (Cat# 74104) according to the manufacturer's protocol. RNA was reverse transcribed with the High-Capacity cDNA Reverse Transcription kit (ThermoFisher, Cat # 4368813). RT-qPCR was performed using the QuantStudio 12K Flex Real-Time PCR System (ThermoFisher, Cat# 4471134). Following primers for TaqMan™ Gene Expression Assay were purchased from ThermoFisher; human NOS2 (Cat #4453320) and human ACTB (Cat # 4333762F). Experiments were performed in triplicate and considered statistically significant when $p < 0.05$.

Statistical analysis.

Two-way analysis of variance (ANOVA) or ordinary one-way ANOVA, when possible, was performed using GraphPad Prism version 7.0 (GraphPad Software, San Diego, CA) to evaluate the effects of two independent factors and their interaction on the dependent variable. Prior to analysis, data were checked for normality and homogeneity of variances. When significant effects were detected, multiple comparisons were conducted using Tukey's test to identify specific group differences. Results were considered statistically significant at $p < 0.05$.

2.3 Results

2.3.1 NOS2 is expressed in ovarian cancer

To first detect the expression of NOS2 both at protein and RNA levels we used The Human Protein Atlas database, an important resource for clinical research. This database represents an integrated omics approach combining protein expression in immunohistochemistry and high-throughput RNA sequencing (RNAseq) data [210]. Transcriptomic was expressed in number of transcripts per million (nTPM). RNA-seq profiles were generated by integrating the HPA (n=69) and the Cancer Cell Line Encyclopedia (CCLE 2019, n=1019). Proteomic data were obtained through mass-spectrometry (MS). The circles represent where mass spectrometry data were available, where no circles means that MS data were not available and white circles that the protein was not detected through MS. NOS2 and iNOS expression profile across these ovarian cancer cell lines is presented in **Figure 2.2**.

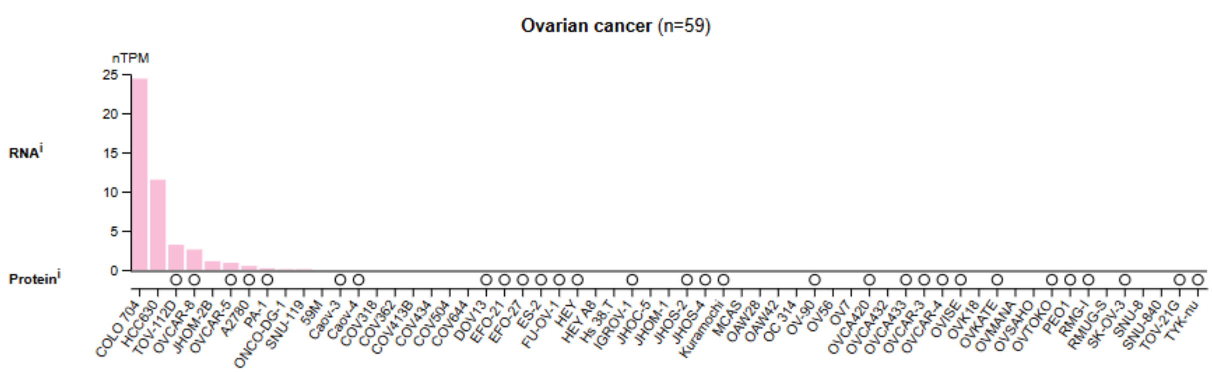

Figure 2.2. The Human Protein Atlas NOS2 expression reports. RNA expression levels of NOS2 in ovarian cancer represented in pink bars and expressed in number of transcripts per million (nTPM).

Some cell lines showed NOS2 expression at RNA levels. Among HGSOC cell lines, OVCAR8 demonstrated the highest NOS2 RNA expression (nTPM 2.6). A2780, a well-studied endometrioid ovarian cancer cell line [211], demonstrated the seventh highest NOS2 RNA expression level (nTPM 0.5). It is important to mention that although two other cell lines, COLO704 and HCC630, showed elevated NOS2 expression, HCC630 was identified as harboring a Y chromosome, indicating a non-female origin as reported in CCLE, while COLO704, despite its high NOS2 expression, has been documented by Moore G.E. as originating from a pleural effusion of a 50-year-old female patient. After analyzing the data available in The Human Protein Atlas, we analyzed the CCLE database. CCLE is a database with an extensive number of cancer cells (n=1019, as mentioned above) and the top ovarian cancer expressing cell lines are shown in the figure below (**Figure 2.3**). In this database, OVCAR8 is still confirmed as the highest High Grade Serous Ovarian Cancer NOS2 expressing cell line (over 1.5 log2 TPM+1) and how A2780 still confirms good NOS2 expression levels.

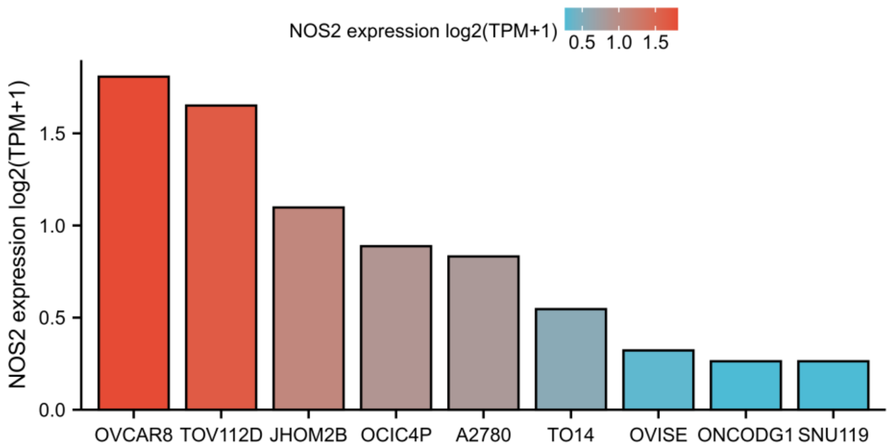

Figure 2.3. CCLE top ovarian cancer cell lines expressing NOS2. The values are represented in a logarithmic scale of Transcript per Million and show how different cell lines express NOS2. OVCAR8 is confirmed to be top HGSOC cell line expressing NOS2.

To complete the analysis, we also screened a third database called CellMiner NCI-60. We selected an ovarian cancer cell line panel among the different cells lines and types available in the dataset and we still found encouraging data supporting how NOS2 expression can be strongly correlated to High Grade Serous Ovarian Cancer. Y-axis represents NOS2 gene expression measured as log2(FPKM+1). FPKM stands for "Fragments Per Kilobase of transcript per Million mapped reads," a common unit for quantifying gene expression from RNA sequencing data. OVCAR8 is still, also in this database, among the top NOS2 expressing ovarian cancer cell lines and. Interestingly, NCI/ADR-RES which in this database shows the highest expression, is a derivative cell line of OVCAR8 obtained after their exposure to Adriamycin (Doxorubicin) to obtain a multidrug-resistant phenotype. The NOS2 expression levels reported in CellMiner NCI-60 are shown in **Figure 2.4.**

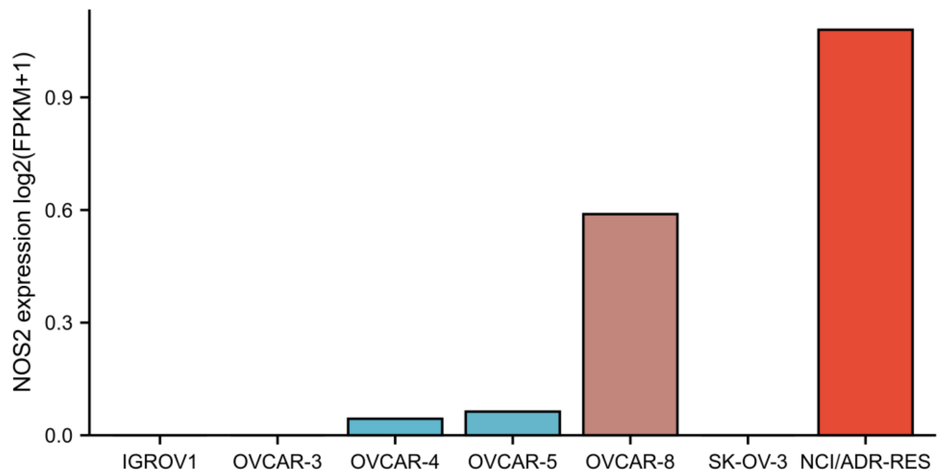

Figure 2.4. NCI-60 top ovarian cancer cell lines expressing NOS2. NOS2 expression is reported as log2(FPKM+1). It is possible to observe as OVCAR8 and NCI/ADR-RES (a derivate of OVCAR8) show the highest expression of iNOS also in this database.

As previously mentioned, CellMiner NCI-60 reports OVCAR8 and its chemoresistant counterpart as the top NOS2-expressing cell lines, suggesting that chemoresistant lines may exhibit a basal expression of this gene. Interestingly, the only other cell line in this database showing higher NOS2 expression than OVCAR8 is also chemoresistant. The connection between chemoresistance and elevated NOS2 expression will be explored in the subsequent sections of this work.

2.3.2 Expression levels in different tissues

After assessing NOS2 expression in various ovarian cancer cell lines, we extended our analysis to compare NOS2 expression levels across non-cancerous or normal, tumour, and metastatic ovarian tissues in a specific database called TNMPlot. This database allows to make cross-analysis not only between healthy ovarian samples and primary tumour sites, but also between metastatic samples with healthy ovarian samples and between metastatic samples and primary tumour sites. TNMplot, an online database compiling Gene chip data from patient samples, showed (**Figure 2.5)**, that NOS2 expression was increased in tumour tissues (N = 744) compared to normal tissues (N = 46). Interestingly, NOS2 expression was reduced in metastatic tissues (N = 44) relative to both normal and tumour tissues. Although the difference in NOS2 expression between normal and tumour tissues was not statistically significant, contrasts between normal versus metastatic and tumour versus metastatic tissues were significant. It is still possible to observe how tumour tissues exhibited a higher median and greater variability in NOS2 expression compared to normal ovarian tissues.

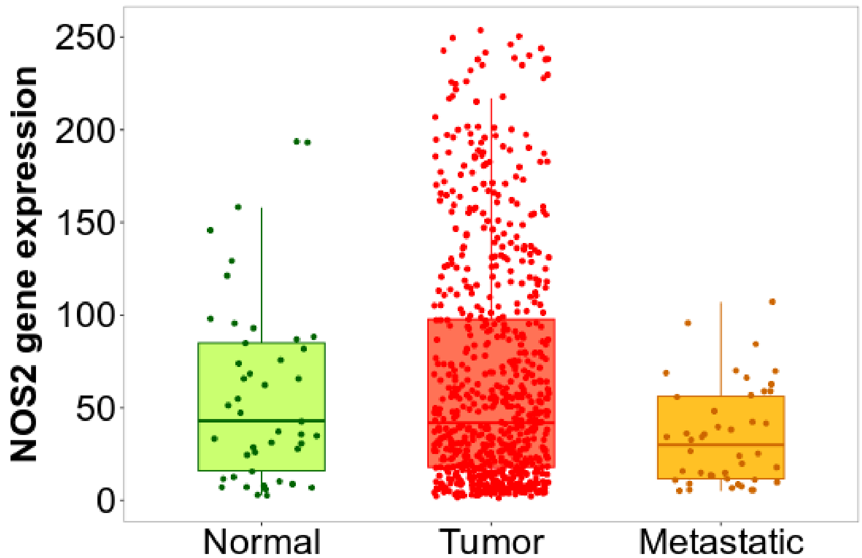

Figure 2.5. NOS2 expression in healthy, primary site tumour and metastatic ovarian samples. The bars obtained from Gene chip analysis in TNMPlot show differences in NOS2 expression among healthy ovaries (normal), ovarian cancer tumour spots (tumour) and metastasis (metastatic). The table shows how different and spread is the expression of NOS2 in tumors compared to the other two groups. The Kruskal-Wallis test (a non-parametric one-way ANOVA) for this comparison yielded a p-value indicating significant differences among groups.

2.4 Ovarian cancer cell lines expression of NOS2 – in-house panel

Following the bioinformatic screening of NOS2 expression, a panel of Ovarian Cancer cell lines were analysed for expression at the protein level using western blotting. OVCAR-3 and CAOV3, A2780 both wild-type and Cisplatin Resistant, as well as OVCAR8, which is the High-Grade-Serous cell line that showed the highest levels of NOS2 according to the databases previously mentioned, were assessed. NOS2 expression levels were detected through qPCR using our in-house ovarian cancer panel (**Figure 2.6**).

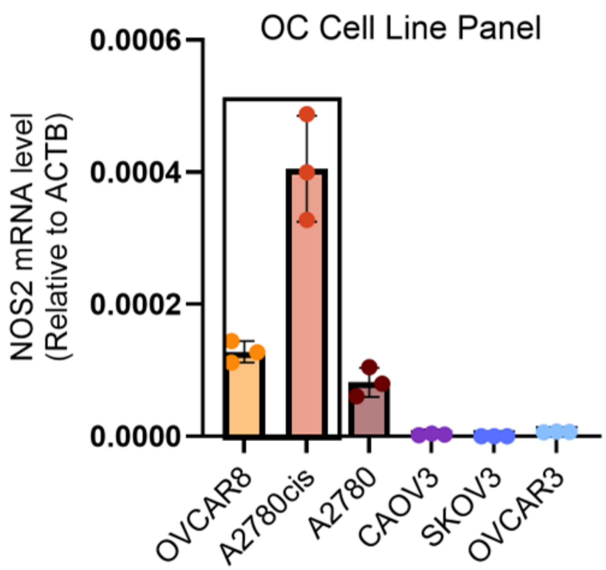

Figure 2.6. qPCR on NOS2 panel. The figure shows the mRNA expression levels in the in-house ovarian cancer panel built to detect the expression of NOS2 in accordance with what was found in different databases. OVCAR8 confirms its high expression of NOS2 and A2780cis shows the highest expression among the cell lines tested. This analysis has been conducted in three independent replicates and expresses the NOS2 mRNA levels related to ACTB.

The graph above presents interesting results, showing NOS2 mRNA levels relative to β-Actin (ACTB when referred to the mRNA) without any group comparisons, simply reflecting pure NOS2 expression. These data align perfectly with the previous bioinformatic findings. According to various databases, particularly CellMiner NCI-60 regarding chemoresistant cell lines, A2780cis appears to be the highest NOS2-expressing cell line with a normalized ratio of 0.0004, followed by OVCAR8, which is confirmed as the highest NOS2-expressing ovarian cancer cell line in HGSOC with a ratio of 0.00017, followed by A2780 wild type with a level of 0.00014.

We also confirmed the expression of iNOS through western blotting procedures. **Figure 2.7** shows the blots and densitometry analysis of all 5 cell lines, confirming expression of iNOS in OVCAR8, A2780 and A2780cis, and no expression in the OVCAR-3 and CAOV3 cell lines, in agreement with The Human Protein Atlas data. These data are in line not only with the previous bioinformatic findings (even if expressed in terms of mRNA expression only), but also with the in-house qPCR panel shown before. Regarding the chemoresistant cell line taken in exam before, A2780cis appears to be the highest iNOS expressing cell line with a normalized expression of iNOS corresponding to 0.4, followed by OVCAR8 with a level of 0.17, which is confirmed again as the highest iNOS-expressing ovarian cancer cell line in HGSOC.

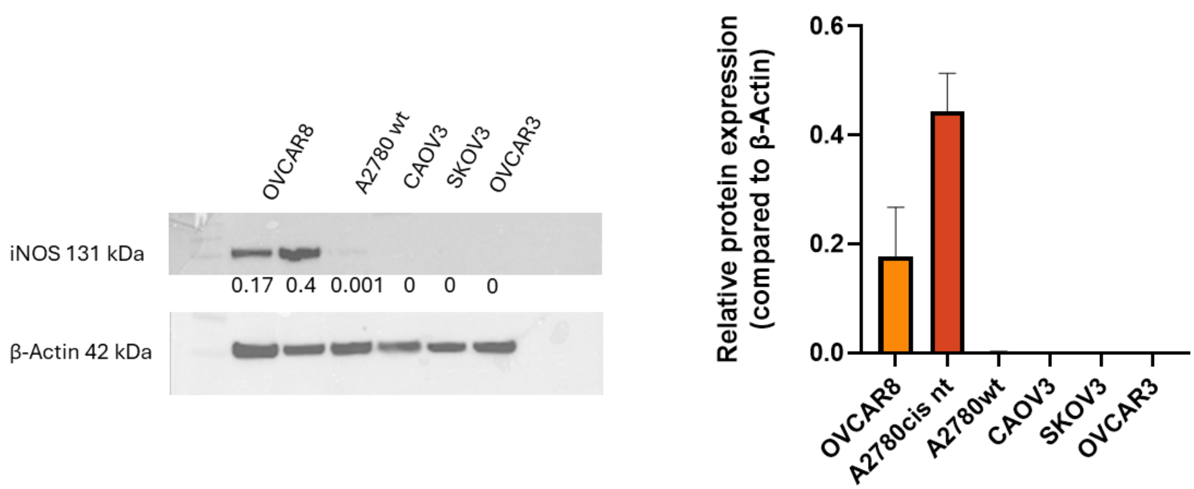

Figure 2.7. Western blot and densitometry analysis showing the in-house iNOS expression panel among different ovarian cancer cell lines. It is possible to observe that only OVCAR8 (HGSOC) and As2780cis show the expression of iNOS at basal level, differently from the other ovarian cancer cell lines. Protein data confirmed what already observed in mRNA data where OVCAR8 and A2780 show a basal and high expression of NOS2. This analysis has been conducted in three independent replicates and expresses the iNOS protein levels related to ACTB.

2.4.1 Cytokine cocktail and iNOS expression in HGSOC cell lines

Cytokine cocktails are a useful tool used in different works [212, 213] to induce iNOS expression, as they simulate an inflammatory environment, an essential component to induce the expression of iNOS

[214]. For that reason, we evaluated iNOS expression in the cell lines which didn't show a basal expression of iNOS by treating them with a cytokine cocktail or LPS [215]. The cytokine cocktail contained IFN-γ (25 ng/mL), TNF-α (10 ng/mL), and IL-1β (10 ng/mL), while LPS was applied at 1 μg/mL. The results , for all cell lines, are shown in **Figure 2.8**.

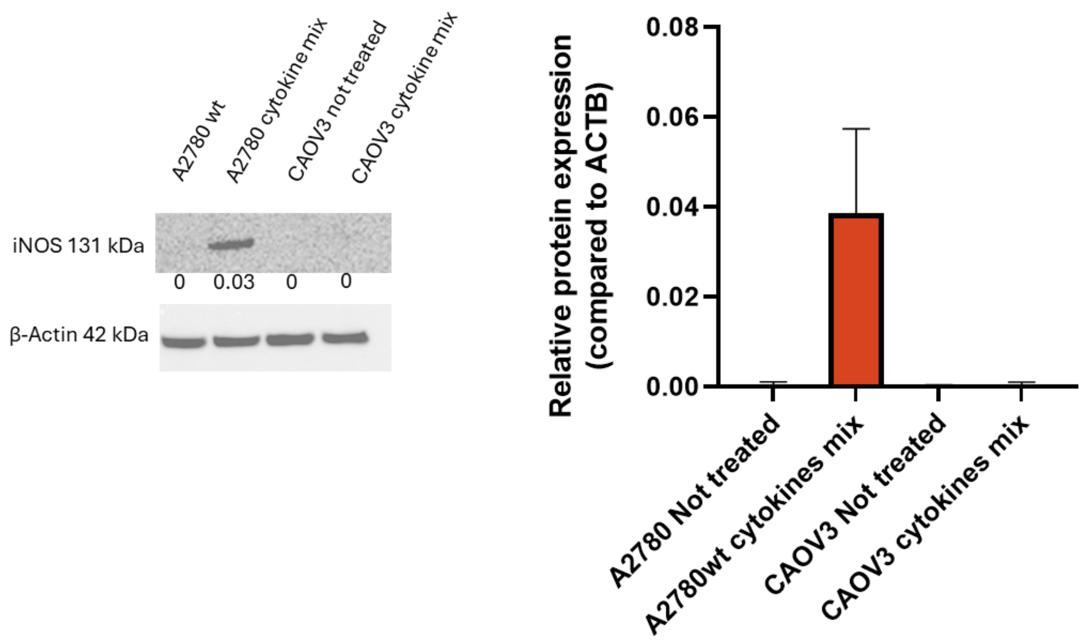

Figure 2.8. Expression of iNOS after the induction of A2780 and CAOV3 with cytokines mix. It is possible to observe how the expression of iNOS2 in A2780 wild type is inducible and strongly related to the use of cytokine mixes, differently from CAOV3. This analysis has been conducted in three independent replicates and expresses the iNOS protein levels related to β-Actin.

For the A2780 wild-type cell line, western blot analysis aligned with data from The Human Protein Atlas as well as our in-house RNA panel, demonstrating NOS2 expression following treatment with a cytokine cocktail. Specifically, A2780 cells treated with the cytokine mix showed a normalized iNOS expression level of approximately 0.03, whereas untreated A2780 cells exhibited no detectable iNOS expression. Similarly, CAOV3 cells showed no iNOS expression regardless of cytokine treatment. These findings align with the Human Protein Atlas data and with the other databases previously mentioned (CCLE and NCI-60).

To assess the effects of cytokine mix on the cell lines shown to have continuous expression of iNOS, western blotting was utilised. **Figure 2.9** shows the results after treating OVCAR8 with Lipopolysaccharide (LPS) (1 μg/mL) or cytokine cocktail (IFN-γ (25 ng/mL), TNF-α (10 ng/mL), and IL-1β (10 ng/mL).

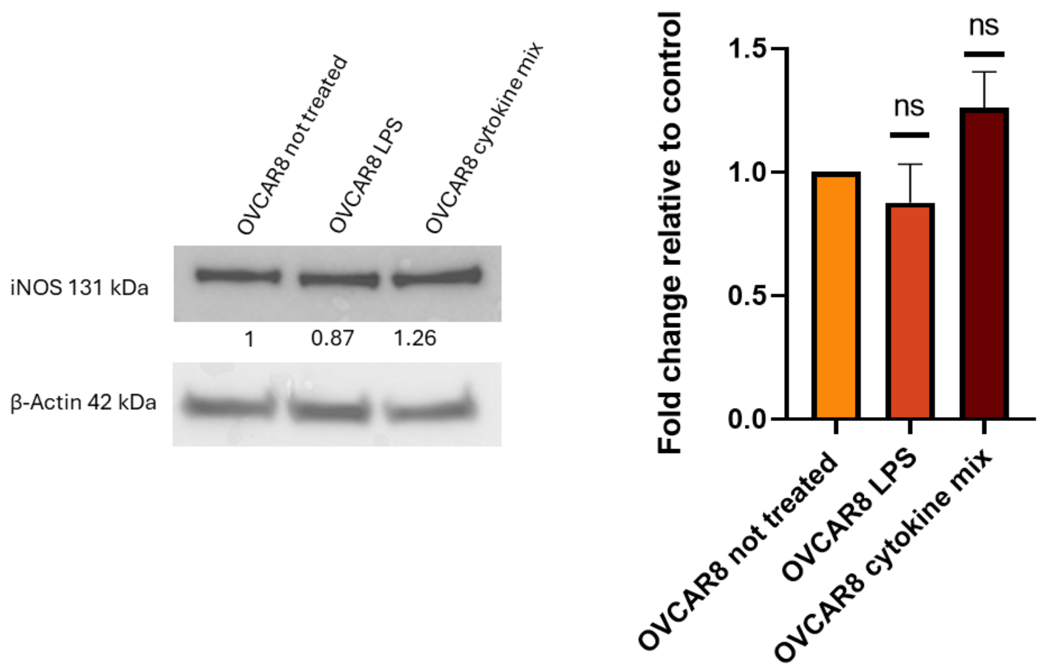

Figure 2.9. OVCAR8 cell line doesn't need stimuli to express or to boost iNOS expression. In this figure it is possible to observe as iNOS is continuously expressed regardless of the administered treatment in OVCAR8 cell line. This analysis has been conducted in three independent replicates and expresses the iNOS protein levels related to β-Actin. Significance was considered only in case of $p < 0,05$. Here it is possible to observe how the two treatments didn't show any significant difference compared with OVCAR8 not treated.

OVCAR8 was identified in The Human Protein Atlas as the most significant expressor of NOS2 and we confirmed it in Figure 2.9 under basal conditions. Following treatment, a similar pattern of NOS2 expression was observed after 24 hours independently from the conditions showing no difference regardless of the treatment and their potential aggressiveness. What can be observed is a not statistically significant change in iNOS expression after the administration of the cocktail even if a little variation has been observed in the two groups where OVCAR8 treated with LPS reached a level of 0.87 (expressed as fold change compared to Not treated) and a level of 1.26 in OVCAR8 Cytokine mix group. These data show how cytokines mix cannot change OVCAR8 iNOS expression.

Following this analysis, the same procedure was adopted for A2780cis. **Figure 2.10** shows the same treatment operated on A2780cis, which consisted in the administration of LPS (1 μg/mL) or cytokine mix (IFN-γ (25 ng/mL), TNF-α (10 ng/mL), and IL-1β (10 ng/mL)

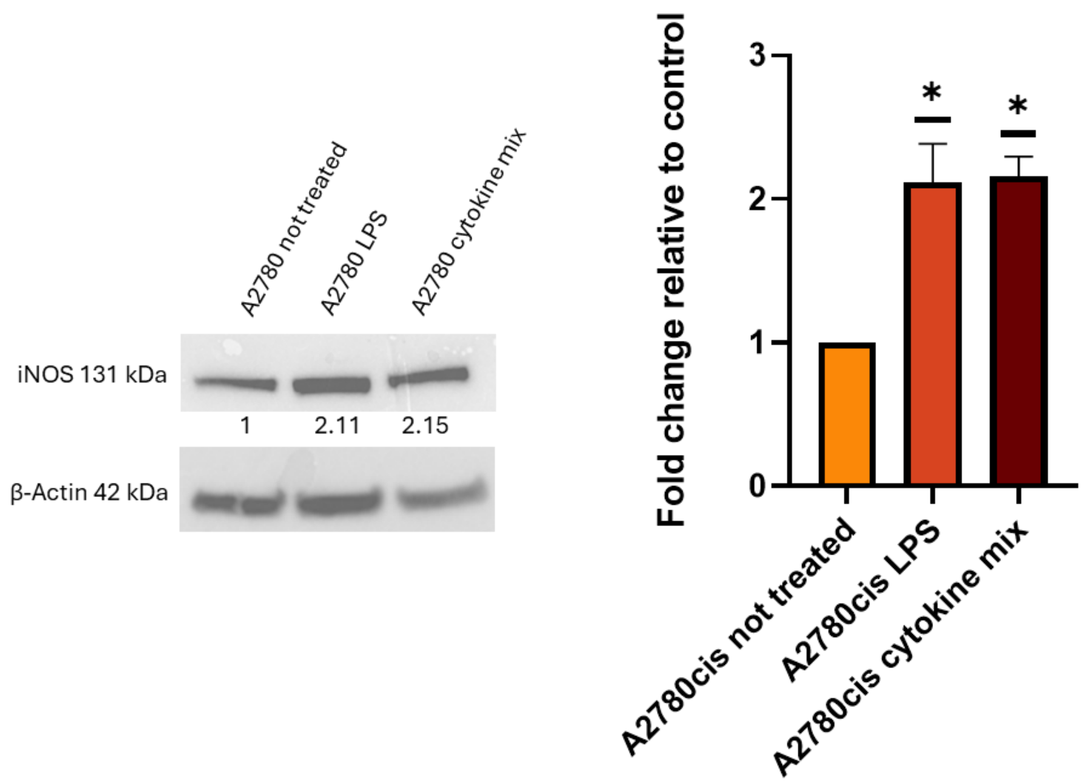

Figure 2.10. A2780cis doesn't need stimuli to express iNOS, but its expression can be increased using a cytokines mix. In this figure it is possible to observe how A2780cis is able to express iNOS at basal levels and how, in this case, the treatment with LPS and cytokine mix can increase iNOS expression.

In particular, A2780cis treated with LPS showed a fold change of 2.11 ($p < 0.05$), compared to A2780cis not treated, and a fold change of 2.15 ($p < 0.05$) in A2780cis cytokine mix group compared to A2780cis not treated. The experiments have been conducted in three independent biological repliates.

A2780cis showed an increase in iNOS expression after the treatments, showing how the environment after the chemoresistance could interfere, and potentially boost iNOS expression. This result shows and confirms also the continuous expression of iNOS operated by this cell line even if the effects of cytokine mixes appear to boost iNOS expression in A2780cis. What can be observed is a change, in this case, in iNOS expression after the administration of the cocktail. A2780cis treated with LPS reached a level of 2.11 ($p < 0.05$), expressed as fold change compared to A2780cis not treated, and a level of 2.15 ($p < 0.05$) in A2780cis cytokine mix group. These data show how cytokines mix can influence iNOS expression which is already expressed at a basal level in this chemoresistant cell line.

2.5 iNOS is expressed at basal levels in OVCAR8 cell line

Since their discovery, short interfering RNA (siRNAs) have increasingly gained a key role in RNA interference (RNAi) therapies and research approaches. They can be used therapeutically as well as to disrupt specific pathways, helping to uncover cancer specific mechanistic functions, *in vitro* [216]. RNAi was employed here, to confirm the specificity of iNOS expression in OVCAR8 cells, which exhibit constitutive iNOS expressions regardless of induction with cytokine cocktail or LPS. The constitutive expression of this enzyme makes them a potential object of study considering the deleterious overexpression of NO in the tumour microenvironment [187]. The results of the iNOS inhibition obtained with siRNA are shown in the western blot and densitometric analysis of **Figure 2.11**.

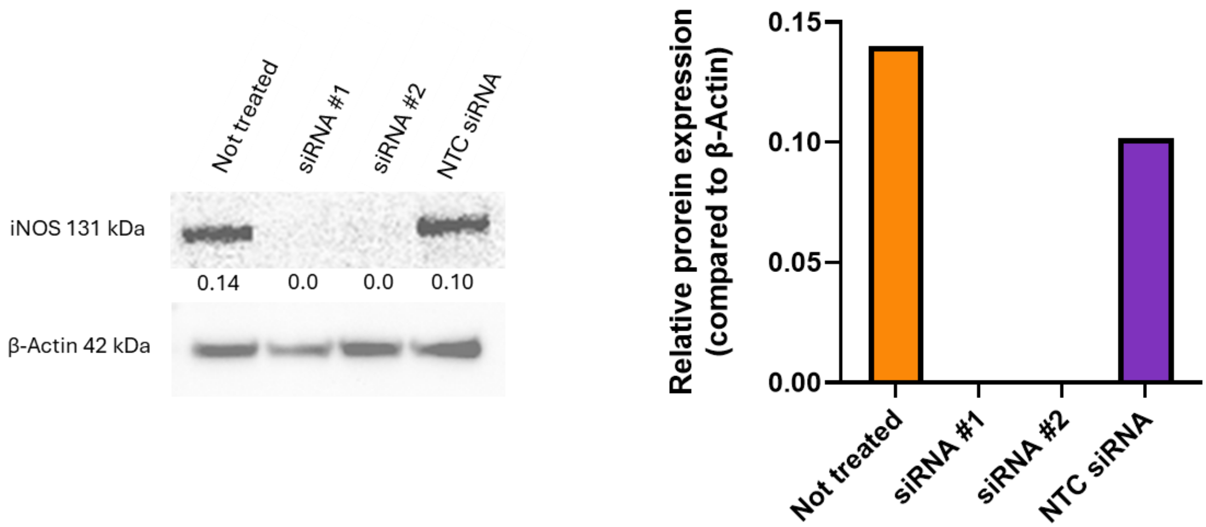

Figure 2.11. **OVCAR8 has basal iNOS expression**. The siRNAs showed the expression of iNOS in the not treated lane. Similar expression in the scramble siRNA lane. Complete knockout has been obtained for the two anti-NOS2 siRNA tested in lane two and three.

Both untreated and NTC-treated OVCAR8 cells maintained iNOS expression, unlike the siRNA-treated samples where iNOS was effectively silenced. Data was presented as relative protein expression (compared to β-Actin) to test the efficacy and specificity of the siRNAs in targeting and silencing iNOS. Untreated cells showed normal iNOS expression corresponding to a relative protein expression of 0.14, while cells treated with a non-targeting control siRNA (NTC siRNA) exhibited 0,10 of relative iNOS expression compared to ACTB. Treatment with both anti-NOS2 siRNAs (siRNA1 and siRNA2) resulted in a complete knockout of the iNOS, with NOS2 expression reduced to 0%.

2.6 L-NMMA shows killing activity on HGSOC NOS expressing cell lines

L-NMMA is structurally similar to L-arginine, the natural substrate for NOS. It binds to the active site of NOS enzymes, competing with L-arginine. By blocking L-arginine binding, L-NMMA prevents the enzymatic conversion of L-arginine to nitric oxide and L-citrulline. Considering the overexpression of iNOS in cancer and inflammation [195], L-NMMA may play a beneficial role by reducing NO release, thereby limiting EMT, acquired chemoresistance, and angiogenesis [196]. Given the constant and consistent expression of NOS2 by OVCAR8 cells, we evaluated the effects of LNMMA treatment on the viability of OVCAR8 cells after 72 hours of treatment. A range of L-NMMA concentrations, from 2 mM to 30 mM, were tested and resulting cell viability shown in **Figure 2.12**.

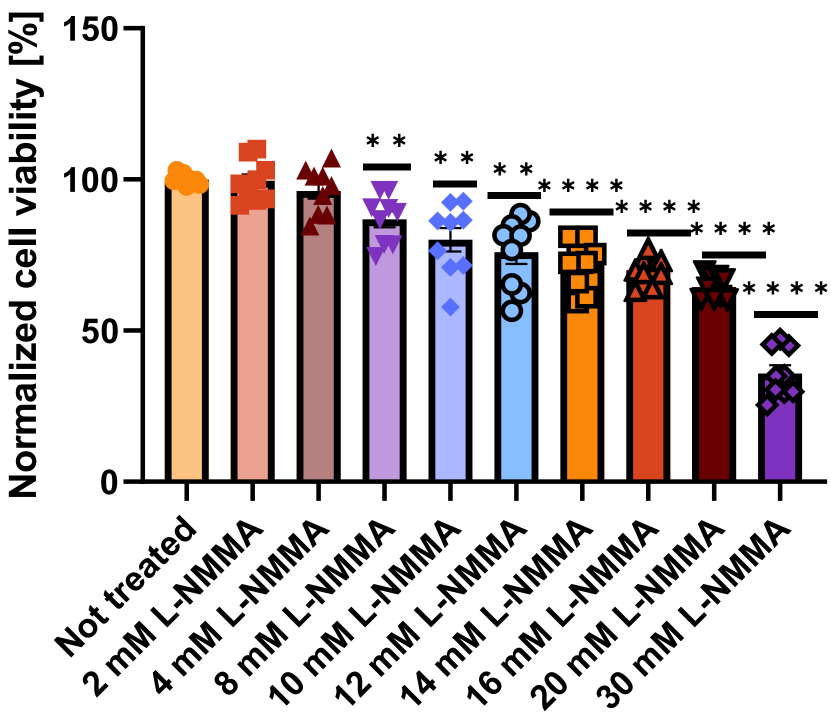

Figure 2.12. Effects of L-NMMA in OVCAR8 cell viability. In this figure it is possible to observe the effect of different concentration of L- NMMA after 72 hours of administration of the drug. Cell viability decreases according to the increasing concentration of L-NMMA adopted. A statistically significant difference ($p< 0.05$) is observed starting with 8 mM of L-NMMA. In particular, the administration of 2 mM and 4 mM of L-NMMA showed no significant impact on cell viability, with values of 102.9% and 100.7%. At 8 mM, cell viability decreased to 91.6% ($p < 0.05$), and at 10 mM, it further declined to 86.7%

($p < 0.05$). Treatment with 12 mM L-NMMA reduced viability to 83.2% ($p < 0.05$), 14 mM led to 76.5% viability ($p < 0.05$). The next three concentrations showed continued reductions: 16 mM resulted in 72.1% viability ($p < 0.05$), 20 mM reduced viability to 65.7% ($p < 0.05$), and the highest concentration tested, 30 mM, caused a substantial drop to 30.8% ($p < 0.05$). All the experiments were conducted in three independent biological replicates and results were considered significant with p values < 0.05.

The lowest concentrations, 2 mM and 4 mM showed no significant impact on cell viability, with values of 102.9% and 100.7%, respectively, compared to untreated cells ($p > 0.05$). At 8 mM, cell viability decreased to 91.6% ($p < 0.05$), and at 10 mM, it further declined to 86.7% ($p < 0.05$). Treatment with 12 mM L-NMMA reduced viability to 83.2% ($p < 0.05$), while 14 mM led to 76.5% viability ($p < 0.05$). The next three concentrations showed continued reductions: 16 mM resulted in 72.1% viability ($p < 0.05$), 20 mM decreased viability to 65.7% ($p < 0.05$), and the highest concentration tested, 30 mM, caused a substantial drop to 30.8% ($p < 0.05$), which is below the IC50 threshold.

2.6.1 Cisplatin IC50 on HGSOC NOS2 expressing cell line

Cisplatin is one of the most used chemotherapeutic agents worldwide. It is also commonly used in ovarian cancer, due to its efficiency in damaging the DNA of cancer cells. [217]. To evaluate the effectiveness of chemotherapeutic agents on OVCAR8, an HGSOC NOS2 expressing cell line, we performed a dose response curve with increasing dose of cisplatin from 4 μM to 24 μM over 72 hours and monitored cellular proliferation using the RealTime-Glo™ MT Cell Viability Assay. The purpose of this assay was to detect and define the IC50 or values close to it to optimize the chemotherapeutic concentration to administer together with L-NMMA, an enzymatic inhibitor of iNOS. The role of combining this known chemotherapy approach based on Cisplatin together with L-NMMA remains unexplored and the opportunity to combine these two drugs represent an interesting opportunity in key of future ovarian cancer treatments and novel therapies. The efficacy of Cisplatin was measured after 72 hours of treatment, consistent with commonly reported protocols in the literature [218] **(Figure 2.13 A-B)**.

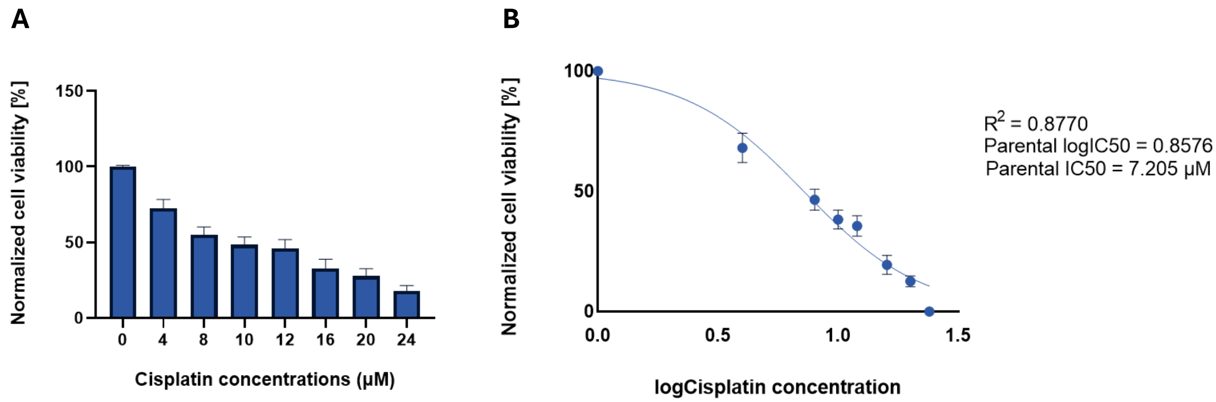

Figure 2.13 (A,B). **Effects of Cisplatin on OVCAR8 cell viability. Figure 2.13A** shows the dorse obtained after administering Cisplatin at different concentrations for 72 hours. It is possible to observe how increasing concentration of Cisplatin cause the reduction in viability over time. **Figure 2.13B** shows a pharmaceutical curve of Cisplatin (in logarithmic concentrations) and the relative percentage of proliferation. The mathematically calculated IC50 for OVCAR8 parental cell il is 7.205 μM. The goodness of the curve has been expressed as R^2 value, in this case corresponding to 0.8770. The experiments have been conducted in three independent replicates.

All tested concentrations resulted in reduced cell proliferation. The lowest dose, 4 μM Cisplatin, induced a normalized residual cell viability of 72.35%. Doubling this concentration to 8 μM decreased viability further to 55.1%. At 10 μM, the IC50 was reached, with cell proliferation reduced to 48.4%. A slightly higher concentration of 12 μM caused a close effect on the previous concentration tested, reducing viability to 46.1%. The three highest concentrations showed more pronounced effects: 16 μM led to 32.9% residual viability, 20 μM to 27.7%, and the maximum tested dose of 24 μM resulted in the lowest residual viability of 17.8%, as shown in **Figure 2.13A**. The IC50 for OVCAR8 has been identified in **Figure 2.13B** to be 7.205 μM, which aligns with previously reported data on the efficacy of platinating agents in OVCAR8 cells. The reliability of the curve is represented by the R squared value obtained over the replicates corresponding to 0.8770.

2.6.2 L-NMMA increases the efficacy of Cisplatin

Considering the novel option that we propose in this study of combining ovarian cancer together with L-NMMA, whose potential application in ovarian cancer remain unexplored, we tested in vitro the combinatorial effects of Cisplatin with L-NMMA. The treatment of the OVCAR8 parental cell line with

Cisplatin, L-NMMA, and their combination resulted in differential proliferation rates after 72 hours (**Figure 2.14A**). The Cisplatin concentration was consistently maintained at 10 μM throughout the experiments, while different concentrations of L-NMMA were tested. Treatment with 10 μM Cisplatin alone resulted in a proliferation rate of 56%.

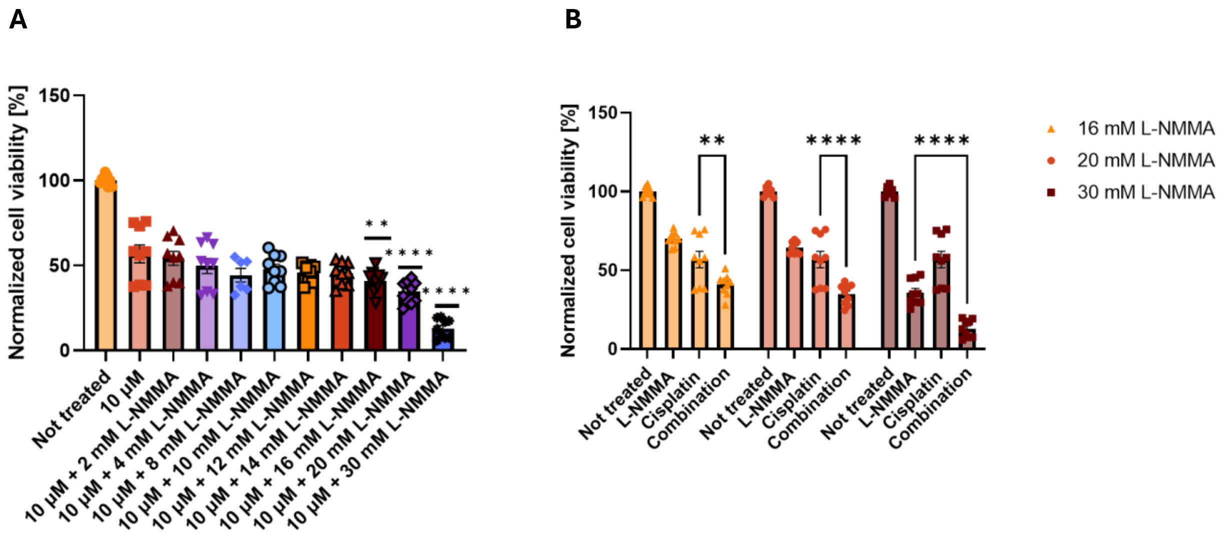

Figure 2.14 (A-B). L-NMMA increases the efficacy of Cisplatin. Figure 2.14A shows the effects of combining Cisplatin with L-NMMA. A gradient of L-NMMA (ranging from 2 mM to 30 mM) demonstrates its ability to enhance the efficacy of Cisplatin in the reduction of proliferation of OVCAR8. Statistically significant results were determined using a two-way ANOVA with a threshold of $p < 0.05$. A significant increase in Cisplatin's effect was observed starting at 16 mM L-NMMA, when comparing the residual proliferation of OVCAR8 parental cells treated with 10 μM Cisplatin only. When combined with L-NMMA, residual proliferation rates were as follows: 54.8% with 2 mM, 49.7% with 4 mM, 44.3% with 8 mM, 47.8% with 10 mM, 45.9% with 12 mM, and 45.3% with 14 mM. At 16 mM L-NMMA combined with 10 μM Cisplatin, proliferation was reduced to 40% ($p < 0.05$). Treatment with 20 mM L-NMMA plus Cisplatin further decreased proliferation to 34.7% ($p < 0.05$). Finally, the combination of 30 mM L-NMMA and 10 μM Cisplatin led to the lowest residual proliferation rate of just 12.9% ($p < 0.05$). The experiments were performed in three independent replicates. **Figure 2.14B** compares four conditions in OVCAR8 parental cells: untreated, treated with L-NMMA alone, treated with Cisplatin alone, and treated with the combination of both drugs. Statistical significance was again assessed using two-way ANOVA ($p < 0.05$). The combination treatment produced a significantly greater reduction in cell proliferation compared to either treatment alone, showing an increased effect in the reduction of OVCAR8 cells proliferation. 16 mM of L-NMMA combined with 10 μM Cisplatin, reduced proliferation to 40% ($p < 0.05$). Treatment with 20 mM L-NMMA plus Cisplatin further decreased proliferation to 34.7% ($p < 0.05$). Finally, the combination of 30 mM L-NMMA and 10 μM Cisplatin led to the lowest residual proliferation rate of just 12.9% ($p < 0.05$). The experiments were performed in three independent replicates.

When combined with L-NMMA, residual proliferation rates were as follows: 54.8% with 2 mM, 49.7% with 4 mM, 44.3% with 8 mM, 47.8% with 10 mM, 45.9% with 12 mM, and 45.3% with 14 mM. At 16 mM L-NMMA combined with 10 μM Cisplatin, proliferation was reduced to 40% ($p < 0.05$). Treatment with 20 mM L-NMMA plus Cisplatin further decreased proliferation to 34.7% ($p < 0.05$). Finally, the combination of 30 mM L-NMMA and 10 μM Cisplatin led to the lowest residual proliferation rate of just 12.9% ($p < 0.05$). **Figure 2.14B** shows a comparison between untreated cells, L-NMMA treated cells, Cisplatin treated cells and treatment from the combination of Cisplatin and L-NMMA.

2.6.3 Notes on the combinatorial effects of Cisplatin and L-NMMA

After evaluating the effects of the combined treatment in comparison with the single agents, it was observed that the combination of cisplatin and L-NMMA produced predominantly additive effects across low to intermediate concentrations, except for 30 mM of L-NMMA, where borderline for synergistic effects was observed. The implications of higher L-NMMA concentrations, particularly in terms of their biological impact and potential clinical applicability, will be discussed in the following chapters. Importantly, at lower concentrations L-NMMA consistently exhibited additive effects in combination with cisplatin, suggesting a potentially favorable therapeutic window for in vivo applications. These findings are further supported by the effects of L-NMMA on Vimentin expression and the epithelial–mesenchymal transition (EMT) process, which will be addressed in the next chapter, highlighting its possible relevance in future clinical investigations.

2.7 iNOS expressing cell line show expression of Vimentin

Vimentin is a protein involved in cytoskeleton reorganization [219] and also plays a role in EMT transition [220]. Numerous studies have investigated the potential implications of Vimentin in cancer progression and its role and involvement in cancer [203]. A recent study highlighted the relationship between iNOS, NO, and EMT [209] in metaplastic breast cancer. To explore a possible correlation between ovarian cancer, iNOS expression, and Vimentin expression, a Vimentin panel, similar to what has been proposed in the sections above, is shown in **Figure 2.15**.

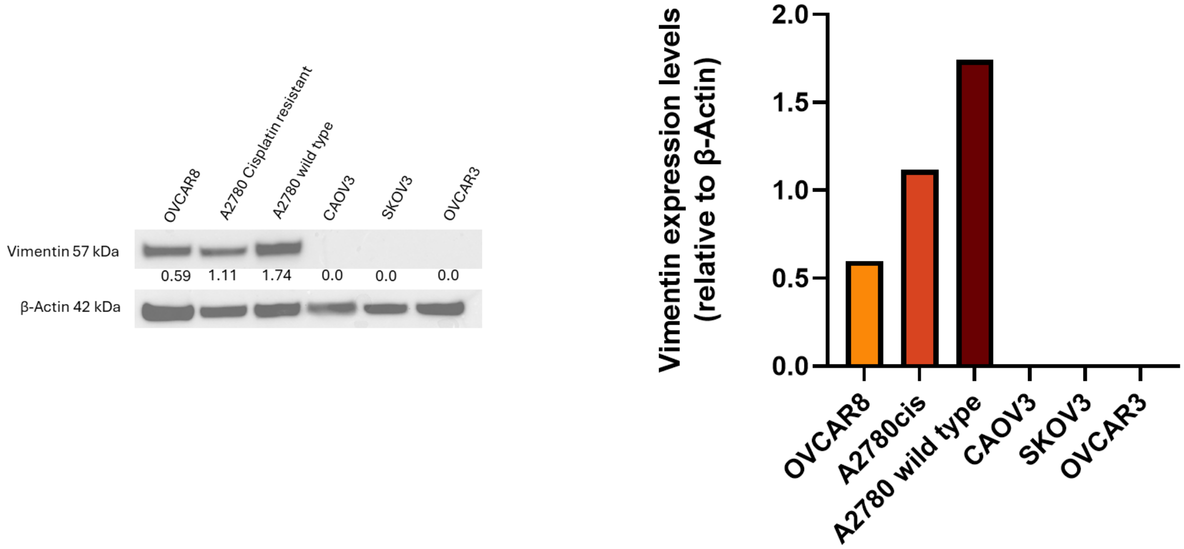

Figure 2.15. Only iNOS expressing cell lines express Vimentin. In the figure it is possible to observe how only the cell lines that have been previously proved to express iNOS which are, OVCAR8, A2780cis and A2780 wild type, express Vimentin. The ovarian cancer cel lines which didn't show Vimentin expression don't have any detectable Vimentin expression. The experiments were performed in three independent replicates.

Notably, OVCAR8, A2780cis, and A2780 wild type are the only cell lines that showed Vimentin expression. Only iNOS-expressing ovarian cancer cell lines are able to express Vimentin, revealing an interesting correlation between this enzyme and Vimentin production. This result is particularly relevant considering a publication on breast cancer showing that Vimentin expression is associated with poor prognosis in breast carcinoma [221]. Another study conducted on patient samples demonstrates that increased Vimentin expression is also correlated with malignant cases of ovarian cancer [222]. Considering this aspect, along with the key role of Vimentin in EMT [187] and recent studies reporting the role of L-NMMA in EMT [187], the following section explores the effect of L-NMMA on Vimentin expression.

2.7.1 L-NMMA reduces Vimentin expression

Vimentin is positively correlated with cancer progression as tumour starts to spread and invade surrounding areas [203]. The changes that occur during metastatic invasion and tumour spread are all related to a phenomenon called Epithelial-to-Mesenchymal Transition (EMT) which is often related to a change in cell shape and morphology. All these changes are supported by a structural reorganization of cells starting from their cytoskeleton where Vimentin is one of the main elements. Targeting NOS2 through L-NMMA and enzymatic inhibitor of nitric oxide synthase could have a potential role in EMT and cytoskeletal reorganization, as described in a recent publication [209]. To assess L-NMMA effect on Vimentin expression, total protein isolates were prepared from OVCAR8 cells following treatment with 4,6, 8 and 10 mM L-NMMA (**Figure 2.16**).

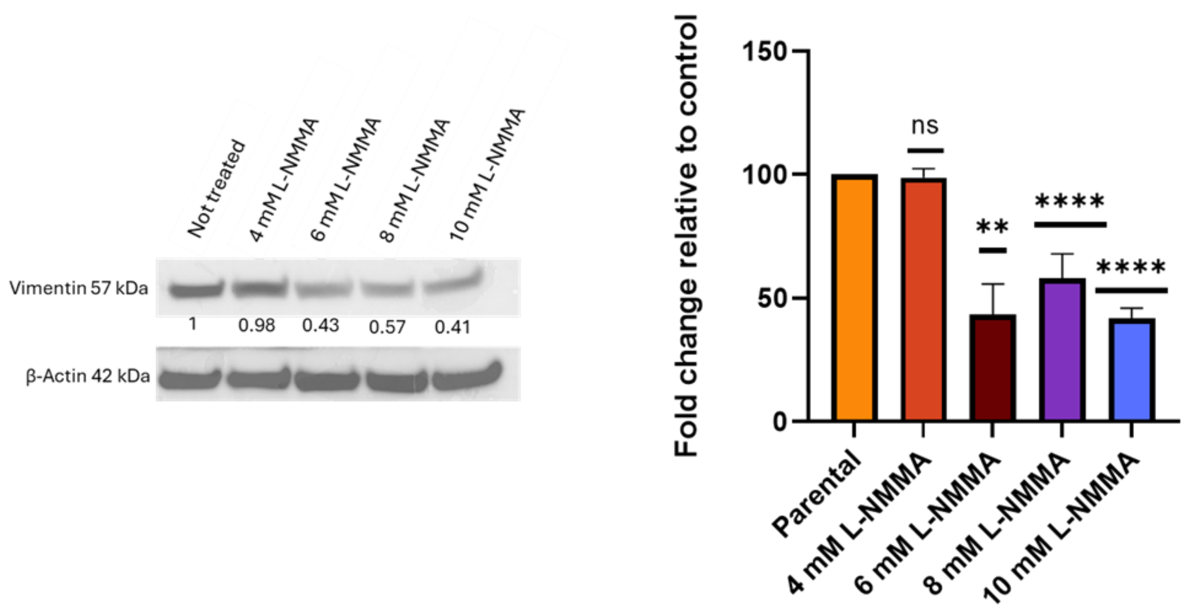

Figure 2.16 (A-B). Effects of L-NMMA administration on Vimentin protein expression. L-NMMA was tested at four different concentrations starting from 4 mM up to 10 mM. It is possible to observe a strong reduction of Vimentin expression that can be observed from 6 mM of L-NMMA to 10 mM. The data obtained were considering significant with $p < 0.05$. At 4 mM, L-NMMA did not cause a significant decrease in Vimentin levels, which remained comparable to untreated cells with a fold change relative to control corresponding to 0.98. After the administration of 6 mM the Vimentin level decreased to 0.43 ($p < 0.05$), 8 mM showed a decrease, but less than the previous one, reaching the level of 0.57 ($p < 0.05$) and at the end, 10 mM showed residual Vimentin levels corresponding to 0.41 ($p < 0.05$). The analysis was performed in three independent replicates.

Treating OVCAR8 parental cell line with L-NMMA for 48 hours resulted in a decrease in Vimentin protein levels. This reduction followed a dose-dependent gradient, particularly noticeable between 6 mM and 10 mM of L-NMMA. At 4 mM, L-NMMA did not cause a significant decrease in Vimentin levels, which remained comparable to untreated cells with a fold change relative to control corresponding to 0.98. We observed a significative reduction in Vimentin levels after the treatment with 6 mM L-NMMA which led to Vimentin residual levels corresponding to a fold change relative to control of 0.43 ($p < 0.05$), 8 mM L-NMMA led to a fold change corresponding to 0.57 ($p < 0.05$), and 10 mM L-NMMA led to 0.42 fold change when compared to control ($p < 0.05$).

2.8 Discussion

NOS2 plays multiple roles within the tumour microenvironment (TME), with many well-known functions in proinflammatory responses, vasodilation, and neurotransmission [151], modulating cancer cell behaviour by targeting specific proteins through S-nitrosylation [223]. In this chapter, a novel approach and findings have been proposed, showing that OvCA cell lines express iNOS both constitutively and following induction with proinflammatory cytokines. OVCAR8 cell line, representative of HGSOC, displayed significantly elevated and constitutive iNOS expression, which persisted regardless of treatment with LPS or a cytokine mixture (IFN-γ, TNF-α, IL-1β). Similarly, the cisplatin-resistant A2780 cell line exhibited constitutive NOS2 expression, whereas its cisplatin-sensitive counterpart expressed iNOS exclusively upon cytokine stimulation. These observations are consistent with data from the Human Protein Atlas, confirming OVCAR8 as one of the highest NOS2-expressing HGSOC cell lines and justifying its selection for knockout studies that have been analyzed in the following chapters. More specifically, the in-house panel, developed in this work, correlated not only with the Human Protein Atlas but also with datasets from CCLE and the NCI-60 panel. What it also to be mentioned in this first part of our work is that, while HGSOC represents around the 70% of all types of ovarian cancer [224], EOC is composed of different subtypes. Although it is known that cancer is associated with a proinflammatory environment [225] and a subsequent release of cytokines [225], there is limited evidence regarding which specific subtype or cell line is capable of expressing iNOS. Even though databases collect data from omics sciences, as we reported in CCLE, NCI-60, and The Human Protein Atlas, the novelty we present lies in demonstrating that iNOS can be expressed both at baseline and in response to a proinflammatory environment. This expression shows differences between Cisplatin-resistant and Cisplatin-sensitive cell lines. We propose a new potential perspective that links iNOS expression to Cisplatin resistance. It is already known that a proinflammatory environment and the release of NO may be related to chemotherapy resistance [171], but in this study, we specifically suggest a potential connection between iNOS expression and chemotherapy resistance in ovarian cancer, as observed in the A2780 cell line. Another important aspect of our findings is that we demonstrated the induction of iNOS by a cytokine cocktail, previously shown to be effective in other cancer types [173], but not yet demonstrated in ovarian cancer. We demonstrated the effect of the cytokine mix on ovarian cancer and identified two important findings. The first is that some ovarian cancer cell lines showed basal expression of iNOS. The second is that iNOS expression in ovarian cancer did not require a pro-inflammatory environment. Additionally, we provided evidence that iNOS is not only expressed at the RNA level, as reported in The Human Protein Atlas, which lacks protein-level data, but also at the protein level. This significantly expands the existing data on ovarian cancer cell lines by showing that not only A2780 wild-type cells express iNOS, but also their Cisplatin-resistant counterparts. These data are absent from the three databases we consulted and are currently lacking in scientific literature. What will make a future impact in tailoring and defining ovarian cancer research is the complete characterization of the (eventual) role of iNOS across all subtypes, as their origin sites differ and the disease progresses differently. This could enable the development of specific combinatorial therapies for each subtype that should be taken into consideration. In our study, we mainly focused on HGSOC due to its prevalence among all EOC subtypes but we also included EndOC, which, although representing approximately 10-15% of all EOC cases [226], is associated with previous endometriosis and obesity in patients [227]. These conditions lead to an increased percentage of adipose tissue and consequently increased release of cytokines, which can potentially increase iNOS expression [228] and provide metabolic support to the tumour, as previously mentioned in the previous chapter of this work. As previously mentioned, tailoring therapies to specifically address the distinct features of each subtype is essential. For this reason, this study identifies the context in which a treatment designed to inhibit NO could be effective in sensitizing cancer cells. This level of discrimination in the use of L-NMMA has not yet been reported in the literature. It has to be reported that, as also previously mentioned in other parts of this work, L-NMMA has been studied for clinical trials in combination with Taxane. L-NMMA is a drug that, considered its effects and according to how reported in literature, is not a drug thought to be a standalone treatment. The same clinical trial Phase I/II reports among the beneficial effects of the combination treatment, apart from the reduced toxicity, also the stimulation of the immune system, as it will be reported in the following sections in a syngeneic in vivo model. The concentrations of the drug reported in this study, even if are in the range of millimolar (from 4mM to 30 mM) have the main aim of proving the potential efficacy of this drug also in ovarian cancer and its effects on EMT. In particular, as it will be reported in the in vivo section of this work, L-NMMA has been modulated to reach optimal doses with no toxicity in vitro sustained by daily injections of L-NMMA in order to avoid side effects avoiding high concentrations of the drug. In addition, the potential applicability of L-NMMA for clinical trials in ovarian cancer has been proved in this work, but still lacks of real tests and optimization of the system. The clinical applicability will be a potential following step of this work to be conducted with medical expertise with knowledge in the exact dosage of the drug into patients. Therefore, this work provides novel insights into where the benefits of combining L-NMMA with Cisplatin are most evident. By analyzing the differences among ovarian cancer subtypes, we demonstrated not only where L-NMMA can be used most efficiently, but also where a proinflammatory environment contributes to increased NO expression, and where it does not. With this knowledge, it becomes possible to enhance treatment specificity by testing the Cisplatin + L-NMMA combination according to the subtype, as has already been done in other cancer types or subtypes [157, 209]. After characterizing iNOS expression, we conducted a series of analyses to evaluate the cells' responses to chemotherapy, L-NMMA, and combinatorial treatment with Cisplatin and L-NMMA. Following determination of the IC50 for Cisplatin and assessment of L-NMMA's effects alone on OVCAR8 (we saw a viability reduction starting at 8 mM), we investigated the combined treatment. Our results were encouraging, demonstrating enhanced efficacy of Cisplatin when combined with various concentrations of L-NMMA, indicating a synergistic interaction with chemotherapy. Following lines of a previous study conducted on breast cancer [18], given EMT's established role in metastasis and chemoresistance, we investigated a potential downregulation of Vimentin related to the deletion of NOS2. Supporting this, treatment of parental OVCAR8 cells with the NOS2 inhibitor L-NMMA resulted in approximately a 50% decrease in Vimentin expression at concentrations starting from 6 mM, reinforcing the connection between NOS2 activity and Vimentin regulation for ovarian cancer. In this chapter, an innovative approach using L-NMMA to increase the susceptibility of ovarian cancer cells to chemotherapy has been proposed. These findings suggest potentially interesting scenarios regarding the connection between chemoresistance, iNOS and Vimentin expression in ovarian cancer [229]. While identifying subtype-specific responses in ovarian cancer treatment was important, as previously stated, equally crucial was the optimization of a treatment regimen to serve as a reference point for future studies involving combination therapies with Cisplatin and nitric oxide synthase inhibitors. This work provides standardized concentrations for in vitro treatments and, as will be shown in the following sections, also for in vivo applications.

These data demonstrate that targeting EMT in ovarian cancer cells is a valid strategy to improve chemotherapy efficiency and potentially extend treatment windows by increasing sensitivity to cisplatin. This association may also connect Vimentin expression with chemoresistance [203] as we found iNOS is constantly expressed in our chemoresistance ovarian cancer cell line. Considered that L-NMMA reduces Vimentin expression levels, it might potentially suggest that reducing Vimentin might lead to an increased chemotherapy sensitivity, considering that after tumour debulk and chemotherapy, 50-70% of patients experience recurrence associated with chemoresistance [230]. Thus, targeting iNOS could be a promising strategy to improve therapy efficacy in patients with acquired chemoresistance, addressing a major challenge in ovarian cancer. Further supporting these hypotheses, immunoblotting revealed that not all ovarian cancer cell lines screened expressed iNOS; some had basal levels while others showed inducible expression following cytokine treatment and only iNOS-expressing cell lines displayed detectable Vimentin protein levels, suggesting a role for iNOS and NO in regulating Vimentin expression. Currently, literature lacks comprehensive information on the relationship between iNOS and Vimentin expression for ovarian cancer. In this work, a new and interesting scenario is proposed in which Vimentin expression may be linked to NO-related pathways. Numerous studies in the literature support the role of S-Nitrosylation in promoting EMT [191, 231, 232]. However, limited evidence exists regarding this mechanism in ovarian cancer. Interestingly, while

Vimentin has already been associated with increased chemoresistance in cancer, as previously mentioned, no studies have directly examined the effect of L-NMMA on reducing Vimentin levels in ovarian cancer. Although one study explored EMT, Vimentin expression, and L-NMMA in metaplastic breast cancer [209], this connection remains largely unexplored in ovarian cancer. Targeting Vimentin may also have implications for modulating the tumour microenvironment, as increased EMT, of which Vimentin is a key marker, is linked to a supportive role of stromal cells. This relationship was discussed in the introductory section of this work. Therefore, future investigations into the role of L-NMMA in regulating a broader panel of EMT markers could further support its potential to disrupt the tumour microenvironment and improve therapeutic outcomes.

Another consideration that can be reached from the previous chapter is the extensive presence of an immune cold microenivornment into the TME with immune cells which also have the capacity of expressing iNOS. This suppression is driven in part by regulatory T cells (Tregs), myeloid-derived suppressor cells (MDSCs), and M2 macrophages [233]. Given NO's role in modulating immune responses and its secretion by multiple immune components, targeting NO represents a promising strategy to reactivate the silenced antitumor immune response silenced by cancer cells or other tumour microenvironment components. For that reason, an important avenue for future research, to be addressed in the following chapter, involves evaluating the effects of L-NMMA in vivo. Developing a system where all these factors can be analyzed represents an interesting and necessary step to elucidate the role of Cisplatin in combination with L-NMMA. What makes an in vivo model an interesting way to study the effects of iNOS and L-NMMA in ovarian cancer is that targeting iNOS, and consequently, NO, could potentially make L-NMMA a pan-tumour microenvironment drug, particularly considering what has been stated in the previous section of this work: many cells are able to express iNOS, not only immune system cells but also other cell types that compose the stroma, such as fibroblasts [234], adipocytes [235], and mesenchymal cells [168]. All these cells have the potential not only to stimulate tumour growth but also to inactivate the immune response, creating a safe environment for cancer cells to grow and proliferate. In addition, the abundance of proinflammatory cytokines, abundant in ovarian cancer [236], can create a deleterious loop where iNOS is continuously expressed, leading to a final overexpression that favours cancer growth. Considering all these aspects, developing a treatment strategy that not only targets cancer cells but also disrupts the tumour microenvironment may represent a key advancement in the fight against ovarian cancer. The ability to modify the composition of the tumour microenvironment, an area often characterized by a dense, drug-resistant stroma, could improve drug penetration and delivery. By compromising this protective barrier formed by stromal components, such an approach could enhance the specificity and efficiency of therapeutic agents, allowing them to reach both tumour cells and other resident cell types more effectively.

Conclusions

In the second part of this work, iNOS expressing ovarian cancer cell lines were identified. An in-house panel has been developed to confirm iNOS expression at both the RNA and protein levels. In this work potential combinatorial treatment has also been proposed using Cisplatin and L-NMMA, demonstrating an increased efficacy of chemotherapy. Additionally, a role for L-NMMA in reducing Vimentin levels has been identified. This result could open interesting possibilities, especially considering that Vimentin is commonly associated with poor prognosis, acquired chemoresistance, and metastatic progression in cancer.

Chapter 3 – L-NMMA increases the efficacy of Cisplatin in vivo and stimulates the immune response

3.1 Introduction

Considering the disease complexity of OvCa, late-stage diagnosis and the clinical challenge of the characteristic cold tumor microenvironment observed in both primary tumors and metastatic niches [237], the development of appropriate *in vivo* models is essential for comprehensive investigation of this disease. Encompassing the diverse stages of disease progression, the various histological subtypes of epithelial ovarian cancer, and their distinct molecular profiles, it is imperative to establish and characterize an optimal in vivo model. Such a model should accurately recapitulate the biological complexity of ovarian cancer to facilitate the investigation of tumor pathogenesis, progression, and therapeutic response. The development of in vivo models for ovarian cancer remains challenging, because it is necessary taking into consideration several intrinsic limitations. These include difficulties in tumor detection, the high metastatic potential of ovarian cancer which complicates the acquisition of consistent and robust signals, as well as the frequent development of ascites [238]. Additionally, the choice of mouse strain also imposes limitations. Immunocompetent models allow the study of the host immune response. However, they cannot support engraftment of human ovarian cancer cell lines, which may better reflect the human disease than murine-derived lines. Conversely, immunocompromised mouse strains facilitate the engraftment and study of human ovarian cancer cell lines, thus allowing the analysis of human tumor progression, but they inherently lack a functional immune system. This limitation is particularly significant given the immunologically “cold” nature of ovarian cancer, characterized by a subdued immune response, which is critical to understand for therapeutic development. In general, there are some in vivo models which are mainly and widely used in research. These models are xenograft models, PDXs and syngeneic models. Xenograft models, which involve engrafting human tumor cells into immunodeficient mice, are limited primarily by the absence of an intact immune system. Another notable limitation is the confinement of tumor formation to the site of injection, resulting in localized tumor aggregates [239, 240]. Nonetheless, these models offer the advantage of permitting the investigation of tumor progression from early to advanced stages [241, 242], In combination with the ability to study tumor development in human cell lines with targeted gene knockout or downregulation, enabling the investigation of how specific genes influence tumor growth and progression. Despite this potential, the lack of an immune response represents a significant drawback, as tumor development in vivo is not merely a function of cellular proliferation but is also modulated by immune-tumor interactions, which are absent in these models [243]. An alternative approach for modeling ovarian cancer involves Patient-Derived Xenografts (PDXs). A key advantage of PDX models is the retention of certain patient-derived stromal components within the murine host, thereby allowing the study of tumor behavior in the context of a microenvironment partially composed of human stromal cells [244]. This is particularly relevant given the critical role of the tumor microenvironment in ovarian cancer. However, a major limitation of PDX models is the progressive replacement of human stroma by murine stromal cells over time, leading to a loss of the original human microenvironmental features. Consequently, although PDXs provide valuable insights, they do not fully recapitulate the complex interactions between human tumor cells and their native stromal microenvironment, thus limiting the comprehensiveness of microenvironmental studies in ovarian cancer [245]. Syngeneic *in vivo* models are widely employed, in particular considering that they possess an intact immune system [246]. Specifically, syngeneic models utilize immunocompetent mice, which enable unique investigations into immune system adaptation within the tumor microenvironment and evaluation of therapeutic strategies aimed at immune reactivation. Given the significant advances and emphasis on immunotherapy in contemporary cancer treatment, syngeneic models offer promising avenues for pre-clinical research [247]. However, it is important to consider that these models require the use of murine cancer cell lines to maintain immune competence. Consequently, the biological features of tumors derived from murine cells do not perfectly replicate human tumor biology. Moreover, murine tumors exhibit less genetic heterogeneity compared to human tumors, which may lead to discrepancies in tumor progression dynamics and limit direct translational applicability [248]. A summary of some of the previously described in vivo models is represented in

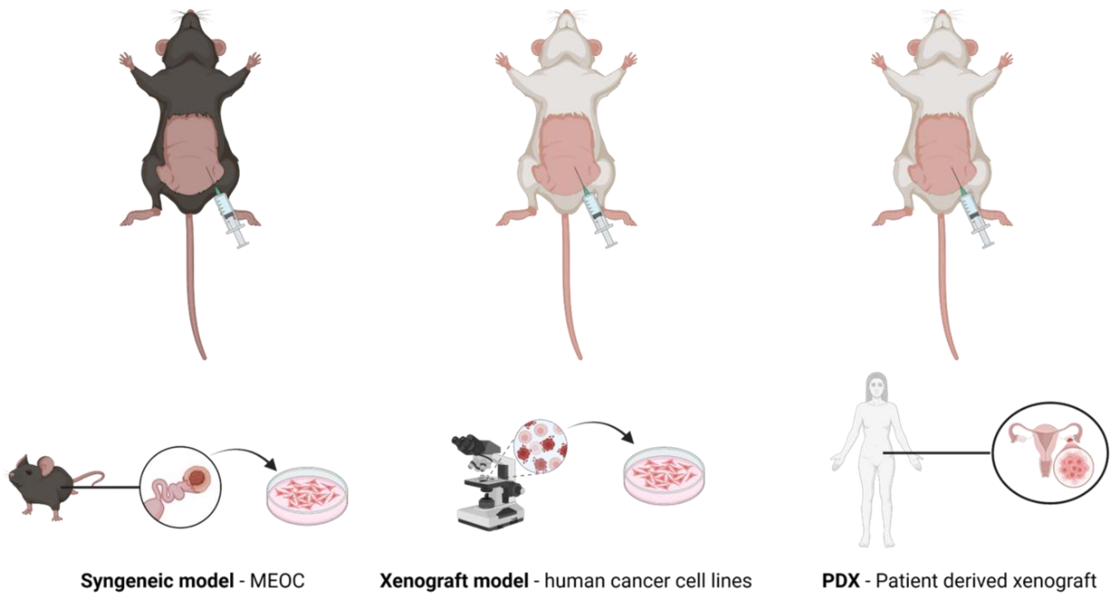

Figure 3.1.

Figure 3.1. Overview of the most common in vivo models used to represent ovarian cancer. Several in vivo models are commonly employed to simulate the heterogeneity of ovarian cancer, each with distinct characteristics and applications. The syngeneic model utilizes murine ovarian cancer cell lines implanted into immunocompetent mice, allowing for the study of tumor progression within an intact immune system. The xenograft model involves the transplantation of human ovarian cancer cell lines into immunodeficient mice, such as nude or NSG strains, enabling the assessment of human tumor biology in the absence of adaptive immunity. The patient-derived xenograft (PDX) model involves engrafting fragments of primary human ovarian tumors, including both malignant and stromal components, into immunocompromised mice, thereby preserving tumor heterogeneity and more closely recapitulating the human tumor microenvironment. Created in https://BioRender.com.

The main features of these models are also summarized in **Table 3.1**.

Type of in vivo model	Advantages	Disadvantages
Syngenic in vivo model	Immune response analysis	Murine cancer cells
Xenograft model	Human cancer cell lines	Immunocompromised mice
PDX model	Cancer and stroma	Immunocompromised mice and risk of false positive for stromal elements

Table 3.1. Main features summary of the syngeneic, xenograft and PDX model. The table present to principal advantages and disadvantages of three of the most common in vivo models adopted to simulate ovarian cancer.

Considering the purpose of our study, an essential factor that drove the selection of in vivo models was iNOS expression. In particular, the potential expression of iNOS in one of these in vivo models was considered a key factor. The reason for the selection of a syngeneic in vivo model was the presence of the immune system which is well known for its response to and production of proinflammatory stimuli. Inflammatory stimuli are an essential factor for iNOS production, also considering that iNOS itself is a key player during the inflammatory response due to its involvement in multiple functions [198, 249, 250]. In particular, the dysregulated expression of this enzyme [251] may contribute to an altered immune response and, as proposed in this work, to enhanced tumor proliferation and increased metastatic potential._An in vivo model that retains intact inducible nitric oxide synthase (iNOS) expression could provide valuable insight into the role of iNOS in modulating both immune dynamics and disease progression. Notably, in this work, it has been detected iNOS expression in the murine epithelial ovarian cancer (MEOC) cell line ID8, particularly in response to proinflammatory cytokine stimulation, making this cell line an interesting candidate for further in vivo studies in an in vivo model where the immune system might play a key role in the release of cytokines. Having the chance of studying an in vivo model which can specifically investigate the immune regulation and tumor progression, makes the ID8 syngeneic in vivo model a solid choice to investigate the role of iNOS in ovarian cancer. In addition to these factors, ID8 murine ovarian cancer cell lines are widely used for the purpose of studying ovarian cancer and its progression in immunocompetent mice [246, 252, 253]. This cell line has extensively been engineered for the expression of some reporters gene like Luciferase, RFP or GFP allowing to study the tumor from the development at the earlier stages up to the latest stages and the development of ascites [246]. Another important factor that can be obtained with this model and not in other in vivo systems is the development of ascites [254] and the characterization of the immune niche into them. The development of this peculiar factor is indicative of the last stage of the disease, similarly to what happens into human patients and represents a source of information about the cell population contained into this extravasation fluid [255]. Developing an in vivo model that faithfully recapitulates the key pathophysiological features of ovarian cancer is critical for translational research. The ID8 syngeneic ovarian cancer model not only mirrors essential aspects of human disease, including tumor growth, ascites formation, and an intact immune microenvironment, but also provides a robust platform for therapeutic evaluation. This model allows for initial assessment of cisplatin efficacy, a key chemotherapeutic agent in ovarian cancer treatment. Importantly, it also facilitates investigation of combination therapies aimed at modulating the tumor microenvironment. For instance, L-NMMA, a potent inhibitor of iNOS, has been extensively studied in preclinical models of triple-negative breast cancer, characterized by elevated iNOS expression, at the Houston Methodist Research Institute under Dr. Jenny Chang's laboratory [157]. Given the role of iNOS in ovarian cancer progression and chemoresistance, combining cisplatin with L-NMMA in the ID8 model represents a promising strategy to disrupt the tumor microenvironment, potentially enhancing therapeutic efficacy and overcoming drug resistance. The option of combining Cisplatin and L-NMMA in ovarian cancer represents an insight which should be considered following the proof provided in the previous chapter about the expression of iNOS in ovarian cancer cell lines together with the well-known iNOS expression from immune cell line components such as macrophages [256] and other different immune cell subtypes [257, 258].

3.1.1 Aims and objective

A combinatorial treatment strategy has been developed by using a syngeneic in vivo ovarian cancer model to study tumor progression, metastasis, and the transition of the tumor immune microenvironment (TIME) from "cold" to "hot." To achieve this, an intraperitoneal injection of the ID8-Luc murine ovarian cancer cell line has been employed, monitorin early-stage tumor development and evaluate treatment effects on metastasis, immune system activation, and physical parameters such as abdominal volume and body weight.

3.2 Materials and methods

Animal model. Training in animal handling procedures for murine models was conducted at the Houston Methodist Research Institute (animal facility, 6670 Bertner Avenue). The training followed institutional requirements and included instruction on cage maintenance, food and water replacement, and euthanasia procedures. All animal protocols for the experiments were approved by the Houston Methodist Hospital Research Institute Animal Care and Review Office (IACUC number IS00007220). ID8 (Millipore Sigma®, Cat. SCC145) and ID8Luc (Creative Biolabs®, Cat. IOC-ZP310) cell lines were regularly cultured at 37ºC in 5% CO2 in High Glucose DMEM with 4% FBS, 1% of Penycillin/Streptomicin and ITS Liquid Media Supplement (Millipore Sigma® Cat. I3146). C57BL/6 mice 6 weeks old female were purchased from Jackson Laboratory. Mice received intraperitoneal (IP) injection of 5 x 10’6 ID8-Luc cells in 200 µL of PBS. Luminescence signals were analysed using Perkin IVIS Spectrum CT with Luminescence detection in automatic mode. Mice were treated daily with L-NMMA, receiving 400 mg/kg at the start of each treatment cycle, followed by 200 mg/kg on subsequent days. Based on previous studies investigating L-NMMA use in both in vivo and clinical settings, stabilization of blood pressure following L-NMMA treatment was achieved by administering amlodipine at a concentration of 1 mg/mL. Cisplatin was administered once weekly at a dose of 2 mg/kg. Mice body weight was detected using a regular laboratory balance and the abdomen diameter with a regular caliper. Mice were monitored for tumor growth and overall health, with body weight measured regularly using a laboratory balance. Bioluminescence signals from labeled cells were analyzed using the Perkin Elmer IVIS Spectrum CT under automatic luminescence detection mode. The experiment was conducted using n = 7 mice per group (control, L-NMMA treatment, cisplatin treatment, and cisplatin

+ L-NMMA treatment). Animals were sacrificed at the study endpoint (12 weeks), in accordance with the previously cited publication and in-house optimization of the model, coinciding with the development of ascites..

Ascites immune profiling. The following mouse antibodies were used for flow cytometry analysis of lymphoid ascites collected from C57BL/6 mice at the experimental endpoint. Samples were processed fresh on the same day as euthanasia. Red blood cells were lysed, and a portion of the remaining cells were reserved for immunoblotting, while the rest were analyzed by flow cytometry. The following antibody panel was used to characterize immune lymphoid cells. The following mouse antibodies were used in a flow cytometry for analyzing mouse lymphoid cells FITC-CD8a (Tonbo, ref. #35-0081-U025), PerCP-Cy5.5-TCR-β (Tonbo, ref. # 65-5961-U025), PE-Cy5-CD25 (Tonbo, ref. # 50-0621-U025), PE-CD62L (Tonbo, ref. # 55-0251-U025), PE-Cy7-CD44 (Tonbo, ref. # 60-0441-U025), APC-Cy7-CD3 (Tonbo, ref. # 25-0032-U025), BV421-NK-1.1 (BDBiosciences, ref. # 562921), violetFluor 500-CD45 (Tonbo, ref. # 85-0451-U025), cFluorV610-CD4 (Cytek, ref. # R7-20270), BV650-CD159a (BDBiosciences, ref. # 755252), CD127 (BDBiosciences, ref. # 567540), Ghost Dye Violet540 (Tonbo, ref. # 13-0879-T100), TruStain FcX™ (CD16/32) (BioLegend, ref. # 101320). The myeloid panel was composed by FITC-CD80 (Tonbo, ref. # 35-0801-U025), PerCP-Cy5.5-Ly-6c (Tonbo, ref. # 65-5932-U025), PE-F4/80 (Tonbo, ref. # 50-4801-U025), PE-Cy5-CD86 (BioLegend, ref. # 105015), PE-Cy7-CD11c (Tonbo, ref. # 60-0114-U025), APC-R700-CD11b (BDBiosciences, ref. # 564985), APC-CD40 (BioLegend, ref. # 124611), APC-R700-MHCII (Tonbo, ref. # 25-5321-U025), violetFluor450-Ly-6G (Cytek, ref. # 75-1276-U025, Ghost Dye Violet540 (Tonbo, ref. # 13-0879-T100), TruStain FcX™ (CD16/32) (BioLegend, ref. # 101320). The experiment was performed with a number of n=7 mice per group and the results were considered statistically significant when $p < 0.05$.

Image analysis. H&E slides from mice tissues were scanned as whole slide images (TIFF based format) using a 20X objective with a DP200 scanner (Roche Diagnostics). The images were then analysed using QuPath open-source software* version Version: 0.5.1. Tumor deposits were identified and annotated by a Consultant/Attending level Clinical Histopathologist (SH). Thereafter the cell detection parameters were set at default. A binary classifier type which was trained to identify tumor cells and lymphocytes was applied within the annotated areas (tumor spots) on the image to prevent overcalling of other cells including mesothelial or other tissue as tumor cells. The tumor areas, tumor cell count, total area and total cell count were calculated based on default cell parameters in QuPath and the classifier as described. Mitotic counts were assessed visually out as per standard clinical assessment using 10 high power fields. Lymphovascular invasion was also assessed by visual assessment of the slide by a Consultant/Attending level Clinical Histopathologist. The analysis was conducted with the contribution of Dr. Sean Hynes, Dr. Fidelma Kaar and Dr. Adam Freegrove from the department of Histopathology, Galway University Hospital, Ireland and the discipline of Pathology, University of Galway, Ireland. Experiments were conducted with n = 7 mice per group, with five slides prepared per tissue from each individual mouse sample. The results were considered statistically significant when $p < 0.05$.

Immunoblotting. Whole-cell lysate was extracted using Cell Signaling lysis buffer (20 mM Tris-HCl (pH 7.5), 150 mM NaCl, 1 mM Na2EDTA, 1 mM EGTA, 1% Triton, 2.5 mM sodium pyrophosphate, 1 mM beta-glycerophosphate, 1 mM Na3VO4, 1 µg/ml leupeptin, Cat #9803). Proteins were separated by SDS-PAGE gel and transferred to a PVDF membrane (Millipore Sigma, Cat #NX0095). The membranes were blocked with 5% non-fat milk and incubated with primary antibody overnight at 4°C with gentle agitation using the following antibody: rabbit anti-human iNOS (1:1000, Cell Signaling, Cat #95423), rabbit anti-β-Actin HRP conjugate (1:7000, Cell Signaling, Cat#5125). Signals from iNOS was detected and amplified by using a secondary anti-rabbit HRP-conjugated antibody (1:3000, Cell Signaling, Cat #7074). Luminescence from antibodies was amplified using Clarity ECL Western Blotting Substrates from Bio-Rad (Cat #1705060S). Experiments were performed in triplicate unless otherwise specified and considered statistically significant when $p < 0.05$).

Cytokine mix administration. Cells were cultured under regular cell culture conditions. In order to stimulate iNOS expression, a cytokine mix composed by IFN-γ (25 ng/mL, Peprotech # 315-05-100UG), TNF-α (10ng/mL, Peprotech # 315-01A-20UG), IL1-β (10 ng/mL, Peprotech # 211-11A-10UG) was administered. Cytokine mix was administered only once and cells were maintained in culture after the cytokine administration for 72 hours.

Statistical analysis

Two-way analysis of variance (ANOVA) or ordinary one-way ANOVA, when possible, was performed using GraphPad Prism version 7.0 (GraphPad Software, San Diego, CA) to evaluate the effects of two independent factors and their interaction on the dependent variable. Prior to analysis, data were checked for normality and homogeneity of variances. When significant effects were detected, multiple comparisons were conducted using Tukey's test to identify specific group differences. Results were considered statistically significant at $p < 0.05$.

3.3 Results

3.3.1 Syngeneic model optimisation

The syngeneic in vivo model has been conducted by using the C57BL/6 mice strain, an immunocompetent mouse strain which received an injection of a MEOC cell line, ID8. ID8 is a well know cell line used for studies in ovarian cancer [246]. The expression of iNOS in this murine epithelial cell line has not been clearly documented, indicating a gap in the scientific literature. Therefore, we chose to stimulate this cell line with a cytokine mix composed by IFN-γ (25 ng/mL), TNF-α (10 ng/mL). IL1-β (10 ng/mL), based on findings from human cell lines discussed in the previous chapter, to determine whether it is capable of expressing iNOS and responding to well-known inflammatory stimuli that typically induce iNOS expression [184, 198, 259, 260]. In the following figure (**Figure 3.2**), it is shown that ID8 cell line responds to proinflammatory stimuli producing iNOS after the administration of cytokines

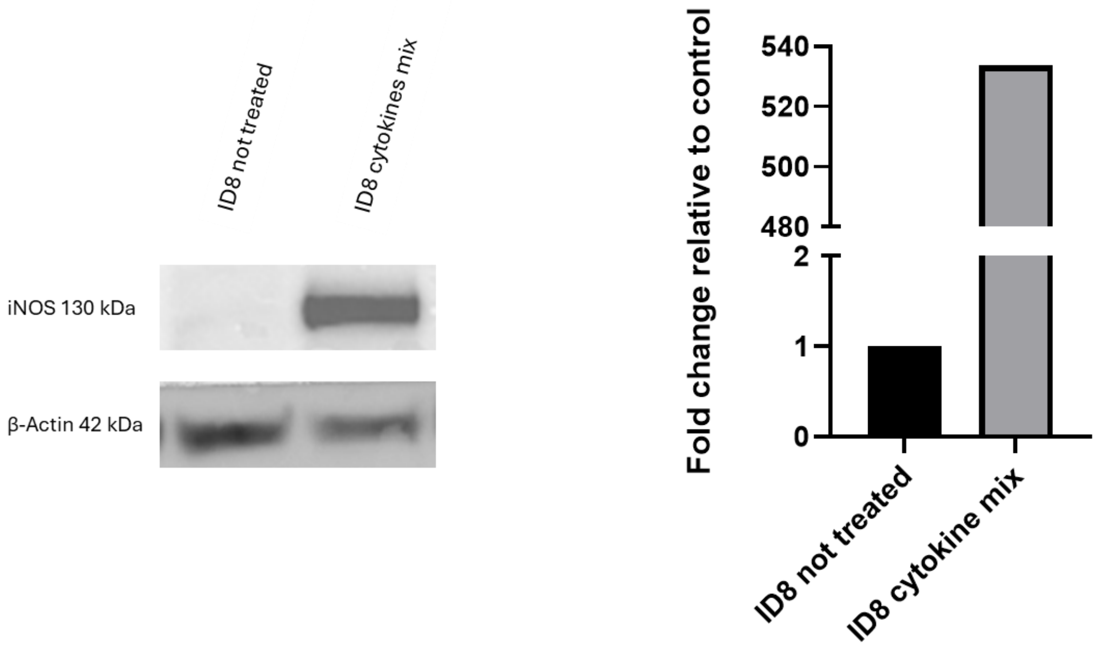

Figure 3.2. ID8 cell line is responsive to proinflammatory stimuli. The figure shows the expression of iNOS obtained after stimulating ID8 cell line with cytokines mix known to induce iNOS expression. The administration of cytokines mix was able to induce a high iNOS expression. Cytokine mix was composed by (IFN-γ (25 ng/mL), TNF-α (10 ng/mL). IL1-β (10 ng/mL).

After detecting the expression of iNOS in the cell line designated for this study, female C57BL/6 mice, 6 weeks old, have been used to conduct the following pilot study. The experiment design is reported in the figure below (**Figure 3.3**).

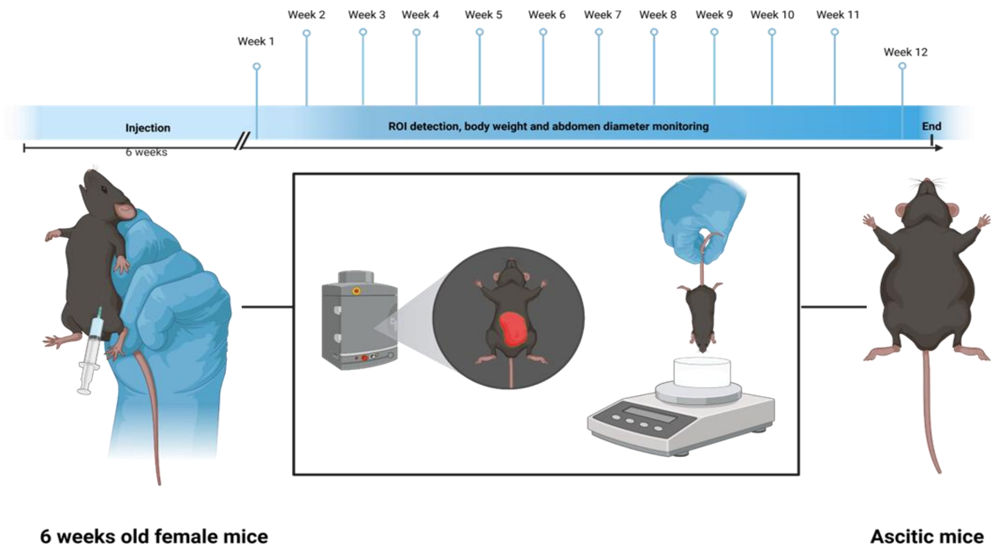

Figure 3.3. Syngeneic in vivo model optimization. Experiment setup showing the beginning of the experiment at week 0 with the injection of murine cancer cells through the constant detection of Region of interest (ROIs) and body weight until the endpoint where ascitic mice were obtained. Created in https://BioRender.com.

The injection has been conducted accordingly to publications related to IP injection of cancer cells with the aim to simulate the late stage of ovarian cancer where ascites is formed. 5 x 10'6 cells were injected IP [246] and were able to show at the experiment endpoint the formation of ascites and the increase of body weight and abdomen diameter.

3.3.2 Body weight and abdomen diameter increase over the weeks

In the syngeneic *in vivo* model used in this study, a consistent increase in body weight was observed from the point of tumor cell injection (week 0) through the endpoint (week 11), suggesting progressive tumor growth and ascites formation. The average body weight of the mice at the time of injection was 19.41 g. Subsequent weekly measurements showed the following increases: week 1 – 20.75 g, week 2 – 21.18 g, week 3 – 21.09 g ($p < 0.05$), week 4 – 21.35 g ($p < 0.05$), week 5 – 21.78 g ($p < 0.05$), week 6 – 22.60 g ($p < 0.05$), week 7 – 22.59 g ($p < 0.05$), week 8 – 24.24 g ($p < 0.05$), week 9 – 24.94 g ($p < 0.05$), week 10 – 25.80 g ($p < 0.05$), and week 11 (endpoint) – 28.28 g ($p < 0.05$). These results reflect the gradual accumulation of fluid and tumor burden associated with advanced disease progression (**Figure 3.4A**). In parallel with the increase in body weight, a progressive enlargement of the abdominal diameter was also observed, consistent with ascites development. The abdominal distension became apparent starting from week 6, when the average abdominal diameter was 6.54 cm. A slight decrease was noted at week 7 (6.52 cm), but a marked increase followed in subsequent weeks: 7.35 cm at week 8 ($p < 0.05$), 7.58 cm at week 9 ($p < 0.05$), and 7.50 cm at week 10 ($p < 0.05$). By the endpoint at week 11, the abdominal diameter reached an average of 7.92 cm ($p < 0.05$). These measurements support the conclusion that ascites accumulation contributed significantly to the observed body weight gain and abdominal swelling in the late stages of disease progression (**Figure 3.4B**).

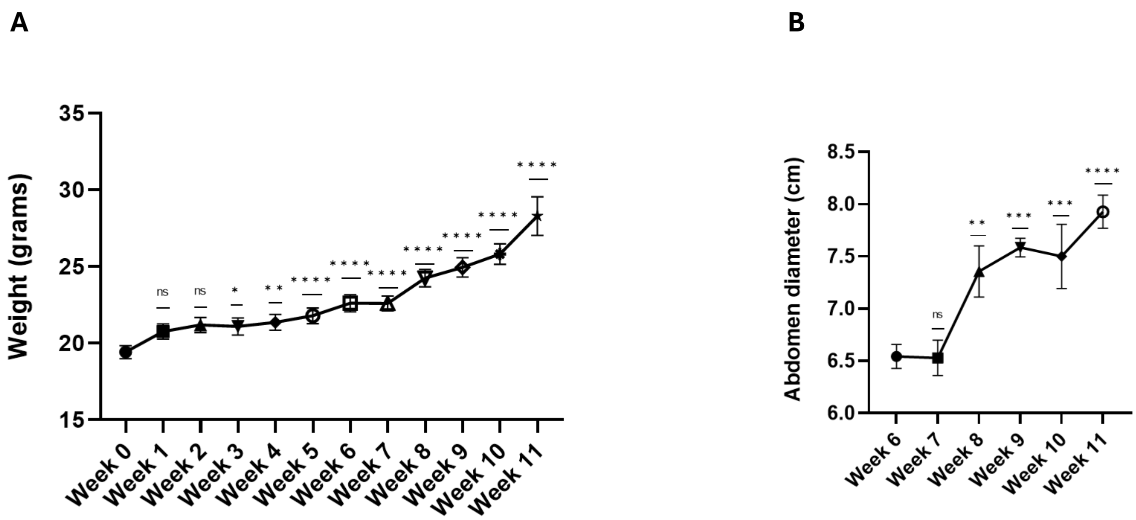

Figure 3.4(A-B). Morphological parameters showed an accumulation of body fluids and an increase in body weight. Figure 3.4A shows the body weight increase week by week in C57BL/6 mice which received an injection of 5 x 10'6 ID8 cells in 200 µL of PBS. A consistent increase in body weight was observed from the point of tumour cell injection (week 0) through the endpoint (week 11), suggesting progressive tumour growth and ascites formation. The average body weight of the mice at the time of injection was 19.41 g. Subsequent weekly measurements showed the following increases: week 1 – 20.75 g, week 2 – 21.18 g, week 3 – 21.09 g ($p < 0.05$), week 4 – 21.35 g ($p < 0.05$), week 5 – 21.78 g ($p < 0.05$), week 6 – 22.60 g ($p < 0.05$), week 7 – 22.59 g ($p < 0.05$), week 8 – 24.24 g ($p < 0.05$), week 9 – 24.94 g ($p < 0.05$), week 10 – 25.80 g ($p < 0.05$), and week 11 (endpoint) – 28.28 g ($p < 0.05$). Results were considered significant with $p < 0.05$. **Figure 3.4B** shows the abdomen diameter in mice detected week by week (starting from week six, where an increase has been observed). The abdominal distension became apparent starting from week 6, when the average abdominal diameter was 6.54 cm. At week 7 a little reduction was observed (6.52 cm), but a significant increase

was observed at week 8 corresponding to 7.35 cm ($p < 0.05$). 7.58 cm were registered at week 9 ($p < 0.05$), and 7.50 cm at week 10 ($p < 0.05$). By the endpoint at week 11, the abdominal diameter reached an average of 7.92 cm ($p < 0.05$).

3.3.3 Metastasis accumulation simulates the late stage of ovarian cancer

At the endpoint of the treatment (week 12) the peritoneum and abdominal cavity of the sacrificed mice were carefully examined. We observed widespread metastases throughout the peritoneal lining as well as within the abdominal cavity. Metastatic lesions were found at multiple sites on the peritoneum (**Figure 3.5 A**), varying in size, which likely reflects different timing and progression of cancer cell invasion into the peritoneal cavity. Notably, several abdominal organs exhibited diffuse metastases (**Figure 3.5 B-C**). The omentum showed numerous metastatic nodules dispersed across this fatty layer. Additional metastatic foci were detected in the stomach and intestines, along with micrometastases in the liver. Corresponding to these findings, serial observations and images revealed a progressive increase in abdominal volumes over the weeks, consistent with substantial ascites accumulation.

A B C

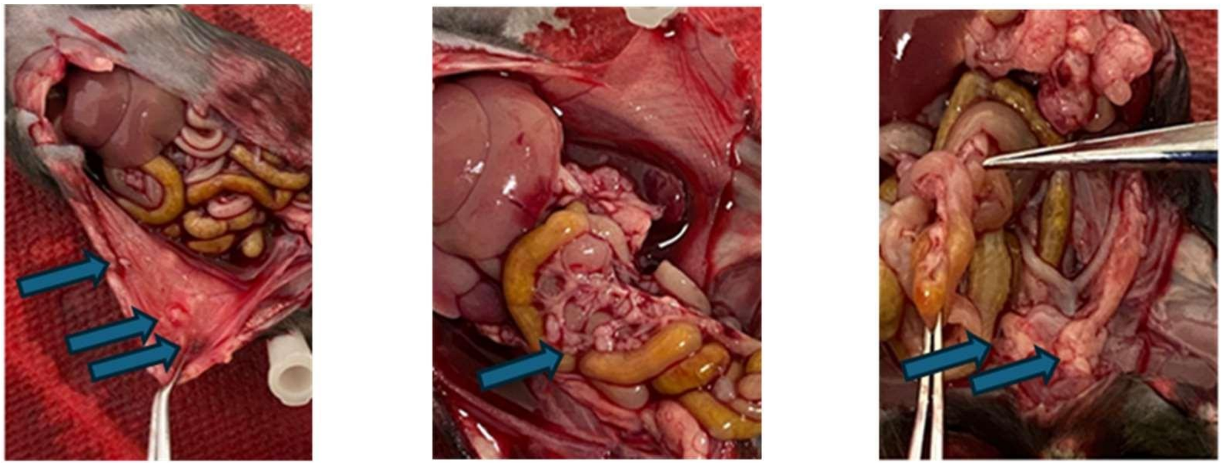

Figure 3.5(A-C). Peritoneum and omentum collected at the endpoint show a high grade of metastasis formation. In **Figure 3.5A**, it is possible to observe (as indicated by the arrows) the presence of metastasis in the peritoneum. **Figures 3.5B and 3.5C** show the accumulation of metastatic lesions in abdominal organs (as indicated by the arrows).

3.3.4 iNOS is expressed in the ascites

To detect NOS2 expression in this in vivo model, and considering the abundant ascitic fluid where cancer cells, immune cells, and tumor spheroids accumulate [261], iNOS expression in ascites samples has been analyzed. Our Controls included a human High-Grade Serous Ovarian Cancer cell line (OVCAR8) and the same cell line treated with NOS2-specific siRNA as a negative control. Samples labeled #1, #2, and #3 exhibited NOS2 expression consistent with our positive control (**Figure 3.6**). It is important to highlit that both human iNOS and murine iNOS shown in the following picture were detected using a human antibody anti-iNOS from Cell Signaling (Cat.Ref. E2M9F).

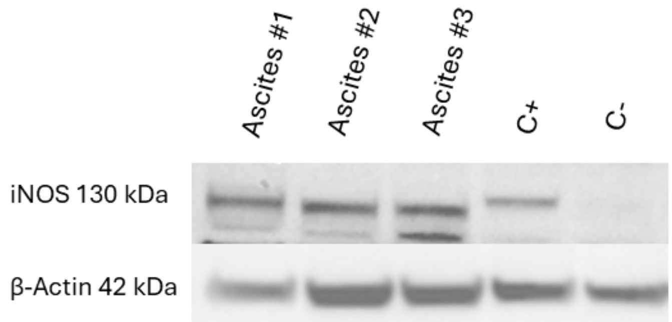

Figure 3.6. Detection of iNOS expression in ascites samples from three mice samples. It is possible to observe as cells recovered from the ascitic fluid from three mice samples, showed iNOS expression. OVCAR8 cells served as positive control, while OVCAR8 cells treated with siRNA targeting iNOS2 were used as the negative control to confirm specificity of the signal.

3.4 Experimental design and treatment regimens in the ID8 syngeneic in vivo model

Based on the characteristics observed during the generation and optimization of the ID8 syngeneic in vivo model, particularly the timing of ascites accumulation, changes in body weight, and progression of abdomen diameter, a four-arm experimental study to evaluate different treatment options was designed. The groups included a control group, in which mice received intraperitoneal (IP) injection of ID8 cells without subsequent treatment; an L-NMMA treatment group, receiving daily L-NMMA administration; a Cisplatin treatment group, receiving Cisplatin only; and a combination treatment group, treated with both Cisplatin and L-NMMA. Treatment began at week 5 post-ID8 cell injection, one week prior to the onset of ascites accumulation as indicated by abdomen diameter measurements from the optimization study. Cisplatin was administered intraperitoneally at a dose of 2 mg/kg every two weeks starting at week 5. L-NMMA was given daily with a dosing regimen of 400 mg/kg on the first day of each week, followed by 200 mg/kg on subsequent days. This treatment schedule was designed to investigate the therapeutic efficacy of L-NMMA alone, Cisplatin alone, and their combination on tumor progression and ascites development in the ID8 model (**Figure 3.7**).

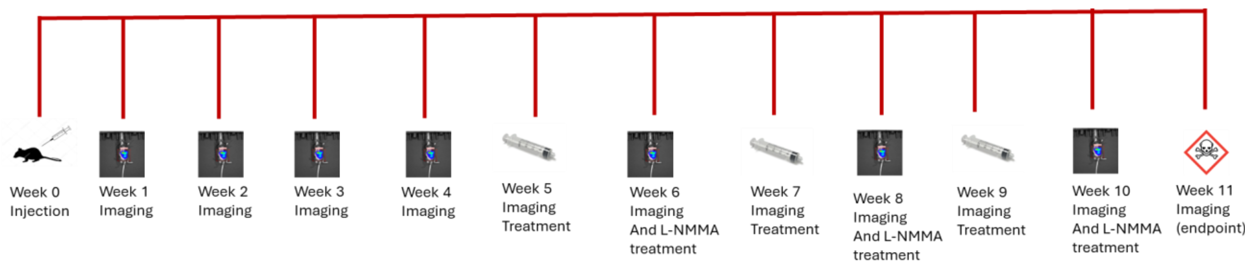

Experimental groups

- Not treated (Cells intraperitoneal injection only)
- Cisplatin treatment (Intraperitoneal injection)
- L-NMMA treatment (Intraperitoneal injection)
- Cisplatin + L-NMMA (Intraperitoneal injection)

Treatments

- **Cisplatin treatment:** One administration every two weeks (**2 mg/kg**)
- **L-NMMA treatment:** Daily treatment (Monday to Friday) starting from week 5 – **400 mg/kg** day 1 (beginning of every week), **200 mg/kg** from day 2 (second day of every week)

Figure 3.7. Experimental design for the syngeneic in vivo model. Experimental design showing the time point of the treatments, experimental groups and the treatment per single group. Three Cisplatin and L-NMMA cycle treatments have been used. The experiment was divided into four arms starting with control group, L-NMMA group, Cisplatin group and a combination between Cisplatin and L-NMMA.

3.4.1 Body weight changes following treatment with L-NMMA, Cisplatin, and their combination

Following administration of the different treatment regimens, L-NMMA alone, Cisplatin alone, and the combination of Cisplatin and L-NMMA, mice's body weight over time was monitored. The following body weight trends are reported: the untreated group (**Figure 3.8A**) showed a general increase in average body weight, starting at 20.32 grams at week 5 and rising to 24.9 grams by week 10. This weight gain likely reflects tumour progression and ascites accumulation. The mice treated with L-NMMA alone (**Figure 3.8B**) displayed a similar pattern to the untreated group, with body weight increasing from 21.12 grams at week 5 to 25.1 grams at week 10, indicating that L- NMMA alone did not significantly inhibit tumour growth or ascites development. Mice receiving Cisplatin alone (**Figure 3.8C**) exhibited a little overall increase in body weight among all groups. Their average body weight decreased from 21.12 grams at week 5 to 19.82 grams at week 6, followed by partial recovery and fluctuations over the subsequent weeks, ultimately reaching 23.4 grams at week 10. This pattern of weight loss followed by partial recovery suggests that Cisplatin treatment could potentially have an impact on both tumour progression and the overall physiological status of the mice. The combination treatment group (**Figure 3.8D**) reported a slower increase of body weight when compared to all groups. Their average body weight rose from 20.32 grams at week 5 to 23.0 grams at week 10. This weight gain might indicate a beneficial effect in the combination of Cisplatin and L-NMMA treatment in slowing disease progression and ascites accumulation relative to single-agent treatments or no treatment.

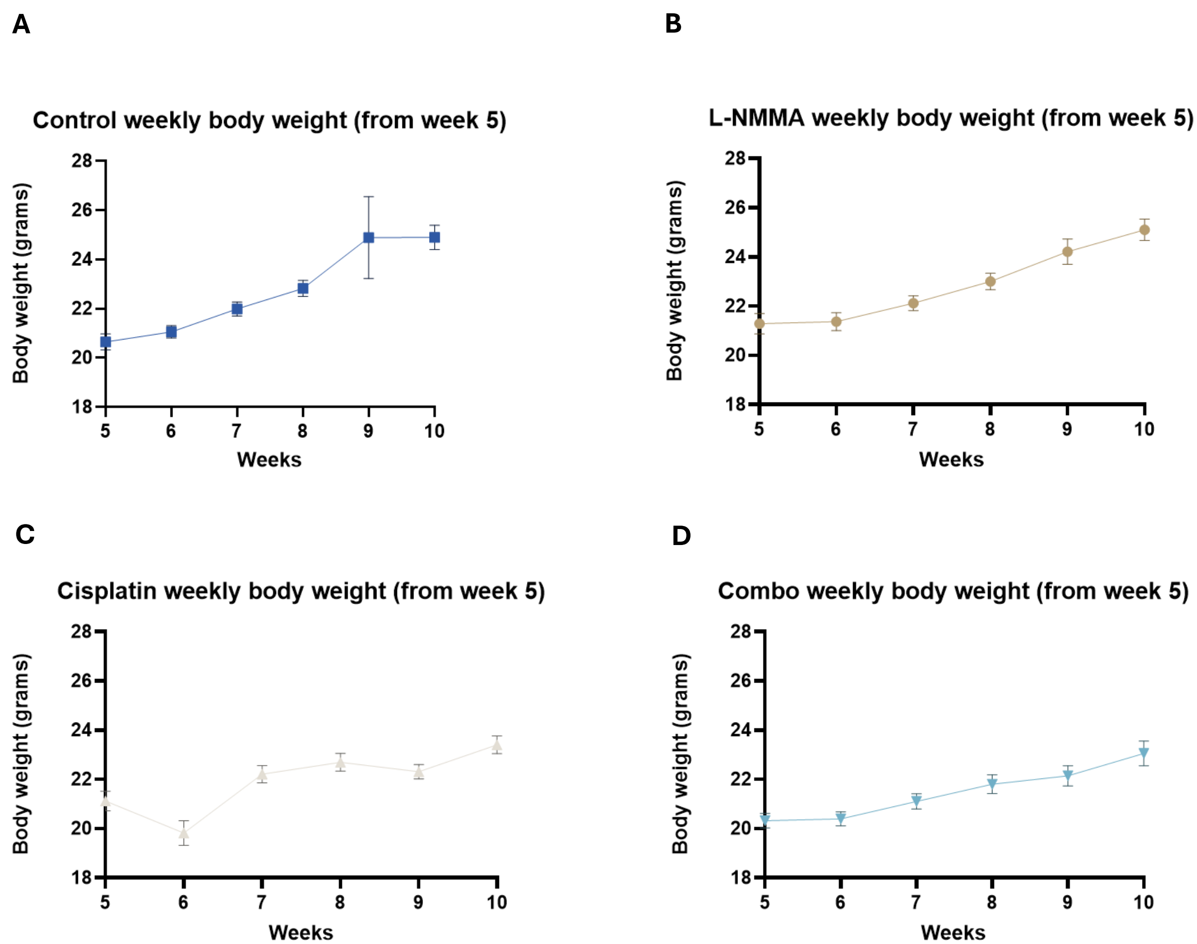

Figure 3.8 (A–D). Body weight trends across different experimental groups over time. **Figure 3.8A** depicts the body weight of the control group, which received no treatment and only cell injections, starting from week 5, the time point when treatments began in the other groups. It is possible to observe an increase in average body weight, starting at 20.32 grams at week 5 and rising to 24.9 grams by week 10. **Figure 3.8B** shows the body weight changes in mice treated with L-NMMA. The pattern was similar to the untreated group, with body weight increasing from 21.12 grams at week 5 to 25.1 grams at week 10. .**Figure 3.8C** illustrates the weight trend for the Cisplatin-treated group. Their group average body weight decreased from 21.12 grams at week 5 to 19.82 grams at week 6, ultimately reaching 23.4 grams at week 10.. **Figure 3.8D** presents the body weight progression in the group receiving the combination treatment, where their average body weight rose from 20.32 grams at week 5 to 23.0 grams at week 10.

Analysis of the body weight curves across all treatment groups revealed that the combination of Cisplatin and L-NMMA resulted in the slowest increase in body weight over time. This group exhibited a reduction in weight gain compared to the untreated control as well as the groups treated with either L-NMMA or Cisplatin alone. Both the control and L-NMMA groups showed a higher increase in body weight, consistent with tumor progression and ascites accumulation. The Cisplatin-only group displayed fluctuations characterized by periods of weight loss and a slower overall increase in body weight. In contrast, the combination therapy group demonstrated the most controlled and gradual body weight gain, suggesting a potential beneficial inluence of combining Cisplatin and L-NMMA inin the attenuation of the disease progression and associated ascites. This comparative analysis underscores the enhanced therapeutic efficacy of combining Cisplatin with L-NMMA in the syngeneic ID8 ovarian cancer model, as reflected by the collective body weight trends (**Figure 3.9**).

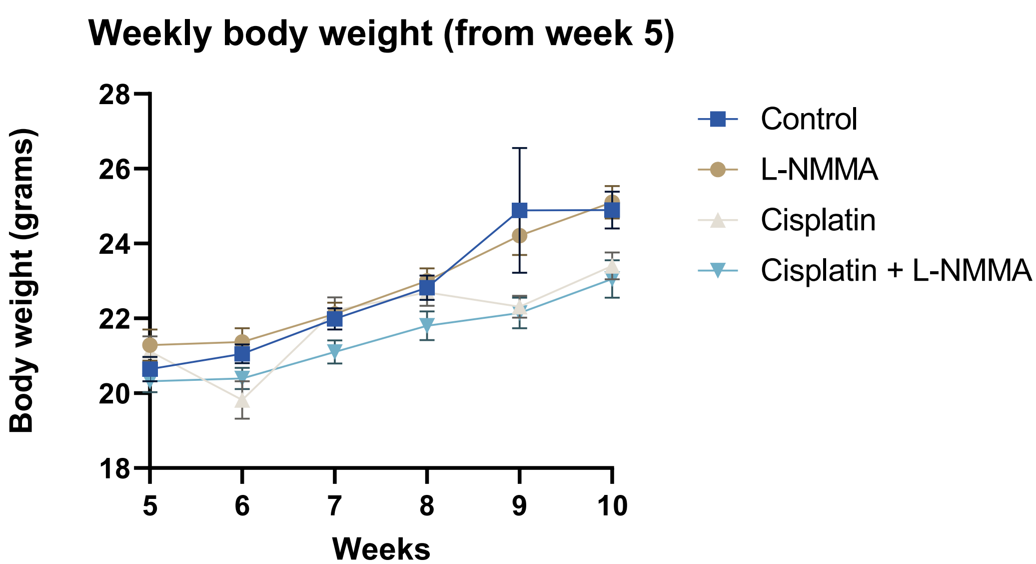

Figure 3.9. Body weight trends comparison per single arm treatment. Body weight trends for each treatment group. L-NMMA alone has minimal impact on body weight, whereas both the Cisplatin and the combination Cisplatin + L-NMMA groups exhibit a reduction in body weight.

The body weight curve showed a decrease following two distinct trends. The L-NMMA and control groups exhibited a similar reduction in body weight by the endpoint. In contrast, the Cisplatin and Cisplatin + L-NMMA groups followed a different trend, with both showing a more pronounced weight loss due to a smaller abdominal volume, as it will be shown in the next section. Notably, these latter groups had the lowest body weight compared to the L- NMMA and control groups, highlighting the impact of chemotherapy on ascites formation and tumour progression. However, no significant difference was observed between the Cisplatin and Cisplatin + L-NMMA groups at this stage.

3.4.2 Abdomen diameter changes following treatment with L-NMMA, Cisplatin, and their combination

In addition to monitoring body weight, it was also measured the abdomen diameter of the mice throughout the treatment period to assess ascites progression, a hallmark of the ID8 syngeneic model characterized by significant accumulation of ascitic fluid. Tracking abdomen diameter thus serves as a critical indicator of both disease progression and treatment efficacy. In the untreated control group (**Figure 3.10A**), abdomen diameter gradually increased over time, starting at 7.00 cm at week 5 and peaking around week 8 at 7.50 cm, followed by a slight decrease in the final weeks. This trend reflects progressive ascites accumulation, with the minor reduction possibly due to biological variability or other physiological factors. Similarly, the L-NMMA treated group (**Figure 3.10B**) exhibited comparable fluctuations in abdomen diameter, with decreases and increases at various time points, including a peak diameter of 7.78 cm at week 9. These variations suggest that while L-NMMA may transiently influence ascites accumulation, it does not consistently prevent the increase in abdomen diameter characteristic of fluid buildup. In contrast, the Cisplatin-treated group (**Figure 3.10C**) displayed a distinct pattern characterized by an overall reduction in abdomen diameter during the treatment period. Beginning at 7.25 cm at week 5, the diameter decreased to 6.36 cm by week 7, with minor fluctuations thereafter, ultimately reaching 6.64 cm at week 10, below the baseline measurement. This trend indicates that Cisplatin had a potential role in limiting ascitic fluid accumulation relative to untreated and L-NMMA groups. The combination treatment group (Cisplatin + L-NMMA) (**Figure 3.10D**), showed a decreasing trend throughout the study despite an increase at week 9. Starting from 6.9 cm at week 5, the diameter declined to 6.22 cm ($p < 0.05$) by week 10. These data collectively indicate that the combination therapy produced the strongest reduction in abdomen diameter and, consequently, ascites accumulation among all treatment groups.

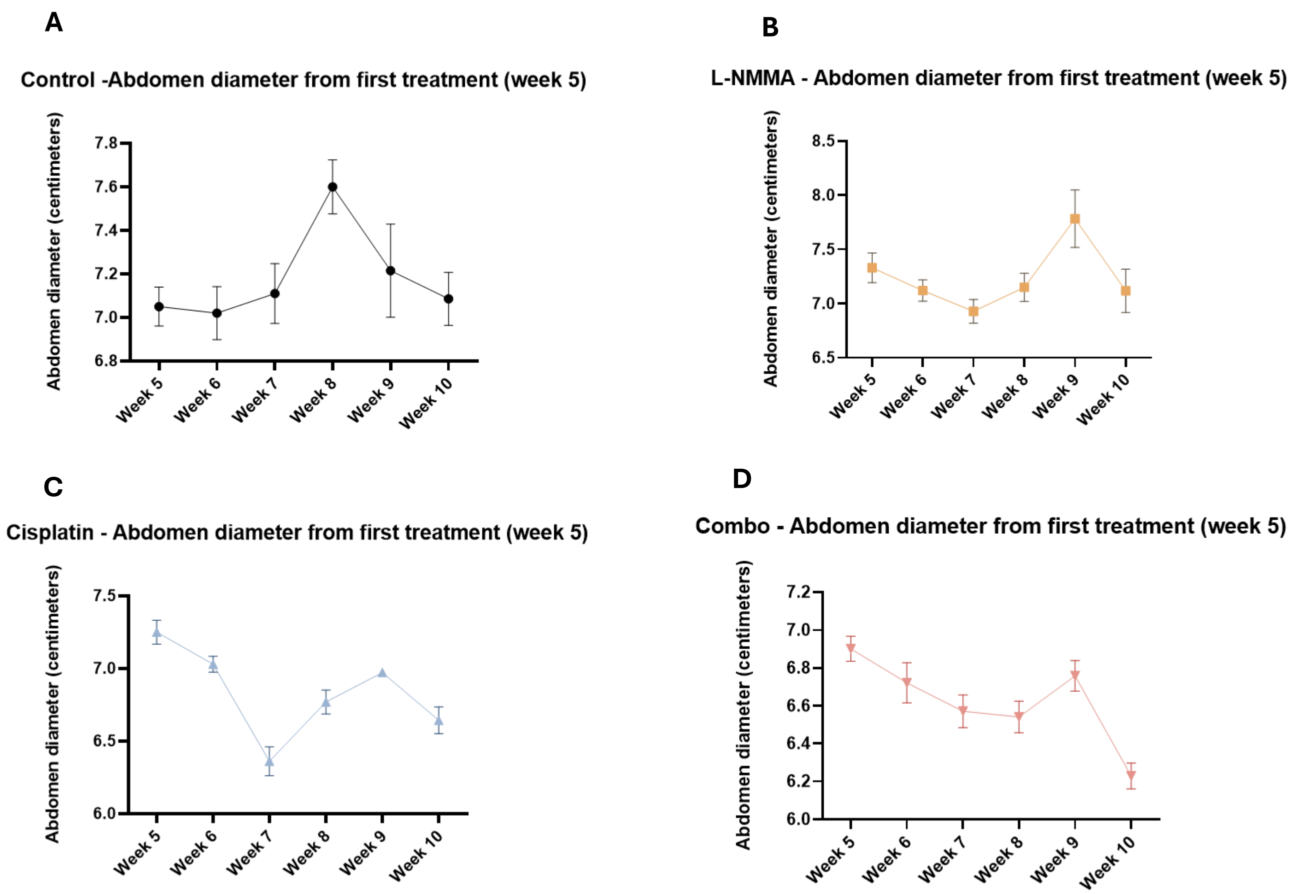

Figure 3.10 (A–D). Abdomen diameter trends over time for each treatment group. In **Figure 3.10A**, the control group shows a consistent abdomen diameter remaining above 7 cm throughout the study. In particular, the abdomen diameter increased over time, starting at 7.00 cm at week 5 and peaking around week 8 at 7.50 cm, followed by a decrease in the final two weeks. **Figure 3.10B** shows the trend of the L-NMMA group, wherethe abdomen diameter at the starting point is less than 7,50 cm and even by including a peak diameter of 7.78 cm at week 9, the diameter comes back to slightly more than 9 cm at the endpoint. **Figure 3.10C** shows that Cisplatin treatment reduces the abdomen diameter to below 7 cm. Beginning at 7.25 cm at week 5, the diameter decreased to 6.36 cm by week 7, ultimately reaching 6.64 cm at week 10.**Figure 3.10D** reveals that the combination treatment further decreases the abdomen diameter to under 6.3 cm. In particular, starting from 6.9 cm at week 5, the diameter declined to 6.22 ($p < 0.05$) cm by week 10.

When comparing the abdomen diameter curves across all treatment groups, the combination therapy (Cisplatin + L-NMMA) produced the most sustained reduction in abdomen diameter over time. This decrease was more impactful in particular at the endpoint, where the control group and L-NMMA had an abdomen diameter higher than 7 cm, the Cisplatin group higher than 6.5 cm and the combination group reached the diameter of 6.3 cm ($p < 0.05$). These results highlight a potential beneficial efficacy of the combinatorial treatment in limiting ascites accumulation, a hallmark of disease progression in the ID8 syngeneic ovarian cancer model (**Figure 3.11**).

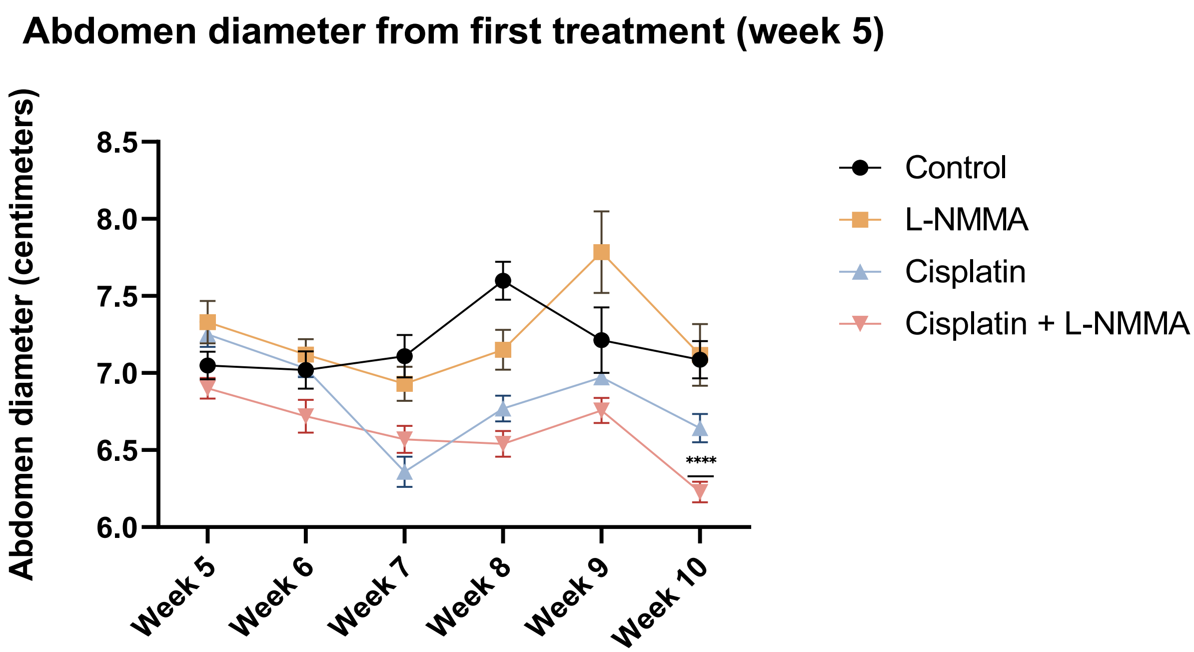

Figure 3.11. Abdomen diameter trends comparison per single arm treatment. This figure presents the abdomen diameter trends for all treatment groups combined. It clearly demonstrates that the combination treatment produced the most pronounced reduction in abdomen diameter, during week 10, compared to the other groups.

When analyzed collectively, a clear distinction emerges between the groups. Specifically, the abdominal diameter trend reveals three distinct patterns. The first, which shows the largest abdominal diameter, corresponds to the control and L-NMMA groups. Similar to the body weight trend, these groups exhibit an abdominal diameter exceeding 7 cm by the endpoint. A different trend is observed in the Cisplatin group, which shows a reduction in abdominal diameter compared to the control and L-NMMA groups, although it does not fall below 6.5 cm. As previously mentioned, the Cisplatin + L-NMMA group demonstrates a higher reduction, with abdominal diameter reaching a minimum of 6.22 cm at the endpoint ($p < 0.05$).

3.4.3 Mice grouping and injection were consistent

As mentioned above, the experiment was conducted by dividing mice into four groups. This in vivo tumor model represents late-stage ovarian cancer characterized by widespread metastasis throughout the peritoneum and abdominal organs. Due to the diffuse nature of tumor spread, traditional measurements of solid tumors are not applicable. Instead, tumor nodules were detected using bioluminescent imaging.

For this purpose, the murine epithelial ovarian cancer cell line ID8 was genetically engineered to express Luciferase, enabling direct detection of ROIs from the intraperitoneally (IP) injected cells. Following injection, bioluminescence signals were monitored weekly to track tumor dissemination within the abdominal cavity and assess progression over time. As will be discussed later, a major reduction in tumor signal was observed in the Cisplatin + L-NMMA and Cisplatin alone treatment groups, consistent with the trends seen in body weight and abdomen diameter measurements. Importantly, in line with previous model optimization, a peak in bioluminescence signal was observed after week 5. The bioluminescence data collected until week 5 were used to form homogeneous groups prior to initiating treatment. Tumor progression during this pre-treatment period followed the expected trend, allowing for balanced distribution of tumor burden across the four experimental arms at the start of therapy. At week 5, on the day of treatment assignment, the mice were divided into groups based on their last recorded bioluminescence maintaining an equal and consistent signal among the new formed groups to start treatments without any bias (**Figure 3.12**).

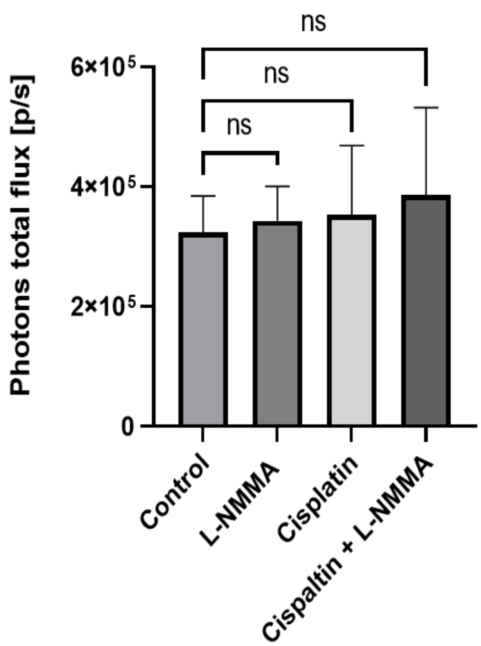

Figure 3.12. ROI level per group at the beginning of the treatments. The ROIs were consistent and equivalent across all groups before starting treatments. For all the considered group, the ROIs were between 4 x 10'5 and 2 x 10'5 with a p value > 0.05.

Mice were divided based on equal ROI values to ensure comparable tumor burden and peritoneal spread across groups, allowing treatment to begin from equivalent baseline conditions and ensuring unbiased, consistent results.

3.4.4 Cisplatin and Cisplatin +L-NMMA showed a reduction in ROI signal

Following the grouping of mice based on bioluminescence signal intensity, treatments were initiated according to the assigned experimental arms. The results are presented sequentially beginning with the control group, followed by the L-NMMA group, the Cisplatin group, and finally the combination treatment group (Cisplatin + L-NMMA). As shown in **Figure 3.13A**, the control group exhibited an increase in bioluminescence signal week by week until the experimental endpoint at week 11. After the initial peak immediately following cell injection (time 0), the luciferase signal began to rise after week 5, reflecting progressive tumour growth within the abdominal cavity. Total Flux values (photons per second [p/s]) reached 1.1×10^6 at week 11, with minor fluctuations along the way, indicating a continuous increase in tumour burden in untreated mice. The L-NMMA-treated group (**Figure 3.13B**) showed fluctuating Total Flux levels throughout the treatment period, until reaching 7.6×10^5 at week 11. These data suggest that while L-NMMA treatment temporarily stabilized tumour growth at certain time points, the overall control of tumour progression was incomplete. The Cisplatin-treated group (**Figure 3.13C**) demonstrated a distinct trend characterized by fluctuating but generally lower tumour burden compared to the control and L-NMMA groups. Total Flux values reached 4.5×10^5 at week 11. This pattern indicates a suppressive effect of Cisplatin on tumour progression. Also, the combination treatment group (**Figure 3.13D**) exhibited a controlled tumour progression overall where Total Flux values reached 4.9×10^5 at week 11. This marked reduction in bioluminescence signal during the final week reflects a decrease in tumour burden under the combinatorial therapy, suggesting a potential improved efficacy compared to single-agent treatments.

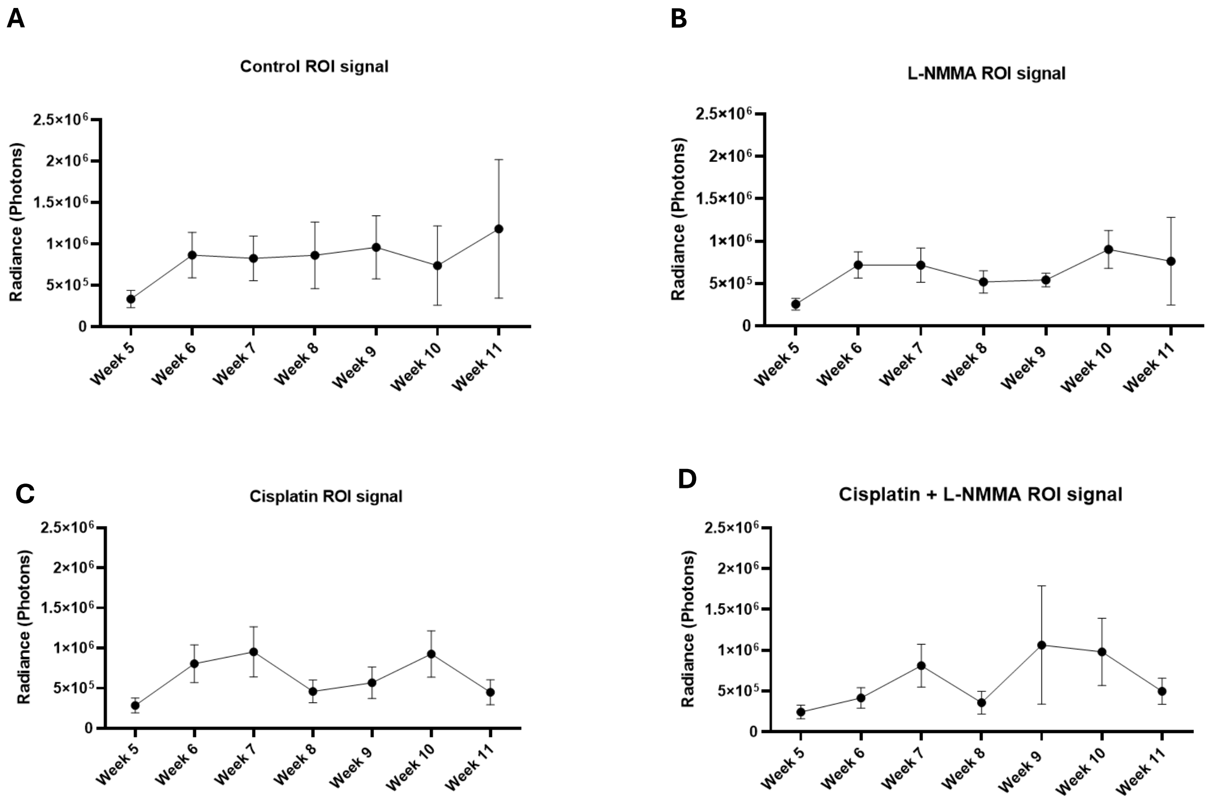

Figure 3.13(A-D). ROI trends over time for each treatment group. Figure 3.13A shows the ROI detected in the control group, The luciferase signal began to increase after week 5, with Total Flux values (photons per second [p/s]) reaching 1.1×10^6 at week 11, indicating a continuous increase in tumour burden in untreated mice. **Figure 13B** shows the ROIs levels obtained in the L-NMMA group. It is possible to observe fluctuating ROIs levels throughout the treatment period, until reaching 7.6×10^5 at week 11. **Figure 3.13C** shows the levels obtained in the cisplatin group, where a different trend of the ROI curve was observed. After the beginning of the treatments at week 5, an increase in the ROI was observed, followed by a decrease at week 8. Week 9 and 10 showed another increase in the trend which resulted again in a reduction of the signal, where Total Flux values reached 4.5×10^5 at week 11. and **Figure 3.11D** shows the ROI trend obtained in the combination group. After treatment began at week 5, a decrease was observed at week 8, followed by an increase in signal in the following weeks. ROI values reached 4.9×10^5 at week 11.

The signal obtained per single arm starting from week five is represented in the following figure (**Figure 3.14**).

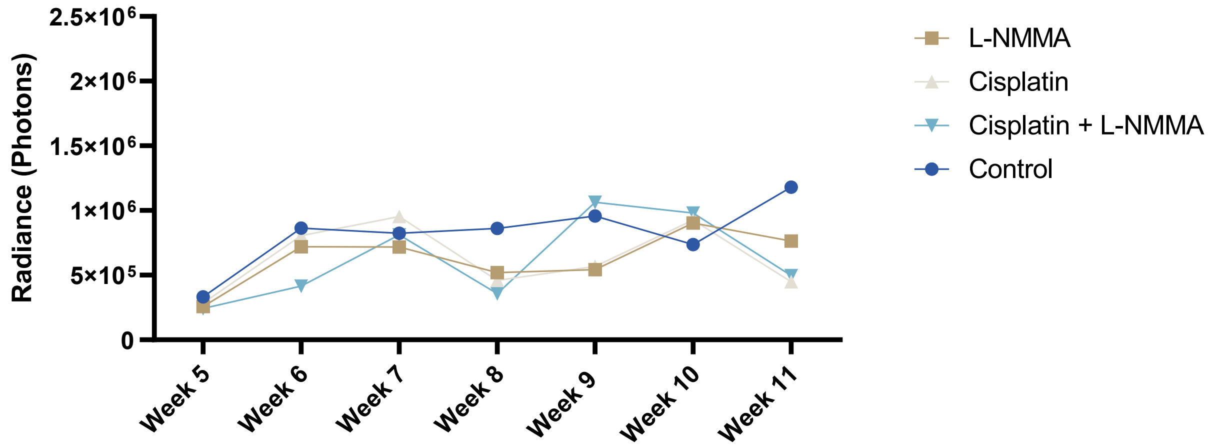

Figure 3.14. ROI trends comparison per single arm treatment. The control group exhibited the highest signal intensity, while the L-NMMA group showed reduced levels. Both the Cisplatin and combination treatment groups demonstrated a reduction in regions of interest (ROIs).

Control Group shows an increase in tumor signal from week 5 to week 11, with some fluctuations but an overall upward trend reaching the highest signal levels toward the endpoint. L-NMMA group follows a similar trend to the control, with increases and decreases, but the signal remains slightly lower than the control at most time points, indicating a mild effect on tumor progression. Cisplatin Group exhibits a more fluctuating tumor signal compared to control and L-NMMA groups. Combination Group shows a tumor bioluminescence comparable with the Cisplatin group. Even with this parameter, it is still possible to distinguish distinct trends for each individual group. Specifically, the control group exhibited the highest ROI peak, reflecting the most extensive tumor spread within the abdominal cavity. The L-NMMA group showed a reduction in ROI signal. However, both the Cisplatin and Cisplatin + L-NMMA groups showed lower ROIs levels compared to the other groups, even the data were not significant, suggesting that while both are effective in limiting tumor spread, the addition of L-NMMA does not further enhance Cisplatin's efficacy in this context.

3.4.5 Omentum revealed a lower signal in the combination treatment

After reaching the endpoint of the treatment, the signal obtained from the omentum, extracted from mice abdominal cavity, was analyzed. The signal has been detected by using ROI, similarly to what we did for the whole abdominal cavity. The signal was measured in Total Flux of Photons [p/s] too. In **Figure 3.15A** it is possible to observe a representative selection of all samples and **Figure 3.15B** shows the ROI quantification (expressed in [p/s]) in each group. Analysis of the signal obtained from the omentum at the study endpoint revealed distinct differences among the treatment groups. The control group exhibited a mean signal intensity of 9×10^5 p/s. Treatment with L-NMMA resulted in an increased mean signal of 4.4×10^6 p/s. Both Cisplatin alone and the combined Cisplatin + L-NMMA treatments demonstrated a reduction in signal intensity compared to control. Specifically, the Cisplatin group showed a mean signal of 3.5×10^5 p/s, while the Cisplatin + L-NMMA group exhibited a further decreased mean signal of 1.3×10^5 p/s (**Figure 3.15C**).

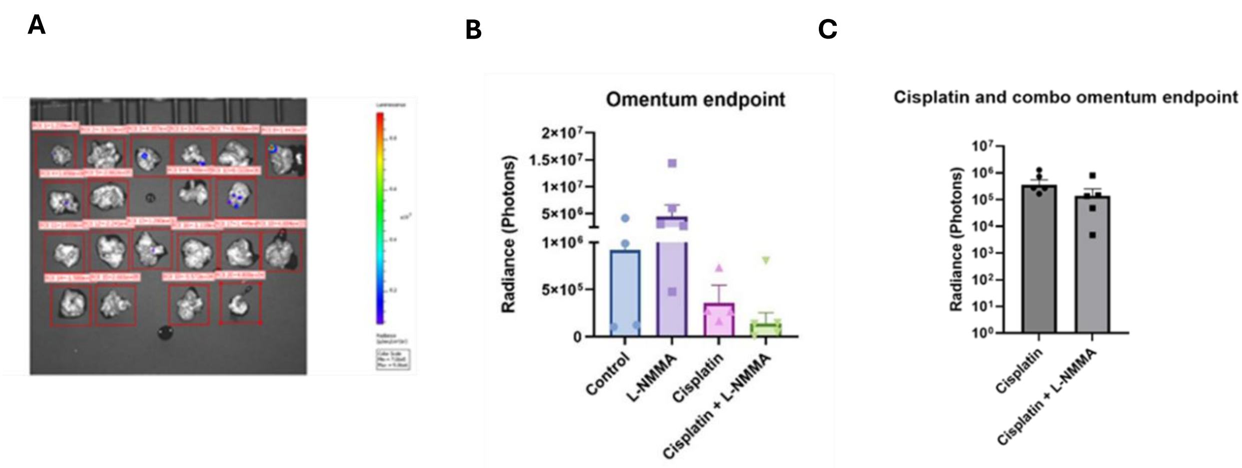

Figure 3.15 (A–C). ROI detection in the omentum at the endpoint. Figure 3.15A presents a representative image of the signal detected in the omentum following mouse sacrifice. **Figure 3.15B** compares the ROI signal from the omentum across all treatment groups. In particular, the control group exhibited a mean signal intensity of 9×10^5 p/s. Treatment with L-NMMA resulted in an increased mean signal of 4.4×10^6 p/s. the Cisplatin group showed a mean signal of 3.5×10^5 p/s, while the Cisplatin + L-NMMA group exhibited a mean signal of 1.3×10^5 p/s **Figure 3.15C** highlights the reduction of ROI observed in the combination treatment group compared to the Cisplatin only group, where the Cisplatin group showed a mean signal of 3.5×10^5 p/s, while the Cisplatin + L-NMMA group exhibited a mean signal of 1.3×10^5 p/s

Omentum colonization exhibited different trends across the groups, although no statistically significant differences were observed. As the omentum is typically the first site of tumor colonization, it appears to be particularly challenging to treat effectively, which may explain the absence of significant group differences. Nonetheless, both the Cisplatin and Cisplatin + L-NMMA groups showed the lowest ROI signals, suggesting a potential inhibitory effect on tumor proliferation. When the data are analyzed and visualized side by side in Figure 3.15C, it is possible to observe that, although not statistically significant, the Cisplatin + L-NMMA group displays a slight lower ROI signal compared to Cisplatin alone.

3.4.6 Flow cytometry reveals a more active phenotype in the combination treatment group

After the collection of the ascites at the endpoint, ascites from each mouse were collected and profiled through FACS. Immune profiling was conducted by using antibodies for myeloid and lymphoid markers. Samples were divided into a myeloid and lymphoid group. In the lymphoid group we found the presence of T lymphocytes, NKT cells, NK_NKT cells and NK cells. There are also Tregs, CD4+ and CD8+ T cells together with markers (CD62L and CD44) both related to the activation status of T cells. For what concerns the myeloid panel, the presence (in terms of percentages) of DC1, DC2, MDSC and neutrophils was analysed. This type of analysis opened to the opportunity to identify the presence of immune cells by comparing four different treatment arms, as reported above. Changes in the immune system collectively present into ascites changes in accordance with the type of treatment administered were observed. We observed an overall improvement by using the combination of Cisplatin and L-NMMA (even if it must be registered an increase of Tregs after the combination treatment) with a significative increase of T lymphocytes, an increase of NK_NKT and an increase of activation markers in the CD4+ T cells population.

3.4.7 Lymphoid panel showed significant changes in the combination treatment group

Analysis of immune cell infiltration revealed that the combination treatment with Cisplatin and L-NMMA significantly enhanced T lymphocyte infiltration compared to single-agent therapies and untreated controls. Specifically, T lymphocyte expression reached 43.5% in the combination group ($p < 0.05$), markedly higher than the Cisplatin (30.7%), L-NMMA (26.34%), and untreated control groups (24.7%) (**Figure 3.16A**). Similarly, NKT cell infiltration was substantially increased in the combination group, reaching 3.27% ($p < 0.05$), which was significantly greater than levels observed in the Cisplatin (0.34%), L-NMMA (0.28%), and untreated (0.14%) groups (**Figure 3.16B**). The NK_NKT cell population also showed a pronounced increase with combination therapy (7.09%) ($p < 0.05$), exceeding the proportions found in the Cisplatin (2.67%), L-NMMA (2.81%), and untreated control groups (2.96%) (**Figure 3.16C**). Although no statistically significant differences were observed in NK cell populations across groups, a positive trend (even if not reaching significance), was observed, with the combination group exhibiting the highest percentage (3.0%), followed by the untreated (2.77%), L-NMMA (2.3%), and Cisplatin (2.16%) groups (**Figure 3.16D**). Additionally, regulatory T cell (Treg) infiltration was influenced by treatment; the combination therapy increased Treg presence to 1.75% ($p < 0.05$), compared to 0.65% in the Cisplatin group, 0.55% in the L-NMMA group, and 0.48% in the untreated controls (**Figure 3.16E**).

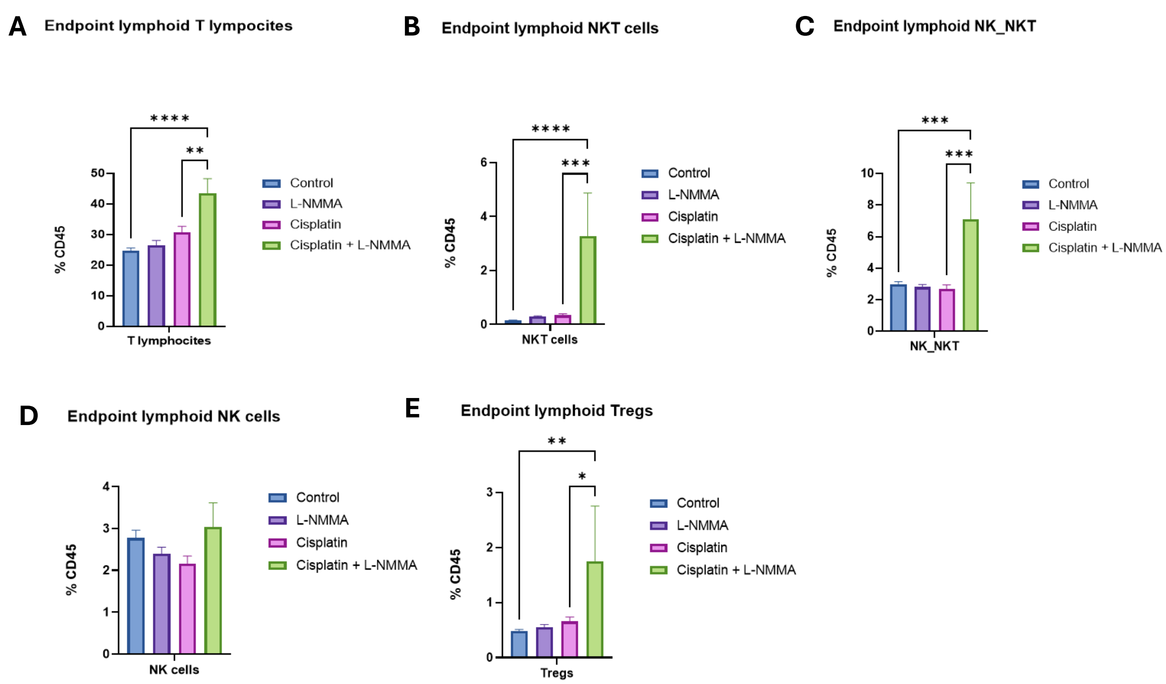

Figure 3.16 (A–E). Levels of various lymphocyte populations in ascites across four different treatment groups. Figure 3.16A shows the levels of T lymphocytes in each group, showing a significant increase in the combination group compared to the others. T lymphocyte expression reached 43.5% in the combination group ($p < 0.05$), markedly higher than the Cisplatin (30.7%), L-NMMA (26.34%), and untreated control groups (24.7%). **Figure 3.16B** highlights the levels of NKT cells, showing a significant increase in the combination group compared to the others. The combination group, reached 3.27% ($p < 0.05$), which was significantly greater than levels observed in the Cisplatin (0.34%), L-NMMA (0.28%), and untreated (0.14%) groups. Similarly, **Figure 3.16C** presents the percentage of NK_NKT cells within the total CD45+ population, revealing an increase in the same group relative to the other treatment groups. The NK_NKT cell population had a pronounced increase with combination therapy (7.09%) ($p < 0.05$), compared to the percentages found in the

cisplatin (2.67%), L-NMMA (2.81%), and untreated control groups (2.96%). **Figure 3.16D** depicts the levels of NK cells, which, although not statistically significant, exhibit a trend toward higher levels in the combination treatment group. The combination group exhibited the highest percentage (3.0%), followed by the untreated (2.77%), L-NMMA (2.3%), and Cisplatin (2.16%) groups. Finally, **Figure 3.16E** shows regulatory T cells (Tregs), which display a significant increase ($p < 0.005$) in the combination group compared to all other treatments. The combination therapy increased Treg presence to 1.75% ($p < 0.05$), compared to 0.65% in the Cisplatin group, 0.55% in the L-NMMA group, and 0.48% in the untreated controls

The results from the initial analysis of the lymphoid panel demonstrate that, at the treatment endpoint, the combination of Cisplatin and L-NMMA was the most effective in reactivating the immune system. Ovarian cancer is well known for its immunologically “cold” tumor microenvironment [237], which poses a challenge for immunotherapy. Numerous strategies have been explored to convert this cold environment into a “hot,” immune-responsive one. In this study, the use of L-NMMA to inhibit nitric oxide release, combined with Cisplatin, led to a significant increase in key immune cell populations, including T lymphocytes, NKT cells, and NK_NKT cells, compared to the other treatment groups. This suggests that the combination therapy promotes a more robust immune activation.

3.4.8 CD4+ and CD8+ T cells

The levels of CD4+ and CD8+ T cells in ascites did not show significant changes across treatment groups. CD4+ T cell infiltration remained stable, with no significant increase observed in response to any therapy, as shown in **Figure 3.17A**. No significant changes were observed for the CD8+ T cells (**Figure 3.17B**) indicating that the combinatorial and single-agent treatments did not significantly impact the levels of these T cell subtypes.

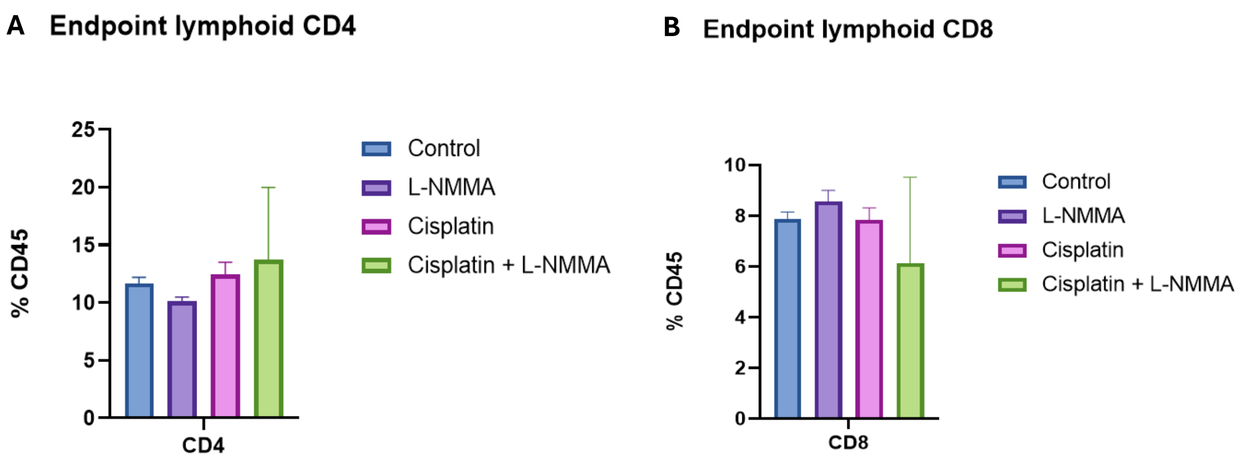

Figure 3.17 (A–B). CD4 and CD8 changes across four different treatment groups. Figure 3.17A shows a trend towards increased levels of CD4 T cells, although this difference is not statistically significant. **Figure 3.17B** illustrates the levels of CD8 T cells across the treatment groups, still not reporting any significant change.

When analyzing the T cell subpopulations, specifically CD8+ and CD4+ T cells, no statistically significant differences were observed among the groups. Although higher levels of CD4+ T cells were detected, these increases did not reach statistical significance. Similarly, CD8+ T cell levels remained unchanged across all groups.

3.4.9 CD4+ T cells are stimulated after the combination treatment

Interestingly, there was an increase in activation markers (CD62L- CD44+) (**Figure 3.18A**) and a decrease in naïve markers (CD62L+ CD44-) (**Figure 3.18B**) on CD4+ T cells following treatment. Specifically, the combination treatment resulted in 59.7% of CD4+ T cells expressing activation markers ($p < 0.05$), compared to 35.66% with Cisplatin alone, 38.6% with L-NMMA alone, and 24.7% in untreated controls. The level of naïve CD4+ cells (CD62L+ CD44-) was significantly reduced in the combination treatment group to 23.35%, while Cisplatin, L-NMMA, and untreated groups showed levels of 50%, 44%, and 62%, respectively.

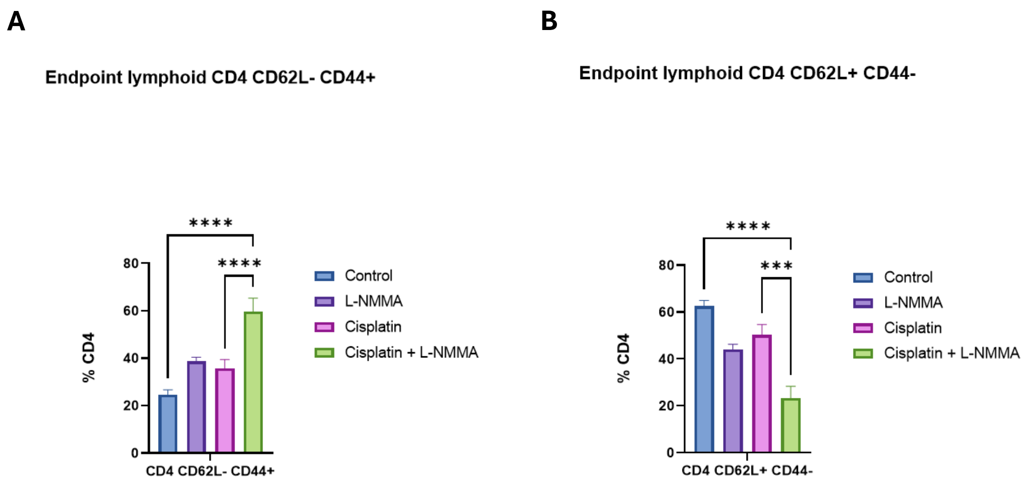

Figure 3.18 (A-B). CD4 T cells increase their activation status and reduce naïve levels after the combination therapy. Figure 3.18A shows an increase in activation markers (CD62L- CD44+) following the combination treatment which resulted in 59.7% of CD4+ T cells expressing activation markers ($p < 0.05$), compared to 35.66% with Cisplatin alone, 38.6% with L-NMMA alone, and 24.7% in untreated controls.. In **Figure 3.18B** the combination group exhibits a more pronounced reduction of naïve markers (CD62L+ CD44-) when compared to the other treatment groups, which was significantly reduced in the combination treatment group to 23.35%, while Cisplatin, L-NMMA, and untreated groups showed levels of 50%, 44%, and 62%, respectively.

These results highlight where the combination treatment exerts its strongest impact on the immune population. Among the lymphoid cells analyzed, the $CD4^{+}CD62L^{-}CD44^{+}$ T cell subpopulation showed a significant increase, indicating enhanced activation of memory T cells. Concurrently, the $CD4^{+}CD62L^{+}CD44^{-}$ T cell population decreased, reflecting a reduction in naïve T cells and, consequently, fewer immune cells in a resting, non-responsive state. This suggests that the combination therapy primarily promotes the expansion and activation of memory T cells, which can, in turn, stimulate and coordinate broader anti-tumor immune responses [262].

3.4.10 CD8+ T cells activation status

No significant changes were observed in the overall percentage of $CD8^{+}$ T cells across treatment groups. Notably, L-NMMA treatment increased the proportion of activated $CD8^{+}$ T cells (CD62L-CD44+) (**Figure 3.19A**), reaching 24.3% ($p < 0.05$) compared to 14.1% in the control group, suggesting a role for L-NMMA in promoting CD8+ T cell activation. Additionally, L-NMMA treatment resulted in a reduction of naïve $CD8^+$ T cells (CD62L+CD44-) (**Figure 3.19B**), decreasing from 56.5% in controls to 42.25% ($p < 0.05$), further indicating a shift toward an activated phenotype.

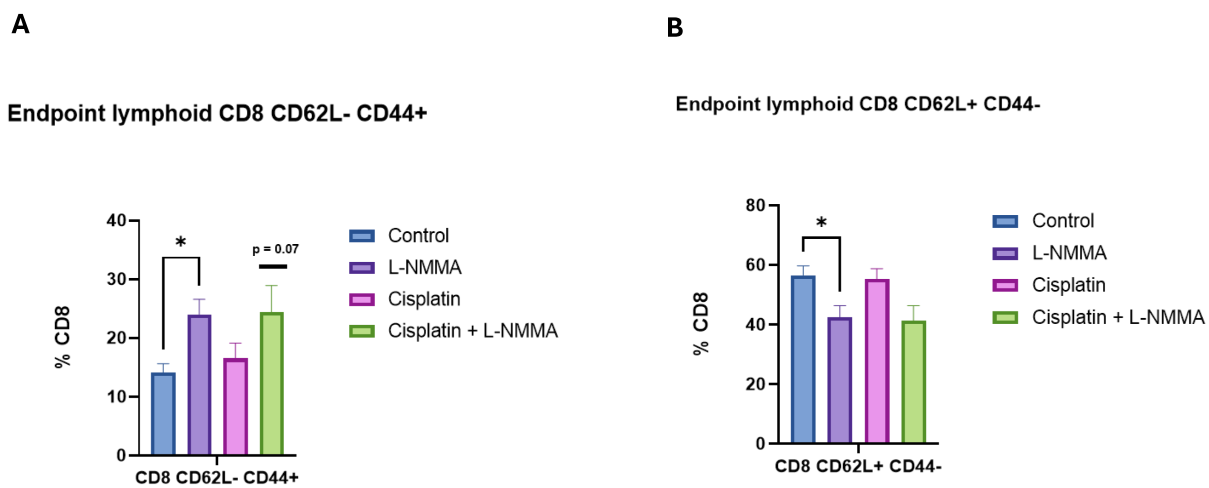

Figure 3.19 (A-B). CD8 T activation and naïve markers don't change after the combination therapy. Figure 3.19A illustrates the effect of each treatment on activation markers of CD8+ T cells, with L-NMMA showing a significant increase. Combination treatment exhibited a p value close to 0.05, value considered as statistically significant. In particular, L-NMMA treatment significantly increased the proportion of activated $CD8^+$ T cells (CD62L- CD44+) (Figure 3.1A), reaching 24.3% ($p < 0.05$) compared to 14.1% in the control group, suggesting a role for L-NMMA in promoting CD8+ T cell activation. **Figure 3.19B** shows a significant decrease in naive CD8+ T cell markers following treatment with L-NMMA, but no difference in the combination treatment. In particular, L-NMMA treatment resulted in a reduction of naïve $CD8^+$ T cells (CD62L+CD44) decreasing from 56.5% in controls to 42.25% ($p < 0.05$), further indicating a shift toward an activated phenotype.

Notably, for what concerns CD8 cells only, L-NMMA alone induced a significant increase in activation markers ($CD62L^-CD44^+$) on $CD8^+$ T cells. Although the combination treatment did not reach statistical significance when compared to control, it showed a strong trend toward increased activation with a p-value approaching 0.05. Similarly, for naïve markers ($CD62L^+CD44^-$), L-NMMA caused a significant decrease, while the combination group exhibited a comparable, albeit less pronounced, trend that did not approach statistical significance as closely.

3.4.11 Myeloid panel showed changes following the four treatment conditions

The myeloid panel revealed several changes across treatment groups. Regarding the myeloid population, combinatorial therapy resulted in a significant reduction in the percentage of type 1 dendritic cells (DC1) ($p < 0.05$) (**Figure 3.20A**). Specifically, the frequency of DC1 was 0.97% in the combination treatment group, compared to 2.7% in the Cisplatin group, 3.07% in the L-NMMA group, and 2.37% in the untreated controls. Type 2 dendritic cells (DC2) showed a similar trend where the combination treatment reached a level of 1.47%, the Cisplatin group showed a level of 3%, L-NMMA a level of 3.48% and the control group a level of 2,76% (**Figure 3.20B**). A marked decrease was also observed in the population of myeloid-derived suppressor cells (MDSCs) following combination therapy (**Figure 3.20C**). The residual MDSC levels were 0.2% in the combination group, versus 1.67% in the Cisplatin group, 2.5% in the L-NMMA group, and 1.045% in untreated animals. No significant differences were detected in neutrophil frequencies among groups (**Figure 3.20D**); however, a modest reduction was noted in the combination treatment group relative to Cisplatin alone. Specifically, neutrophil percentages were 11.5% in the combination group, 13.49% in the Cisplatin group, 11.6% in the L-NMMA group, and 9.87% in the untreated control.

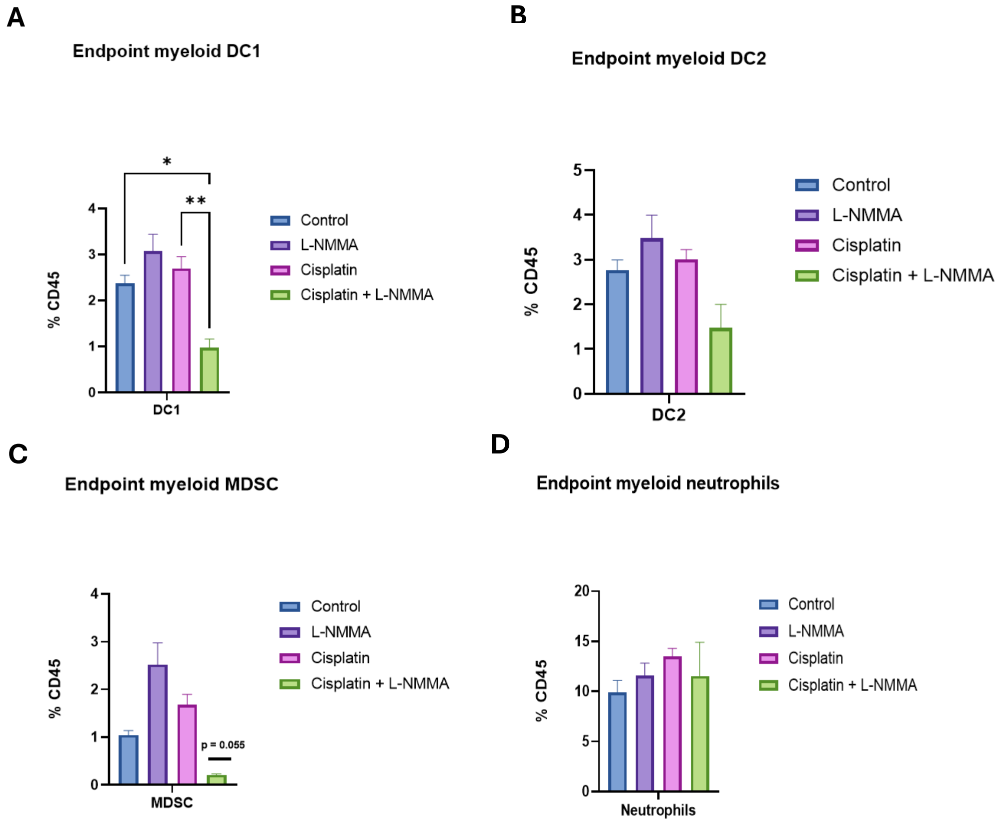

Figure 3.20 (A–D). **Myeloid immune population has slight changes after the combination therapy. Figure 3.20A** shows the levels of DC1 cells following treatments across all groups, with a noticeable decrease in the combination group compared to the others. The frequency of DC1 was 0.97% ($p < 0.05$) in the combination treatment group, compared to 2.7% in the Cisplatin group, 3.07% in the L-NMMA group, and 2.37% in the untreated controls. **Figure 3.20B** illustrates the levels of DC2 cells, which are also reduced after combination treatment, which reached a level of 1.47%,. The Cisplatin group showed a level of 3%, L-NMMA a level of 3.48% and the control group a level of 2,76%. **Figure 3.20C** shows the levels of MDSC which were 0.2% in the combination group, versus 1.67% in the Cisplatin group, 2.5% in the L-NMMA group, and 1.045% in untreated animals. . **Figure 3.20D** presents the levels of neutrophils after treatment. In the combination group, neutrophil percentages were 11.5% 13.49% in the Cisplatin group, 11.6% in the L-NMMA group, and 9.87% in the untreated control.

In this case, a decrease in conventional type 1 Dendritic Cells (DC1) was observed. This result can be considered a side effect, as DC1 cells are often correlated with a good prognosis. However, it should also be noted that dendritic cells are capable of expressing and producingcan express and produce NO [263], which could make them an intrinsic target of L-NMMA. Furthermore, regarding the MDSC population, although the reduction did not reach statistical significance, a strong decrease was observed following Cisplatin + L-NMMA treatment, with a p-value of 0.055.

3.5 Pathologic evaluation reveals a tumor regression in the peritoneum

To evaluate the effects of the treatments on tumor progression within the peritoneum and omentum, histological sections from these tissues were analyzed. Several quantitative parameters were assessed, including tumor area, number of tumor cells, percentage of tumor cells, percentage of tumor area, number of tumor foci (tumor spots), and mitotic counts. All measurements were performed using QuPath software, as illustrated in the accompanying images (**Figure 3.21A-E**).

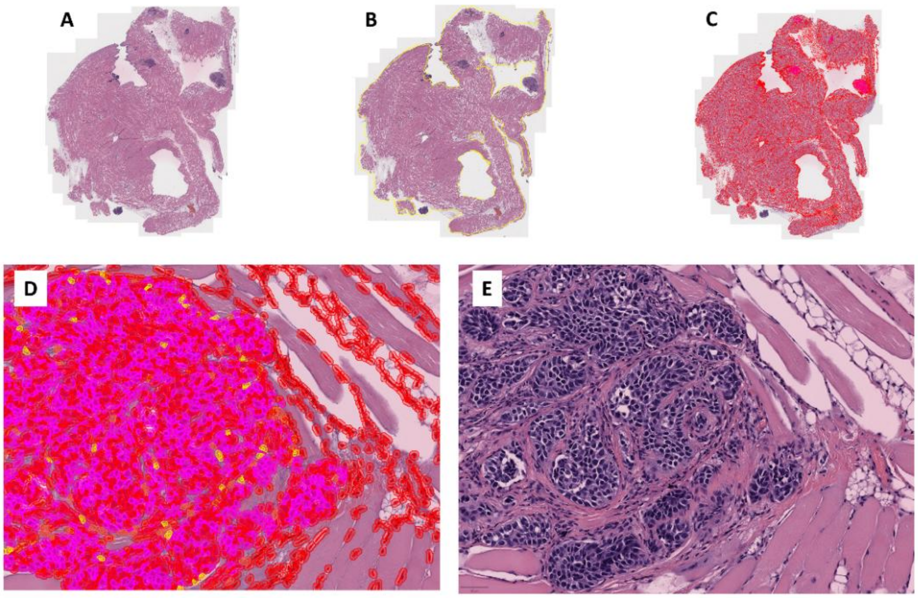

Figure 3.21. Representative image of the pathological analysis workflow. Representative tissue section examined as a whole slide image (**Figure 3.21A**) with a total cell count carried out using QuPath (**Figure 3.21B,C**). One of the areas of tumor is shown inset (**Figure 3.21D**). The tumor cells (pink) and lymphocytes (yellow) as identified by the classifier are seen (**Figure 3.21E**).

By using QuPath we were also able to identify micrometastasis which were nest into peritoneum, omentum, but also in the vascular structure (**Figure 3.22 A-C**).

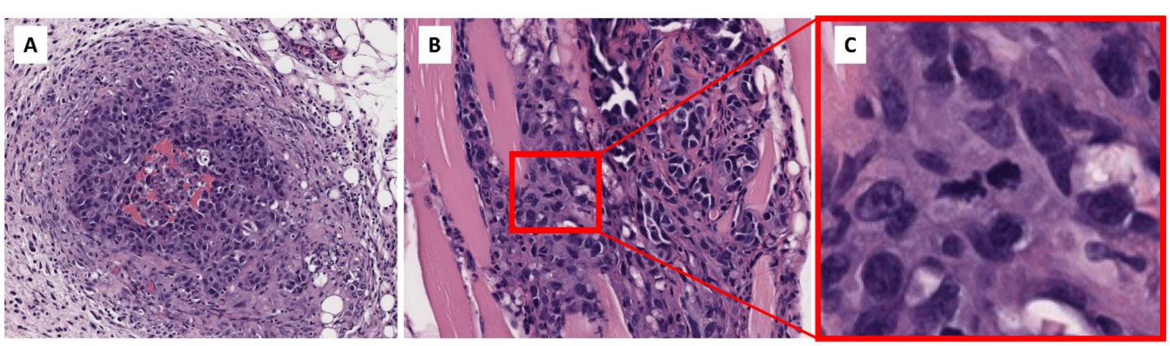

Figure 3.22. Representative image of metastatic spread in the mice abdominal cavity. An example of the lymphovascular invasion is identified in **Figure 3.22A** as well as a mitosis identified in **Figure 3.22B** and at higher magnification in **Figure 3.22C**.

As previously discussed, both figures show tumour dissemination in the peritoneum and vasculature of the mice's abdominal cavity. Given the extent of these micrometastases and their often small size, an analysis was performed slide by slide using automated software capable of detecting even the smallest tumour spots.

3.5.1 Tumor area is reduced in the peritoneum after the combination treatment

The images below show the tumor area (in μm^2) in the peritoneum and omentum across different treatment groups. In the peritoneum (**Figure 3.23**), a significant reduction in tumor area was observed in the treatment groups compared to the control. Specifically, the control group exhibited an average tumor area of 4.67×10^6 μm^2. Treatment with Cisplatin alone reduced the tumor area to 2.23×10^6 μm^2, while the combination treatment group showed the most pronounced reduction, with an average area of 9×10^5 μm^2 ($p < 0.05$).

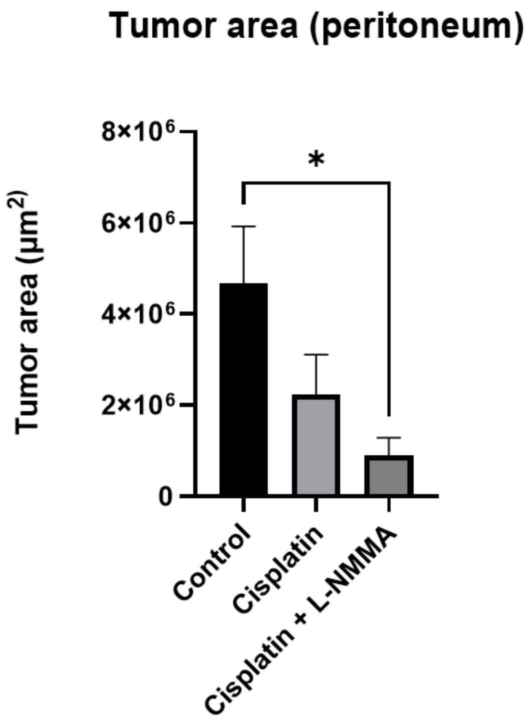

Figure 3.23. Tumor area has a significant reduction after the combination therapy. In the figure it is possible to observe a significant reduction in tumor area within the peritoneum following treatment with the combination group. In particular, the control group showed an average tumour area of 4.67×10^6 μm^2. Treatment with Cisplatin alone showed an average tumour area to 2.23×10^6 μm^2, while the combination treatment group showed the strongest reduction, with an average area of 9×10^5 μm^2 ($p < 0.05$).

Peritoneal metastases are the condition in which most patients are diagnosed, often because diagnosis occurs at a late stage of the disease [266]. Given this, the first line of treatment typically involves surgery to achieve tumor debulking, followed by chemotherapy to prevent tumor progression and eliminate any residual cancer cells within the abdominal cavity. In this study, the combination of Cisplatin and L-NMMA demonstrated a significant reduction in tumor area compared to Cisplatin alone, suggesting that this combination therapy has the potential to enhance the effects of chemotherapy while also promoting immune cell reactivation, as shown earlier.

3.5.2 Tumor cell number is reduced in the peritoneum after the combination treatment

In the peritoneum, for what concern tumor cell number showed interesting results (**Figure 3.24**). The control group showed the highest number of tumor cells, with an average of 2.8×10^4 cells. Treatment with Cisplatin alone reduced this number to 1.2×10^4, while the combination treatment (Cisplatin + L-NMMA) resulted in the most substantial reduction, with 5.7×10^3 tumor cells ($p < 0.05$). These results indicate that the combination therapy was significantly more effective in reducing tumor cell numbers compared to both the control and the Cisplatin-only group.

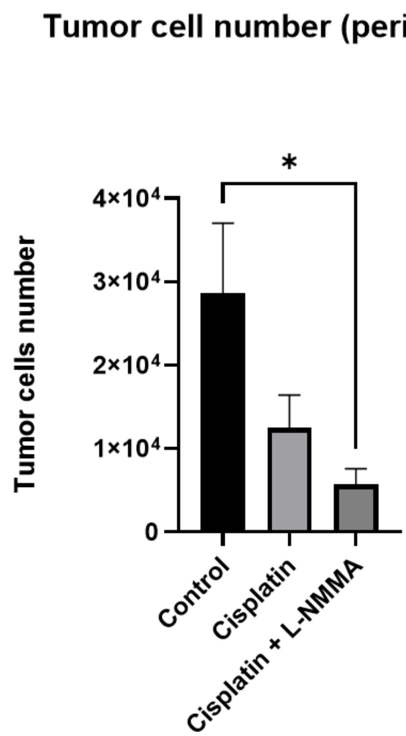

Figure 3.24. Tumor cell number has a significant reduction after the combination therapy. In the figure it is possible to observe a significant reduction in tumor cell numbers following the combination treatment, with a greater impact than the Cisplatin-only group. The control group showed the highest number of tumour cells, with an average of 2.8×10^4 cells. Treatment with Cisplatin alone reduced this number to 1.2×10^4, while the combination treatment (Cisplatin + L-NMMA) resulted in the most impactful reduction compared to Cisplatin, with 5.7×10^3 tumour cells ($p < 0.05$).

In addition to the reduction in tumor area, a decrease in the total number of tumor cells was also observed. This finding highlights how the combination treatment of Cisplatin and L-NMMA not only reduces tumor burden but also lowers the overall number of cancer cells. This provides a more specific and integrative analysis compared to standard ROI measurements. Furthermore, this approach enables the detection of micrometastases and small tumor spots that are often difficult to identify in the murine abdominal cavity due to physiological barriers such as ascites, fur, and limitations in imaging sensitivity.

3.5.3 Percentage of tumor cells is reduced in the peritoneum after the combination treatment

We also analyzed the percentage of tumor cells in the peritoneum (**Figure 3.25).** This analysis confirmed the trends observed in absolute tumor cell numbers in the peritoneum. The control group exhibited a tumor cell percentage of 10.3%. Treatment with Cisplatin reduced this to 5.3%, while the combination treatment resulted in the lowest percentage at 2.6%. This reduction observed in the combination group was statistically significant when compared to the control ($p < 0.05$), whereas the difference between the Cisplatin group and control did not reach statistical significance.

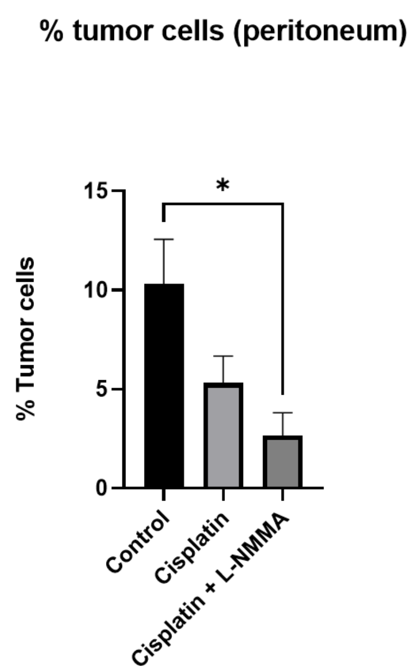

Figure 3.25. Percentage of tumor cells has a significant reduction after the combination therapy. The stronger impact of the combination treatment in the peritoneum is shown. A significant reduction has been obtained following the combination treatment, which exhibited a tumour cell percentage of 10.3%. Treatment with Cisplatin reduced this to 5.3%, while the combination treatment resulted in the lowest percentage at 2.6% ($p < 0.05$)

This result also demonstrates a strong and significant reduction in the percentage of tumor cells relative to all cells identified in the tissue sections following treatment with the Cisplatin + L-NMMA combination. Overall, these findings suggest not only a reduction in tumor burden but also an improved clearance of metastatic spots in the peritoneum compared to treatment with Cisplatin alone, which did not show a similar decrease.

3.5.4 Percentage of tumor area is reduced after the combination treatment

We also confirmed the strong impact of the combination treatment by analyzing the percentage of tumor area. Similar to the analysis of tumor cell percentages, this was calculated as the ratio between the total area occupied by tumor cells and the total tissue area within each section. In the peritoneum (**Figure 3.26**), the control group showed the highest percentage of tumor area at 2.8%. The Cisplatin-treated group exhibited a reduced percentage of 1.3%, while the combination treatment resulted in the lowest tumor area percentage at 0.89% ($p < 0.05$). These findings further support the enhanced therapeutic efficacy of the combination treatment in this murine model, confirming its stronger impact compared to Cisplatin alone or no treatment.

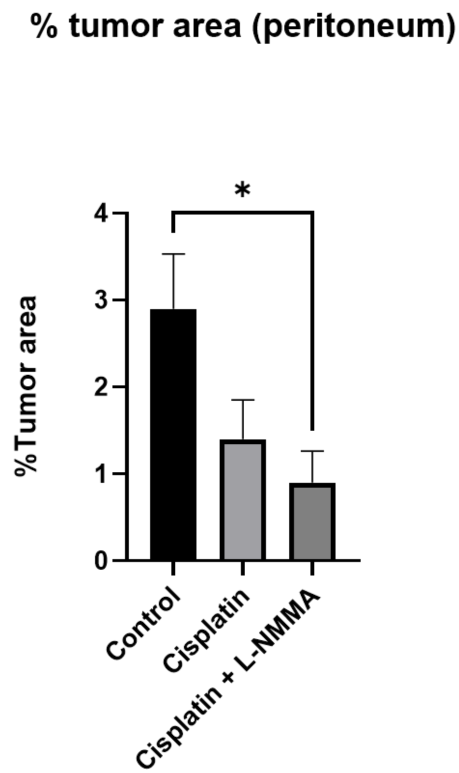

Figure 3.26. Percentage of tumor area has a significant reduction after the combination therapy. The figure shows the reduction in the percentage of tumor area in the peritoneum among different treatment groups. The stronger effect was observed in the combination treatment group which showed the strongest reduction among the different conditions. More specifically, the control group had the highest percentage of tumour area corresponding to 2.8%. The Cisplatin-treated group exhibited a percentage of 1.3%, while the combination treatment resulted in the lowest tumour area percentage corresponding to 0.89% ($p < 0.05$).

The percentage of tumor area followed the same trend as the percentage of tumor cells, where a reduced number of cells corresponded to, as mentioned above, a clearer peritoneal area with fewer metastases compared to the Cisplatin and control groups.

3.6 Discussion

Identifying an ideal in vivo ovarian cancer model remains challenging due to the distinct characteristics related to each in vivo system. What can be achieved is the selection of the in vivo model that best aligns with the specific objectives of the study. We selected an immunocompetent mouse strain, the C57BL/6 mice, which allows the investigation of both the cancer progression from the early stage and immunosuppressive effects on the immune system during tumor development. Additionally, this model enables the assessment of the impact of our combination and single-agent therapies on immune modulation and tumor regression. Previous studies have investigated the use of L-NMMA in vivo [156, 157]. The combination of Cisplatin and L-NMMA presented in this section represents a novel strategy. Exploring the effects of L-NMMA in ovarian cancer further may offer significant therapeutic potential. This is particularly relevant given the demonstrated expression of iNOS in both ascites and cancer cells, as well as in immune cell populations known to produce nitric oxide, including MDSCs [265], macrophages [266], dendritic cells [263], and also in stromal components [167]. This combination therapy provides an innovative strategy to assess the therapeutic effects of L-NMMA in ovarian cancer, targeting both tumor and immune compartments. It was also confirmed that this in vivo model expresses iNOS both in vitro and in vivo. Recapitulating what this work has showed about the use of ID8 synegenic in vivo model for ovarian cancer is that, first, the intraperitoneal injection of the ID8 cell line induces the formation of ascites in mice, accompanied by an increase in abdominal volume and body weight due to fluid accumulation. This work demonstrated that different treatment regimens exert distinct effects on tumor progression, not only when comparing control versus treated groups but also between single-agents and combination therapies. In particular the single-agent that have been used are L-NMMA, a drug previously employed in breast cancer clinical trials [157] , and recognized for its potent inhibitory effect on iNOS activity in vivo, and cisplatin, the standard chemotherapy agent for ovarian cancer patients. The combination of Cisplatin and L-NMMA may offer synergistic benefits for several reasons. As extensively discussed in the introduction, the immunosuppressive tumor microenvironment not only maintains the tumor in a “cold” state but also actively promotes tumorigenesis. The crosstalk within the tumor microenvironment profoundly influences and often counteracts the beneficial effects of the immune response [267]. In this context, the immune system acquires an immunosuppressive phenotype, predominantly silencing anti-tumor immunity. Tumor-associated macrophages play a critical role in this process, exhibiting immunosuppressive functions, promoting tumor progression, and being stimulated by the tumor microenvironment to produce iNOS [268]. Furthermore, iNOS drives the accumulation of myeloid-derived suppressor cells MDSCs at sites of expression, thereby reinforcing immune suppression [271]. In this chapter, it was also demonstrated that iNOS can be induced in MEOC cell lines following stimulation with pro-inflammatory cytokines, agents previously shown to induce iNOS in other cancer types [213]. Importantly, iNOS expression is not confined to cell lines but persists in late-stage disease within ~~our~~this syngeneic model, as evidenced by iNOS detection in ascites samples. Therefore, administration of L-NMMA may reduce NO production, thereby mitigating the deleterious effects of iNOS overexpression in the tumor microenvironment [270]. While the efficacy of platinating agents is well established, their associated side effects are also well documented. For example, Cisplatin can induce renal tubular damage as a side effect by increasing the levels of ROS in the kidneys [271]. Considering this, the administration of L-NMMA may also mitigate the deleterious off-target effects of Cisplatin, and potentially its less toxic derivative, Carboplatin, thereby reducing therapy-associated toxicity and allowing a more focused cytotoxic effect on cancer cells. Moreover, it has been previously reported that the immune system is capable not only of expressing iNOS but also of responding to inflammatory stimuli, which may either initiate or result from iNOS production [198]. In the study presented in this chapter, it was also observed that the combination of L-NMMA and Cisplatin not only reduced body weight and abdominal diameter, indicating morphological improvements, but also promoted reactivation of the immune system. These effects were evident exclusively with the combination therapy, highlighting that monotherapy was less effective in exerting broad impacts involving both direct cancer cell targeting and immune stimulation. This combination demonstrated the potential to modulate the TIME by influencing the release and activity of molecules such as NO, which are critical regulators of immune cell migration, activation, and function. Specifically, administration of the combinatorial treatment led to increased infiltration of T lymphocytes into ascites, elevated numbers of NK cells, further expansion of NK_NKT cells, and notably, an increase in activation markers accompanied by a decrease in naïve markers within the CD4+ T cell population. Many publications have highlighted the importance of $CD4^{+}$ T cells and their memory subpopulations in ovarian cancer, suggesting these cells play a crucial role in stimulating and activating immune responses against tumors [262]. While L-NMMA has already been evaluated in clinical trials for breast cancer [157], the results presented in the previous sections of this study suggest a potential role for L-NMMA, especially in combination with Cisplatin, in reactivating and stimulating the memory compartment of the immune system in ovarian cancer. Alongside the reactivation of effector $CD4^+$ T cells, a reduction in naïve markers was observed, indicating that the shift in memory populations involves not only increased activation but also clearance of inactive or unstimulated cells within the ascites. Future studies should aim to elucidate the mechanisms underlying the enhanced $CD4^+$ T cell activity and their interaction with L-NMMA. These findings underscore the role of NO-mediated inflammatory signaling in the recruitment and activation of immune effector cells. Another significant observation was that the combination therapy not only enhanced the immune response within ascitic fluid but also effectively reduced tumor progression in the peritoneum. The combination treatment uniquely decreased tumor area, tumor cell count, and the proportion of tumor cells, demonstrating a better efficacy compared to Cisplatin alone. This ability to simultaneously suppress metastasis formation and boost immune recruitment may improve chemotherapy outcomes. While initial responses to chemotherapy, especially with platinating agents, are often favorable, approximately 80% of patients become refractory after initial treatments [272]. This represents a major therapeutic challenge in ovarian cancer. The proposed model and combinatorial treatment indicate that adding L-NMMA sensitizes cancer cells to chemotherapy, suggesting that iNOS may contribute not only to tumor progression but also to chemoresistance. Also, based on a previous publication demonstrating metastatic accumulation in the peritoneum along with an immune composition characterization [246], this study quantified and characterized peritoneal metastases to evaluate the effect of chemotherapy combined with L-NMMA on reducing tumor burden. Overall, the combination treatment increases cancer cell sensitivity to chemotherapy. This approach could help delay or overcome chemoresistance, which commonly develops in a large proportion of patients after initial treatment with platinating agents. Additionally, it suggests potential for longer or adjusted treatment schedules to maintain therapeutic response. Another key aspect is the development of an in vivo model that replicates essential features of late-stage ovarian cancer in humans. This model also offers a valuable platform to study cytokine responses, inflammatory status, and the role of nitric oxide within the tumour microenvironment.As highlighted in the introduction, the heterogeneity and diverse characteristics of ovarian cancer complicate the selection of an appropriate model. With this work it has been established a model which, although it does not employ human cells for studying tumor progression, demonstrates ascites formation and may serve as a useful tool for future investigations related to the role of nitric oxide and, specifically, iNOS. Importantly, this expression is not confined to cancer cells alone but also involves the heterogeneous cell populations that emerge following ascites accumulation. The optimization of an iNOS-expressing in vivo model may hold significant utility, especially in light of ongoing clinical trials employing L-NMMA in other cancer types, as mentioned earlier. Such a model could facilitate a deeper understanding of the interplay between iNOS, NO, and tumor progression, thereby aiding the development of targeted therapeutic strategies. A future perspective for extensively studying ovarian cancer involves the development of in vivo models that consider one of the most critical and detrimental aspects of the disease, relapse. As previously mentioned, 70–80% of patients experience relapse [273], which complicates therapeutic approaches due to the acquisition of resistance to commonly used chemotherapeutic agents, particularly platinating agents like Cisplatin. The resensitization of Cisplatin- or platin-resistant cancer cell lines could reveal a potential connection between NO signaling and acquired chemoresistance. A previous study has already shown that NO plays a role in chemoresistance [274], but demonstrating that L-NMMA can effectively treat ovarian cancer cells that no longer respond to chemotherapy would represent a significant advancement in combating this disease. Another important aspect for future research is to investigate how treatment with Cisplatin, L-NMMA, and their combination affects survival rates in mice over time. If the combination therapy can extend the efficacy of Cisplatin, potentially allowing longer treatment durations while reducing the dosage, it could widen the therapeutic window. Therefore, performing survival assays in mice would provide valuable insights into how effectively these treatments improve survival outcomes. Additionally, since the mice in this study did not undergo any surgical procedures to remove metastatic tumor nodules, there is translational potential in using the Cisplatin + L-NMMA combination at lower doses to reduce side effects. This approach could be applied before tumor debulking surgery to shrink tumor masses, making physical removal of metastases easier, and possibly also post-surgery to eliminate residual metastatic spots. Such a strategy might optimize the surgical outcome and overall treatment effectiveness. Moreover, as demonstrated, the reactivation of the immune system not only converts the tumor microenvironment from immunologically cold to hot but also enhances the cytotoxic activity of chemotherapy combined with L-NMMA. Taken together, these considerations highlight the value of developing in vivo models that evaluate treatment efficacy at lower doses, which could optimize traditional chemotherapy and pave the way for innovative combination therapies, including immunotherapies. Optimizing tumor killing in this way may be crucial for improving outcomes in ovarian cancer patients.

Conclusions

Taken together, we present a novel perspective on treating ovarian cancer by proposing a dual combination therapy as a potential strategic approach. The relationship between ovarian cancer and the role of iNOS, and consequently, nitric oxide (NO), within the tumour microenvironment remains underexplored. Building upon previous findings presented in this work, which support the deleterious role of iNOS in ovarian cancer, an in vivo model was developed that recapitulates the late-stage disease conditions observed in human patients. This model demonstrated that combining platinating agents with iNOS inhibitors exerts beneficial effects, not only by shifting the tumour immune microenvironment from “cold” to “hot,” but also by inhibiting metastatic progression, as confirmed through pathological analysis of collected samples. These findings suggest new opportunities for targeting ovarian cancer that extend beyond direct cytotoxicity against cancer cells to include rebalancing the inflammatory response and modulating the tumour microenvironment. Such an approach holds promise as a component of combinatorial therapeutic strategies which can be applied in future for innovative therapies.

Chapter 4 – iNOS knockout cell line reveals a higher sensitivity to Cisplatin in vitro and in vivo

4.1 Introduction

Given the detrimental features of the OC-TME, targeting the cross-talk among its primary components represents a promising therapeutic strategy. Specifically, the OC-TME is enriched with EVs [275], pro-inflammatory cytokines [181], hormones like estrogens [276], and NO [277]. All of them is part of an established and solid network all made and developed to allow tumour progression guaranteeing protection from drugs and immune escape. There is substantial evidence about the role of pro-inflammatory cytokines in the establishment and induction of signals that can inhibit the immune response in the tumour niche [278], and it has also been reported that oestrogens are able to stimulate and influence tumour progression in ovarian cancer [279]. Also, EVs can stimulate cancer progression by releasing pro-cancer miRNAs [280]. Even if the pathological role of dysregulated NO has been extensively studied in other cancers, particularly in breast cancer [281], its precise functions in ovarian cancer remain insufficiently understood. As previously discussed, multiple cell populations within the TME express iNOS, leading to increase NO levels. Among the diverse functions attributed to NO, S-nitrosylation stands out as a key post-translational modification. This process involves the addition of a NO group to cysteine thyol residues of target proteins, thereby altering protein activity and modulating downstream signalling pathways [223]. Through this mechanism, NO can influence a wide range of cellular functions and contribute to tumour progression. S-nitrosylation is also known to play a role in stabilizing proteins and, consequently, preventing their degradation. Several studies proposed the involvement of S-Nitrosylation in EMT [191, 231, 282] and one study proposed a mechanism in which S-nitrosylation acts as a stabilizer of proteins, including Vimentin, by inhibiting the binding of ubiquitin units. Specifically, a NO group can interact with the thiol group of the E3 subunit, thereby preventing its interaction with ubiquitinase subunits and, as a result, regulating the activity of this enzyme [283]. It has also been showed that S-nitrosylation targets the Cys328 residue of Vimentin, potentially influencing its functions and stability [284]. The primary mechanism by which NO groups prevent ubiquitinase binding is through mechanical impairment of the interaction between the enzyme's active site and its substrate. Other detrimental effects of excessive S- nitrosylation include the interaction of NO moieties with transcription factors, leading to conformational changes that alter their activity and transcriptional potential [282]. Additionally, the accumulation of NO, beyond its role in S-nitrosylation, can act as a ROS, disrupting the redox balance within the tumour microenvironment [285]. To investigate the molecular consequences of NO depletion, a NOS2 knockout (KO) model was generated. This approach allowed us to study the impact of sustained iNOS loss on tumour cell behavior, mimicking the pharmacological inhibition of NO synthesis by L-NMMA. The NOS2 KO cell line provides an advanced tool to characterize NO-dependent pathways, as previously demonstrated in other cancer types [209]. Furthermore, the analysis conducted in this work was extended to a second OC cell line, A2780cis, to determine whether iNOS plays a consistent role across different OC subtypes. In A2780cis cell lines, the effects of iNOS knockdown were evaluated by using siRNA, a strategy widely adopted since their discovery and increasingly explored for therapeutic applications [286]. siRNA-mediated silencing reproduced the phenotypic changes seen with L-NMMA treatment in the OVCAR8 parental cell line. This supports the validity of our pharmacological model across another ovarian cancer subtype. The results highlight the link between nitric oxide, EMT, and cancer cell migration. The opportunity to temporarily disrupt NO-related pathways provides a valuable approach for gaining deeper insight into the deleterious effects of NO overexpression in a second cell line. Investigating the potential role of iNOS in regulating Vimentin expression could offer a meaningful perspective on one of the mechanisms contributing to EMT. In addition to EMT progression through Vimentin, bulk RNAseq was employed to comprehensively map the transcriptomic alterations induced by iNOS depletion. This omics approach, now a standard in modern research, offers broad insights into transcriptomic, proteomic, genomic, and lipidomic changes [287], especially valuable given the complexity of NO signalling. The impact of iNOS loss in HGSOC cells was investigated through RNA-seq to identify the most affected pathways. The importance of omic sciences has already been discussed in previous sections; however, it is worth emphasizing how impactful these approaches can be in contexts where NO has a broad and diverse range of potential targets. In this context, the selective inhibition of only one of the three nitric oxide synthase isoforms allowed for the specific correlation of pathway activation with NO produced exclusively by iNOS. This type of analysis has already been applied to metaplastic breast cancer, where Reddy et al. [209] identified a potential connection between iNOS expression and the EMT, opening new avenues for understanding iNOS-driven mechanisms. Given the encouraging data presented thus far, applying a similar approach to ovarian cancer could reveal a broader role for iNOS across various cancer types. While omic sciences are undoubtedly valuable, conducting meta-analyses across omic datasets from different contexts is even more critical. The data presented in the previous section of this work have been cross-referenced with patient-derived data from external databases. This meta-analysis has yielded more consistent and robust evidence supporting the essential role of iNOS, not only in vitro but also in clinical settings, bridging the gap between laboratory research and patient outcomes. To validate the in vitro findings presented in this work, an in vivo model was also developed. Tumour growth and metastatic potential were compared between mice injected with parental OVCAR8 cells and those injected with OVCAR8 iNOS KO cells, with or without Cisplatin treatment. This experimental design allowed the evaluation of the role of iNOS in tumorigenesis and therapy response in vivo. The importance of proceeding with a second in vivo model lies in the fact that, as previously mentioned, each in vivo model, particularly for ovarian cancer, has distinct features. Introducing an additional model allows for the investigation of aspects that a syngeneic in vivo model cannot fully address due to its intrinsic characteristics. The heterogeneity of ovarian cancer necessitates, when feasible and contextually appropriate, the expansion of available in vivo models to better reflect the disease's complexity. In this regard, the genetic background of the tumour plays a crucial role in selecting a suitable model. When aiming to study the immune system in its entirety, syngeneic in vivo models offer the advantage of preserving immune integrity; however, the genetic characteristics of the cancer cells remain equally important. As previously discussed, one of the most common and widely distributed mutations in ovarian cancer is the TP53 mutation [200]. Utilizing human ovarian cancer cell lines that harbor typical mutations in TP53 as well as BRCA1 and BRCA2, such as the OVCAR8 cell line, enables the generation of a second in vivo model that more closely resembles the genetic landscape observed in human patients. This approach offers a more accurate representation of how treatments like Cisplatin and L-NMMA might perform in a clinically relevant context. To overcome this limitation, we utilized NSG mice, which enabled the study of tumour development, metastatic potential, tumour dissemination, and the efficacy of chemotherapeutic agents using human ovarian cancer cell lines. Previous studies using human ovarian cancer cell lines have demonstrated that different lines produce varying outcomes in immunocompromised mouse models. Mitra et al. tested several human ovarian cancer cell lines and reported that OVCAR3 did not generate peritoneal metastases in any of the six mice tested. A similar lack of metastatic behavior was observed for OVCAR4 and OVCAR5. OVSAHO and CAOV3 also followed this trend, with CAOV3 producing peritoneal metastases in only one mouse. Notably, OVCAR8 induced metastases in all five mice tested [288]. This highlights the unique ability of OVCAR8 to closely mimic the clinical scenario of advanced-stage ovarian cancer, where patients are often diagnosed after peritoneal metastasis has already occurred [289]. Continuing with the same study, OVCAR8 showed complete tumour uptake in all mice following intraperitoneal injection, in contrast to other cell lines such as COV362, OVKATE, Kuramochi, SNU119, and UWB1.289 (BRCA-null), where no tumour uptake was observed [288]. Furthermore, at endpoint analysis, OVCAR8 exhibited full omental colonization in all five mice tested. This feature was not replicated in other cell lines: OVCAR3 showed omental metastasis in only two of six mice, OVCAR5 showed none, and OVSAHO also failed to demonstrate this behavior [288]. Considering these findings, along with the previously discussed genetic profile of OVCAR8, particularly its TP53 and BRCA mutations, the decision to include OVCAR8 in an expanded in vivo panel was driven by the goal of more accurately mimicking the human ovarian cancer setting. In addition, the benefits of including this second in vivo model are further supported by its ability to evaluate chemotherapy responses in human cell lines, specifically by comparing OVCAR8 parental and OVCAR8 iNOS KO cell lines. This aspect enabled the completion of the translational framework initiated in the first part of the study through L-NMMA administration, providing a comprehensive evaluation of iNOS depletion in both in vitro and in vivo settings. Considered the encouraging results that have been obtained in vitro still working with OVCAR8, and, as will be showed in the above sections of this work, on A2780cis, having the opportunity of bridging in vitro results with in vivo results presented an excellent opportunity to give solid proofs about the real effect of Cisplatin in combination with L-NMMA in ovarian cancer. Another significant advantage of this model is the absence of ascites formation, which allowed for improved follow-up of tumour initiation and progression. Collectively, this study presents a comprehensive approach, spanning genetic models, pharmacological inhibition, siRNA knockdown, and transcriptomic profiling, to elucidate the multifaceted role of iNOS and NO in ovarian cancer highlighting the effects on EMT, chemotherapy treatment and combination of chemotherapy with L-NMMA.

4.1.1 Hypothesis and aim of the study

iNOS plays a critical role in regulating EMT, and its depletion has been associated with reduced tumor growth, downregulation of Vimentin, and enhanced sensitivity to Cisplatin, both in vitro and in vivo. To better replicate the sustained suppression of nitric oxide observed with clinical administration of L-NMMA, NOS2 knockout clones were generated to investigate the long-term consequences of iNOS loss. Considered the encouraging results that have been showed in the previous sections of this work, for what concerns in vitro administration of L-NMMA on OVCAR8 cell lines, generation of an in vivo model expanded the consistency of the data previously reported. In this work, to even give more information spanning also to different ovarian cancer subtypes increasing consistency about the role of iNOS expressed at basal condition, a second cell line has been added, A2780cis, in order to detect the effects of iNOS on EMT in different ovarian cancer subtypes.

4.2 Materials and methods

Cell culture. HGSOC OVCAR8 was a gift from Nermin Kahraman (Houston Methodist Research Institute). OVCAR8-RFP-Luc were generated after transfection using a lentiviral vector. OVCAR8 and OVCAR8-RFP-Luc were cultured in RPMI1640 with 10% FBS and 1% Penicillin/Streptomycin at 37ºC supplied with 5% CO2. A2780cis was cultured using RPMI1640 supplied with 10%FBS, 1% penicillin/streptomycin and 2 mM glutamine at 37ºC and 5% CO2 with the addition of 1 μM of Cisplatin weekly.

Immunoblotting. Whole-cell lysate was extracted using Cell Signaling lysis buffer (20 mM Tris-HCl (pH 7.5), 150 mM NaCl, 1 mM Na2EDTA, 1 mM EGTA, 1% Triton, 2.5 mM sodium pyrophosphate, 1 mM beta-glycerophosphate, 1 mM Na3VO4, 1 μg/ml leupeptin, Cat #9803). Proteins were separated by SDS-PAGE gel and transferred to a PVDF membrane (Millipore Sigma, Cat #NX0095). The membranes were blocked with 5% non-fat milk and incubated with primary antibody overnight at 4∘C with gentle agitation using the following antibody: rabbit anti-iNOS (1:1000, Cell Signaling, Cat #95423), rabbit anti-Vimentin (1:1000, Cell Signaling, Cat #5741), rabbit anti-β-Actin HRP conjugate (1:7000, Cell Signaling, Cat#5125). Signals from iNOS and Vimentin were detected and amplified by using a secondary anti-rabbit HRP-conjugated antibody (1:3000, Cell Signaling, Cat #7074). Signals were detected using Clarity ECL Western Blotting Substrates from Bio-Rad (Cat #1705060S). Experiments were conducted in triplicates, or duplicates, where indicated in the relative results section. Results were considered statistically significant when $p < 0.05$.

RealTime-Glo™ MT Cell Viability Assay. 1.500 cells were seeded in white opaque 96-well plate (Greiner Bio-One, Cat# 655074). After 24 hours, gradients of Cisplatin (MCE®, Cat #HY- 17394) concentration (from 4μM to 24 μM) were added to the desired well together with MT Cell Viability Substrate and NanoLuc® luciferase (Promega, Catalog #G9711). Cells were maintained under regular culture conditions and luminescence was measured 72 hours after Cisplatin administration using a luminometer (GloMax navigator, Promega, Cat# E5302). Experiments were conducted in triplicates, and the results were considered statistically significant when $p < 0.05$.

Reverse Transcription, Quantitative Real-Time PCR (RT-qPCR). Total RNA was extracted using RNeasy mini kit from Qiagen (Cat# 74104) according to the manufacturer's protocol. RNA was reverse transcribed with the High-Capacity cDNA Reverse Transcription kit (ThermoFisher, Cat # 4368813). RT-qPCR was performed using the QuantStudio 12K Flex Real-Time PCR System (ThermoFisher, Cat# 4471134). Following primers for TaqMan™ Gene Expression Assay were purchased from ThermoFisher; human NOS2 (Cat #4453320) and human ACTB (Cat # 4333762F). Experiments were conducted in triplicates, and the results were considered statistically significant when $p < 0.05$.

Double nickase assay. Double nickase plasmids were obtained from Santa Cruz Biotechnology. Transfections were performed in 6-well plates, with 1.5×10^5 cells seeded per well. All reagents used in the procedure, including the double nickase plasmid (SC- 400666-NIC), the transfection reagent (SC-395739), and the transfection medium (SC- 108062), were also purchased from Santa Cruz. Puromycin was sourced from Gibco. For the transfection, 3 μg of the double nickase plasmid was resuspended in transfection medium and incubated for 5 minutes. The transfection reagent was prepared using the same procedure. The plasmid solution was then combined with the transfection reagent and incubated for 30 minutes at room temperature to allow complex formation. The resulting transfection mixture was added dropwise to the cells in antibiotic-free medium. After five hours, the transfection solution was removed and replaced with fresh antibiotic-free medium. Forty-eight hours post-transfection, the medium was replaced with fresh medium containing 1 µg/mL puromycin to initiate selection. Surviving clones were selected for GPF, expanded and screened for successful NOS2 knockout using Western blot analysis.

RNAseq. Differential expression analysis was performed using R (version 4.2.1) with the limma package. The parental cell line was used as the control group. Genes with an absolute log fold change (|LogFC|) greater than 0.58 and an adjusted p-value (p.adj) less than 0.05 were considered differentially expressed. Gene ontology (GO) and KEGG pathway analyses were visualized using ggplot2 (version 3.4.4) in R. The development of the pipeline, data mining, and pathway analysis were obtained with the contribution of Dr. Hong Zhao and Agne Baseviciene, who also contributed to the visualization of the results.

Scratch wound assay. The scratch wound assay was conducted on the OVCAR8 parental cell line and knockout clones KO1 and KO2. Cells were seeded at a density of 3×10^4 cells per well in Sartorius ImageLock plates, which are compatible with the Incucyte® S3 live-cell imaging system. This seeding density ensured 100% confluency within 24 hours, a prerequisite for the assay. After 24 hours, a uniform scratch was introduced in each well using the Sartorius WoundMaker™ tool. Wound closure was monitored at six-hour intervals over a 24-hour period using the Incucyte® S3 system. Image analysis and quantification of wound closure were performed using the Incucyte 2022B Rev2 software. Experiments were conducted in triplicates, and the results were considered statistically significant when $p < 0.05$.

Clones phenotype. The pictures of the KO clones were taken using Revolve microscope (Echo®). The images were taken at different magnifications, from 4X to 20X.

siRNA transfection. siRNA transfection was performed using siRNA Dharmacon validated and transfection reagent, both purchased from Dharmacon®. The siRNA was prepared at a final concentration of 50 nM by diluting in 195 µL of serum-free medium. Separately, 5 µL of transfection reagent was also diluted in 195 µL of serum-free medium. Both solutions were incubated at room temperature for 5 minutes. Following this initial incubation, the siRNA and transfection reagent solutions were combined and gently mixed. The resulting complex was incubated for an additional 20 minutes at room temperature to allow for complex formation. The transfection mixture was then added dropwise to each well, followed by the addition of 1.6 mL of serum-free medium. After six hours, the transfection solution was removed and replaced with standard complete growth medium. Total RNA was extracted 24 hours post- transfection, and protein samples were collected after 48 hours for downstream analysis.

Colony Formation Assay. Cells were seeded in 6-well plates at a density of 500 cells per well. After seeding, cells were incubated at 37 °C in a humidified atmosphere with 5% CO_2 and allowed to grow undisturbed for 14 days, or until visible colonies (≥50 cells per colony) had formed. Growth medium was replaced every 4 days to maintain optimal conditions. At the endpoint, colonies were gently washed twice with phosphate-buffered saline (PBS) to remove residual medium and non-adherent cells and stained with crystal violet solution for 15 minutes at room temperature. Excess stain was removed by washing the wells thoroughly with tap water until background was minimal. Plates were air-dried at room temperature before imaging and analysis. Stained colonies were visualized and imaged using a flatbed scanner or imaging system. Quantification was performed either manually by counting the total area of colonies or using ImageJ software (NIH) with a colony analysis plugin. All experiments were independently repeated in triplicates and considered statistically significant when $p < 0.05$.

Animal model. Training in animal handling procedures for murine models was conducted at the animal facility of the Houston Methodist Research Institute (6670 Bertner Avenue, Houston, TX, 77030). The training followed institutional requirements and included instruction on cage maintenance, food and water replacement, and euthanasia procedures. All animal protocols for the experiments were approved by the Houston Methodist Hospital Research Institute Animal Care and Review Office (IACUC number IS00007220). NOD SCID gamma mice 4 weeks old females were used for the xenograft in vivo model. Mice received IP injection of 5 x 10^6 OVCAR8-RFP-Luc and OVCAR8NOS2-KO-RFP-Luc in 200 µL of PBS. For this experiment, a number n=6 of mice which received the injection of OVCAR8-RFP-Luc (parental group) and a number of n=6 of mice which received the injection of OVCAR8NOS2-KO-RFP-Luc was used for the tumor development detection through the ROIs and a number of n=6 of mice which received the injection of OVCAR8-RFP-Luc (parental group) and a number of n=6 of mice which received the injection of OVCAR8NOS2-KO-RFP-Luc was used for the survival experiment. Mice body weight was detected using a regular laboratory balance and luminesce signal from labelled cells was analysed using Perkin IVIS Spectrum CT with Luminescence detection in automatic mode. Mice received a single injection of cisplatin (6.4 mg/kg) during the second week of treatment. ROIs were monitored every four days, and the survival analysis was conducted until the last mouse in one of the two experimental groups had died. For the survival experiments, in addition to animals found dead due to illness or distress, mice were euthanized in accordance with the Houston Methodist Research Institute animal facility guidelines when body weight fell below 15 g or upon veterinary assessment indicating severe illness and animal distress. The experiment was considered concluded when the number of mice in any one of the study groups was depleted.

Statistical analysis.

Two-way analysis of variance (ANOVA) or ordinary one-way ANOVA, when possible, was performed using GraphPad Prism version 7.0 (GraphPad Software, San Diego, CA) to evaluate the effects of two independent factors and their interaction on the dependent variable. Prior to analysis, data were checked for normality and homogeneity of variances. When significant effects were detected, multiple comparisons were conducted using Tukey's test to identify specific group differences. Results were considered statistically significant at $p < 0.05$.

4.3 Results

4.3.1 Double nickase assay causes iNOS expression loss

The double nickase system works by transfecting two plasmids which encode for a gDNA which guides the CRISPR/CAS9 system to cut in the desired area of the genome, in this case, NOS2 gene. After the cut, positive clones are selected through Puromycin treatment (1 μg/mL) as the plasmids carry the resistance to this antibiotic giving cells a temporary resistance to it. After 72 hours from the administration of Puromycin, positive clones were expanded and screened through western blotting. Shown in **Figure 4.1** is the expression of iNOS following treatment and sub clone isolation. A clear difference in protein expression was observed between the parental OVCAR8 cells and the three clones, named KO1 and KO2. The immunoblot above shows the strong impairment that has been obtained after the double nickase assay.

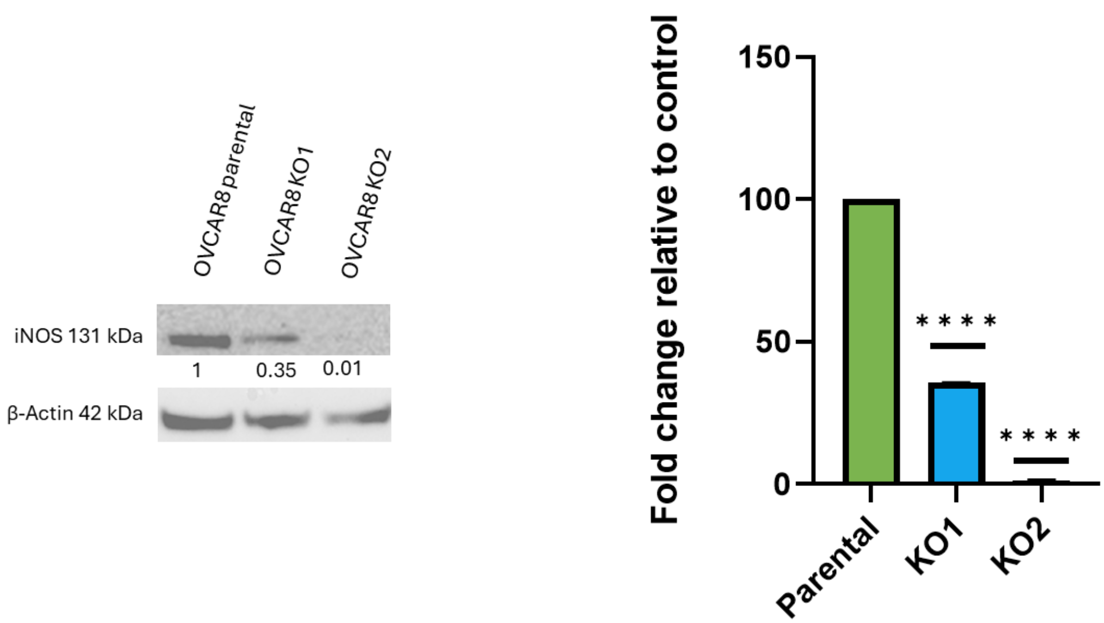

Figure 4.1. Generation of NOS2 OVCAR8 knockout clones. Figure 4.1A shows the expression of NOS2 into OVCAR8 parental and the knockout 1, 2 and 3 obtained by using the SantaCruz double nickase assay. It is also possible to observe the consistency of protein loading through the β-Actin expression levels. The knockout clone 1 showed a strong reduction of iNOS with residual iNOS levels corresponded only to 35% ($p < 0.05$). An even stronger reduction has been observed for the KO clone 2 (KO2) with a minimal residual level of iNOS corresponding to 1% ($p < 0.05$). Experiments were conducted in three independent replicates.

It is possible to observe how the knockout clone 1 showed a solid reduction of iNOS where the residual iNOS levels corresponded only to 35% with a strong statistically significant p value ($p < 0.05$). An even stronger reduction has been observed for the KO clone 2 (KO2) with a minimal residual level of iNOS corresponding to 1% ($p < 0.05$). These results showed how the constitutive expression of iNOS can be significantly reduced, as it has already been conducted in a recent publication in Nature communications for metaplastic breast cancer [209], with similar reduction in protein expression levels showing the consistency of these results.

4.3.2 NOS2 impacts on cell morphology

Impairment of iNOS function, and consequently of NO production, affected cell morphology. As previously mentioned in the first part of this work, it has already been demonstrated that L-NMMA, and therefore iNOS inhibition, has a direct impact not only on cell viability but also on Vimentin expression. Vimentin is a protein associated with EMT [203] and cytoskeleton organization [220], and it may play important roles in regulating cell morphology and structural organization. **Figure** 4.**2** shows the morphological differences between the OVCAR8 parental cell line and OVCAR8 knockout clones.

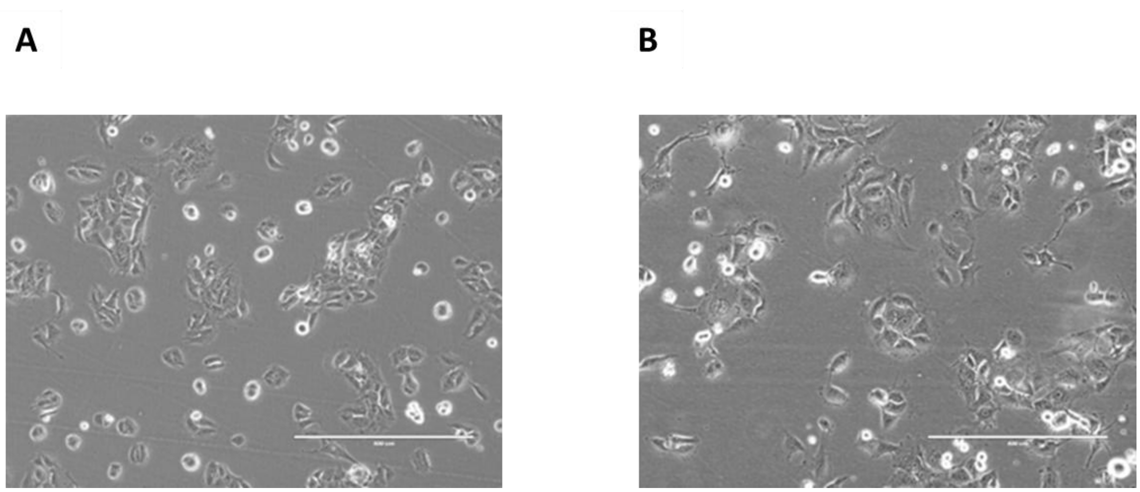

Figure 4.2. Morphology of OVCAR8 NOS2 knockout clones. The two images on **Figure 4.2A** show on the left a 4X magnification of parental OVCAR8 (left) and OVCAR8 KO in 4X. In **Figure 4.2B** It is possible to observe a change from an epithelial shape to a rounded and clustered shape of the knockout clones with a more senescent aspects and vacuolization procedures.

Clones KO1, KO2, and KO3 showed a clear morphological change as it is possible to observe in Figure 4.2. These changes also influenced their growth patterns; all the clones mentioned above (clone KO1, clone KO2) showed a greater tendency to grow in clusters rather than spreading evenly across the culture plate surface. An entire reorganization of cell shape can indicate a total reassert of cells cytoskeleton which may influence their potential to spread in the plate in vitro, in vivo in terms of metastatic spread. It is important to highlight that this morphological reorganization didn't afflict cell viability inducing senescence, as it will be demonstrated in the following viability assays comparing parental and knockout cell lines without receiving any treatments. Interestingly, as it will also be reported in the following sections, the downregulation of iNOS lead to vimentin downregulation, higher sensitivity to Cisplatin and a slower efficiency in formation of colonies and migration.

4.3.3 Vimentin reduction following NOS2 KO

As targeting NOS2 could have an important role in the EMT transition, the morphology change was investigated in the context of EMT marker Vimentin [219-221]. A recent publication reports, in breast cancer, a role of NOS2 in the expression of some EMT markers [209]. One of the markers analyzed is Vimentin. It is one of the key players in EMT [203] and considering the late diagnosis that occurs in most patients, metastasis is an event that is already present at the moment of the diagnosis. For this reason, the potential impact of iNOS reduction on Vimentin expression in ovarian cancer was investigated (**Figure 4.3**).

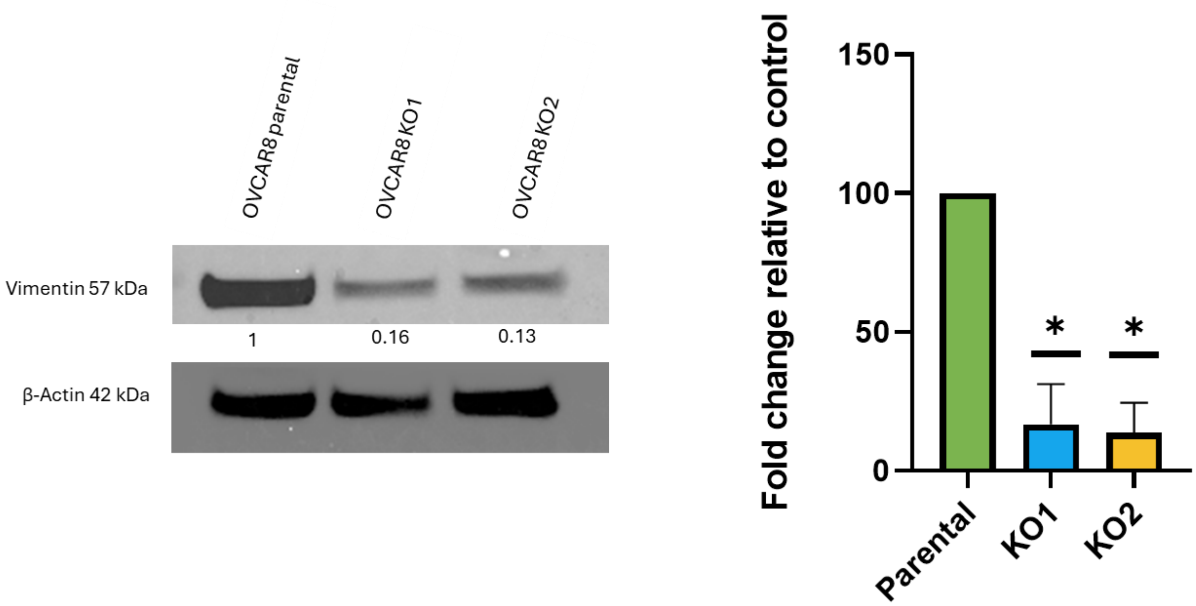

Figure 4.3. iNOS is related to Vimentin expression. The figure shows the level of Vimentin in parental OVCAR8 and in the knockout clones. The reduction of Vimentin is observed when iNOS2 is downregulated. β-Actin shows the consistency in the protein loading. Vimentin expression was reduced to 16% ($p < 0.05$) in clone KO1 and 13% ($p < 0.05$) in clone KO2. Experiments were conducted in three independent replicates.

The reduction of NOS2 levels resulted in decreased expression of downstream genes associated with NOS2 activity. Specifically, Vimentin levels in the two knockout clones were lower than those in the parental cells, as illustrated in Figure 4.3. Vimentin expression was reduced to 16% ($p < 0.05$) in clone KO1 and 13% ($p < 0.05$) in clone KO2, compared to 100% in the parental line. The observed effects were comparable with the impact observed when parental cell lines were treated with L-NMMA, indicating similar outcomes in the knockout clones and how potentially these knockout clones are potentially more sensitized for chemotherapy, as will be shown in the following sections.

4.3.4 Vimentin reduction is confirmed through siRNA knockout in another iNOS expressing cancer cell lines resistant to chemotherapy

To validate previous findings presented in this work, where L-NMMA treatment resulted in reduced Vimentin expression and consistent observations in our KO model, two siRNAs targeting NOS2 were administered to assess whether RNAi would replicate these effects in A2780cis ovarian cancer cell line, which exhibits basal NOS2 expression as demonstrated earlier, to further corroborate the results identified in this work ~~results~~ across different cellular models. NOS2 mRNA levels were significantly reduced following siRNA treatment as shown in **Figure 4.4** where A2780cis cells exhibited a substantial decrease in NOS2 mRNA, with both siRNAs achieving reductions lower than 50% of fold change.

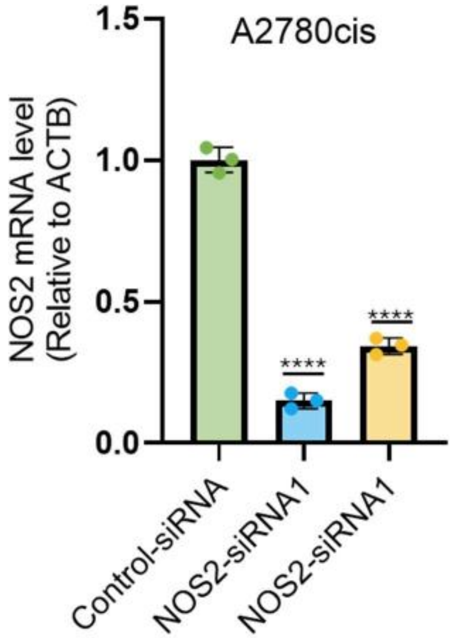

Figure 4.4. siRNA1 and siRNA2 led to a complete reduction of NOS2 mRNA. In the figure it is shown a strong reduction of NOS2 mRNA in A2780cis too where over a 50% of reduction is observed. siRNA1 resulted in a strong reduction of NOS2 mRNA levels, reaching a level of 0.2 compared to scramble siRNA ($p < 0.05$). siRNA2 also produced a significant decrease, reducing NOS2 mRNA to 0.37 relative to scramble siRNA ($p < 0.05$).Experiments were conducted in three independent replicates.

The results shown above led to an interesting observation, already discussed in earlier sections of this work. Specifically, siRNA1 resulted in a significant reduction of NOS2 mRNA levels, reaching a fold change of 0.2 compared to scramble siRNA ($p < 0.05$), while siRNA2 also produced a significant decrease, reducing NOS2 mRNA to 0.37 relative to scramble siRNA ($p < 0.05$). This siRNA-mediated knockdown demonstrated, first, that iNOS is expressed at a basal level in A2780 cells (as previously shown in this study), and second, that it is possible to achieve specific targeting of NOS2 using siRNA technology. Together with RNA reduction levels, a reduction was observed in iNOS protein levels, followed by a reduction in Vimentin expression levels as shown in **Figure 4.5**. The levels of Vimentin went down together with the levels of iNOS reaching a fold change level of 0.4 for siRNA1 and 0.3 for siRNA2. These results showed how also for other types of cancer there might be a correlation between the expression and release of NO with the expression of Vimentin.

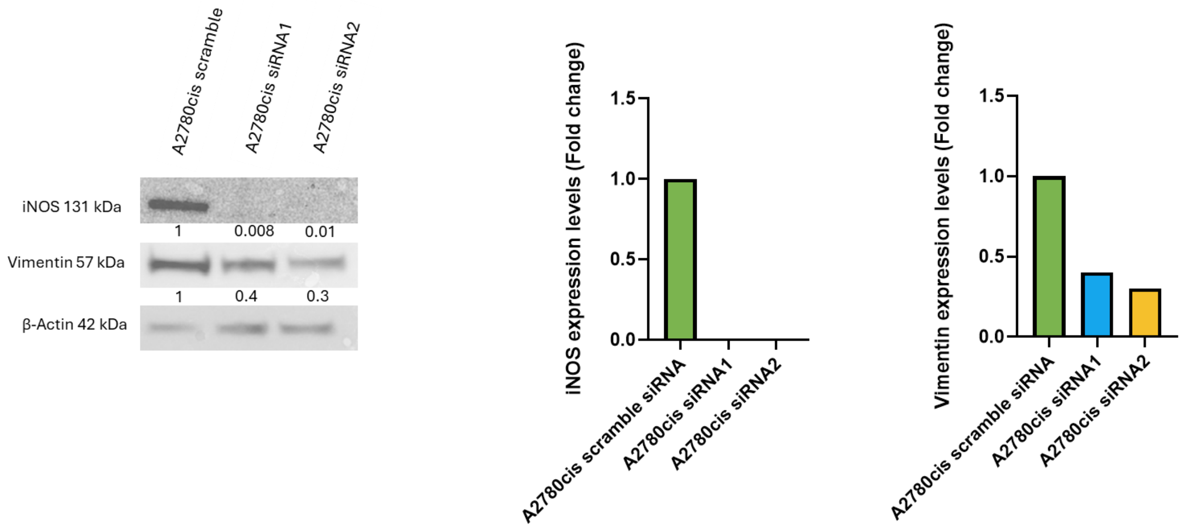

Figure 4.5. siRNA treatments show that iNOS expression levels are related to the levels of Vimentin expression. The Figure on the left shows a complete iNOS expression inhibition following the administration of two different siRNAs, confirmed by densitometric analysis in the center. The Figure on the right shows that concurrently, Vimentin levels also decreased reaching a fold change level of 0.4 for siRNA1 and 0.3 for siRNA2, suggesting a potential relationship between iNOS and Vimentin across different subtypes of ovarian cancer. Experiments were conducted in two independent replicates.

It is also possible to observe that, in a different ovarian cancer subtype, vimentin expression remains impacted. While the differences between ovarian cancer subtypes, as well as the known transcriptional and translational variations between chemosensitive and chemoresistant cell lines, must be considered, iNOS appears to play a regulatory role in vimentin expression in this second cell line as well. Given this, and considering the high recurrence rate of ovarian cancer (approximately 80% of patients) [290], the administration of L-NMMA could potentially be explored as part of innovative therapeutic strategies following relapse.

4.3.5 NOS2 KO has a higher sensitivity to Cisplatin

Platinating agents are the first-line treatment approach for ovarian cancer [291]. Chemotherapy is administered immediately after tumour debulking surgery, during which metastatic lesions are removed [291]. This strategy aims to prevent any residual tumourigenic events in the abdominal cavity, especially in cases where complete removal of all metastatic spots is not achievable during surgery. Unfortunately, a significant proportion of patients experience relapse, and cancer cells often acquire chemoresistance, rendering standard treatments ineffective. Here, it has been demonstrated that the modulation of iNOS can enhance the efficacy of cisplatin in cancer cells, thereby increasing the cytotoxic effects of chemotherapy. This improvement may translate to reduced side effects for patients, prolonged treatment effectiveness, and a decreased likelihood of developing chemoresistance due to the drug's heightened killing efficiency. MT-Glo Viability assay (also known as RT-Glo viability assay) is an efficient procedure to detect viability over time of cell with or without any treatments. The purpose of the experiment was to detect the effect of Cisplatin in the parental cell line after 72 hours, similarly to what has been done to detect the IC50 in the parental cell line. Viability was measured detecting luminescence produced after the reduction of a substrate (RT-Glo Max substrate, Promega®) which can be reduced only if cells are viable. The proliferation assay showed higher sensitivity of the knockout models compared to the parental OVCAR8 cells. Across the entire tested range of Cisplatin concentrations (4 μM to 24 μM), both clones consistently showed lower proliferation rates (**Figure 4.6**).

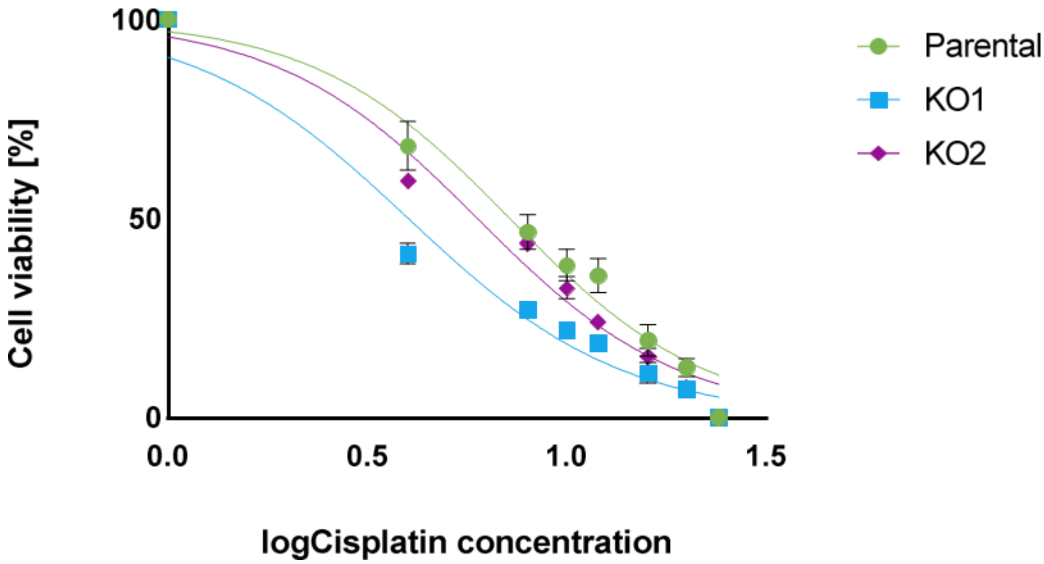

Figure 4.6. NOS2 knockout clones show higher sensitivity to Cisplatin. 4 μM of cisplatin achieved the IC50 for KO1 where the cell viability was 42.41% ($p < 0.05$), 58% in KO2 and 72.35% of OVCAR8 parental. At 8 μM Cisplatin, viability for KO1 was 55.1% in the parental cells compared to 28.71% ($p < 0.05$) in KO1 and 43.71% in KO2. At 10 μM, viability decreased to 48.43% in the parental line and 23.7% ($p < 0.05$) in KO1 and 33.1 % ($p < 0.05$) in KO2. At 12 μM, the viability values were 46.1% for parental cells and 20.53% ($p < 0.05$) in KO1 and 33.1% ($p < 0.05$) in KO2. With 16 μM, viability dropped to 32.9% in parental cells versus 13.1% ($p < 0.05$) in KO1 and 17.01% ($p < 0.05$) in KO2. At 20 μM, parental cells showed 27.75% viability, while KO1 was at 9.17% ($p < 0.05$) and 9.78% ($p < 0.05$) in KO2. Finally, at the highest concentration of 24 μM, proliferation was reduced to 17.86% in the parental cells and only 2.23% ($p < 0.05$) in KO1 and 2.72% ($p < 0.05$) in KO2. Experiments were performed in three independent replicates.

The lowest tested concentration (4 μM) already achieved the IC50 for KO1 where the cell viability was 42.41% ($p < 0.05$), 58% in KO2 and 72.35% of OVCAR8 parental. At 8 μM Cisplatin, viability for KO1 was 55.1% in the parental cells compared to 28.71% ($p < 0.05$) in KO1 and 43.71% in KO2. At 10 μM, viability decreased to 48.43% in the parental line and 23.7% ($p < 0.05$) in KO1 and 33.1 % ($p < 0.05$) in KO2. At 12 μM, the viability values were 46.1% for parental cells and 20.53% ($p < 0.05$) in KO1 and 33.1% ($p < 0.05$) in KO2. With 16 μM, viability dropped to 32.9% in parental cells versus 13.1% ($p < 0.05$) in KO1 and 17.01% ($p < 0.05$) in KO2. At 20 μM, parental cells showed 27.75% viability, while KO1 was at 9.17% ($p < 0.05$) and 9.78% ($p < 0.05$) in KO2. Finally, at the highest concentration of 24 μM, proliferation was reduced to 17.86% in the parental cells and only 2.23% ($p < 0.05$) in KO1 and 2.72% ($p < 0.05$) in KO2.

4.3.6 Scratch wound assay

NO can modify cytoskeletal components directly through nitrosylation [231] or indirectly by modulating signaling pathways such as focal adhesion kinase [292], and MMPs [293]. These pathways collectively influence cellular migration and invasion. The scratch wound assay is a widely used technique to evaluate the efficiency of cells in recovering from an artificially induced scratch in a fully confluent well. The purpose of this experiment was to monitor the cells' capacity to close the wound after scratch induction in a 96-well plate. In this study, we compared the wound closure efficiency between OVCAR8 parental cells and the knockout cell lines. The results are presented in **Figure 4.7A** and **Figure 4.7B**.

A B

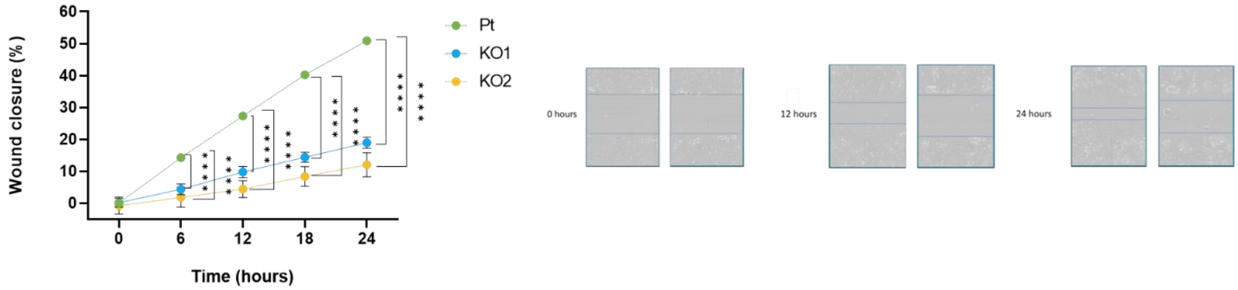

Figure 4.7 (A-B). **NOS2 knockout clone OVCAR8 cell line shows a lower migration efficiency. Figure 4.7A** shows the wound closure efficiency over a period of 24 hours. After six hours, wound closure was 4.3% ($p < 0.05$) for KO1 and 1.8% ($p < 0.05$) for KO2, compared to 14.27% in the parental cells. At twelve hours, closure increased to 9.74% ($p < 0.05$) for KO1 and 4.39% ($p < 0.05$) for KO2, while the parental line reached 27.43%. After eighteen hours, KO1 showed 14.34% ($p < 0.05$) efficacy of wound closure and KO2 for 8.35% ($p < 0.05$), whereas the parental cells had closed 40.18% of the wound. At the 24-hour endpoint, wound closure was 18.93% ($p < 0.05$) for KO1 and 12.05% ($p < 0.05$) for KO2, significantly lower than the 50.85% closure observed in the parental OVCAR8 cells. **Figure 4.7B** shows pictures of different time lapses comparing the closure of the wound in OVCAR8 parental and KO2. Experiments were performed in three independent replicates.

The knockout had a significant impact on the migration ability of the knockout models. The percentage of wound closures in KO1 and KO2 clones differed significantly from the OVCAR8 parental cell line. Wound closure was monitored every six hours over a 24-hour period. After six hours, wound closure was 4.3% for KO1 and 1.8% for KO2, compared to 14.27% in the parental cells. At twelve hours, closure increased to 9.74% for KO1 and 4.39% for KO2, while the parental line reached 27.43%. After eighteen hours, KO1 showed 14.34% efficacy of wound closure and KO2 for 8.35%, whereas the parental cells had closed 40.18% of the wound. At the 24-hour endpoint, wound closure was 18.93% for KO1 and 12.05% for KO2, significantly lower than the 50.85% closure observed in the parental OVCAR8 cells. In figure 4.7B it is possible also to observe the difference in migration over the time and how OVCAR8 parental had a quicker efficiency in wound closure compared to the knockout clones.

4.3.7 Colony formation assay

As mentioned in the section above, iNOS plays a significant role in cell motility. It has already been demonstrated that Vimentin expression decreases following iNOS inhibition, and that wound closure efficiency is markedly impaired in NOS2 knockout clones. In line with these findings, a colony formation assay was conducted to specifically assess the ability of ovarian cancer cells to proliferate and spread across the surface of a 12-well plate (**Figure 4.8A-B**). For that reason, the efficacy of forming colonies was tested by seeding OVCAR8 parental and the two knockout clones at a density of 500 cells per well in a 12-well plate. the same experiment was performed on the second cell line taken into analysis, A2780cis, by administering two different siRNAs to simulate, also in this cell line, which were the effects of iNOS depletion in terms of colony formation.

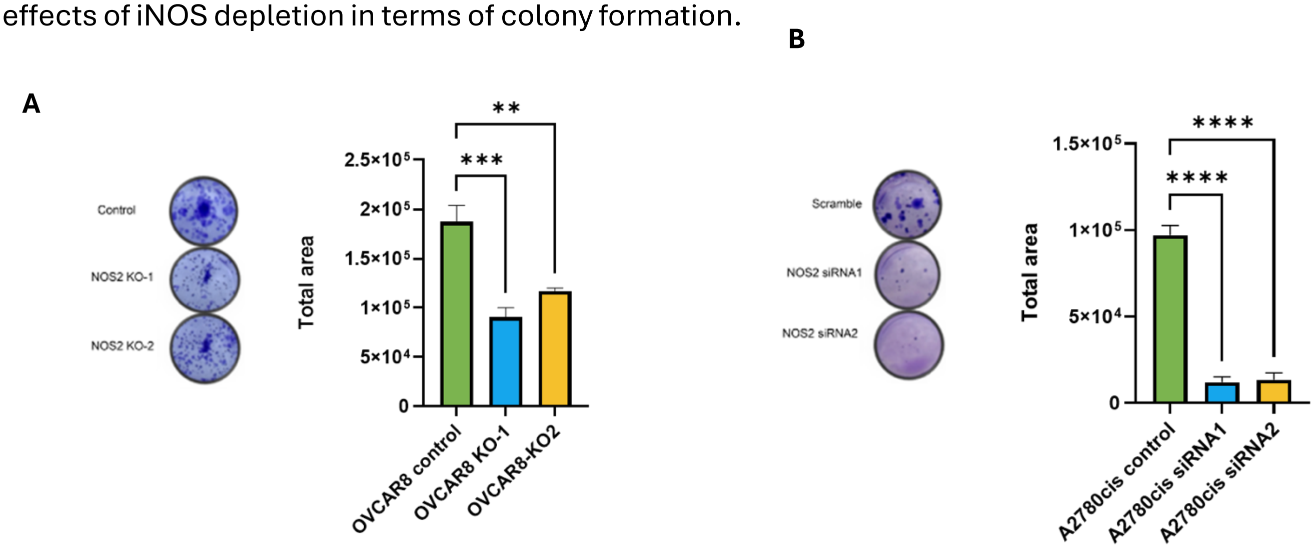

Figure 4.8 (A-B). Reduction in colony formation is related to iNOS depletion. Figure 4.8A shows a marked reduction in colony formation in the knockout (KO) clones compared to the parental cell line, with more than of a 50% decrease observed in KO1 ($p < 0.05$) and more than the 40% for KO2 ($p < 0.05$).. Similarly, **Figure 4.8B** highlights a significant reduction in colony formation in A2780cis cells, with over 85% reduction noted for both siRNAs ($p < 0.05$). Experiments were performed in three different replicates.

A significant reduction in colony formation was observed in OVCAR8 (**Figure 4.8A**), as well as in A2780cis (**Figure 4.8B**). In Figure 4.8A it is possible to observe how KO-1 and KO-2 had a reduction close to the 50% when compared with the total area of the control. Same results showed in Figure 4.8B even with a stronger impact, where more than the 85% of reduction of colony formation was observed using siRNA1 and siRNA2 on A2780cis. This experiment confirmed that iNOS plays a crucial role in cellular motility, morphology, and migration, three key features involved in EMT. The effects observed with the use of L-NMMA suggest that inhibiting iNOS can directly impact EMT, potentially limiting one of the most deleterious aspects of ovarian cancer: metastasis, which often occurs alongside acquired chemoresistance.

4.4 Mechanistic understanding through transcriptome level analysis

Phenotypic alterations associated initially with the activity of L-NMMA and subsequently with the generation of a knockout were observed. These alterations impacted overall cellular viability following Cisplatin treatment and were evident in markers of the Epithelial to Mesenchymal transition, with particular emphasis on Vimentin expression. Morphological changes, including vacuolization and alterations in cellular morphology, were also detected, collectively indicative of cytoskeletal reorganization. These changes, linked to iNOS and consequently to NO, the terminal enzymatic product, may modulate S-Nitrosylation, a post-translational modification characterized by the covalent attachment of a NO group to a thiol residue of a protein Cysteine group [285]. Overproduction of NO, resulting from upregulated expression of NOS enzymes, can lead to dysregulated cellular states frequently associated with oncogenesis [294]. Due to the unique properties of NO, including its capacity to diffuse across cellular membranes independent of specific receptors, the abundance of cysteine residues in diverse proteins, and the extensive repertoire of potential post-translational modifications, a comprehensive analysis was warranted to delineate the molecular pathways involving iNOS and NO. Accordingly, bulk RNA sequencing was conducted, the results of which will be presented in the subsequent chapter.

4.4.1 Molecular level understanding of NOS2 KO in OVCAR8 cells.

Omics technologies have fundamentally transformed the analysis of cellular pathways and interactions. Since their initial applications in the early 2000s, these technologies have made significant advancements and have become indispensable tools for comprehensive analyses at resolutions previously unimaginable. Transcriptomic profiling offers a revolutionary approach to gaining deep insights into cellular mechanisms. Consequently, as mentioned above, bulk RNAseq was conducted to compare the transcriptional landscapes of OVCAR8 parental cells and OVCAR8 KO cells. In **Figure 4.9**, the procedure and experimental plan adopted from the generation of the knockout to the sequencing are illustrated.

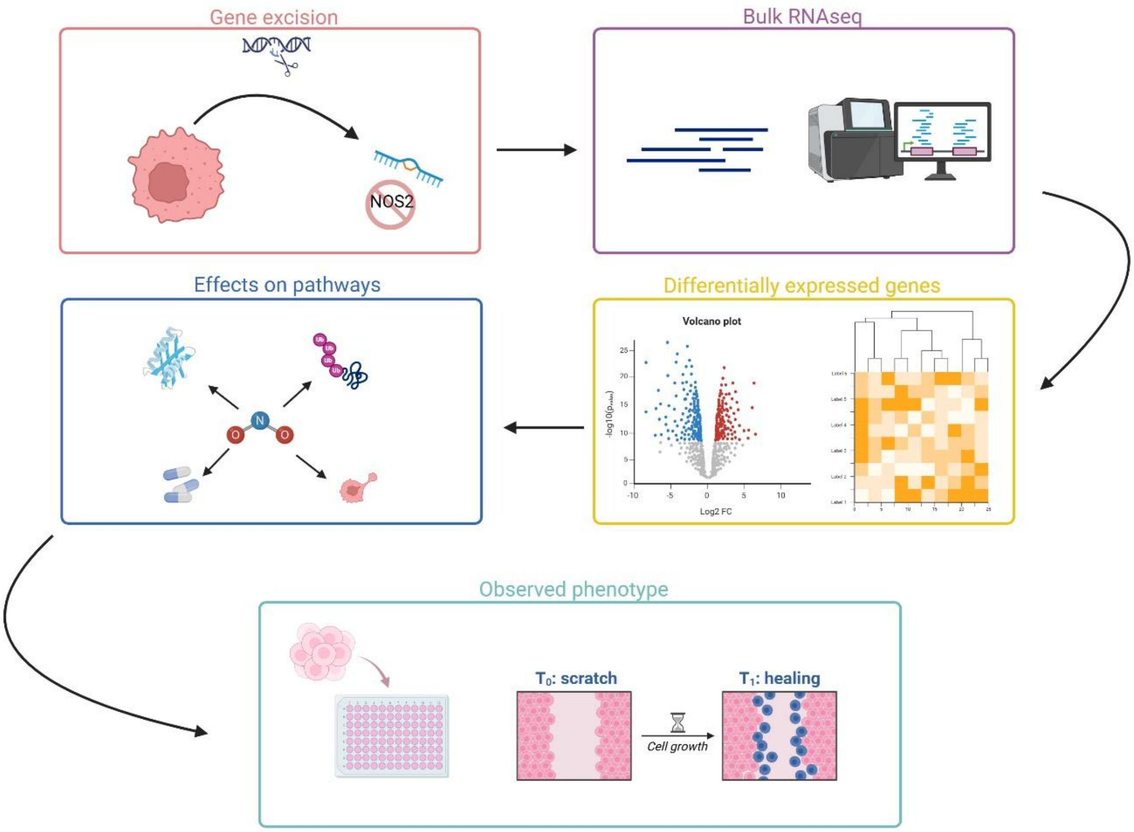

Figure 4.9. From the generation of a knockout to the observed phenotype. The following map shows the procedures adopted to identify all the possible dysregulated pathways after the generation of a knockout. Created in https://BioRender.com.

4.4.2 RNAseq workflow

RNA samples were analyzed following this grouping system **(Table 4.1).** OVCAR8 NOS2 parental were considered as control and were compared with OVCAR8 NOS2 KO.

Samples grouping	
ID	**Condition**
Pt-3	Control
Pt-2	Control
Pt-1	Control
KO-1	KO
KO-3	KO
KO-2	KO

Table 4.1. Samples grouping for the RNAseq. OVCAR8 parental and OVCAR8 KO cells were analyzed in triplicate. Pt-1, Pt-2, and Pt-3 represent the three replicates of the OVCAR8 parental cells, while KO-1, KO-2, and KO-3 represent the three replicates of the OVCAR8 KO clone.

After grouping our samples, a library from the transcripts obtained from each sample has been prepared. A schematic representation of the RNAseq library preparation workflow is represented in figure below **(Figure 4.10).**

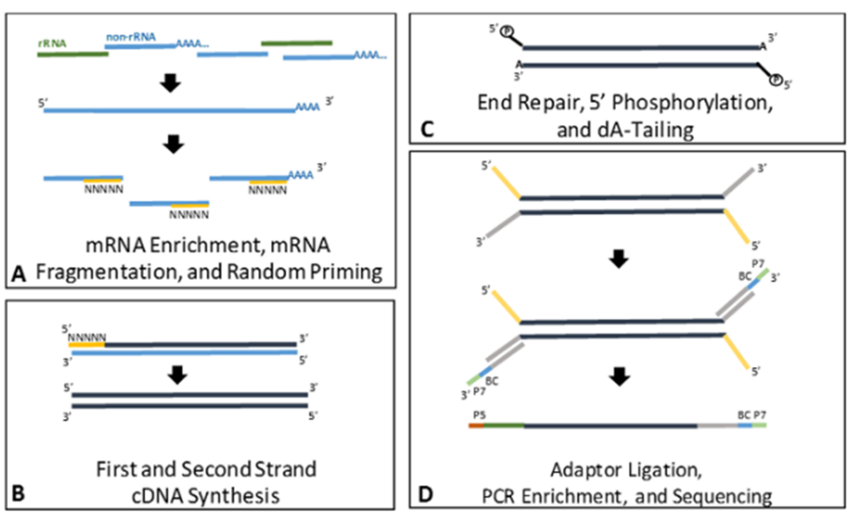

Figure 4.10. Schematic representation of the RNA-seq library preparation workflow. The figure illustrates each step of the library preparation process, starting from mRNA enrichment, followed by cDNA synthesis, dA-tailing, and concluding with sequencing.

After the library preparation step and the final sequencing, the sequenced fragments are undergone to a bioinformatic procedure which is represented in the following figure **(Figure 4.11)**

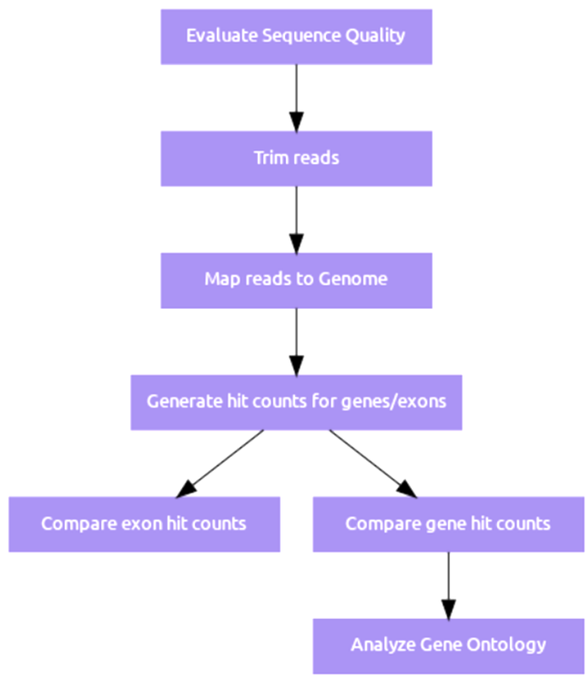

Figure 4.11. Workflow summarizing the procedure step by step for the bioinformatic analysis. In this figure it is possible to observe the bioinformatic pipeline needed to generate the data presented above.

4.4.3 Sample sequencing statistics

A summary of the sequencing statistics is represented in **Table 4.2.**

Sample ID	# Reads	Yield (Mbases)	Mean Quality Score	% Bases >= 30
Pt-1	35118395	10536	38.48	92.82
Pt-2	34438978	10332	38.46	92.73
Pt-3	37877451	11363	38.47	92.77
KO-3	37804510	11341	38.51	92.92
KO-1	33821953	10147	38.52	92.98
KO-2	32764103	9829	38.5	92.91

Table 4.2. Sample sequencing statistics. In the following table are reported the statistics per sample. It is possible to observe the high-quality score (the maximum score is considered 40).

The mapped reads to the reference genome and all the statistics related to the mapping are reported in **Table 4.3**

Sample ID	Total Reads	Total Mapped Reads	% Total Mapped Reads	Unique Mapped Reads	% Unique Mapped Reads
KO-1	33512193	32911547	98.20767922	32039428	95.60528611
KO-2	32469284	31899705	98.24579131	30979705	95.41234417
KO-3	37449049	36789880	98.23982446	35770360	95.51740553
Pt-1	34764310	34121082	98.1497461	33220093	95.55803926
Pt-2	34068887	33420664	98.09731677	32502934	95.40356866
Pt-3	37508849	36800460	98.11140832	35802442	95.45065486

Table 4.3. Statistics related to the mapping phase of the amplified transcripts. In the following table is represented a summary of the statistic after mapping the reads to the reference genome.

After extracting gene hit counts, the resulting count table was used for downstream differential expression analysis. Using DESeq2, we compared gene expression between the user-defined groups of samples. The Wald test was applied to generate p-values and $\log_2$ fold changes. Genes with an adjusted p-value < 0.05 and an absolute $\log_2$ fold change > 1 were considered significantly differentially expressed in each comparison. The number of significantly differentially expressed genes for all comparisons is summarized below in **Table 4**.4.

Comparison	Upregulated Genes	Downregulated Genes	Total Significantly Differentially Expressed Genes
Control-vs-KO	199	203	402

Table 4.4. Statistics from the comparison of gene expression between OVCAR8 parental and OVCAR8 KO using DESeq2. In this table it is possible to observe a summary of the upregulated, dysregulated and significantly differentially expressed genes.

Next, a Gene Ontology (GO) analysis was performed on the set of statistically significant genes using GeneSCF v1.1-p2. The goa_human GO list was used to cluster the genes based on their associated biological processes and to assess their statistical significance. The resulting list of genes, grouped according to their Gene Ontology categories, is presented in **Table 4.5**.

Comparison	Number of Enriched GO Terms	Total GO Terms	% Enriched GO Terms
Control-vs-KO	200	1656	12.07729469

Table 4.5. Gene ontology analysis statistics obtained through the software GeneSCF v.1.1-p2. In this table it is possible to observe a summary of the GO analysis obtained after sequencing and comparing the samples in order to associate the genes for their biological function.

4.4.4 Distribution of read counts

The distribution of read counts in the libraries was examined before and after normalization. Original read counts were normalized to account for factors such as variation in sequencing yield between samples. These normalized read counts were then used to accurately identify differentially expressed genes. **Figure 4.12** shows the read counts for each sample before normalization.

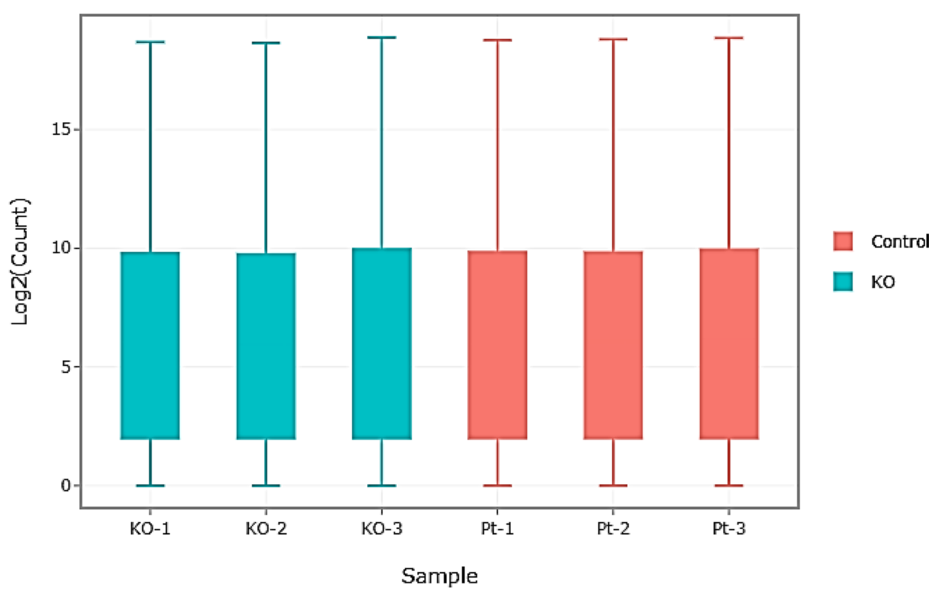

Figure 4.12. Distribution of unnormalized reads count for gene.

Figure 4.13 shows the read counts for each sample after the normalization.

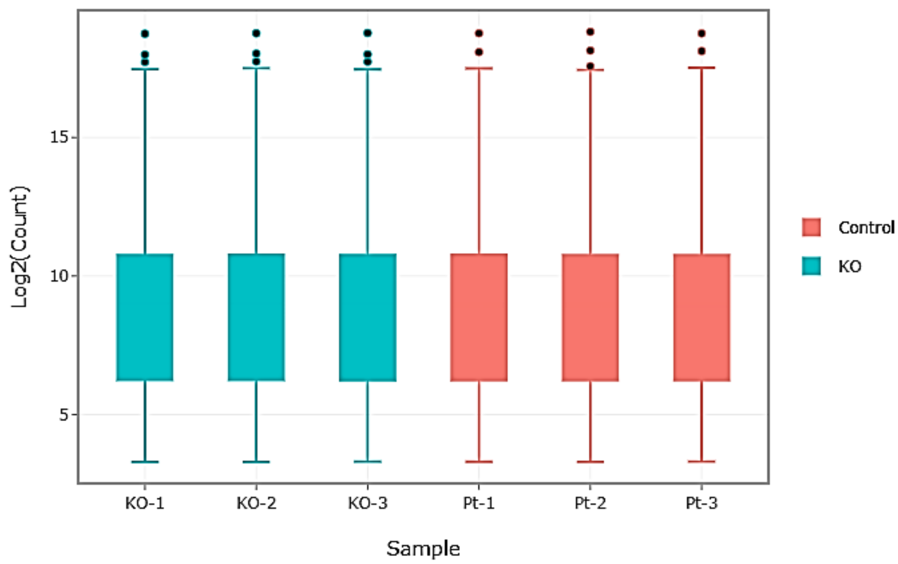

Figure 4.13. Distribution of normalized reads count for genes.

4.4.5 Sample similarity assessment

Data quality assessments were performed to identify any samples that were not representative of their group and could potentially affect the analysis quality. The overall similarity among samples was evaluated using the Euclidean distance between them. This method allowed us to examine which samples were similar or different and whether they conformed to the expectations of the experimental design. A shorter distance indicates greater similarity between samples. Based on these distances, samples were clustered as shown in **Figure 4.14**.

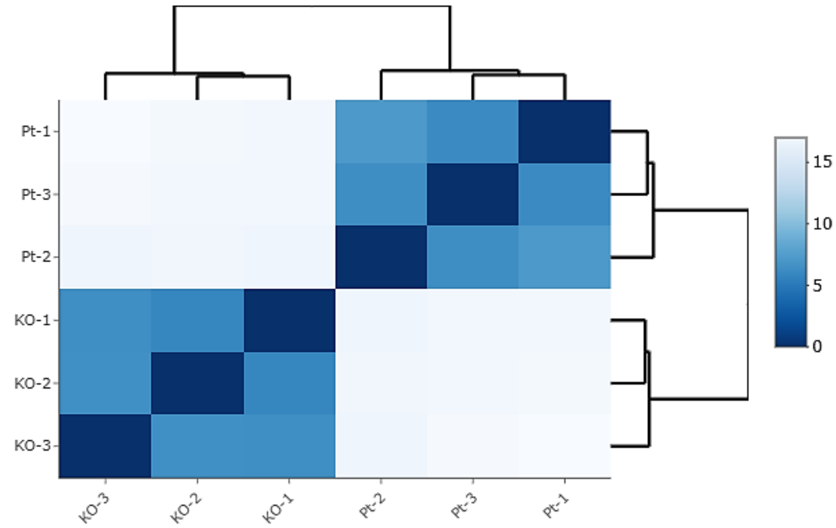

Figure 4.14. Heatmap of sample-to-sample distance. In this map it is possible to observe how close and how different are the samples related to each others, in a colorimetric scale from light blue to dark blue (considered as the closest match).

4.4.6 PCA analysis

Principal component analysis (PCA) is another method used to reveal similarities between samples based on the distance matrix. In **Figure 4.15**, samples are projected onto a 2D plane defined by the first two principal components. This type of plot is useful for visualizing the overall effects of experimental covariates and potential batch effects. The x-axis represents the component explaining the greatest variance, while the y-axis represents the second greatest. The percentage of total variance explained by each component is indicated in the axis labels.

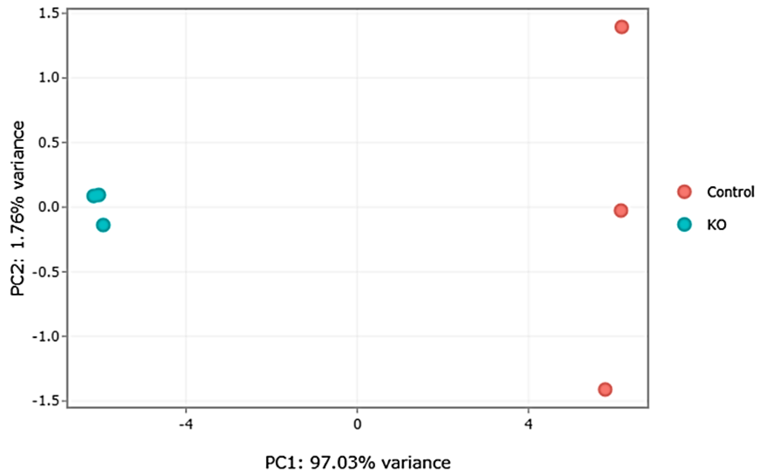

Figure 4.15. PCA of gene expression profiles. Samples are projected onto the first two principal components, which explain 97.03% (PC1) and 1.76% (PC2) of the total variance, respectively. Red dots represent control (OVCAR8 parental) samples, while blue dots represent KO samples. The separation along PC1 indicates distinct transcriptional profiles between the two groups.

4.4.7 GO reveals differentially expressed pathways

After assessing the quality of our samples through PCA and Euclidean distance analysis, we clustered the significantly differentially expressed genes based on their GO terms. The enrichment of GO terms was tested using Fisher's exact test implemented in **GeneSCF v1.1-p2**. **Figure 4.16** displays the GO terms with an adjusted p-value less than 0.05 from the differentially expressed gene sets, showing up to 40 terms.

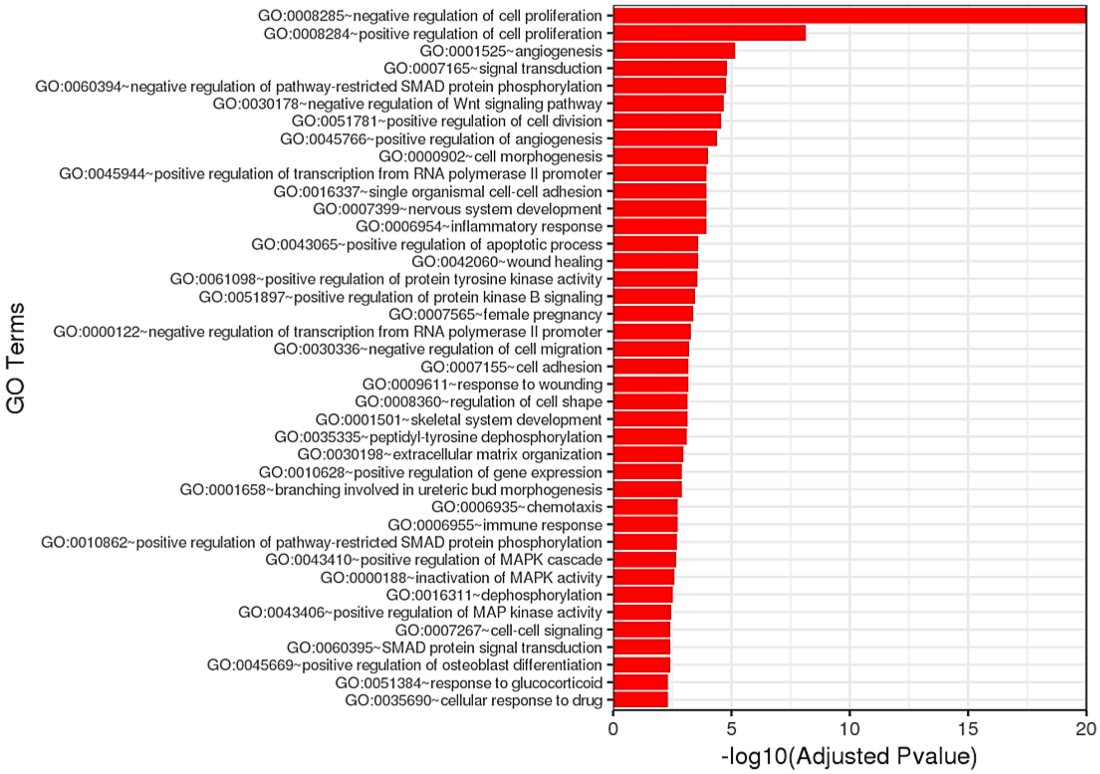

Figure 4.16. GO biological process enrichment analysis of differentially expressed genes. The bar plot displays the top GO terms significantly enriched in the set of differentially expressed genes, ranked by the negative log10 of the adjusted p-value. Enrichment was assessed using Fisher's exact test via GeneSCF v1.1-p2, and only terms with an adjusted p-value < 0.05 are shown (up to 40 terms). The x-axis represents the –log10(adjusted p-value), indicating the statistical significance of each term's enrichment, while the y-axis lists the GO biological process terms. The most significantly enriched processes include regulation of cell proliferation, angiogenesis, signal transduction, and various developmental and immune responses.

This GO enrichment analysis represents 40 significantly enriched terms associated with differentially expressed genes. Several GO terms align well with our previous in vitro results, including negative regulation of cell proliferation, negative regulation of pathway-restricted SMAD protein phosphorylation, cell morphogenesis, wound healing, negative regulation of cell migration, cell adhesion, and response to wounding.

4.4.8 Dysregulated pathways are associated to NO

After comparing the OVCAR8 parental cell line with its knockout counterpart using **DESeq2** to identify differentially expressed genes, we visualized the results with a volcano plot (**Figure 4.17A**) generated using the **EnhancedVolcano** software. The plot clearly shows the separation of genes between knockout and parental clones, highlighting the involvement of NO in regulating various genes. **Figure 4.17B** presents a heatmap of gene expression data, displaying the top 30 upregulated and top 30 downregulated genes identified by DESeq2. These genes exhibit a log fold change of approximately ±2. The heatmap also demonstrates the clustering of these genes across samples, confirming the consistency of the sample groups used in our analysis.

A

B

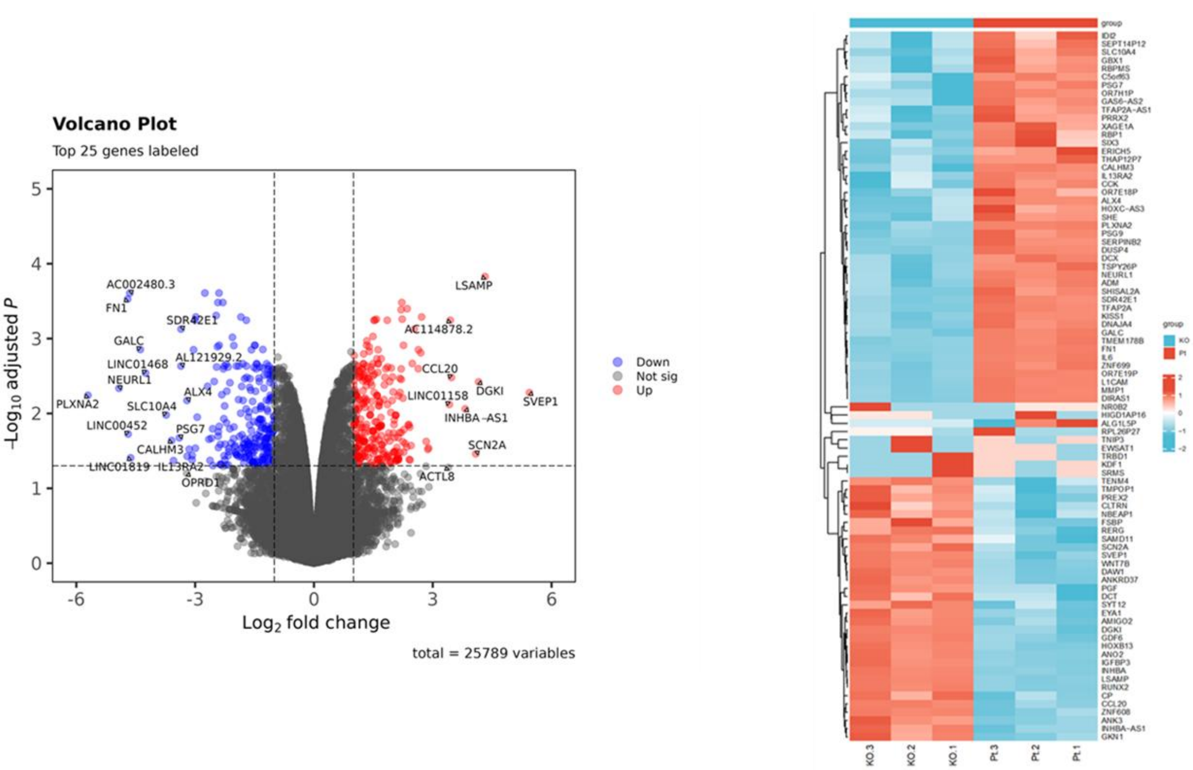

Figure 4.17 (A-B). Volcano plot showing the top up and down-regulated genes obtained in a visual output through EnhancedVolcano. The gene names present in **Figure 4.17A** are representative of the top 25 dysregulated genes. **Figure 4.17B** represents a Heatmap which shows the clustering of the top up- and downregulated genes with a logFC =/- 2. The heatmap provides also a representation of consistency over replicated among samples.

We also generated a table representative of the top up- and down-regulated genes summarizing each single logFC, Average expression and adjusted p value. In **Table 4.6A** it is possible to observe the list of the top downregulated genes, in **Table 4.6B** it is possible to observe the list of the top upregulated genes. All these comparisons are made by analyzing the knockout clones in relation to their parental counterparts.

A

ID	logFC	AveExpr	P.Value	adj.P.Val
PLXNA2	-5.70864946	-3.16500055	7.4818E-05	0.00572549
NEURL1	-4.92389026	0.73303619	4.395E-05	0.00460742
FN1	-4.7059306	5.71945887	5.7613E-08	0.00029715
LINC00452	-4.69264445	-1.14863136	0.00080417	0.01883616
AC002480.3	-4.64930804	0.07169838	3.5387E-08	0.00024644
LINC01819	-4.62967454	-1.00488484	0.00320345	0.03915344
GALC	-4.38619495	-0.12067555	2.0076E-06	0.00139927
LINC01468	-4.25273146	0.18422573	1.3144E-05	0.00288274
SLC10A4	-3.73251927	-0.2968499	0.00025293	0.01047107
CALHM3	-3.59452909	-1.02387305	0.00117115	0.02296784
IL13RA2	-3.54636641	0.23518143	0.00383191	0.04267046
PSG7	-3.39911195	-2.76307867	0.0010004	0.021147
AL121929.2	-3.35840395	-1.93567564	6.2708E-06	0.00232607
SDR42E1	-3.35627126	-1.78313817	6.8291E-07	0.00074658
OPRD1	-3.21092374	-3.94279881	0.00768244	0.06332971
ALX4	-3.20538839	-3.18323137	0.0001071	0.00670393
CCK	-3.20142974	-0.69491305	0.00291615	0.03726698
AC002480.1	-3.1507857	-0.35173419	0.00196012	0.03003926
AC093227.2	-3.07873995	-1.25053921	0.00365101	0.04166189
RPL26P27	-3.07462387	-0.89542528	0.00277568	0.03643595
TMEM178B	-3.03951788	-0.4908275	2.155E-06	0.00141025
IL6	-3.00460592	2.79125006	4.3488E-07	0.00056957
TFAP2A-AS1	-2.99452745	-1.35872561	0.00184883	0.0291261
OR7E19P	-2.98245631	7.16381148	2.6315E-07	0.00051466
MAPK8IP1P2	-2.97403598	-2.0847324	0.0359944	0.15622005
OR7H1P	-2.94837342	1.82287205	0.00029626	0.01120478
MMP1	-2.75380297	9.27905251	3.8224E-08	0.00024644
AC108463.3	-2.73929914	-1.02562317	0.01184239	0.08056009
FCGR3B	-2.73072826	-1.38239339	0.02270922	0.11701263

B

ID	logFC	AveExpr	P.Value	Adj.P.Val
NR0B2	2.45185001	-2.47467919	0.00155262	0.02687279
AC022335.1	2.45866778	-1.6342122	0.04320073	0.17578605
CALCRL	2.48393627	-4.21240769	0.01963206	0.1078807
ANKRD37	2.48396323	3.72068048	4.1736E-06	0.00215268
GGT8P	2.50680032	0.37224848	0.02708577	0.13125045
AC083967.1	2.53456222	6.14007792	6.9479E-07	0.00074658
AC108062.1	2.57849868	-2.02558804	0.04608609	0.18225948
TSSK1A	2.59782235	-1.39541008	0.04097968	0.17053816
LINC01109	2.63475975	-1.21657436	8.5174E-06	0.00252478
GDF6	2.63706944	3.0744881	2.1437E-06	0.00141025
SORBS2	2.64935841	-4.55601062	0.02028712	0.10963633
CDK15	2.66378285	-2.41944995	0.03465482	0.15261497
DISP3	2.69066711	-4.35743589	0.00781046	0.06390355
DAW1	2.69610994	3.90463976	2.6427E-06	0.0015489
HOXB13	2.71844842	1.24078007	2.6303E-07	0.00051466
NTSR1	2.72135716	-3.11741149	0.02052408	0.11031585
DHRS4L1	2.732927	-2.30102905	0.039035	0.16491261
AP000695.1	2.83295959	-0.78795326	0.00523873	0.05072625
FSBP	2.83558564	-3.04399403	0.00123939	0.02367606
AC114912.1	2.87517838	-0.05174927	0.00198193	0.03020805
AC087854.1	2.89514323	-0.91267237	0.00182771	0.0289526
CDR1	2.90181448	-2.33656446	0.01620856	0.09585018
ACTL8	3.39268156	-1.21968208	0.00565795	0.05271916
LINC01158	3.41823075	-0.78661174	0.00013928	0.00758802
AC114878.2	3.4410976	-1.34119152	4.8589E-07	0.00056957
CCL20	3.47122757	1.85922143	2.1787E-05	0.00330508
INHBA-AS1	3.82015445	-2.984237	0.00017753	0.00868864
SCN2A	4.08713508	-4.13489823	0.00252548	0.03458822
DGKI	4.15920434	-3.33810646	3.0756E-05	0.00379501
LSAMP	4.31945952	-0.30849792	5.7617E-09	0.00014859
SVEP1	5.44228661	-1.65903231	6.1307E-05	0.00528256

Table 4.6(A-B). Representative table of the top up- and downregulated genes. Table 4.6A shows the top thirty downregulated genes identified through DESeq2 analysis. Among these, genes such as FN1, MMP1, and IL6 are notable. These genes are known to influence the tumor microenvironment and are implicated in regulating Vimentin expression, a key marker of EMT and tumor invasiveness. **Table 4.6B** presents the top thirty upregulated genes from the same analysis. Interestingly, LSAMP, a gene typically reported as downregulated in many cancers, is strongly upregulated here. This upregulation correlates with reduced tumor growth, invasion, and metastasis, highlighting a potential tumor-suppressive role in this specific context.

Within the downregulated genes list, it is possible to identify several genes associated with the tumor microenvironment and its stability, many of which are potentially involved in regulating Vimentin expression. Notably, Fibronectin 1, one of the most downregulated genes, plays a role in modulating cell adhesion and consequently affects EMT-related markers, including Vimentin [295, 296]. Another significant gene, IL6, is also strongly downregulated and has been reported to regulate vimentin expression [297]. Additionally, MMP1, a member of the MMP family known for its crucial role in the tumor microenvironment and its potential expression by fibroblasts [298], has been shown to influence Vimentin expression. Specifically, studies in cervical cancer have demonstrated that MMP1 knockdown correlates with decreased Vimentin levels [27].

4.4.9 DEGs find correspondence in patient's data

After obtaining the list of differentially expressed genes and assessing the differences between samples through the heatmap and volcano plot described earlier, we performed a cross-analysis comparing our cell line data with patient data from the TNMplot database introduced at the beginning of this chapter. To identify overlapping genes between the two datasets, we generated a Venn diagram. **Figure 4.18** presents the results of this cross-analysis, highlighting the shared and unique differentially expressed genes.

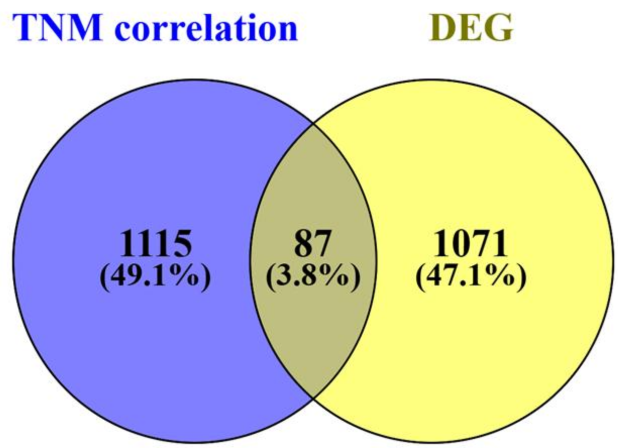

Figure 4.18. Venn Diagram showing the cross-analysis between the differentially expressed genes list on TNMplot and the differentially expressed gens list obtained in our RNAseq analysis. In this figure it is possible to observe the intersection between the two datasets, one produced in this work and a second one extrapolated from TNMplot. The intersection corresponded to 87 differentially expressed genes list, equivalent to 3.8%.

This cross-analysis gave us the opportunity to identify potential candidates of the changes of phenotype identified in our in vitro experiment having the consistency of matching our results with one related to patients obtained through TNMplot. According to the intersection obtained in this diagram we moved with the selection of more specific pathways which could be linked to observed phenotypes in our OVCAR8 NO2 KO cell lines. More details about the selected pathways will be given in the following paragraphs.

4.5 Pathways analysis reveal involvement of NOS2 in proliferation, migration and apoptosis

4.5.1 Apoptosis

After identifying the differentially expressed genes, we mapped these genes to their respective pathways. We used ggplot2 to visualize the dysregulated pathways found when comparing the OVCAR8 parental cell line to the C20 KO clone. Several significantly dysregulated pathways were identified. **Figure 4.19** presents a dot plot highlighting apoptosis-related pathways that were affected. All pathways considered significant had an adjusted p-value below 0.05. The size of the dots in the plot (shown on the right side of **Figure 4.19**) represents the number of counts per transcript. The pathways with the highest counts included the regulation of apoptotic signaling, intrinsic apoptotic signaling, and extrinsic apoptotic signaling pathways. Along with other pathways shown in the figure, these results demonstrate that apoptosis regulation and cell death are strongly influenced by NOS2.

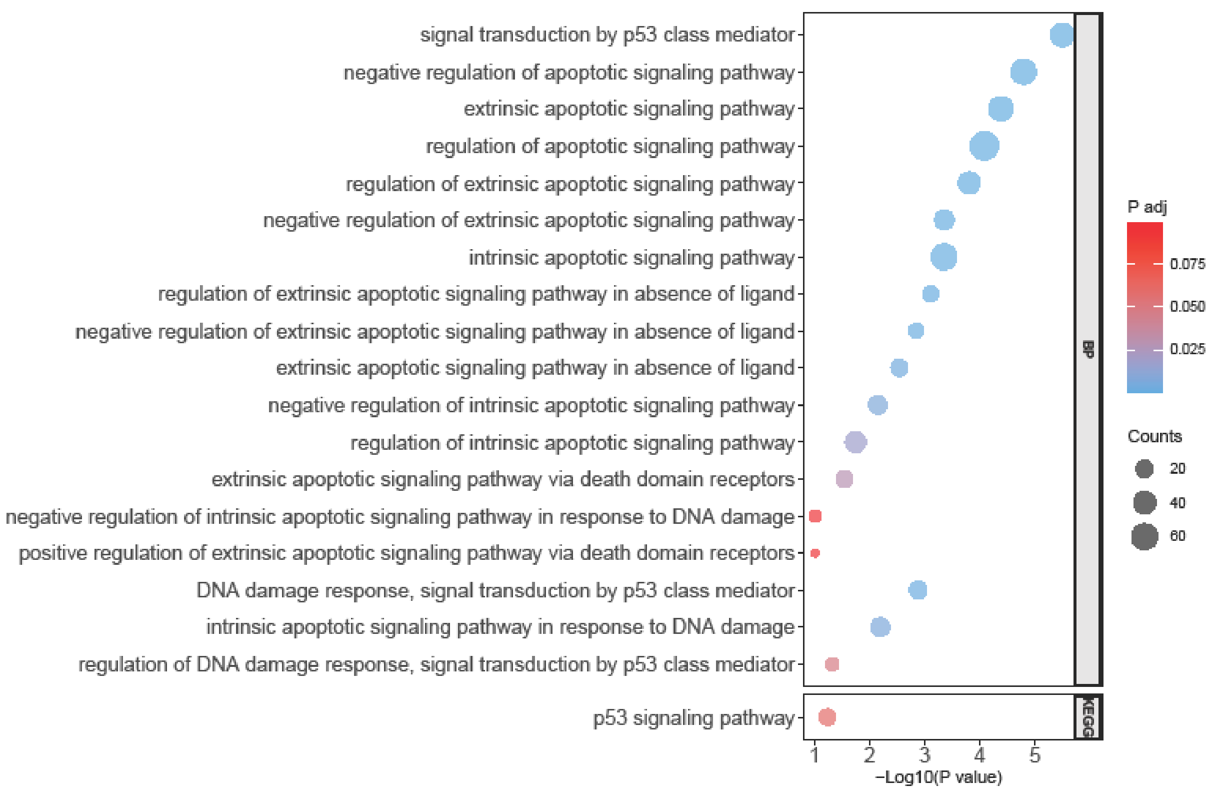

Figure 4.19. **Bubble plot showing dysregulated pathways related to apoptosis and p53 activity.** In the figure it is possible to observe how some dysregulated genes belong to transduction by p53 class mediator, negative regulation of apoptotic signaling pathways, regulation of apoptotic signalling pathway. All might have an important role in determining cancer cell proliferation.

4.5.2 Cell growth

The deletion of NOS2 has impacted not only the regulation of apoptosis and cell death, but also the regulation of growth in the KO clones. Pathways like negative regulation of growth and positive regulation of cell cycle are afflicted by the deletion of NOS2 in the KO clones (as it is possible to observe in **Figure 4.20**). Another factor which is dysregulated and has a key role in ovarian cancer is transforming growth factor beta production. In line with this dysregulated pathway, there are others which follow this trend with a key role in ovarian cancer, always related to the transforming growth factor. These pathways are, respectively, regulation of cellular response to transforming growth factor beta stimulus, negative regulation of cellular response to growth factors stimulus and regulation of transforming growth factor beta receptor signaling pathway. What it is possible to observe is that NOS2 has a connection and can influence the production and response of cells related to transforming growth factor beta.

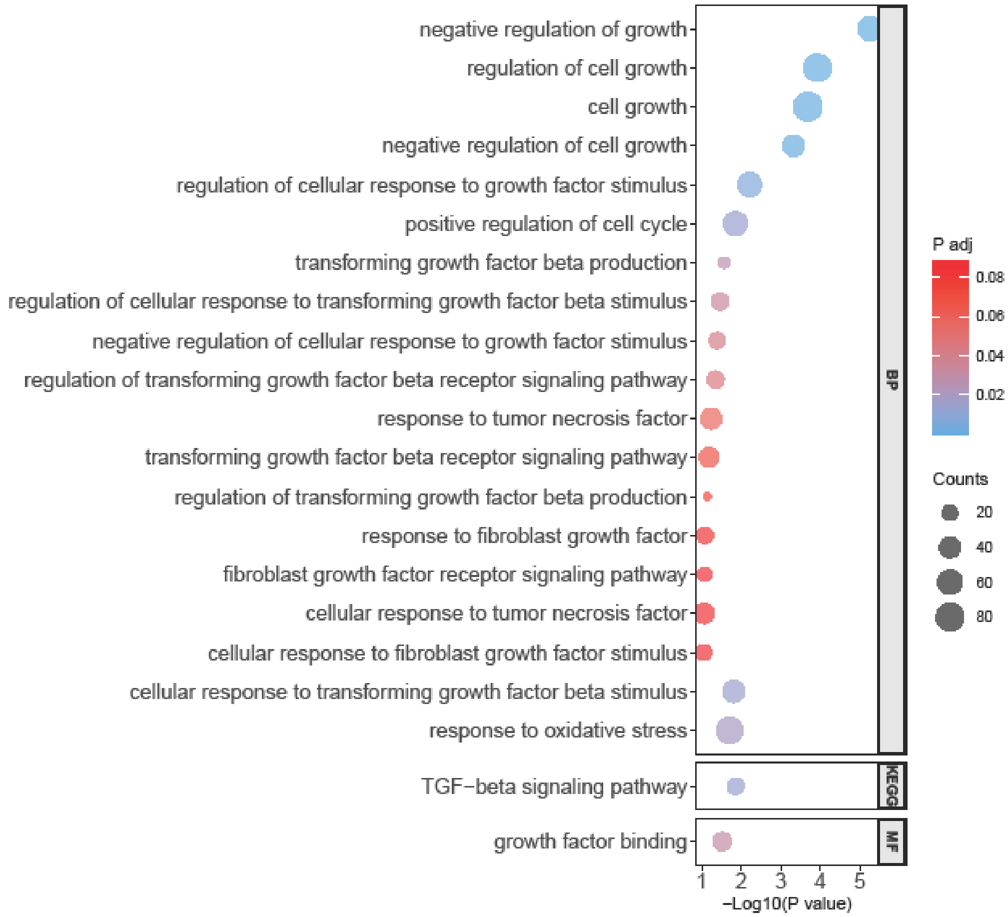

Figure 4.20. **Bubble plot shows dysregulated genes related to cell growth.** Relevant pathways related to cell growth are showed in the picture like regulation of cell growth, transforming growth factor beta production or regulation of cellular response to transforming growth factor beta stimulus.

4.5.3 Hypoxia pathways

The knockout also led to dysregulation of hypoxia-related pathways. Specifically, pathways involved in the cellular response to oxidative stress, regulation of reactive oxygen species metabolism, response to hypoxia, and response to decreased oxygen levels were affected (**Figure 4.21**). These pathways are closely linked to cancer development considering that hypoxia is a common feature of the tumor microenvironment and that plays a critical role in tumor progression. In addition, literature supports that HIF-1 alpha can directly induce NOS2 expression and regulate key factors in cancer, such as Vimentin expression. This regulation may contribute to metastasis, cancer progression, and chemoresistance.

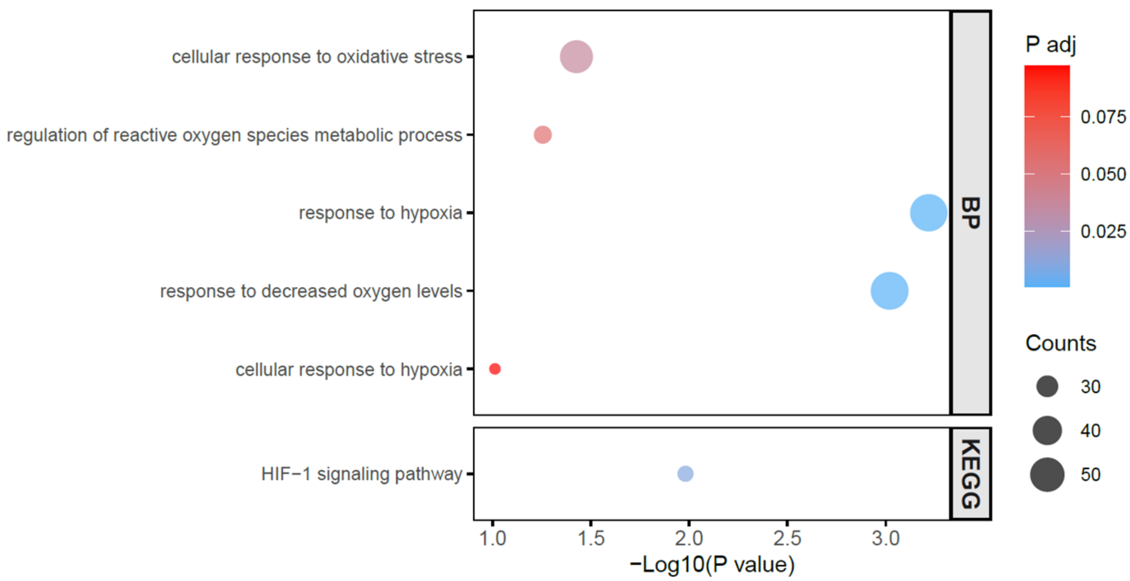

Figure 4.21. Bubble plot shows dysregulated pathways related to hypoxia. Hypoxia related pathways are shown in this figure, all with a potential involvement in cancer progression and proliferation.

4.5.4 Morphogenesis and migration

Dysregulated pathways were also obtained in morphogenesis, proliferation, differentiation and wound healing. All these pathways have a fundamental role in terms of migration of cells, metastasis formation and stemness. In the list of dysregulated pathways represented in the dot plot of **Figure 4.22**. It is possible to observe the presence of pathways like extracellular structure organization, and this might be important also considering the role of the extracellular matrix in the ovarian cancer microenvironment. Other relevant pathways are positive regulation of cell projection organization, mesenchymal cell differentiation, epithelial to mesenchymal transition, microtubule polymerization.

All together these pathways suggest an implication of NOS2 in cell EMT and polymerization of microtubules which are essential for cell cytoskeleton formation and structure. Other significant pathways are regulation of epithelial cell proliferation, positive regulation of epithelial to mesenchymal transition and epithelial cell migration.

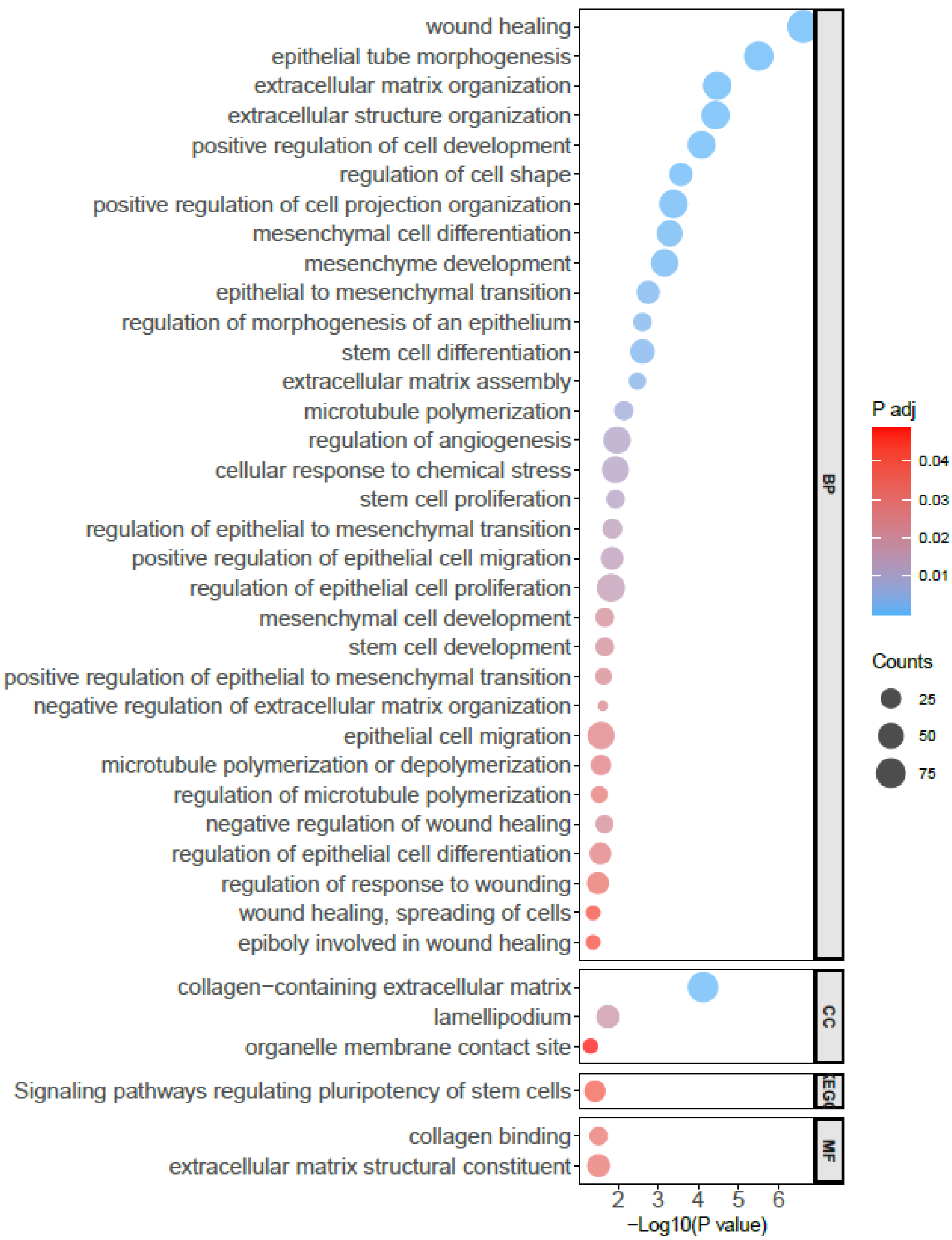

Figure 4.22. **Bubble plot shows dysregulated genes related to morphogenesis and migration.** Relevant pathways related to EMT function are shown in this figure. It is possible to mention some dysregulated pathways like wound healing, epithelial tube morphogenesis, epithelial to mesenchymal transition with a potential relevant involvement in the metastatic process.

4.6 In vivo OVCAR8 KO model optimization

After analysing an immunocompetent murine model (ID8 syngeneic in vivo model), the following aim was to optimize a second in vivo model in order to assess the metastatic potential and tumour proliferation specifically related to iNOS. This model involved a comparison between a human ovarian cancer cell line with normal iNOS expression (OVCAR8 parental) and a genetically edited counterpart, in which iNOS expression was inhibited using the CRISPR-Cas9 double nickase system. To facilitate the engraftment of human cells, NSG mice were adopted, as they are an immunocompromised murine strain specifically designed to tolerate xenografts derived from different species, including Homo sapiens. The primary goal of this experiment was to evaluate tumour spread and overall survival at the experimental endpoint. Based on previously published studies conducted in athymic nude mice, key experimental parameters were identified, including the approximate duration of tumour progression, the lack of ascites formation, the high metastatic potential of the model, and the recommended number of cells for inoculation [288]. The study was structured into two arms respectively including a group of mice (n=3) which received the inoculation of OVCAR8 parental and the second group composed of mice (n=5) which received the inoculation of OV8 NOS2 KO cell line. Both OVCAR8 parental and OVCAR8 NOS2 KO cells were injected intraperitoneally at a concentration of 5×10^6 cells in 200 µL of PBS per mouse. Following injection (week 0), mice were monitored weekly using an IVIS Spectrum CT imaging system to detect and quantify ROIs, expressed as photons per second $[p/s]$, as a measure of tumour burden. The endpoint was established at the week corresponding to the death of the first mouse part of the experiment.

4.6.1 KO group shows a decrease in the ROIs levels

As we previously mentioned, at the dead of the first mouse (parental group), we analyzed the ROI levels obtained during the weeks from this first experiment. The levels of ROIs, expressed in photons per second [p/s], were monitored over time to assess tumor progression in mice injected with either the NOS2 parental or NOS2 knockout (KO) OVCAR8 cell lines (**Figure 4.23**). At baseline (Week 0), both groups exhibited comparable ROI levels, with an average of 4.34×10^9 [p/s], indicating similar initial tumor engraftment. By Week 1, a divergence in tumor signal became evident. The parental group showed a significant increase to 7.5×10^{10} [p/s], whereas the KO group displayed a much lower signal at 5.2 [p/s], suggesting delayed tumor proliferation in the absence of NOS2. At Week 2, the gap persisted but narrowed, with ROI levels rising to 1.99×10^{11} [p/s] in the parental group and 8.81×10^{10} [p/s] in the KO group. By Week 3, the difference between groups further diminished. The parental group reached 2.93×10^{11} [p/s], while the KO group exhibited a comparable signal of 2.52×10^{11} [p/s]. At the endpoint of the experiment reached by the death of a mouse belonging to the parental group, the signal showed still a separation in the two group. The gap is reduced compared to the biggest difference observed at week two, but it is still possible to observe also how at the endpoint the signal remains separated between parental and knockout.

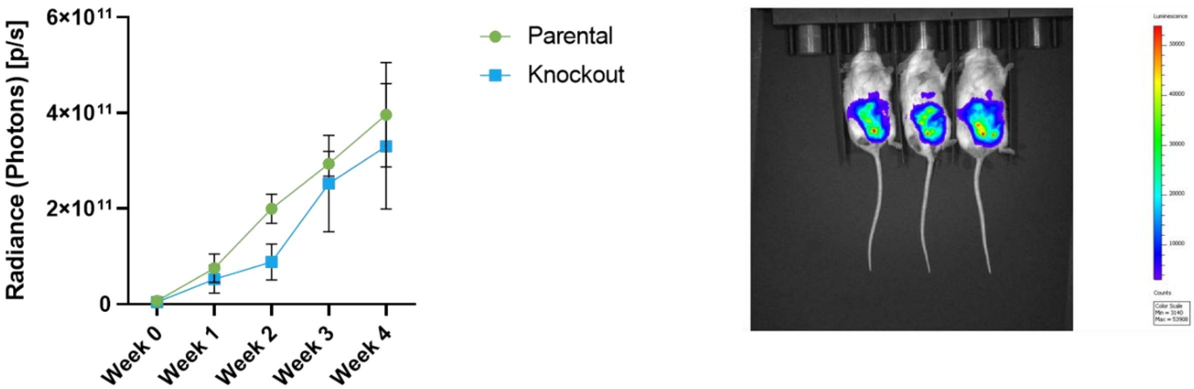

Figure 4.23. ROI signal from day 0 to week 4 (day 28) in the two group analyzed, OVCAR8 parental and OVCAR8 knockout. The left panel displays the region of interest (ROI) signal measured over four weeks in the in vivo model, showing a reduced tumour signal in the OVCAR8 knockout (KO) group compared to controls. The right panel illustrates an example of tumour dissemination observed in the OVCAR8 parental group. At baseline (Week 0), both groups exhibited comparable ROI levels, with an average of 4.34×10^9 [p/s], indicating similar initial tumour engraftment. By Week 1, a divergence in tumour signal became evident. The parental group showed a significant increase to 7.5×10^{10} [p/s], whereas the KO group displayed a much lower signal at 5.2 [p/s], suggesting delayed tumour proliferation in the absence of NOS2. At Week 2, the gap persisted but narrowed, with ROI levels rising to 1.99×10^{11} [p/s] in the parental group and 8.81×10^{10} [p/s] in the KO group. By Week 3, the difference between groups further diminished. The parental group reached 2.93 $\times 10^{11}$ [p/s], while the KO group exhibited a comparable signal of 2.52×10^{11} [p/s]. At the endpoint of the experiment, reached by the death of a mouse belonging to the parental group, the signal showed still a separation in the two group with the KO group reaching levels lower than 4 x 10’11 [p/s].

It is possible to observe that, during the initial optimization of the model, tumor uptake was achieved in all mice. Starting from similar baseline signals, due to a consistent number of cells injected per group, a separation between groups emerged, gradually diminishing by week four, which was the endpoint of this model. This initial optimization revealed a potentially reduced proliferation rate of the knockout clones in vivo compared to the parental cells. Another observation was the extensive tumor dissemination and the high ROI levels detected, indicating rapid and widespread tumor growth starting as early as the first week.

4.6.2 OVCAR8 KO has a slower tumor growth into the peritoneum and higher sensitivity to Cisplatin

Consistent with earlier observations in this study where the combination of Cisplatin with L-NMMA or NOS2 knockout (KO) clones led to increased sensitivity to Cisplatin, along with impaired migratory and colony-forming abilities, a second in vivo experiment was conducted with a larger cohort size (n = 6 per group) and expanded treatment conditions. One cohort of six mice received an intraperitoneal (IP) injection of the OVCAR8 NOS2 parental cell line, while a second cohort received an IP injection of the OVCAR8 NOS2 KO cell line. Tumour growth and proliferation were monitored via region of interest (ROI) measurements every four days. In parallel, two additional cohorts, following the same injection regimen, were treated with Cisplatin. For this second experiment, a survival analysis was performed to evaluate Cisplatin efficacy detecting how Cisplatin could affect the spread of cancer cells and proliferation in vivo. The experimental timeline and protocol are outlined in **Figure 4.24**.

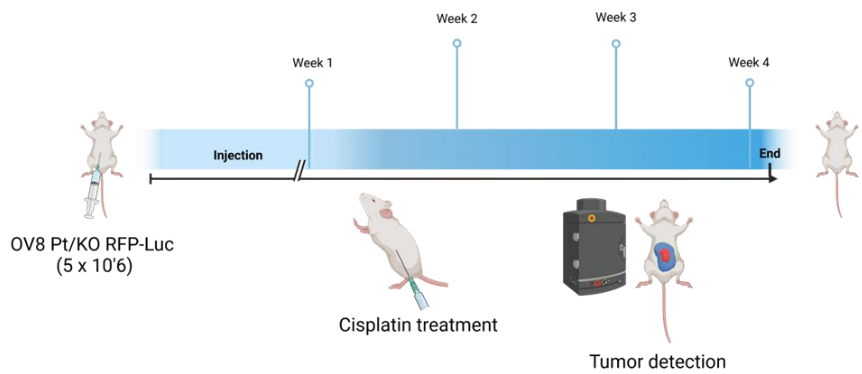

Figure 4.24. In vivo project plan for the OV8RFP-Luc NOD SCID Gamma model. After the injection of cancer cell lines, we monitored the tumor growth for four weeks with repeated measurements every four days. We also administered Cisplatin to designated group for the survival experiment. Created in https://BioRender.com.

Upon reaching the experimental endpoint, defined, in accordance with the optimized model, as the death of the first mouse within any group (in this case, from the OVCAR8 parental group), we analyzed the ROI data collected throughout the study. The resulting ROI curve demonstrated a clear divergence in tumor growth dynamics, with a distinct separation observed for the OVCAR8 KO group. This group exhibited a marked decline in signal intensity over time, consistent with our in vitro findings that OVCAR8 KO cells possess reduced proliferative and migratory capacities. The ROI curve illustrating these differences is presented in **Figure 4.25**.

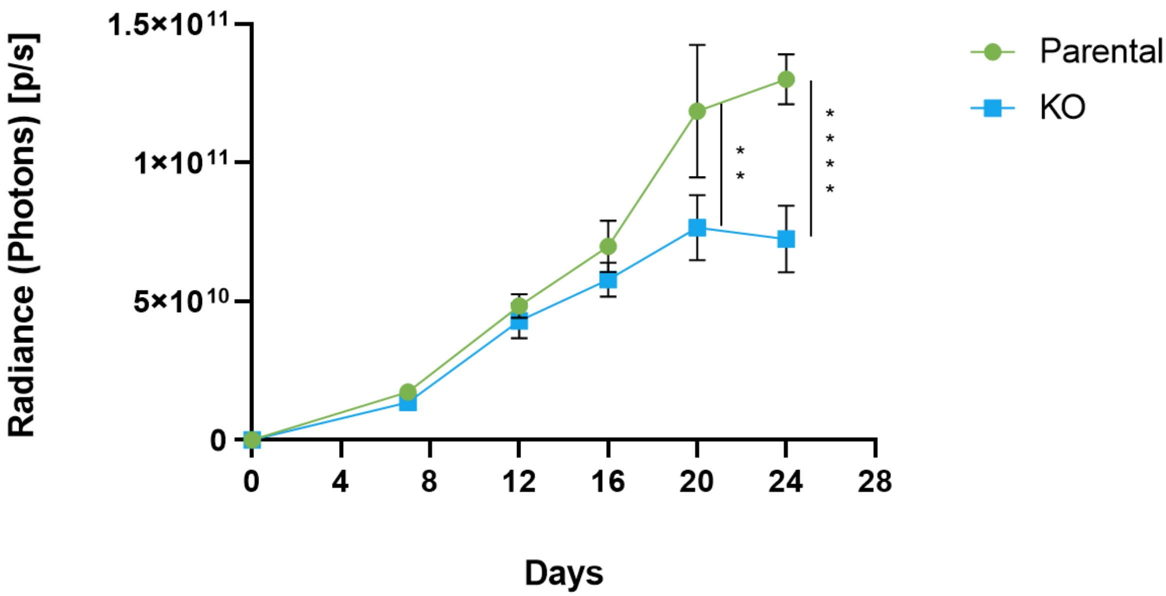

Figure 4.25. OVCAR8 KO has a slower growth rate compared to its parental counterpart. In the figure it is possible to observe how the signal detected from the mice starts to separate as early as eight days and how at the endpoint a significant separation is observed in the knockout group when compared to the parental group at the endpoint. Significant reductions in ROI were observed at day 20 where the parental ROI was1.18 x 10^{11} [p/s] against 7.6 x 10^{10} [p/s] of parental group ($p < 0.05$) and day 24 where parental ROI was 1.3 x 10^{11} [p/s] against 7.24 x 10^{10} [p/s] of knockout group ($p < 0.05$).

The results presented above lead to an important observation regarding the proliferation efficiency of the knockout cells, which is further detailed in the following figure. Specifically, there is a strong and significant reduction in the ROI signal, indicating a lower proliferation rate and decreased metastatic potential within the abdomen of mice. This finding aligns with earlier observations in this study, where impaired migration efficiency in the scratch wound assay and reduced colony formation capacity collectively supports the role of iNOS in promoting migration and EMT when overexpressed. Notably, significant reductions in ROI were observed at day 20 where the parental ROI was1.18 x 10^{11} [p/s] against 7.6 x 10^{10} [p/s] of parental group ($p < 0.05$) and day 24 where parental ROI was 1.3 x 10^{11} [p/s] against 7.24 x 10^{10} [p/s] of knockout group ($p < 0.05$), with a final drop at day 24, highlighting how targeting NO in ovarian cancer correlates with diminished cancer cell proliferation. In accordance with the previously described experimental design, we conducted a parallel survival assay under the same conditions. Mice were treated with the standard in vivo dose of Cisplatin for the OVCAR8 model (6.4 mg/kg), taking into account the rapid tumor progression characteristic of this model. The results strongly supported our in vitro findings, demonstrating that OVCAR8 KO tumors are more sensitive to Cisplatin treatment. Notably, 33% of the mice bearing OVCAR8 KO tumors survived beyond the established endpoint, in contrast to the parental group, which exhibited no survival beyond this timepoint. The Kaplan–Meier curve is presented in **Figure 4.26**.

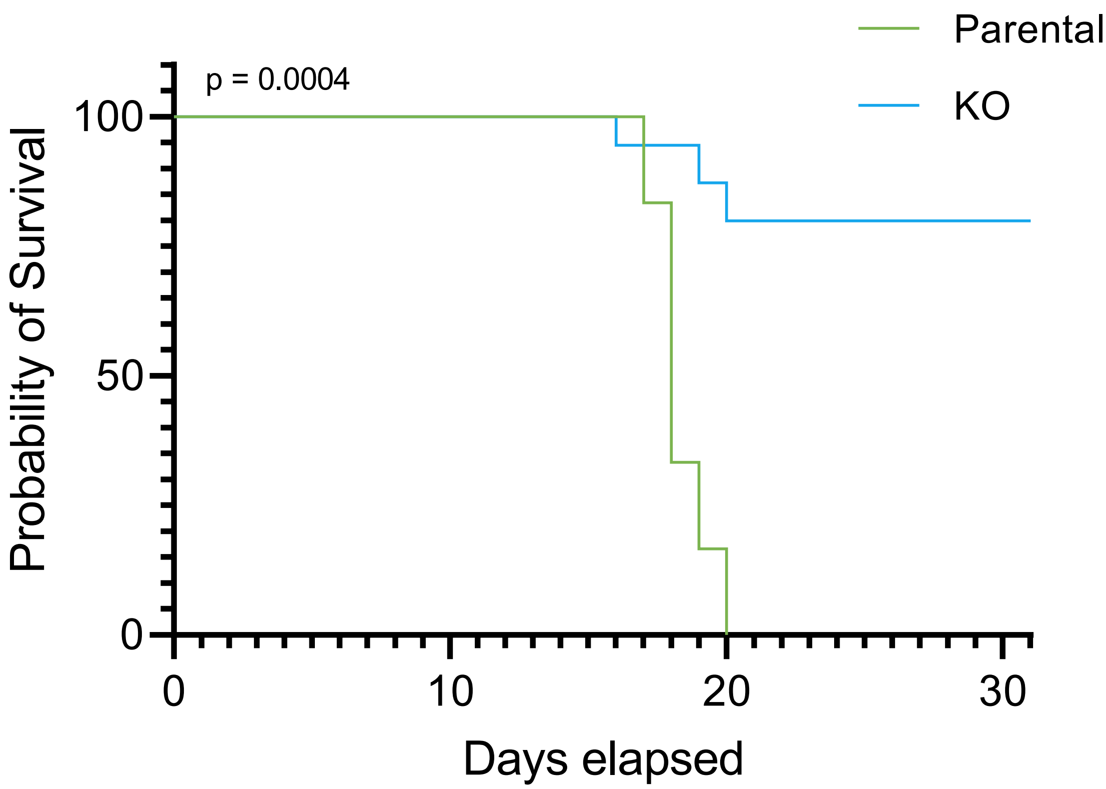

Figure 4.26. Kaplan-Meyer curve shows better survival of the OVCAR8 KO group. The figure illustrates the survival timepoints for the two experimental groups. Notably, 33% of mice in the OVCAR8 KO group survived beyond the predefined endpoint, in contrast to the OVCAR8 parental group, in which no mice survived past this timepoint. In particular, 33% ($p < 0.0004$) of the mice bearing OVCAR8 KO tumours survived beyond the established endpoint, in contrast to the parental group, which exhibited no survival beyond this timepoint. The experiment was conducted using six mice per group and was terminated once any group had no remaining mice.

In line with previous sections of this work, a significant Kaplan-Meier survival curve ($p < 0.0004$) demonstrated that the knockout group survives longer compared to the parental group. It has already been shown that knockout cell lines are more sensitive to cisplatin, indicating increased chemotherapy-induced cell killing relative to the parental cell line. Here, we confirm the in vitro observation of heightened chemotherapy sensitivity, which translates into prolonged survival due to improved tumor targeting by the treatment. This finding is further supported by Figure 4.25, where a significant reduction in the detected ROI indicates that knockout cell lines grow more slowly and proliferate less within the mouse abdomen. These results suggest the potential for extending cisplatin treatment duration in clinical settings, along with enhanced drug efficacy.

4.7 Discussion

One of the main challenges in the treatment of ovarian cancer is represented by the metastatic process, as this disease is frequently diagnosed at a late stage, when metastatic spread has already occurred [299]. Following tumor debulking through surgical intervention, a chemotherapy regimen is typically initiated. A diffuse metastatic process complicates surgical debulking, rendering the procedure both technically challenging and prolonged due to the difficulty in identifying all metastatic sites [300]. For this reason, appropriate chemotherapy plays a dual role: firstly, in eradicating residual malignant cells, and secondly, in preventing further tumorigenesis. Chemotherapeutic intervention thus has a pivotal role in mitigating the deleterious effects associated with the ovarian cancer metastatic process [301]. Although chemotherapy is initially highly effective, relapse occurs in approximately 70% of patients, rendering subsequent treatments less effective [273]. Given these considerations, enhancing the efficacy of chemotherapy and preventing the development of chemoresistance are critical goals. Numerous mechanisms underlying chemoresistance have been proposed, including the involvement of NO pathways [274], although further research is required to fully elucidate the mechanisms by which resistance to platinum-based agents is acquired in ovarian cancer. Strategies aimed at increasing cancer cell sensitivity to chemotherapeutic agents, thereby prolonging the therapeutic window and preventing the survival of subpopulations that could develop chemoresistance, represent a promising approach. Such strategies may lead to the development of novel therapeutic interventions that enhance the cytotoxic efficacy of chemotherapy and reduce the likelihood of treatment failure due to acquired resistance. Motivated by these findings, we generated a NOS2 knockout clone to mimic the effects of L-NMMA by substantially reducing nitric oxide (NO) production in the target cell line. Generation of knockout clones is an advanced approach that enables functional, metabolic, and phenotypic investigations of gene depletion [302]. Another study has reported the generation of an iNOS knockout model in metaplastic breast cancer, demonstrating that iNOS, and consequently nitric oxide (NO), can influence chemosensitivity and epithelial-mesenchymal transition (EMT) markers [209]. Motivated by these findings, this work proposes the development of an iNOS knockout model for ovarian cancer to explore similar regulatory mechanisms. Previous studies have shown that NOS knockouts can produce diverse biological outcomes, affecting multiple pathways associated with the targeted gene's depletion [303]. Although the role of NOS2 depletion remains underexplored, especially in ovarian cancer, this study showed that NOS2 knockout clones lost their typical epithelial morphology. Instead, they adopted a more rounded, senescent-like appearance with pronounced vacuolization.. This morphological change was accompanied by a significant reduction in Vimentin, a key mesenchymal marker linked to epithelial-to-mesenchymal transition (EMT) [203]. The importance of expanding current knowledge about the role of vimentin in ovarian cancer lies in the fact that this protein is often associated with epithelial-mesenchymal transition (EMT) [203]. EMT is a key phenomenon in many types of cancer; however, given the high metastatic spread typically observed at the time of diagnosis in ovarian cancer, it represents a particularly critical and deleterious factor impacting patient survival. By targeting this protein, especially considering its constitutive expression in chemoresistant ovarian cancer cell lines, the potential involvement of iNOS inhibitors as therapeutic agents against chemoresistant ovarian cancer warrants further investigation. The reduction in Vimentin correlated with decreased cell migration and proliferation, as evidenced by impaired wound healing and increased sensitivity to Cisplatin in NOS2 knockout clones. These NOS2 knockout clones also exhibited a significantly lower IC50 for cisplatin compared to parental cells, consistent with prior reports involving OVCAR8. While L-NMMA monotherapy had a limited effect on cell viability, it markedly potentiated cisplatin's cytotoxicity at sub-IC50 doses. The combination of cisplatin and L-NMMA reduced cell viability more effectively than either agent alone. We observed a pronounced decrease in viability, particularly when considering the IC50 values of the cell lines analyzed. The knockout clone exhibited an IC50 of 4 µM whereas its parental counterpart showed higher tolerance at this concentration, remaining far from its own IC50. In this study, as previous findings confirmed, it has been demonstrated that inhibition of iNOS in knockout models enhances the sensitivity of the cells to chemotherapeutic agents, thereby advancing the current understanding of Cisplatin sensitivity in ovarian cancer cells. The results obtained in our ovarian cancer NOS2 knockout model suggest novel therapeutic opportunities, potentially supporting combined treatment regimens incorporating cisplatin to enhance efficacy. Furthermore, as also mentioned before, scratch wound assays revealed that NOS2 knockout clones displayed severely impaired migratory capacity, achieving less than 15% wound closure over 24 hours compared to nearly 50% closure by parental cells. To strengthen the consistency of our findings, we employed siRNAs targeting NOS2 to induce its knockdown and investigate potential correlations with a second cell line belonging to another ovarian cancer subtype, A2780cis, characterized by cisplatin resistance, to broaden the scope of our study. This approach was motivated by several factors: first, to validate results in an independent cell line; second, to evaluate a distinct ovarian cancer subtype; third, to analyze a model exhibiting resistance to platinum-based agents. Since its discovery in the early 2000s, siRNA technology has been widely utilized as a mean to induce RNA interference (RNAi) in laboratory settings [304], and increasingly, as a therapeutic strategy in clinical contexts [305-307]. This versatility makes siRNA an ideal tool for assessing the effects of NOS2 depletion in our models. Following treatment with two distinct siRNAs, we observed a significant reduction in Vimentin expression in A2780, consistent with the effects seen upon L-NMMA treatment and in knockout models obtained from OVCAR8. These findings corroborate our previous observations, reinforcing the role of NOS2 in regulating this mesenchymal marker across different ovarian cancer models. Furthermore, we examined the impact of NOS2 knockdown on cellular proliferation by conducting colony formation assays in both OVCAR8 knockout clones and A2780cis cells treated with siRNAs. Administration of the two siRNAs led to a marked impairment in colony growth A2780cis cell line as well as in OVCAR8 KO clones, suggesting that inducible Nitric Oxide Synthase (iNOS) plays a critical role in promoting cell proliferation when overexpressed. Overall, the reduction in colony formation upon NOS2 silencing complements our experiments demonstrating decreased cell viability following combined treatment with L-NMMA and cisplatin, thereby reinforcing the potential of targeting iNOS as a therapeutic strategy to overcome chemoresistance. The opportunity to arrest colony proliferation, which in vivo may correspond to omentum or peritoneal colonization, is a crucial possibility. Specifically, as has already been reported, the metastatic cascade can be associated with various factors, such as Vimentin [203], as well as different pathways like JAK/STAT [308]. An important contribution of this work is the evidence that Nitric Oxide Synthase also plays a key role in the metastatic cascade in ovarian cancer. Collectively, these data underscore NOS2's role in regulating Vimentin expression and thereby modulating cancer cell morphology, migration, proliferation, and chemotherapy response, consistently with findings in the literature [220, 309]. To elucidate the transcriptional pathways influenced by NOS2, and to have a full overview of its involvement in different pathways, we performed bulk RNA sequencing comparing NOS2 knockout and parental OVCAR8 cells. Differential gene expression analysis identified significant alterations in pathways associated with epithelial morphogenesis, stem cell differentiation, hypoxia response, and cellular growth. Notably impacted pathways included wound healing, epithelial tube morphogenesis, regulation of cell shape, epithelial-to-mesenchymal transition (EMT), stem cell proliferation and development, and epithelial cell migration. These pathways are critical regulators of cancer cell proliferation, metastasis, and tumor microenvironment interactions. Collectively, these data suggest that targeting NOS2 could disrupt multiple oncogenic signaling cascades, thereby attenuating cancer cell migration, proliferation, and chemoresistance. Moreover, our findings indicate that L-NMMA may prolong chemotherapy efficacy and enable dose reduction, potentially mitigating cisplatin-associated toxicities. Although it remains to be definitively demonstrated that L-NMMA can resensitize cisplatin-resistant ovarian cancer cells, our data suggests that it may delay resistance onset or enhance chemotherapy susceptibility, that must still be elucidated in further investigation. This is particularly relevant given the differential NOS2 expression observed between cisplatin-resistant A2780 cells (constitutive NOS2 expression) and their cisplatin-sensitive counterparts (inducible NOS2 expression). Taken together, these findings position NOS2 as a promising therapeutic target for combination regimens in ovarian cancer, alongside NOS1, which has been studied previously [310]. After extensively investigating the involvement of iNOS in various pathways, including its relationship with cell proliferation, EMT, and colony formation, we progressed to testing an in vivo model. Using immunocompromised mice, we optimized parameters such as timing, ROI capture efficiency, and endpoint duration to establish the most suitable experimental conditions. Once optimized, we conducted our experiments under these conditions. Consistent with previous in vivo experiments performed in immunocompetent mice, we observed dissemination of cancer cells throughout the peritoneum and abdominal cavity, characteristic of late-stage ovarian cancer. However, the extent of tumor spread differed notably between the OVCAR8 parental and OVCAR8 knockout cell lines. Despite starting with comparable [p/s] signal intensities, longitudinal measurements over five time points revealed a slower progression of tumor spread in mice injected with knockout clones. Remarkably, prior reaching the experimental endpoint, the knockout group exhibited a decrease in signal intensity, suggesting reduced tumor burden. These in vivo findings support our prior in vitro data demonstrating significantly impaired colony formation following NOS2 knockdown with siRNAs. Moreover, our in vivo model corroborated previous observations regarding cisplatin sensitivity. Initial screenings revealed that co-treatment with cisplatin and L-NMMA enhanced cisplatin's cytotoxic efficacy at IC50 doses. Similarly, the knockout clones displayed increased cisplatin sensitivity, consistent with colony formation and scratch wound assays where the clones exhibited reduced proliferation and migration capacity over 24 hours. Notably, mice injected with OVCAR8 knockout cells and treated with cisplatin showed improved survival compared to those receiving parental cells, with 33% survival observed in the knockout group. As explained before, patients have a poor survival rate over five years from the time of cancer diagnosis and the start of treatments [311]. In this in vivo model, mice with iNOS inhibition survived longer compared to their counterparts with basal iNOS expression, suggesting that the integration of Nitric Oxide Synthase inhibitors could be a potential and effective addition to current therapies to extend treatment duration as well as reduce the side effects of the drug itself. By first reducing the IC50 for Cisplatin, then showing a reduced ROI, and finally demonstrating longer survival, L-NMMA, an enzymatic inhibitor of Nitric Oxide Synthases, may represent strong candidates to support patients and extend their survival following cancer detection. This further reinforces the critical role of iNOS in tumor progression, proliferation, and metastasis. Although much remains to be clarified regarding iNOS's role in ovarian cancer, our study proposes that combining conventional chemotherapy with iNOS inhibition may enhance therapeutic efficacy and improve tumor clearance. Future investigations are necessary to explore iNOS's involvement in chemoresistance, a major challenge in ovarian cancer treatment. Developing in vivo models using chemoresistant cell lines and knockout clones will be crucial for elucidating the mechanisms underlying resistance and for determining whether iNOS depletion, demonstrated here in a pre-chemoresistance context, can modulate proliferation, migration, metastasis, and chemosensitivity. The opportunity to further investigate the specific role of iNOS and NO in promoting chemoresistance, as already reported in another study relative to OC [171], could represent a future direction in ovarian cancer research. This may lead to more effective responses to relapses and ultimately help ensure longer survival for patients.

Conclusions

Taken together, our results reveal a novel role for iNOS in cancer cell development, proliferation, and chemotherapy sensitivity. We demonstrated that NOS2 depletion, achieved through siRNA-mediated knockdown and genetic knockout in in vitro models, significantly impairs tumor cell growth and migratory capacity. Importantly, our in vivo studies further confirmed that iNOS depletion reduces tumor proliferation and enhances sensitivity to cisplatin, highlighting the therapeutic potential of targeting iNOS to improve treatment outcomes in ovarian cancer.

Final considerations - contribution to the field

This PhD presented a comprehensive preclinical investigation into the role of inducible nitric oxide synthase (iNOS) inhibition in ovarian cancer (OC), integrating bioinformatics, in vitro modelling, and in vivo experimentation to elucidate its therapeutic potential.

Major results

Initial bioinformatic analyses leveraged publicly available patient and cell lines datasets to establish differential iNOS expression across OC subtypes and correlate its upregulation with a more aggressive phenotype and potentially acquired chemoresistance, particularly to platinating agents. These findings provided a rationale for targeting iNOS as a therapeutic strategy and informed the subsequent experimental design. In vitro studies employed OC cell lines to test, as first, the efficacy of L-NMMA in cell viability, then the efficacy of Cisplatin in ovarian cancer cell lines which showed a basal expression of iNOS. The combination of the two drugs has been tested showing how L-NMMA has beneficial effects in increasing the efficacy of Cisplatin. Relevantly, L-NMMA was also reported to significantly impair the overexpression of Vimentin with its implication in EMT. Inhibition of iNOS through knockout of its gene, NOS2, led to increased sensitivity to Cisplatin with a strong reduction of Vimentin levels correlated to an impaired migration efficacy, implicating nitric oxide signalling in modulating EMT. These results were cross-referenced with transcriptomic data, reinforcing the link between iNOS activity and EMT together with apoptotic signalling, growth stimuli and extracellular matrix organization.

Building on these in vitro insights, the thesis transitioned to in vivo models to assess the translational relevance of iNOS inhibition. A syngeneic mouse model was employed, enabling evaluation of iNOS inhibition alone and in combination with cisplatin. The administration of the combination of Cisplatin and L-NMMA led, also in this in vivo model, to a significant reduction of tumour area, tumour cells number and, in general, presence of metastasis in the peritoneum when compared to Cisplatin only. Importantly, immune profiling of treated tumours revealed increased infiltration of T cells and an increase of activation markers and reduced immunosuppressive populations for CD4+ T cells, suggesting that iNOS inhibition may also potentiate anti-tumour immunity. In addition to the previous model, a xenograft mouse model was developed by injecting KO NOS2 human cell lines to investigate the role of iNOS in tumour growth, progression and establishment, revealing a significant reduction in tumour burden in the knockout group when compared with its parental counterpart together with an increased survival when Cisplatin was administered. These findings suggested that iNOS contributes not only to tumour cell- intrinsic resistance but also to shaping the tumour microenvironment. Collectively, this work provides a robust preclinical foundation for the clinical exploration of iNOS-targeted therapies in OC, particularly in combination with platinum-based chemotherapy.

What this work helped to overcome

This study, based on the initial aims and hypotheses, aimed to evaluate the current standards of care for ovarian cancer while exploring novel avenues for combinatorial treatment strategies. Traditional chemotherapy, which primarily targets cancer cells, does not adequately address the complex deleterious interactions occurring within the TME. In particular, the intercellular crosstalk mediated by NO plays a significant role in tumour progression and resistance mechanisms. Therefore, the use of NOS inhibitors may represent a promising approach to disrupt the nitric oxide-mediated communication within the tumour microenvironment, potentially enhancing therapeutic efficacy (as shown in **Figure 4.27**)

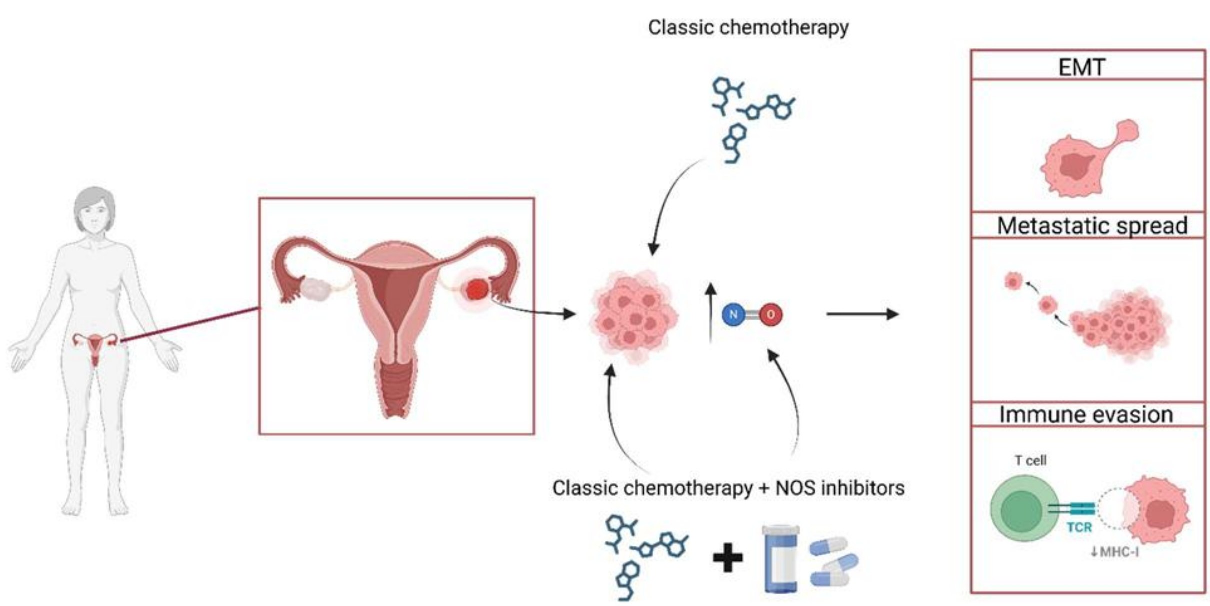

Figure 4.27. The beneficial effects of combining NOS inhibitors to chemotherapy. The figure illustrates how NOS inhibitors have the potential to suppress all NO related functions within the tumour niche when NO is overexpressed. Created in https://BioRender.com.

Why NO is important – Uncovering iNOS expression in ovarian cancer

TME is highly heterogeneous, with many cell types being reprogrammed through continuous crosstalk. All stromal components contribute to this, including cancer-associated fibroblasts [144], adipose cells [21], mesenchymal stem cells [20], and the tumour immune microenvironment (TIME), which is part of the tumour niche and plays a key role in tumour progression and maintaining an immunosuppressive status [17]. There is intense cross- communication between these cell types, mediated by EVs [312], cytokines [225] and, nitric oxide (NO) [277]. Nitric oxide (NO) is a versatile signaling molecule that plays diverse physiological roles in the human body. It functions as a neurotransmitter, a regulator of vascular tone, and a mediator of intracellular signaling in conjunction with reactive oxygen species (ROS) [151]. Additionally, NO is produced by cells of the immune system as a key effector in inflammatory responses [151]. Inducible NOS is expressed primarily in immune cells, such as macrophages, upon stimulation by pro-inflammatory cytokines or bacterial endotoxins, resulting in sustained and high-output NO production. Inflammatory stimuli critically regulate iNOS expression and consequent NO production [152]. As previously reported, the widespread expression of inducible nitric oxide synthase (iNOS) by various cell types within the tumour niche results in a systemic overexpression of this enzyme where the continuous and basal expression of iNOS leads to overproduction of NO within the niche, which can, according to studies in other cancer types, result in increased chemoresistance [274]. However, in ovarian cancer, iNOS expression has not been as extensively or thoroughly investigated as in this work. Although biobank data and existing literature have documented iNOS expression, there remains a lack of definitive evidence regarding the basal levels of iNOS expression specifically in ovarian cancer.

The inflammatory status in ovarian cancer has a role in iNOS upregulation

In the TME, chronic inflammation often leads to the recruitment of immunosuppressive cell populations rather than effector immune cells, thereby facilitating immune evasion. This phenomenon is exemplified in ovarian cancer, characterized by an immunologically "cold" microenvironment, where the presence of immunosuppressive cells expressing iNOS may promote immune tolerance by dampening anti-tumour immune responses [313]. Furthermore, the TME is typically characterized by factors that inhibit effective immune cell infiltration and activate oncogenic signaling pathways that support tumour cell survival and proliferation. A key finding of this study is the role of immunosuppression, often associated with chronic inflammation, in the upregulation of iNOS expression. Rather than activating immune cells, this immunosuppressive environment inhibits them and contributes to increased iNOS levels. Additionally, cytokine expression can stimulate ovarian cancer cell lines that do not express iNOS at basal levels, leading to enhanced aggressiveness. This observation aligns with previous reports linking nitric oxide overexpression in the tumour microenvironment to increased tumour malignancy.

The role of NO in EMT and the interference operated by L-NMMA

The finding that only the iNOS-expressing ovarian cancer cell lines show expression of Vimentin it was a field this work helped to uncover. Vimentin has already been linked to iNOS expression in metaplastic breast cancer [209], and this study proves that a similar condition is present in ovarian cancer. Considering the expression of iNOS demonstrated in this context, new scenarios open for anti-Nitric Oxide Synthase drugs in the treatment of this cancer type. In particular, L-NMMA was tested in OVCAR8 with encouraging results. The reduction in viability observed in this cell line, which continuously expresses iNOS, showed that at high concentrations L-NMMA affects viability, but most importantly, the combination of Cisplatin and L-NMMA demonstrated that L-NMMA can increase the efficacy of Cisplatin's IC50. In addition, an innovative aspect which wasn't taken into consideration before this work is related to the use of L-NMMA to impair EMT by reducing Vimentin levels by over 50%. In particular, according to data reported in literature, the potential activity of L-NMMA on Vimentin might be related to a key Cysteine residue on Vimentin itself. More specifically, it has been reported how Vimentin has one key point which is responsible for all the post-translational modifications which are related to Vimentin. This hotspot is its Cysteine 328 which can be, because of its thiolic residue, potentially nitrosylated. In particular, the role of nitric oxide could be interacting with this Cysteine residue through nitrosylation and by acquiring NO moiety, making the Cysteine residues not accessible to the ubiquitinase proteins, making Vimentin more stable by avoiding degradation. The hypothesis of Cys328 nitrosylation and the role of L-NMMA in increasing Vimentin stability, is reported in the figure above (**Figure 4.28**).

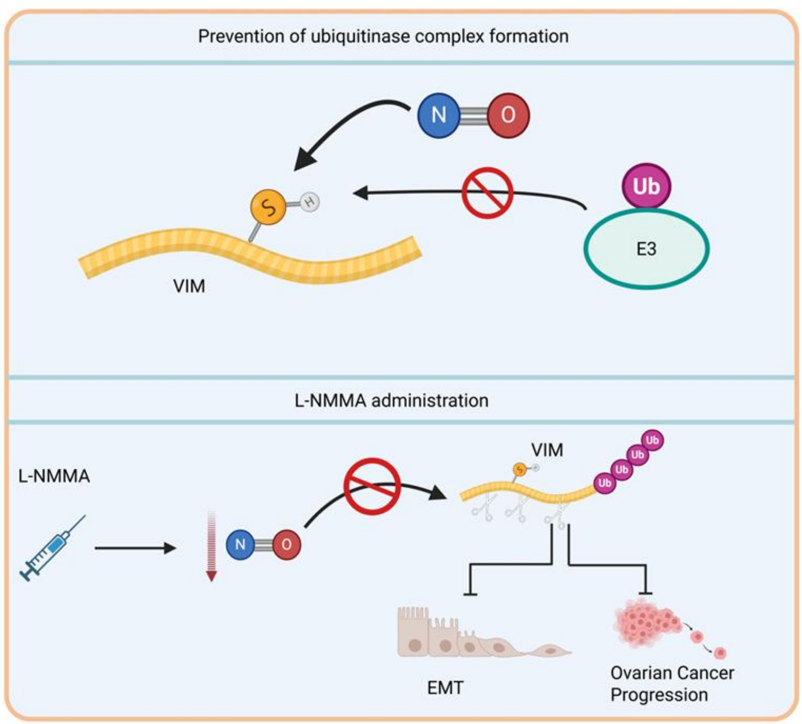

Figure 4.28. Vimentin nitrosilatyion and L-NMMA activity. The hypothesis reported in the figure above shows how NO is able to interact through nitrosylation in the Cys328 residue of Vimentin through S-Nitrosylation avoiding ubiquitination. When administered, L-NMMA is able to reduce NO levels, and consequently, S-Nitrosylation which, in turn is not able to prevent Vimentin degradation through ubiquitination. Created in https://BioRender.com.

The administration of L-NMMA in ovarian cancer cell lines expressing iNOS shows a potential direct effect on EMT, which may influence many aspects of ovarian cancer, starting from metastatic spread, where Vimentin is involved [203], to global EMT transition [203] and even acquired resistance to chemotherapy. These results were also confirmed by the generation of KO cell lines which reported the same effects in the NOS2 knockout clones generated as model for L-NMMA clinical administration. The connection between L-NMMA and Vimentin in ovarian cancer opens new frontiers in treating this condition, with the potential to both kill cancer cells and limit their spread by targeting and disrupting the communications between cells into the tumour niche.

The effect of combining Cisplatin + L-NMMA

The appropriate use of chemotherapy is a critical factor in the fight against OC. While Cisplatin is an effective drug, it also presents many side effects, such as nephrotoxicity, organ damage, and increased release of ROS [314]. The effectiveness of the drug also depends on how well the patient can tolerate the treatment, including the concentrations and number of cycles that can be sustained. For this reason, reducing side effects can help improve both the duration and effectiveness of treatment. Another important aspect is that, even with the first-line approach, comprising surgical tumour debulking and chemotherapy, almost 70-80% of patients experience relapse [290], making chemotherapy less effective as cancer cells develop resistance to treatment. A drug that is effective at low doses and suitable for long-term use could provide significant benefits in the treatment of this disease. A drug exhibiting strong anticancer activity at low doses could help minimize the risk of chemoresistance. Beyond treatment efficacy and duration, the tumour microenvironment plays a critical role in cancer progression. Therefore, this study proposes a novel approach that not only enhances the cytotoxic effects of Cisplatin, allowing for dose reduction and decreased likelihood of chemoresistance, but also targets the disruption of cellular communication within the tumour microenvironment. This strategy aims to destabilize and inhibit epithelial-mesenchymal transition (EMT) and immune suppression, thereby delivering a comprehensive assault on the entire tumour niche.

The combination therapy reactivates the immune system and reduces the metastatic spread

The selection of a syngeneic in vivo model enabled the study not only of tumour progression but also of the possible effects of iNOS in an immunocompetent mouse model. It is well known that many immune cells can express iNOS, as previously stated. Additionally, the ovarian cancer tumour microenvironment is recognized as a cold immune environment, where the immune response is low [315], and immune suppression is maintained by immunosuppressive cells, which may play a critical role. For this reason, targeting iNOS and interfering with NO release and intercellular communication may have significant implications in modulating immune responses. Using this in vivo model, a novel approach was explored, combining a pan-microenvironment drug with a classical chemotherapeutic agent, which demonstrated enhanced efficacy. This combination increased the activity of Cisplatin and was associated with the reactivation of key immune cells such as NK, NKT, and increased infiltration of T lymphocytes. This study also showed that L-NMMA treatment led not only to greater immune cell infiltration into ascites but also to increased expression of activation markers on CD4+ T cells. Specifically, L-NMMA enhanced CD4+ T cell activation while simultaneously reducing naïve cell markers, indicating a more activated and functionally engaged T cell population. Furthermore, the combination of Cisplatin and L- NMMA demonstrated a stronger effect in inducing tumour cell death, as confirmed by pathological analysis. The combined treatment significantly reduced tumour area, tumour cell count, and the percentage of tumour cells in peritoneal tissues when compared to Cisplatin alone. These findings support the potential of combining L-NMMA with Cisplatin not only to enhance cytotoxic efficacy but also to modulate the tumour microenvironment and immune response, offering a promising therapeutic strategy for ovarian cancer. Considering all the aspects, this work opened a new scenario of the benefits of a combination therapy between Cisplatin and L-NMMA not only in more aggressively targeting cancer cells, but also, as previously stated, in destabilizing the tumour niche. If, as already stated, the immune cold tumour microenvironment represents one of the main challenges in this disease, this work showed how L-NMMA has specificity in the increase of T cells infiltration and activation of CD4+ T cells showing again that NO plays an important role in the immune suppression of cancer.

KO cells in xenograft mice models are more sensitive to Cisplatin

A specific iNOS KO model has already been tested in vitro in metaplastic breast cancer [209], a type of cancer known for its iNOS expression and consequent overproduction of NO. In this work, OVCAR8 NOS2 KO clones were injected intraperitoneally into NOD SCID gamma (NSG) mice to closely mimic human ovarian cancer, including its specific subtype and the genotypical and phenotypical characteristics of the adopted cell line. Cisplatin treatment was more effective in the iNOS KO model, as shown by a marked reduction in tumour burden and prolonged survival of the mice belonging to the knockout group. The impairment of pathways such as wound healing, epithelial tube morphogenesis, extracellular matrix organization, EMT transition, and other proliferation-related mechanisms, as observed in the RNAseq data, might play a strong role in regards with what was observed. This was further supported by the observed drop in ROI (region of interest) signal at the final measurement point upon reaching the experimental endpoint, confirming that iNOS knockout cells led to slower tumourigenesis and increased survival in mice compared to those injected with parental cells. This model was intended to demonstrate that the observed effects are not limited to immunocompetent mice, where immune system reactivation may contribute to reduced tumour proliferation, but also hold true in a context where NO signaling is directly suppressed. Notably, the use of L-NMMA in this study revealed a dual mechanism of action: targeting the tumour microenvironment and simultaneously reducing both primary tumour growth and metastatic progression.

Future work priorities: current status of iNOS knowledge in ovarian cancer compared to other cancer types

This thesis aims to investigate the role of iNOS in ovarian cancer, a topic that remains insufficiently explored in the current literature. In contrast, iNOS has been extensively studied in breast cancer, where it has been associated with adverse clinical outcomes. Notably, iNOS has been shown to promote epithelial–mesenchymal transition (EMT), while its inhibition increases cellular sensitivity to chemotherapy. Furthermore, clinical studies conducted in Dr. Jenny Chang's laboratory have evaluated the use of the nitric oxide synthase inhibitor L-NMMA, which is now being incorporated into clinical treatment protocols. Collectively, these studies, including clinical trials, demonstrate a comprehensive understanding of iNOS function in breast cancer, highlighting the need to further elucidate its role in ovarian cancer. To establish L-NMMA as an effective therapeutic option for ovarian cancer, several steps are required. These include optimizing its dosage in vivo and, ultimately, in patients. Ovarian cancer presents unique biological challenges that complicate treatment. For instance, the accumulation of ascites in the abdominal cavity can act as a barrier, limiting drug penetration and reducing therapeutic efficacy. Additionally, the activity of fibroblasts and the deposition of extracellular matrix create a dense stromal environment that further impedes the delivery of drugs and immune cells to both primary and metastatic tumor sites. These obstacles underscore the need for innovative strategies to improve treatment outcomes. One potential approach involves optimizing L-NMMA delivery through nanoparticles designed to enhance drug distribution within the tumor microenvironment. Moreover, the development of improved in vivo models will be essential to determine the optimal concentration and therapeutic window of L-NMMA, as well as to assess its combined efficacy with chemotherapy across different experimental systems. With the accumulation of robust preclinical data, it may become feasible to initiate clinical trials in ovarian cancer, similar to those already conducted in breast cancer. Ultimately, this could lead to the development of a novel therapeutic strategy, offering an additional treatment option for patients with high iNOS expression.

Weaknesses of the study

This study aims to introduce and demonstrate the potential applicability of L-NMMA as a novel therapeutic agent in ovarian cancer. To date, both the use of this drug and its investigation in the context of ovarian cancer remain largely unexplored in the literature. Given the challenges associated with this work, and considering that L-NMMA has been extensively studied in breast cancer but not in ovarian cancer, dose optimization represents a critical aspect for future research. As with any emerging therapeutic approach, further studies are required to refine its use, particularly in combination with standard chemotherapy. Moreover, since L-NMMA is often administered alongside Amlodipine as a blood pressure stabilizer, careful optimization of dosing regimens will be essential to minimize potential side effects associated with treatment. Another important area for improvement is the expansion of in vivo studies. Increasing the number of experimental models, including a larger cohort of animals, would strengthen the robustness of the findings presented in this thesis. In particular, the use of patient-derived xenograft (PDX) models could provide valuable insights into the efficacy of L-NMMA in systems that more closely recapitulate human disease, thereby enhancing the translational relevance of the results. Finally, further investigation into the role of iNOS in cisplatin-resistant ovarian cancer cells is needed. It is well established that ovarian cancer frequently develops chemoresistance, typically within approximately 18 months of treatment. Therefore, evaluating the effects of L-NMMA in chemoresistant models would be a crucial step toward addressing one of the most significant challenges in ovarian cancer therapy, namely, the loss of treatment efficacy over time. Such studies could contribute to the development of more effective strategies to overcome resistance and improve patient outcomes.

Future perspectives

While the role of iNOS has been extensively studied in other cancers, this research introduces new insights into its role in ovarian cancer. By identifying ovarian cancer cell lines that express iNOS at basal levels, as well as after cytokine stimulation, it was also demonstrated that iNOS is expressed at basal levels in Cisplatin-resistant ovarian cancer cell lines. This opens new avenues for investigating the connection between iNOS overexpression and chemoresistance. New and promising approaches are emerging in the fight against cancer, especially those that combine drug treatments to target both cancer cells and their supporting microenvironment. The opportunity to pair chemotherapy with agents that can disrupt the tumour microenvironment, inhibit EMT, and simultaneously stimulate the immune response presents a potential breakthrough. This combined strategy may help prevent metastatic spread, overcome acquired chemoresistance, and, in part, reactivate the suppressed immune landscape in ovarian cancer. Taken all together, considered the most recent application in immunotherapy, where many efforts of the scientific community are directed, L-NMMA represents also a potential drug to pair in immunotherapy as it can also implement the immune response by reactivating and stimulating the immune response.

Bibliography

1. Hollis, R.L., *Molecular characteristics and clinical behaviour of epithelial ovarian cancers.* Cancer Lett, 2023. **555**: p. 216057.
2. Gaitskell, K., et al., *Angiogenesis inhibitors for the treatment of epithelial ovarian cancer.* Cochrane Database Syst Rev, 2023. **4**(4): p. CD007930.
3. Sellers, T.A., et al., *Prevention of Epithelial Ovarian Cancer.* Cold Spring Harb Perspect Med, 2023. **13**(8).
4. Feeley, K.M. and M. Wells, *Precursor lesions of ovarian epithelial malignancy.* Histopathology, 2001. **38**(2): p. 87-95.
5. Cho, K.R. and M. Shih Ie, *Ovarian cancer.* Annu Rev Pathol, 2009. **4**: p. 287-313.
6. Duska, L.R. and E.C. Kohn, *The new classifications of ovarian, fallopian tube, and primary peritoneal cancer and their clinical implications.* Ann Oncol, 2017. **28**(suppl_8): p. viii8-viii12.
7. Feki, A., et al., *Dissemination of intraperitoneal ovarian cancer: Discussion of mechanisms and demonstration of lymphatic spreading in ovarian cancer model.* Crit Rev Oncol Hematol, 2009. **72**(1): p. 1-9.
8. Pradeep, S., et al., *Hematogenous metastasis of ovarian cancer: rethinking mode of spread.* Cancer Cell, 2014. **26**(1): p. 77-91.
9. Pecot, C.V., et al., *A novel platform for detection of CK+ and CK- CTCs.* Cancer Discov, 2011. **1**(7): p. 580-6.
10. Phillips, K.G., et al., *Optical quantification of cellular mass, volume, and density of circulating tumor cells identified in an ovarian cancer patient.* Front Oncol, 2012. **2**: p. 72.

11. Colombo, N., et al., *ESMO-ESGO consensus conference recommendations on ovarian cancer: pathology and molecular biology, early and advanced stages, borderline tumours and recurrent diseasedagger*. Ann Oncol, 2019. **30**(5): p. 672-705.
12. Vergote, I., et al., *Neoadjuvant chemotherapy or primary surgery in stage IIIC or IV ovarian cancer*. N Engl J Med, 2010. **363**(10): p. 943-53.
13. Hennessy, B.T., R.L. Coleman, and M. Markman, *Ovarian cancer*. Lancet, 2009. **374**(9698): p. 1371-82.
14. Coukos, G. and S.C. Rubin, *Chemotherapy resistance in ovarian cancer: new molecular perspectives*. Obstet Gynecol, 1998. **G1**(5 Pt 1): p. 783-92.
15. Xiao, X., D.W. Melton, and C. Gourley, *Mismatch repair deficiency in ovarian cancer -- molecular characteristics and clinical implications*. Gynecol Oncol, 2014. **132**(2): p. 506-12.
16. Albrengues, J., et al., *Epigenetic switch drives the conversion of fibroblasts into proinvasive cancer-associated fibroblasts*. Nat Commun, 2015. **6**: p. 10204.
17. Almeida-Nunes, D.L., et al., *Immune Tumor Microenvironment in Ovarian Cancer Ascites*. Int J Mol Sci, 2022. **23**(18).
18. Attane, C. and C. Muller, *Drilling for Oil: Tumor-Surrounding Adipocytes Fueling Cancer*. Trends Cancer, 2020. **6**(7): p. 593-604.
19. Dasari, S., Y. Fang, and A.K. Mitra, *Cancer Associated Fibroblasts: Naughty Neighbors That Drive Ovarian Cancer Progression*. Cancers (Basel), 2018. **10**(11).
20. McLean, K., et al., *Human ovarian carcinoma-associated mesenchymal stem cells regulate cancer stem cells and tumorigenesis via altered BMP production*. J Clin Invest, 2011. **121**(8): p. 3206-19.
21. Nieman, K.M., et al., *Adipocytes promote ovarian cancer metastasis and provide energy for rapid tumor growth*. Nat Med, 2011. **17**(11): p. 1498-503.
22. Da Silva, A.C., et al., *The Role of Stroma in Ovarian Cancer*. Immunol Invest, 2020. **4G**(4): p. 406-424.
23. Desbois, M. and Y. Wang, *Cancer-associated fibroblasts: Key players in shaping the tumor immune microenvironment*. Immunol Rev, 2021. **302**(1): p. 241-258.
24. Dulauroy, S., et al., *Lineage tracing and genetic ablation of ADAM12(+) perivascular cells identify a major source of profibrotic cells during acute tissue injury*. Nat Med, 2012. **18**(8): p. 1262-70.
25. Jotzu, C., et al., *Adipose tissue derived stem cells differentiate into carcinoma-associated fibroblast-like cells under the inffuence of tumor derived factors*. Cell Oncol (Dordr), 2011. **34**(1): p. 55-67.
26. Potenta, S., E. Zeisberg, and R. Kalluri, *The role of endothelial-to-mesenchymal transition in cancer progression*. Br J Cancer, 2008. **GG**(9): p. 1375-9.
27. Quante, M., et al., *Bone marrow-derived myofibroblasts contribute to the mesenchymal stem cell niche and promote tumor growth*. Cancer Cell, 2011. **1G**(2): p. 257-72.
28. Sharon, Y., et al., *Tumor-derived osteopontin reprograms normal mammary fibroblasts to promote inffammation and tumor growth in breast cancer*. Cancer Res, 2015. **75**(6): p. 963-73.
29. Thiery, J.P. and J.P. Sleeman, *Complex networks orchestrate epithelial-mesenchymal transitions*. Nat Rev Mol Cell Biol, 2006. **7**(2): p. 131-42.
30. Paget, S., *The distribution of secondary growths in cancer of the breast. 188S*. Cancer Metastasis Rev, 1989. **8**(2): p. 98-101.
31. Kalluri, R., *The biology and function of fibroblasts in cancer*. Nat Rev Cancer, 2016. **16**(9): p. 582-98.

32. Gerard, N.P., et al., *An anti-inffammatory function for the complement anaphylatoxin C5a-binding protein, C5L2*. J Biol Chem, 2005. **280**(48): p. 39677-80.
33. Guido, C., et al., *Metabolic reprogramming of cancer-associated fibroblasts by TGF-beta drives tumor growth: connecting TGF-beta signaling with "Warburg-like" cancer metabolism and L-lactate production*. Cell Cycle, 2012. **11**(16): p. 3019-35.
34. Kanzaki, R. and K. Pietras, *Heterogeneity of cancer-associated fibroblasts: Opportunities for precision medicine*. Cancer Sci, 2020. **111**(8): p. 2708-2717.
35. Mhaidly, R. and F. Mechta-Grigoriou, *Fibroblast heterogeneity in tumor micro-environment: Role in immunosuppression and new therapies*. Semin Immunol, 2020. **48**: p. 101417.
36. Nurmik, M., et al., *In search of definitions: Cancer-associated fibroblasts and their markers*. Int J Cancer, 2020. **146**(4): p. 895-905.
37. Flavell, R.A., et al., *The polarization of immune cells in the tumour environment by TGFbeta*. Nat Rev Immunol, 2010. **10**(8): p. 554-67.
38. Delaine-Smith, R.M., et al., *Modelling TGFbetaR and Hh pathway regulation of prognostic matrisome molecules in ovarian cancer*. iScience, 2021. **24**(6): p. 102674.
39. Mei, D., et al., *The Role of CTHRC1 in Regulation of Multiple Signaling and Tumor Progression and Metastasis*. Mediators Inflamm, 2020. **2020**: p. 9578701.
40. Wu, Y.H., et al., *COL11A1 promotes tumor progression and predicts poor clinical outcome in ovarian cancer*. Oncogene, 2014. **33**(26): p. 3432-40.
41. Wu, Y.H., et al., *COL11A1 activates cancer-associated fibroblasts by modulating TGF-beta3 through the NF-kappaB/IGFBP2 axis in ovarian cancer cells*. Oncogene, 2021. **40**(26): p. 4503-4519.
42. Yeung, T.L., et al., *TGF-beta modulates ovarian cancer invasion by upregulating CAF-derived versican in the tumor microenvironment*. Cancer Res, 2013. **73**(16): p. 5016-28.
43. Yue, H., et al., *Stromal POSTN induced by TGF-beta1 facilitates the migration and invasion of ovarian cancer*. Gynecol Oncol, 2021. **160**(2): p. 530-538.
44. Zhang, Q., et al., *LY21572SS Monohydrate, a TGF-betaR1 Inhibitor, Suppresses Tumor Growth and Ascites Development in Ovarian Cancer*. Cancers (Basel), 2018. **10**(8).
45. Curtis, M., et al., *Fibroblasts Mobilize Tumor Cell Glycogen to Promote Proliferation and Metastasis*. Cell Metab, 2019. **2G**(1): p. 141-155 e9.
46. Kinugasa, Y., T. Matsui, and N. Takakura, *CD44 expressed on cancer-associated fibroblasts is a functional molecule supporting the stemness and drug resistance of malignant cancer cells in the tumor microenvironment*. Stem Cells, 2014. **32**(1): p. 145-56.
47. Su, S., et al., *CD10(+)GPR77(+) Cancer-Associated Fibroblasts Promote Cancer Formation and Chemoresistance by Sustaining Cancer Stemness*. Cell, 2018. **172**(4): p. 841-856 e16.
48. Wang, W., et al., *Effector T Cells Abrogate Stroma-Mediated Chemoresistance in Ovarian Cancer*. Cell, 2016. **165**(5): p. 1092-1105.
49. Wang, L., et al., *Cancer-associated fibroblasts enhance metastatic potential of lung cancer cells through IL-C/STAT3 signaling pathway*. Oncotarget, 2017. **8**(44): p. 76116-76128.
50. Li, W., et al., *TGFbeta1 in fibroblasts-derived exosomes promotes epithelial-mesenchymal transition of ovarian cancer cells*. Oncotarget, 2017. **8**(56): p. 96035-96047.
51. Wang, L., et al., *CAFs enhance paclitaxel resistance by inducing EMT through the IL-C/JAK2/STAT3 pathway*. Oncol Rep, 2018. **3G**(5): p. 2081-2090.
52. Kai, F., H. Laklai, and V.M. Weaver, *Force Matters: Biomechanical Regulation of Cell Invasion and Migration in Disease*. Trends Cell Biol, 2016. **26**(7): p. 486-497.
53. Kieffer, Y., et al., *Single-Cell Analysis Reveals Fibroblast Clusters Linked to Immunotherapy Resistance in Cancer*. Cancer Discov, 2020. **10**(9): p. 1330-1351.

54. Gerber, H.P., et al., *Complete inhibition of rhabdomyosarcoma xenograft growth and neovascularization requires blockade of both tumor and host vascular endothelial growth factor*. Cancer Res, 2000. **60**(22): p. 6253-8.
55. Fukumura, D., et al., *Tumor induction of VEGF promoter activity in stromal cells*. Cell, 1998. **G4**(6): p. 715-25.
56. Qiao, L., et al., *Dkk-1 secreted by mesenchymal stem cells inhibits growth of breast cancer cells via depression of Wnt signalling*. Cancer Lett, 2008. **26G**(1): p. 67-77.
57. Djouad, F., et al., *Immunosuppressive effect of mesenchymal stem cells favors tumor growth in allogeneic animals*. Blood, 2003. **102**(10): p. 3837-44.
58. Muehlberg, F.L., et al., *Tissue-resident stem cells promote breast cancer growth and metastasis*. Carcinogenesis, 2009. **30**(4): p. 589-97.
59. Yang, J., et al., *Adipocytes promote ovarian cancer chemoresistance*. Sci Rep, 2019. **G**(1): p. 13316.
60. El-Arabey, A.A., M. Abdalla, and A.R. Abd-Allah, *GATA3 and stemness of high-grade serous ovarian carcinoma: novel hope for the deadliest type of ovarian cancer*. Hum Cell, 2020. **33**(3): p. 904-906.
61. Noy, R. and J.W. Pollard, *Tumor-associated macrophages: from mechanisms to therapy*. Immunity, 2014. **41**(1): p. 49-61.
62. Ruffell, B. and L.M. Coussens, *Macrophages and therapeutic resistance in cancer*. Cancer Cell, 2015. **27**(4): p. 462-72.
63. Sica, A., et al., *Macrophage polarization in tumour progression*. Semin Cancer Biol, 2008. **18**(5): p. 349-55.
64. Takaishi, K., et al., *Involvement of M2-polarized macrophages in the ascites from advanced epithelial ovarian carcinoma in tumor progression via Stat3 activation*. Cancer Sci, 2010. **101**(10): p. 2128-36.
65. Wang, X., et al., *Interaction of monocytes/macrophages with ovarian cancer cells promotes angiogenesis in vitro*. Cancer Sci, 2013. **104**(4): p. 516-23.
66. Hornell, T.M., et al., *Regulation of the class II MHC pathway in primary human monocytes by granulocyte-macrophage colony-stimulating factor*. J Immunol, 2003. **171**(5): p. 2374-83.
67. Del Prete, A., et al., *Dendritic cell subsets in cancer immunity and tumor antigen sensing*. Cell Mol Immunol, 2023. **20**(5): p. 432-447.
68. Cubillos-Ruiz, J.R., et al., *ER Stress Sensor XBP1 Controls Anti-tumor Immunity by Disrupting Dendritic Cell Homeostasis*. Cell, 2015. **161**(7): p. 1527-38.
69. Charles, K.A., et al., *The tumor-promoting actions of TNF-alpha involve TNFR1 and IL-17 in ovarian cancer in mice and humans*. J Clin Invest, 2009. **11G**(10): p. 3011-23.
70. Fridlender, Z.G., et al., *Polarization of tumor-associated neutrophil phenotype by TGF-beta: "N1" versus "N2" TAN*. Cancer Cell, 2009. **16**(3): p. 183-94.
71. Karre, K., et al., *Selective rejection of H-2-deficient lymphoma variants suggests alternative immune defence strategy*. Nature, 1986. **31G**(6055): p. 675-8.
72. Morvan, M.G. and L.L. Lanier, *NK cells and cancer: you can teach innate cells new tricks*. Nat Rev Cancer, 2016. **16**(1): p. 7-19.
73. Krockenberger, M., et al., *Macrophage migration inhibitory factor contributes to the immune escape of ovarian cancer by down-regulating NKG2D*. J Immunol, 2008. **180**(11): p. 7338-48.
74. Pesce, S., et al., *B7-HC-mediated downregulation of NKp30 in NK cells contributes to ovarian carcinoma immune escape*. Oncoimmunology, 2015. **4**(4): p. e1001224.
75. Zhou, Y., et al., *B7-HC expression correlates with cancer progression and patient's survival in human ovarian cancer*. Int J Clin Exp Pathol, 2015. **8**(8): p. 9428-33.

76. Radke, J., et al., *[-Cytokine level in malignant ascites and peripheral blood of patients with advanced ovarian carcinoma-].* Geburtshilfe Frauenheilkd, 1996. **56**(2): p. 83-7.
77. Trotta, R., et al., *TGF-beta utilizes SMAD3 to inhibit CD1C-mediated IFN-gamma production and antibody-dependent cellular cytotoxicity in human NK cells.* J Immunol, 2008. **181**(6): p. 3784-92.
78. Theoharides, T.C. and P. Conti, *Mast cells: the Jekyll and Hyde of tumor growth.* Trends Immunol, 2004. **25**(5): p. 235-41.
79. Starkey, J.R., P.K. Crowle, and S. Taubenberger, *Mast-cell-deficient W/Wv mice exhibit a decreased rate of tumor angiogenesis.* Int J Cancer, 1988. **42**(1): p. 48-52.
80. Gooch, J.L., A.V. Lee, and D. Yee, *Interleukin 4 inhibits growth and induces apoptosis in human breast cancer cells.* Cancer Res, 1998. **58**(18): p. 4199-205.
81. Raskov, H., et al., *Cytotoxic CD8(+) T cells in cancer and cancer immunotherapy.* Br J Cancer, 2021. **124**(2): p. 359-367.
82. Hwang, W.T., et al., *Prognostic significance of tumor-infiltrating T cells in ovarian cancer: a meta-analysis.* Gynecol Oncol, 2012. **124**(2): p. 192-8.
83. Ovarian Tumor Tissue Analysis, C., et al., *Dose-Response Association of CD8+ Tumor-Infiltrating Lymphocytes and Survival Time in High-Grade Serous Ovarian Cancer.* JAMA Oncol, 2017. **3**(12): p. e173290.
84. Tiper, I.V., et al., *VEGF Potentiates GD3-Mediated Immunosuppression by Human Ovarian Cancer Cells.* Clin Cancer Res, 2016. **22**(16): p. 4249-58.
85. Zhang, L., et al., *Intratumoral T cells, recurrence, and survival in epithelial ovarian cancer.* N Engl J Med, 2003. **348**(3): p. 203-13.
86. Hamanishi, J., et al., *Programmed cell death 1 ligand 1 and tumor-infiltrating CD8+ T lymphocytes are prognostic factors of human ovarian cancer.* Proc Natl Acad Sci U S A, 2007. **104**(9): p. 3360-5.
87. Curiel, T.J., et al., *Blockade of B7-H1 improves myeloid dendritic cell-mediated antitumor immunity.* Nat Med, 2003. **G**(5): p. 562-7.
88. Kaech, S.M. and W. Cui, *Transcriptional control of effector and memory CD8+ T cell differentiation.* Nat Rev Immunol, 2012. **12**(11): p. 749-61.
89. Lynch, E.A., et al., *Cutting edge: IL-1C/CD4 preferentially induces Th1 cell migration: requirement of CCR5.* J Immunol, 2003. **171**(10): p. 4965-8.
90. Speiser, D.E., et al., *CD4(+) T cells in cancer.* Nat Cancer, 2023. **4**(3): p. 317-329.
91. Yu, P. and Y.X. Fu, *Tumor-infiltrating T lymphocytes: friends or foes?* Lab Invest, 2006. **86**(3): p. 231-45.
92. Lehar, S.M. and M.J. Bevan, *Immunology: polarizing a T-cell response.* Nature, 2004. **430**(6996): p. 150-1.
93. Shedlock, D.J. and H. Shen, *Requirement for CD4 T cell help in generating functional CD8 T cell memory.* Science, 2003. **300**(5617): p. 337-9.
94. Bennett, S.R., et al., *Help for cytotoxic-T-cell responses is mediated by CD40 signalling.* Nature, 1998. **3G3**(6684): p. 478-80.
95. Cella, M., et al., *Ligation of CD40 on dendritic cells triggers production of high levels of interleukin-12 and enhances T cell stimulatory capacity: T-T help via APC activation.* J Exp Med, 1996. **184**(2): p. 747-52.
96. Elgueta, R., et al., *Molecular mechanism and function of CD40/CD40L engagement in the immune system.* Immunol Rev, 2009. **22G**(1): p. 152-72.
97. Devarajan, P., et al., *Pathogen Recognition by CD4 Effectors Drives Key Effector and Most Memory Cell Generation Against Respiratory Virus.* Front Immunol, 2018. **G**: p. 596.

98. Juno, J.A., et al., *Cytotoxic CD4 T Cells-Friend or Foe during Viral Infection?* Front Immunol, 2017. **8**: p. 19.
99. Takeuchi, A. and T. Saito, *CD4 CTL, a Cytotoxic Subset of CD4(+) T Cells, Their Differentiation and Function*. Front Immunol, 2017. **8**: p. 194.
100. Eshima, K., et al., *Ectopic expression of a T-box transcription factor, eomesodermin, renders CD4(+) Th cells cytotoxic by activating both perforin- and FasL-pathways*. Immunol Lett, 2012. **144**(1-2): p. 7-15.
101. Reis, B.S., et al., *Transcription factor T-bet regulates intraepithelial lymphocyte functional maturation*. Immunity, 2014. **41**(2): p. 244-56.
102. Sledzinska, A., et al., *Regulatory T Cells Restrain Interleukin-2- and Blimp-1-Dependent Acquisition of Cytotoxic Function by CD4(+) T Cells*. Immunity, 2020. **52**(1): p. 151-166 e6.
103. Artis, D. and H. Spits, *The biology of innate lymphoid cells*. Nature, 2015. **517**(7534): p. 293-301.
104. Fang, D. and J. Zhu, *Dynamic balance between master transcription factors determines the fates and functions of CD4 T cell and innate lymphoid cell subsets*. J Exp Med, 2017. **214**(7): p. 1861-1876.
105. Vivier, E., et al., *Innate Lymphoid Cells: 10 Years On*. Cell, 2018. **174**(5): p. 1054-1066.
106. Cherrier, D.E., N. Serafini, and J.P. Di Santo, *Innate Lymphoid Cell Development: A T Cell Perspective*. Immunity, 2018. **48**(6): p. 1091-1103.
107. Barnett, J.C., et al., *Ovarian cancer tumor infiltrating T-regulatory (T(reg)) cells are associated with a metastatic phenotype*. Gynecol Oncol, 2010. **116**(3): p. 556-62.
108. Qiao, S., et al., *Tregs are involved in VEGFA/ VASH1-related angiogenesis pathway in ovarian cancer*. Transl Oncol, 2023. **32**: p. 101665.
109. Lasser, S.A., et al., *Myeloid-derived suppressor cells in cancer and cancer therapy*. Nat Rev Clin Oncol, 2024. **21**(2): p. 147-164.
110. Gabrilovich, D.I. and S. Nagaraj, *Myeloid-derived suppressor cells as regulators of the immune system*. Nat Rev Immunol, 2009. **G**(3): p. 162-74.
111. Cui, T.X., et al., *Myeloid-derived suppressor cells enhance stemness of cancer cells by inducing microRNA101 and suppressing the corepressor CtBP2*. Immunity, 2013. **3G**(3): p. 611-21.
112. Groth, C., et al., *Blocking Migration of Polymorphonuclear Myeloid-Derived Suppressor Cells Inhibits Mouse Melanoma Progression*. Cancers (Basel), 2021. **13**(4).
113. Lim, H.X., T.S. Kim, and C.L. Poh, *Understanding the Differentiation, Expansion, Recruitment and Suppressive Activities of Myeloid-Derived Suppressor Cells in Cancers*. Int J Mol Sci, 2020. **21**(10).
114. Pan, P.Y., et al., *Immune stimulatory receptor CD40 is required for T-cell suppression and T regulatory cell activation mediated by myeloid-derived suppressor cells in cancer*. Cancer Res, 2010. **70**(1): p. 99-108.
115. Vergote, I., et al., *Timing of debulking surgery in advanced ovarian cancer*. Int J Gynecol Cancer, 2008. **18 Suppl 1**: p. 11-9.
116. Jaaback, K., N. Johnson, and T.A. Lawrie, *Intraperitoneal chemotherapy for the initial management of primary epithelial ovarian cancer*. Cochrane Database Syst Rev, 2016. **2016**(1): p. CD005340.
117. Tewari, D., et al., *Long-term survival advantage and prognostic factors associated with intraperitoneal chemotherapy treatment in advanced ovarian cancer: a gynecologic oncology group study*. J Clin Oncol, 2015. **33**(13): p. 1460-6.

118. Wright, A.A., et al., *Use and Effectiveness of Intraperitoneal Chemotherapy for Treatment of Ovarian Cancer*. J Clin Oncol, 2015. **33**(26): p. 2841-7.
119. McCloskey, C.W., et al., *Ovarian Cancer Immunotherapy: Preclinical Models and Emerging Therapeutics*. Cancers (Basel), 2018. **10**(8).
120. Yang, Y., et al., *Tumor Microenvironment in Ovarian Cancer: Function and Therapeutic Strategy*. Front Cell Dev Biol, 2020. **8**: p. 758.
121. Chester, C., et al., *Immunotherapeutic approaches to ovarian cancer treatment*. J Immunother Cancer, 2015. **3**: p. 7.
122. Hata, K., et al., *Expression of the vascular endothelial growth factor (VEGF) gene in epithelial ovarian cancer: an approach to anti-VEGF therapy*. Anticancer Res, 2011. **31**(2): p. 731-7.
123. Bellone, S., et al., *Overexpression of epithelial cell adhesion molecule in primary, metastatic, and recurrent/chemotherapy-resistant epithelial ovarian cancer: implications for epithelial cell adhesion molecule-specific immunotherapy*. Int J Gynecol Cancer, 2009. **1G**(5): p. 860-6.
124. Linke, R., A. Klein, and D. Seimetz, *Catumaxomab: clinical development and future directions*. MAbs, 2010. **2**(2): p. 129-36.
125. Berek, J.S., et al., *Catumaxomab for the treatment of malignant ascites in patients with chemotherapy-refractory ovarian cancer: a phase II study*. Int J Gynecol Cancer, 2014. **24**(9): p. 1583-9.
126. Mantovani, A., et al., *Macrophage polarization: tumor-associated macrophages as a paradigm for polarized M2 mononuclear phagocytes*. Trends Immunol, 2002. **23**(11): p. 549-55.
127. Curiel, T.J., et al., *Specific recruitment of regulatory T cells in ovarian carcinoma fosters immune privilege and predicts reduced survival*. Nat Med, 2004. **10**(9): p. 942-9.
128. Ries, C.H., et al., *Targeting tumor-associated macrophages with anti-CSF-1R antibody reveals a strategy for cancer therapy*. Cancer Cell, 2014. **25**(6): p. 846-59.
129. Egen, J.G., M.S. Kuhns, and J.P. Allison, *CTLA-4: new insights into its biological function and use in tumor immunotherapy*. Nat Immunol, 2002. **3**(7): p. 611-8.
130. Maine, C.J., et al., *Programmed death ligand-1 over-expression correlates with malignancy and contributes to immune regulation in ovarian cancer*. Cancer Immunol Immunother, 2014. **63**(3): p. 215-24.
131. Bijker, M.S., et al., *Superior induction of anti-tumor CTL immunity by extended peptide vaccines involves prolonged, DC-focused antigen presentation*. Eur J Immunol, 2008. **38**(4): p. 1033-42.
132. Liu, M.A., *DNA vaccines: an historical perspective and view to the future*. Immunol Rev, 2011. **23G**(1): p. 62-84.
133. Pardi, N., et al., *mRNA vaccines - a new era in vaccinology*. Nat Rev Drug Discov, 2018. **17**(4): p. 261-279.
134. Uchijima, M., et al., *Optimization of codon usage of plasmid DNA vaccine is required for the effective MHC class I-restricted T cell responses against an intracellular bacterium*. J Immunol, 1998. **161**(10): p. 5594-9.
135. Trollet, C., et al., *Generation of high-titer neutralizing antibodies against botulinum toxins A, B, and E by DNA electrotransfer*. Infect Immun, 2009. **77**(5): p. 2221-9.
136. Lopes, A., et al., *Codon-Optimized P1A-Encoding DNA Vaccine: Toward a Therapeutic Vaccination against P815 Mastocytoma*. Mol Ther Nucleic Acids, 2017. **8**: p. 404-415.

137. Su, B., et al., *Sequential administration of cytokine genes to enhance cellular immune responses and CD4 (+) T memory cells during DNA vaccination*. Hum Vaccin Immunother, 2012. **8**(11): p. 1659-67.
138. Dorrie, J., et al., *Therapeutic Cancer Vaccination with Ex Vivo RNA-Transfected Dendritic Cells-An Update*. Pharmaceutics, 2020. **12**(2).
139. Larocca, C. and J. Schlom, *Viral vector-based therapeutic cancer vaccines*. Cancer J, 2011. **17**(5): p. 359-71.
140. Li, M., et al., *Microenvironment remodeled by tumor and stromal cells elevates fibroblast-derived COL1A1 and facilitates ovarian cancer metastasis*. Exp Cell Res, 2020. **3G4**(1): p. 112153.
141. Harper, J. and R.C. Sainson, *Regulation of the anti-tumour immune response by cancer-associated fibroblasts*. Semin Cancer Biol, 2014. **25**: p. 69-77.
142. Xouri, G. and S. Christian, *Origin and function of tumor stroma fibroblasts*. Semin Cell Dev Biol, 2010. **21**(1): p. 40-6.
143. Batlle, E. and J. Massague, *Transforming Growth Factor-beta Signaling in Immunity and Cancer*. Immunity, 2019. **50**(4): p. 924-940.
144. Zhang, M., et al., *The Role of Cancer-Associated Fibroblasts in Ovarian Cancer*. Cancers (Basel), 2022. **14**(11).
145. Desbois, M., et al., *Integrated digital pathology and transcriptome analysis identifies molecular mediators of T-cell exclusion in ovarian cancer*. Nat Commun, 2020. **11**(1): p. 5583.
146. Ozdemir, B.C., et al., *Depletion of carcinoma-associated fibroblasts and fibrosis induces immunosuppression and accelerates pancreas cancer with reduced survival*. Cancer Cell, 2014. **25**(6): p. 719-34.
147. Rocconi, R.P., et al., *Gemogenovatucel-T (Vigil) immunotherapy as maintenance in frontline stage III/IV ovarian cancer (VITAL): a randomised, double-blind, placebo-controlled, phase 2b trial*. Lancet Oncol, 2020. **21**(12): p. 1661-1672.
148. Wang, X., L. Jiang, and Q. Liu, *miR-18a-5p derived from mesenchymal stem cells-extracellular vesicles inhibits ovarian cancer cell proliferation, migration, invasion, and chemotherapy resistance*. J Transl Med, 2022. **20**(1): p. 258.
149. Fan, H., et al., *Epigenomic Reprogramming toward Mesenchymal-Epithelial Transition in Ovarian-Cancer-Associated Mesenchymal Stem Cells Drives Metastasis*. Cell Rep, 2020. **33**(10): p. 108473.
150. Tang, J., et al., *Epigenetic Targeting of Adipocytes Inhibits High-Grade Serous Ovarian Cancer Cell Migration and Invasion*. Mol Cancer Res, 2018. **16**(8): p. 1226-1240.
151. Snyder, S.H. and D.S. Bredt, *Biological roles of nitric oxide*. Sci Am, 1992. **266**(5): p. 68-71, 74-7.
152. Kobayashi, Y., *The regulatory role of nitric oxide in proinffammatory cytokine expression during the induction and resolution of inffammation*. J Leukoc Biol, 2010. **88**(6): p. 1157-62.
153. Xu, W., et al., *The role of nitric oxide in cancer*. Cell Res, 2002. **12**(5-6): p. 311-20.
154. Hess, D.T., et al., *Protein S-nitrosylation: purview and parameters*. Nat Rev Mol Cell Biol, 2005. **6**(2): p. 150-66.
155. Wang, Z., *Protein S-nitrosylation and cancer*. Cancer Lett, 2012. **320**(2): p. 123-9.
156. Mayer, B.X., et al., *Pharmacokinetic-pharmacodynamic profile of systemic nitric oxide-synthase inhibition with L-NMMA in humans*. Br J Clin Pharmacol, 1999. **47**(5): p. 539-44.

157. Chung, A.W., et al., *A phase 1/2 clinical trial of the nitric oxide synthase inhibitor L-NMMA and taxane for treating chemoresistant triple-negative breast cancer*. Sci Transl Med, 2021. **13**(624): p. eabj5070.
158. Hanahan, D. and L.M. Coussens, *Accessories to the crime: functions of cells recruited to the tumor microenvironment*. Cancer Cell, 2012. **21**(3): p. 309-22.
159. Hanahan, D. and R.A. Weinberg, *Hallmarks of cancer: the next generation*. Cell, 2011. **144**(5): p. 646-74.
160. Quail, D.F. and J.A. Joyce, *Microenvironmental regulation of tumor progression and metastasis*. Nat Med, 2013. **1G**(11): p. 1423-37.
161. Romanska, H.M., et al., *iNOS gene upregulation is associated with the early proliferative response of human lung fibroblasts to cytokine stimulation*. J Pathol, 2002. **1G7**(3): p. 372-9.
162. Calvisi, D.F., et al., *Aberrant iNOS signaling is under genetic control in rodent liver cancer and potentially prognostic for the human disease*. Carcinogenesis, 2008. **2G**(8): p. 1639-47.
163. PeNarando, J., E. Aranda, and A. RodrIguez-Ariza, *Immunomodulatory roles of nitric oxide in cancer: tumor microenvironment says "NO" to antitumor immune response*. Transl Res, 2019. **210**: p. 99-108.
164. Rahat, M.A. and B. Hemmerlein, *Macrophage-tumor cell interactions regulate the function of nitric oxide*. Front Physiol, 2013. **4**: p. 144.
165. Orucevic, A., et al., *Nitric-oxide production by murine mammary adenocarcinoma cells promotes tumor-cell invasiveness*. Int J Cancer, 1999. **81**(6): p. 889-96.
166. Monteran, L. and N. Erez, *The Dark Side of Fibroblasts: Cancer-Associated Fibroblasts as Mediators of Immunosuppression in the Tumor Microenvironment*. Front Immunol, 2019. **10**: p. 1835.
167. Xiang, H., et al., *Cancer-Associated Fibroblasts Promote Immunosuppression by Inducing ROS-Generating Monocytic MDSCs in Lung Squamous Cell Carcinoma*. Cancer Immunol Res, 2020. **8**(4): p. 436-450.
168. Ren, G., et al., *Mesenchymal stem cell-mediated immunosuppression occurs via concerted action of chemokines and nitric oxide*. Cell Stem Cell, 2008. **2**(2): p. 141-50.
169. Belgorosky, D., et al., *Relevance of iNOS expression in tumor growth and maintenance of cancer stem cells in a bladder cancer model*. J Mol Med (Berl), 2020. **G8**(11): p. 1615-1627.
170. Gochman, E., et al., *The expression of iNOS and nitrotyrosine in colitis and colon cancer in humans*. Acta Histochem, 2012. **114**(8): p. 827-35.
171. Kielbik, M., I. Szulc-Kielbik, and M. Klink, *The Potential Role of iNOS in Ovarian Cancer Progression and Chemoresistance*. Int J Mol Sci, 2019. **20**(7).
172. Wang, G.Y., et al., *Anti-cancer effect of iNOS inhibitor and its correlation with angiogenesis in gastric cancer*. World J Gastroenterol, 2005. **11**(25): p. 3830-3.
173. Chu, S.C., et al., *Analysis of the cytokine-stimulated human inducible nitric oxide synthase (iNOS) gene: characterization of differences between human and mouse iNOS promoters*. Biochem Biophys Res Commun, 1998. **248**(3): p. 871-8.
174. Okura, Y., et al., *Characterization of cytokine and iNOS mRNA expression in situ during the course of experimental autoimmune myocarditis in rats*. J Mol Cell Cardiol, 1997. **2G**(2): p. 491-502.
175. Rabinovitch, A., et al., *Inducible nitric oxide synthase (iNOS) in pancreatic islets of nonobese diabetic mice: identification of iNOS- expressing cells and relationships to cytokines expressed in the islets*. Endocrinology, 1996. **137**(5): p. 2093-9.

176. Fain, J.N., *Release of interleukins and other inffammatory cytokines by human adipose tissue is enhanced in obesity and primarily due to the nonfat cells*. Vitam Horm, 2006. **74**: p. 443-77.
177. Calon, A., D.V. Tauriello, and E. Batlle, *TGF-beta in CAF-mediated tumor growth and metastasis*. Semin Cancer Biol, 2014. **25**: p. 15-22.
178. Hensler, M., et al., *M2-like macrophages dictate clinically relevant immunosuppression in metastatic ovarian cancer*. J Immunother Cancer, 2020. **8**(2).
179. Redd, P.S., et al., *SETD1B Activates iNOS Expression in Myeloid-Derived Suppressor Cells*. Cancer Res, 2017. **77**(11): p. 2834-2843.
180. Brown, E.R., et al., *A clinical study assessing the tolerability and biological effects of inffiximab, a TNF-alpha inhibitor, in patients with advanced cancer*. Ann Oncol, 2008. **1G**(7): p. 1340-1346.
181. Kulbe, H., et al., *A dynamic inffammatory cytokine network in the human ovarian cancer microenvironment*. Cancer Res, 2012. **72**(1): p. 66-75.
182. Burger, R.A., et al., *Incorporation of bevacizumab in the primary treatment of ovarian cancer*. N Engl J Med, 2011. **365**(26): p. 2473-83.
183. Perren, T.J., et al., *A phase 3 trial of bevacizumab in ovarian cancer*. N Engl J Med, 2011. **365**(26): p. 2484-96.
184. Cinelli, M.A., et al., *Inducible nitric oxide synthase: Regulation, structure, and inhibition*. Med Res Rev, 2020. **40**(1): p. 158-189.
185. Li, L., et al., *iNOS-derived nitric oxide promotes glycolysis by inducing pyruvate kinase M2 nuclear translocation in ovarian cancer*. Oncotarget, 2017. **8**(20): p. 33047-33063.
186. Saied, E.M. and N.M. El-Etreby, *The role and prognostic value of inducible nitric oxide synthase (iNOS) and interleukin-33 (IL-33) in serous and mucinous epithelial ovarian tumours*. Ann Diagn Pathol, 2017. **27**: p. 62-68.
187. Granados-Principal, S., et al., *Inhibition of iNOS as a novel effective targeted therapy against triple-negative breast cancer*. Breast Cancer Res, 2015. **17**(1): p. 25.
188. Vannini, F., K. Kashfi, and N. Nath, *The dual role of iNOS in cancer*. Redox Biol, 2015. **6**: p. 334-343.
189. Westergaard, M.C.W., et al., *Changes in the Tumor Immune Microenvironment during Disease Progression in Patients with Ovarian Cancer*. Cancers (Basel), 2020. **12**(12).
190. Sikora, A.G., et al., *Targeted inhibition of inducible nitric oxide synthase inhibits growth of human melanoma in vivo and synergizes with chemotherapy*. Clin Cancer Res, 2010. **16**(6): p. 1834-44.
191. Ehrenfeld, P., et al., *S-nitrosylation and its role in breast cancer angiogenesis and metastasis*. Nitric Oxide, 2019. **87**: p. 52-59.
192. Li, F., et al., *Regulation of HIF-1alpha stability through S-nitrosylation*. Mol Cell, 2007. **26**(1): p. 63-74.
193. Zhang, H., et al., *HIF-1-dependent expression of angiopoietin-like 4 and L1CAM mediates vascular metastasis of hypoxic breast cancer cells to the lungs*. Oncogene, 2012. **31**(14): p. 1757-70.
194. Martinez-Ruiz, A. and S. Lamas, *S-nitrosylation: a potential new paradigm in signal transduction*. Cardiovasc Res, 2004. **62**(1): p. 43-52.
195. Connelly, S.T., et al., *Increased nitric oxide levels and iNOS over-expression in oral squamous cell carcinoma*. Oral Oncol, 2005. **41**(3): p. 261-7.
196. Chiarugi, V., L. Magnelli, and O. Gallo, *Cox-2, iNOS and p53 as play-makers of tumor angiogenesis (review)*. Int J Mol Med, 1998. **2**(6): p. 715-9.

197. Rak, J.W., B.D. St Croix, and R.S. Kerbel, *Consequences of angiogenesis for tumor progression, metastasis and cancer therapy*. Anticancer Drugs, 1995. **6**(1): p. 3-18.
198. Xue, Q., et al., *Regulation of iNOS on Immune Cells and Its Role in Diseases*. Int J Mol Sci, 2018. **1G**(12).
199. Jang, T.J. and D.K. Kim, *Inducible nitric oxide synthase expression of tumor and stromal cells is associated with the progression of 7,12-dimethylbenz[a]anthracene-induced rat mammary tumors*. Cancer Lett, 2002. **182**(2): p. 121-6.
200. Zhang, Y., et al., *TP53 mutations in epithelial ovarian cancer*. Transl Cancer Res, 2016. **5**(6): p. 650-663.
201. Christie, E.L. and D.D.L. Bowtell, *Acquired chemotherapy resistance in ovarian cancer*. Ann Oncol, 2017. **28**(suppl_8): p. viii13-viii15.
202. Kossai, M., et al., *Ovarian Cancer: A Heterogeneous Disease*. Pathobiology, 2018. **85**(1-2): p. 41-49.
203. Usman, S., et al., *Vimentin Is at the Heart of Epithelial Mesenchymal Transition (EMT) Mediated Metastasis*. Cancers (Basel), 2021. **13**(19).
204. Tabatabaee, A., et al., *Targeting vimentin: a multifaceted approach to combatting cancer metastasis and drug resistance*. Cancer Metastasis Rev, 2024. **43**(1): p. 363-377.
205. Tendulkar, S. and S. Dodamani, *Chemoresistance in Ovarian Cancer: Prospects for New Drugs*. Anticancer Agents Med Chem, 2021. **21**(6): p. 668-678.
206. Chowanadisai, W., et al., *Cisplatin Resistant Spheroids Model Clinically Relevant Survival Mechanisms in Ovarian Tumors*. PLoS One, 2016. **11**(3): p. e0151089.
207. Chang, K.E., et al., *The protein phosphatase 2A inhibitor LB100 sensitizes ovarian carcinoma cells to cisplatin-mediated cytotoxicity*. Mol Cancer Ther, 2015. **14**(1): p. 90-100.
208. Yellepeddi, V.K., et al., *Comparative evaluation of small-molecule chemosensitizers in reversal of cisplatin resistance in ovarian cancer cells*. Anticancer Res, 2012. **32**(9): p. 3651-8.
209. Reddy, T., et al., *NOS inhibition sensitizes metaplastic breast cancer to PI3K inhibition and taxane therapy via c-JUN repression*. Nat Commun, 2024. **15**(1): p. 10737.
210. Lindskog, C., *The Human Protein Atlas - an important resource for basic and clinical research*. Expert Rev Proteomics, 2016. **13**(7): p. 627-9.
211. Barnes, B.M., et al., *Distinct transcriptional programs stratify ovarian cancer cell lines into the five major histological subtypes*. Genome Med, 2021. **13**(1): p. 140.
212. Adams, V., et al., *Induction of iNOS expression in skeletal muscle by IL-1beta and NFkappaB activation: an in vitro and in vivo study*. Cardiovasc Res, 2002. **54**(1): p. 95-104.
213. Burke, S.J., et al., *Regulation of iNOS gene transcription by IL-1beta and IFN-gamma requires a coactivator exchange mechanism*. Mol Endocrinol, 2013. **27**(10): p. 1724-42.
214. Wong, M.L., et al., *Inducible nitric oxide synthase gene expression in the brain during systemic inffammation*. Nat Med, 1996. **2**(5): p. 581-4.
215. Kwon, S. and S.C. George, *Synergistic cytokine-induced nitric oxide production in human alveolar epithelial cells*. Nitric Oxide, 1999. **3**(4): p. 348-57.
216. Dorsett, Y. and T. Tuschl, *siRNAs: applications in functional genomics and potential as therapeutics*. Nat Rev Drug Discov, 2004. **3**(4): p. 318-29.
217. Zon, A. and I. Bednarek, *Cisplatin in Ovarian Cancer Treatment-Known Limitations in Therapy Force New Solutions*. Int J Mol Sci, 2023. **24**(8).
218. Florkemeier, I., et al., *Combined PARP and Dual Topoisomerase Inhibition Potentiates Genome Instability and Cell Death in Ovarian Cancer*. Int J Mol Sci, 2022. **23**(18).

219. Battaglia, R.A., et al., *Vimentin on the move: new developments in cell migration*. F1000Res, 2018. **7**.
220. Liu, C.Y., et al., *Vimentin contributes to epithelial-mesenchymal transition cancer cell mechanics by mediating cytoskeletal organization and focal adhesion maturation*. Oncotarget, 2015. **6**(18): p. 15966-83.
221. Domagala, W., et al., *Vimentin expression appears to be associated with poor prognosis in node-negative ductal NOS breast carcinomas*. Am J Pathol, 1990. **137**(6): p. 1299-304.
222. Bhuyan, G., et al., *Epithelial-mesenchymal transition in serous and mucinous epithelial tumors of the ovary*. J Cancer Res Ther, 2019. **15**(6): p. 1309-1315.
223. Foster, M.W., T.J. McMahon, and J.S. Stamler, *S-nitrosylation in health and disease*. Trends Mol Med, 2003. **G**(4): p. 160-8.
224. Lheureux, S., et al., *Epithelial ovarian cancer*. Lancet, 2019. **3G3**(10177): p. 1240-1253.
225. Maccio, A. and C. Madeddu, *Inffammation and ovarian cancer*. Cytokine, 2012. **58**(2): p. 133-47.
226. Alexandrova, E., et al., *An Overview of Candidate Therapeutic Target Genes in Ovarian Cancer*. Cancers (Basel), 2020. **12**(6).
227. Yoshikawa, H., et al., *Prevalence of endometriosis in ovarian cancer*. Gynecol Obstet Invest, 2000. **50 Suppl 1**: p. 11-7.
228. Engeli, S., et al., *Regulation of the nitric oxide system in human adipose tissue*. J Lipid Res, 2004. **45**(9): p. 1640-8.
229. Muerkoster, S., et al., *Tumor stroma interactions induce chemoresistance in pancreatic ductal carcinoma cells involving increased secretion and paracrine effects of nitric oxide and interleukin-1beta*. Cancer Res, 2004. **64**(4): p. 1331-7.
230. Kim, S., et al., *Tumor evolution and chemoresistance in ovarian cancer*. NPJ Precis Oncol, 2018. **2**: p. 20.
231. Koning, T., et al., *S-Nitrosylation in endothelial cells contributes to tumor cell adhesion and extravasation during breast cancer metastasis*. Biol Res, 2023. **56**(1): p. 51.
232. Switzer, C.H., et al., *S-nitrosylation of EGFR and Src activates an oncogenic signaling network in human basal-like breast cancer*. Mol Cancer Res, 2012. **10**(9): p. 1203-15.
233. Nowak, M. and M. Klink, *The Role of Tumor-Associated Macrophages in the Progression and Chemoresistance of Ovarian Cancer*. Cells, 2020. **G**(5).
234. Tian, B., et al., *Mechanisms of cytokine induced NO-mediated cardiac fibroblast apoptosis*. Am J Physiol Heart Circ Physiol, 2002. **283**(5): p. H1958-67.
235. Unno, Y., et al., *Nitric oxide-induced downregulation of leptin production by 3T3-L1 adipocytes*. Nitric Oxide, 2006. **15**(2): p. 125-32.
236. Santiago, A.E., et al., *Systemic Inffammatory Patterns in Ovarian Cancer Patients: Analysis of Cytokines, Chemokines, and Microparticles*. Rev Bras Ginecol Obstet, 2023. **45**(12): p. e780-e789.
237. Yang, Y., et al., *Nanomedicine Strategies for Heating "Cold" Ovarian Cancer (OC): Next Evolution in Immunotherapy of OC*. Adv Sci (Weinh), 2022. **G**(28): p. e2202797.
238. Qin, T., et al., *Harnessing preclinical models for the interrogation of ovarian cancer*. J Exp Clin Cancer Res, 2022. **41**(1): p. 277.
239. Fu, X. and R.M. Hoffman, *Human ovarian carcinoma metastatic models constructed in nude mice by orthotopic transplantation of histologically-intact patient specimens*. Anticancer Res, 1993. **13**(2): p. 283-6.
240. Vanderhyden, B.C., T.J. Shaw, and J.F. Ethier, *Animal models of ovarian cancer*. Reprod Biol Endocrinol, 2003. **1**: p. 67.

241. Fiebig, H.H., et al., *In vitro and in vivo evaluation of US-NCI compounds in human tumor xenografts*. Cancer Treat Rev, 1990. **17**(2-3): p. 109-17.
242. Voskoglou-Nomikos, T., J.L. Pater, and L. Seymour, *Clinical predictive value of the in vitro cell line, human xenograft, and mouse allograft preclinical cancer models*. Clin Cancer Res, 2003. **G**(11): p. 4227-39.
243. Bareham, B., et al., *Modeling human tumor-immune environments in vivo for the preclinical assessment of immunotherapies*. Cancer Immunol Immunother, 2021. **70**(10): p. 2737-2750.
244. Chen, J., et al., *Patient-Derived Xenografts Are a Reliable Preclinical Model for the Personalized Treatment of Epithelial Ovarian Cancer*. Front Oncol, 2021. **11**: p. 744256.
245. Liu, Y., et al., *Gene expression differences between matched pairs of ovarian cancer patient tumors and patient-derived xenografts*. Sci Rep, 2019. **G**(1): p. 6314.
246. Pisano, S., et al., *Assessment of the immune landscapes of advanced ovarian cancer in an optimized in vivo model*. Clin Transl Med, 2021. **11**(10): p. e551.
247. Quinn, B.A., et al., *Development of a syngeneic mouse model of epithelial ovarian cancer*. J Ovarian Res, 2010. **3**: p. 24.
248. Fong, M.Y. and S.S. Kakar, *Ovarian cancer mouse models: a summary of current models and their limitations*. J Ovarian Res, 2009. **2**(1): p. 12.
249. Giatromanolaki, A., et al., *iNOS Expression by Tumor-Infiltrating Lymphocytes, PD-L1 and Prognosis in Non-Small-Cell Lung Cancer*. Cancers (Basel), 2020. **12**(11).
250. Suschek, C.V., O. Schnorr, and V. Kolb-Bachofen, *The role of iNOS in chronic inffammatory processes in vivo: is it damage-promoting, protective, or active at all?* Curr Mol Med, 2004. **4**(7): p. 763-75.
251. Ambs, S., et al., *Up-regulation of inducible nitric oxide synthase expression in cancer-prone p53 knockout mice*. Proc Natl Acad Sci U S A, 1998. **G5**(15): p. 8823-8.
252. Lee, Y., et al., *Wounding promotes ovarian cancer progression and decreases efficacy of cisplatin in a syngeneic mouse model*. J Ovarian Res, 2018. **11**(1): p. 56.
253. Wilkinson-Ryan, I., et al., *A Syngeneic Mouse Model of Epithelial Ovarian Cancer Port Site Metastases*. Transl Oncol, 2019. **12**(1): p. 62-68.
254. Mo, L., et al., *Syngeneic Murine Ovarian Cancer Model Reveals That Ascites Enriches for Ovarian Cancer Stem-Like Cells Expressing Membrane GRP78*. Mol Cancer Ther, 2015. **14**(3): p. 747-56.
255. Ayhan, A., et al., *Ascites and epithelial ovarian cancers: a reappraisal with respect to different aspects*. Int J Gynecol Cancer, 2007. **17**(1): p. 68-75.
256. Weinberg, J.B., et al., *Human mononuclear phagocyte inducible nitric oxide synthase (iNOS): analysis of iNOS mRNA, iNOS protein, biopterin, and nitric oxide production by blood monocytes and peritoneal macrophages*. Blood, 1995. **86**(3): p. 1184-95.
257. Choy, J.C., et al., *CXCL12 induction of inducible nitric oxide synthase in human CD8 T cells*. J Heart Lung Transplant, 2008. **27**(12): p. 1333-9.
258. Jayaraman, P., et al., *iNOS expression in CD4+ T cells limits Treg induction by repressing TGFbeta1: combined iNOS inhibition and Treg depletion unmask endogenous antitumor immunity*. Clin Cancer Res, 2014. **20**(24): p. 6439-51.
259. Kim, M.E. and J.S. Lee, *Advances in the Regulation of Inffammatory Mediators in Nitric Oxide Synthase: Implications for Disease Modulation and Therapeutic Approaches*. Int J Mol Sci, 2025. **26**(3).

260. Kitasato, A., et al., *Inffammatory cytokines promote inducible nitric oxide synthase-mediated DNA damage in hamster gallbladder epithelial cells*. World J Gastroenterol, 2007. **13**(47): p. 6379-84.
261. Ford, C.E., et al., *The untapped potential of ascites in ovarian cancer research and treatment*. Br J Cancer, 2020. **123**(1): p. 9-16.
262. Sarkar, I., et al., *T-memory cells against cancer: Remembering the enemy*. Cell Immunol, 2019. **338**: p. 27-31.
263. Lowes, M.A., et al., *Increase in TNF-alpha and inducible nitric oxide synthase-expressing dendritic cells in psoriasis and reduction with efalizumab (anti-CD11a)*. Proc Natl Acad Sci U S A, 2005. **102**(52): p. 19057-62.
264. Doubeni, C.A., A.R. Doubeni, and A.E. Myers, *Diagnosis and Management of Ovarian Cancer*. Am Fam Physician, 2016. **G3**(11): p. 937-44.
265. Stiff, A., et al., *Nitric Oxide Production by Myeloid-Derived Suppressor Cells Plays a Role in Impairing Fc Receptor-Mediated Natural Killer Cell Function*. Clin Cancer Res, 2018. **24**(8): p. 1891-1904.
266. MacMicking, J., Q.W. Xie, and C. Nathan, *Nitric oxide and macrophage function*. Annu Rev Immunol, 1997. **15**: p. 323-50.
267. Lavoue, V., et al., *Immunity of human epithelial ovarian carcinoma: the paradigm of immune suppression in cancer*. J Transl Med, 2013. **11**: p. 147.
268. Tsai, C.S., et al., *Macrophages from irradiated tumors express higher levels of iNOS, arginase-I and COX-2, and promote tumor growth*. Int J Radiat Oncol Biol Phys, 2007. **68**(2): p. 499-507.
269. Jayaraman, P., et al., *Tumor-expressed inducible nitric oxide synthase controls induction of functional myeloid-derived suppressor cells through modulation of vascular endothelial growth factor release*. J Immunol, 2012. **188**(11): p. 5365-76.
270. Chen, T., *Unveiling the significance of inducible nitric oxide synthase: Its impact on cancer progression and clinical implications*. Cancer Lett, 2024. **5G2**: p. 216931.
271. Soni, H., et al., *Cisplatin-induced oxidative stress stimulates renal Fas ligand shedding*. Ren Fail, 2018. **40**(1): p. 314-322.
272. Guo, C., et al., *Revisiting chemoresistance in ovarian cancer: Mechanism, biomarkers, and precision medicine*. Genes Dis, 2022. **G**(3): p. 668-681.
273. Ushijima, K., *Treatment for recurrent ovarian cancer-at first relapse*. J Oncol, 2010. **2010**: p. 497429.
274. Wongvaranon, P., et al., *Acquired resistance to chemotherapy in lung cancer cells mediated by prolonged nitric oxide exposure*. Anticancer Res, 2013. **33**(12): p. 5433-44.
275. Hergueta-Redondo, M. and H. Peinado, *The inffuence of secreted factors and extracellular vesicles in ovarian cancer metastasis*. EJC Suppl, 2020. **15**: p. 38-48.
276. Rothenberger, N.J., A. Somasundaram, and L.P. Stabile, *The Role of the Estrogen Pathway in the Tumor Microenvironment*. Int J Mol Sci, 2018. **1G**(2).
277. El-Sehemy, A., L.M. Postovit, and Y. Fu, *Nitric oxide signaling in human ovarian cancer: A potential therapeutic target*. Nitric Oxide, 2016. **54**: p. 30-7.
278. Botti, C., et al., *Immunosuppressive factors: role in cancer development and progression*. Int J Biol Markers, 1998. **13**(2): p. 51-69.
279. Jeon, S.Y., K.A. Hwang, and K.C. Choi, *Effect of steroid hormones, estrogen and progesterone, on epithelial mesenchymal transition in ovarian cancer development*. J Steroid Biochem Mol Biol, 2016. **158**: p. 1-8.

280. Sepulveda, F., et al., *EV-miRNA-Mediated Intercellular Communication in the Breast Tumor Microenvironment*. Int J Mol Sci, 2023. **24**(17).
281. Thomsen, L.L., et al., *Nitric oxide synthase activity in human breast cancer*. Br J Cancer, 1995. **72**(1): p. 41-4.
282. Aranda, E., et al., *Nitric oxide and cancer: the emerging role of S-nitrosylation*. Curr Mol Med, 2012. **12**(1): p. 50-67.
283. Hess, D.T. and J.S. Stamler, *Regulation by S-nitrosylation of protein post-translational modification*. J Biol Chem, 2012. **287**(7): p. 4411-8.
284. Huang, B., S.C. Chen, and D.L. Wang, *Shear ffow increases S-nitrosylation of proteins in endothelial cells*. Cardiovasc Res, 2009. **83**(3): p. 536-46.
285. Fernando, V., et al., *S-Nitrosylation: An Emerging Paradigm of Redox Signaling*. Antioxidants (Basel), 2019. **8**(9).
286. Walton, S.P., et al., *Designing highly active siRNAs for therapeutic applications*. FEBS J, 2010. **277**(23): p. 4806-13.
287. Chen, C., et al., *Applications of multi-omics analysis in human diseases*. MedComm (2020), 2023. **4**(4): p. e315.
288. Mitra, A.K., et al., *In vivo tumor growth of high-grade serous ovarian cancer cell lines*. Gynecol Oncol, 2015. **138**(2): p. 372-7.
289. Halkia, E., J. Spiliotis, and P. Sugarbaker, *Diagnosis and management of peritoneal metastases from ovarian cancer*. Gastroenterol Res Pract, 2012. **2012**: p. 541842.
290. Pignata, S., et al., *Treatment of recurrent ovarian cancer*. Ann Oncol, 2017. **28**(suppl_8): p. viii51-viii56.
291. Bookman, M.A., *First-line chemotherapy in epithelial ovarian cancer*. Clin Obstet Gynecol, 2012. **55**(1): p. 96-113.
292. Rizza, S., et al., *GSNOR deficiency promotes tumor growth via FAK1 S-nitrosylation*. Cell Rep, 2023. **42**(1): p. 111997.
293. Babykutty, S., et al., *Insidious role of nitric oxide in migration/invasion of colon cancer cells by upregulating MMP-2/S via activation of cGMP-PKG-ERK signaling pathways*. Clin Exp Metastasis, 2012. **2G**(5): p. 471-92.
294. Mishra, D., V. Patel, and D. Banerjee, *Nitric Oxide and S-Nitrosylation in Cancers: Emphasis on Breast Cancer*. Breast Cancer (Auckl), 2020. **14**: p. 1178223419882688.
295. Ramos Gde, O., et al., *Fibronectin Modulates Cell Adhesion and Signaling to Promote Single Cell Migration of Highly Invasive Oral Squamous Cell Carcinoma*. PLoS One, 2016. **11**(3): p. e0151338.
296. Griggs, L.A., et al., *Fibronectin fibrils regulate TGF-beta1-induced Epithelial-Mesenchymal Transition*. Matrix Biol, 2017. **60-61**: p. 157-175.
297. Sullivan, N.J., et al., *Interleukin-C induces an epithelial-mesenchymal transition phenotype in human breast cancer cells*. Oncogene, 2009. **28**(33): p. 2940-7.
298. Cui, Q., et al., *Upregulating MMP-1 in carcinoma-associated fibroblasts reduces the efficacy of Taxotere on breast cancer synergized by Collagen IV*. Oncol Lett, 2018. **16**(3): p. 3537-3544.
299. Burges, A. and B. Schmalfeldt, *Ovarian cancer: diagnosis and treatment*. Dtsch Arztebl Int, 2011. **108**(38): p. 635-41.
300. Song, Y.J., *Prediction of optimal debulking surgery in ovarian cancer*. Gland Surg, 2021. **10**(3): p. 1173-1181.
301. Christian, J. and H. Thomas, *Ovarian cancer chemotherapy*. Cancer Treat Rev, 2001. **27**(2): p. 99-109.

302. Hong, T., et al., *Guide for generating single-cell-derived knockout clones in mammalian cell lines using the CRISPR/CasS system*. Mol Cells, 2024. **47**(7): p. 100087.
303. Qin, A., et al., *Knockout of NOS2 Promotes Adipogenic Differentiation of Rat MSCs by Enhancing Activation of JAK/STAT3 Signaling*. Front Cell Dev Biol, 2021. **G**: p. 638518.
304. Jones, S.W., P.M. Souza, and M.A. Lindsay, *siRNA for gene silencing: a route to drug target discovery*. Curr Opin Pharmacol, 2004. **4**(5): p. 522-7.
305. Devi, G.R., *siRNA-based approaches in cancer therapy*. Cancer Gene Ther, 2006. **13**(9): p. 819-29.
306. Ozpolat, B., A.K. Sood, and G. Lopez-Berestein, *Liposomal siRNA nanocarriers for cancer therapy*. Adv Drug Deliv Rev, 2014. **66**: p. 110-6.
307. Duxbury, M.S., et al., *Systemic siRNA-mediated gene silencing: a new approach to targeted therapy of cancer*. Ann Surg, 2004. **240**(4): p. 667-74; discussion 675-6.
308. Mullen, M. and R.R. Gonzalez-Perez, *Leptin-Induced JAK/STAT Signaling and Cancer Growth*. Vaccines (Basel), 2016. **4**(3).
309. Vuoriluoto, K., et al., *Vimentin regulates EMT induction by Slug and oncogenic H-Ras and migration by governing Axl expression in breast cancer*. Oncogene, 2011. **30**(12): p. 1436-48.
310. Li, X., et al., *NOS1 upregulates ABCG2 expression contributing to DDP chemoresistance in ovarian cancer cells*. Oncol Lett, 2019. **17**(2): p. 1595-1602.
311. Tingulstad, S., et al., *Survival and prognostic factors in patients with ovarian cancer*. Obstet Gynecol, 2003. **101**(5 Pt 1): p. 885-91.
312. Tian, W., et al., *Extracellular vesicles in ovarian cancer chemoresistance, metastasis, and immune evasion*. Cell Death Dis, 2022. **13**(1): p. 64.
313. Baert, T., et al., *Myeloid Derived Suppressor Cells: Key Drivers of Immunosuppression in Ovarian Cancer*. Front Immunol, 2019. **10**: p. 1273.
314. Oun, R., Y.E. Moussa, and N.J. Wheate, *The side effects of platinum-based chemotherapy drugs: a review for chemists*. Dalton Trans, 2018. **47**(19): p. 6645-6653.
315. Gao, Y., et al., *Heterogeneity of immune microenvironment in ovarian cancer and its clinical significance: a retrospective study*. Oncoimmunology, 2020. **G**(1): p. 1760067.